Investigation of FAD Chemical Models to Study the Monoamine Oxidase Catalyzed Oxidation of Cyclic Tertiary Allylamines

Akiko Nakamura

Dissertation submitted to the faculty of the Virginia Polytechnic Institute and State University in partial fulfillment of the requirements for the degree of

Doctor of Philosophy

In

Chemistry

James M. Tanko, Chair

Neal Castagnoli, Jr.

Paul A. Deck

David R. Bevan

Richard D. Gandour

June 21st, 2013
Blacksburg, VA

Keywords: single electron transfer, FAD chemical model, monoamine oxidase, cyclic tertiary-allylamine, Parkinson's disease

Investigation of FAD Chemical Models to Study the Monoamine Oxidase Catalyzed Oxidation of Cyclic Tertiary Allylamines

Akiko Nakamura

ABSTRACT

Flavin adenine dinucleotide (FAD) is a coenzyme that participates in the redox process of flavoenzymes. Attempts to characterize the catalytic pathways of these enzymes have relied in part on the use of FAD chemical models. The efforts described in this dissertation focus on the chemical model approach to investigate the mechanism of the monoamine oxidase (MAO) catalyzed oxidation of the cyclic tertiary allylamine 1-methyl-4-(2-methyl-1*H*-pyrrol-2-yl)-1,2,3,6-tetrahydropyridine (TMMP), which is a close analog of the parkinsonian-inducing designer drug 1-methyl-4-phenyl-1,2,3,6-tetrahydropyridine (MPTP). MAO-B catalyzes the conversion of MPTP and its derivatives into active neurotoxins in the brain that subsequently mediate neurogenerative processes that mimic the events leading to idiopathic Parkinson's disease. Monoamine oxidase inhibitors are currently used to treat early stages of Parkinson's disease. Two FAD chemical models are examined in this project: 5-ethyl-3-methyllumiflavinium perchlorate ($5Et3MLF^+ClO_4^-$) and 3-methyllumiflavin (3MLF). The flavinium salt $5Et3MLF^+ClO_4^-$ is an activated form of 3MLF.

These FAD chemical models have been used to examine the MAO catalyzed oxidation. MAO-B is expressed in the brain and is known to be involved in the conversion of TMMP into the neurotoxic metabolite 1-methyl-4-phenyl pyridnium (MMP^+). MAO-B is responsible for the alpha-carbon oxidation of TMMP to yield 1-methyl-4-(2-methylpyrrol-2-yl)-2,3-dihydropyridinium (DHP^+), which then undergoes a second 2-electron oxidation to MMP^+. Previous findings demonstrated that 3MLF and $5Et3MLF^+ClO_4^-$ promoted the oxidation reaction of primary and secondary amines but not tertiary amines. However, the cyclic tertiary allylamine TMMP has not been examined experimentally. Therefore, the alpha-carbon oxidation of TMMP in the presence of the FAD chemical models is reported in this dissertation. The effect of dioxygen and water on the activity of these FAD models is also investigated.

ACKNOWLEDGEMENT

I would like to express my deepest appreciation to all those who helped me complete this dissertation. A special gratitude I give to my advisor Professor James M. Tanko, whose contribution with stimulating suggestions and encouragement helped me to complete my project. I am particularly grateful that you helped me to focus in the lab, but also permitted me to have experiences outside of the lab as well. Your trust allowed me to develop multifaceted capabilities that I will always cherish.

Furthermore, I would also like to acknowledge Professor Neal Castagnoli, Jr who invested his full effort in guiding me to achieve this goal. You also worked with me to develop my understanding of chemistry and organic chemistry techniques from a novice to professional.

Also, I would like to express my appreciation to Dean Karen DePauw. You truly inspired me. You showed me totally different vision of graduate education and gave me opportunities to gain diverse experiences that I could never had without your support.

Many thanks go to my friends who provided encouragement and support. You always helped me when I needed to push myself. Because of you, I never felt alone during this journey.

Most importantly, none of this would have been possible without the love and patience of my family. I cannot find words to express my gratitude to my parents, Mr. Tsuneo Nakamura and Mrs. Miyako Nakamura, and my grandmother, Mrs. Toku Nakamura. You have been a constant source of love, concern, support and strength all these years. Also, my sincere thank-you goes to my siblings, Takahiro Nakamura and Rie Nakamura. You have also shown patience and love. I also would like to express my sincere admiration to Dr. Ikusai Nakamura. I have always regarded your accomplishments throughout my life as my inspiration.

I owe my deepest gratitude to my husband Dr. Arthur Stiles for your assistance and your encouragement. You have been with me through all the great times and comforted me in the challenging times of this journey. Your love and support helped me to stay down to earth.

TABLE OF CONTENTS

LIST OF FIGURES

LIST OF TABLES

CHAPTER ONE

INTRODUCTION AND HISTORICAL

1.1 Introduction to Parkinson's and Other Neurodegenerative Diseases

1.1.1 Mechanisms of Neurodegenerative Diseases

Neurodegenerative diseases are a group of progress disorders and are associated with microglia-derived inflammatory neurotoxins.[1] Examples of neurodegenerative diseases include Alzheimer's disease, Parkinson's disease (PD), amyotrophic lateral sclerosis and HIV-associated dementia. Oxidative stress may play a key role in triggering neurodegenerative processes involving dopaminergic neurons and may be linked to microglia-derived inflammatory neurotoxins.[1]

PD was named after the English physician James Parkinson who published "An Essay on the Shaking Palsy" in 1817.[2] This monograph described different stages of "the Shaking Palsy", later recognized as PD. The four primary symptoms of PD are gait instability, rigidity, slowness of movement and tremor.[3]

PD affects approximately 1% of the population over the age of 70 years in the United States.[3] According to the age-specific prevalence for Western Europe and the world's 10 most populous countries, the number of PD patients over 50 years of age was between 4.1 and 4.6 million in 2005.[4] In the report, the authors predicted that this number would grow substantially over the next 25 years to reach 8.7 million by 2050. The pathological hallmark of PD is the loss of the nigrostriatal neurons and the resulting depletion of the neurotransmitter dopamine.

Dopamine is a catecholaminyl neurotransmitter that is present in the periphery and in the central nervous system.[5] Other catecholamines include epinephrine and norepinephrine. Catecholamine breakdown is mainly mediated by the flavoenzymes monoamine oxidase-A and B (MAO-A and MAO-B).[6] Additionally, activation of microglia and the ensuing production of reactive oxygen species (ROS) stimulate the release of neurotoxic factors, such as NADPH oxidase-derived superoxide radical anion, which are involved in degeneration of dopaminergic neurons.[1] ROS include free radicals, such as superoxide radical anion and hydroxyl radical, and non-radicals, such as hydrogen peroxide and peroxynitrite. Also, it has been reported that α-synuclein plays a

key role in PD. The abnormal aggregation of α-synuclein protofibrils has been reported to occur in the dopaminergic neurons of patients with PD.[7] [8]

As mentioned above, dopamine deficiency is a hallmark of PD. In the late 1950's, the neurotransmitter dopamine and its effects in PD were demonstrated by Carlsson *et al*.[9] Later, decreased levels of dopamine in the brain were found in other patients with a parkinsonian syndrome.[10] It was estimated that the symptoms of Parkinson's disease appear after concentrations of the striatal dopamine decrease to 20% of the normal level.[10] These discoveries have led to improvements in diagnosis and treatment of PD.

1.1.2 The MPTP Model of PD

A potentially important finding relative to the etiology of PD is the parkinsonian-inducing neurotoxin 1-methyl-4-phenyl-1,2,3,6-tetrahydropyridine [(MPTP)(**1**)]. This compound can cause the selective destruction of dopaminergic nigrostriatal neurons, the same neurons that are lost in idiopathic PD.[11] An understanding of the mechanisms by which MPTP causes the loss of nigrostriatal dopaminergic neurons may lead to a better understanding of the causes of PD and, perhaps, to improved therapeutics.

MPTP is a cyclic tertiary allylamine that is bioactivated to the neurotoxin MPP^+ in brain cells by MAO-B (Scheme 1-1). MPTP is capable of crossing the blood-brain barrier rapidly and, once in the CNS, undergoes oxidation in glial cells to yield the dihydropyridinium metabolite [$MPDP^+$ (**2^+**)].[12] This intermediate is further oxidized into the ultimate neurotoxin, the 1-methyl-4-phenylpyridinium species [MPP^+ (**3^+**)]. MPP^+ (**3^+**) is taken up into the nigrostriatal nerve terminals by the dopamine transporter, where it inhibits ATP formation, leading to cell death.[11a, 12-13]

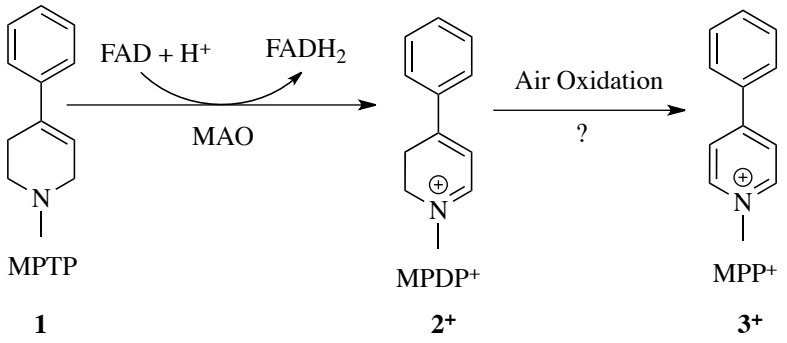

Scheme 1-1

Figure 1-1 illustrates the mechanism of mitochondrial dysfunction with **3**$^{+}$.[12] The pyridinium metabolite **3**$^{+}$ is known to inhibit Complex I of the mitochondrial respiratory system and also to cause apoptosis of dopaminergic neurons.[14] Complex I is NADH-quinone 1 oxidoreductase and is located on the inner membrane of mitochondria. It has been shown that exposure of human neuroblastoma cells to **3**$^{+}$ leads to the inhibition of mitochondrial Complex I and to increase hydrogen peroxide (H_2O_2) levels.[15] Also, caspase-3 activity, a biomarker of apoptosis, increased significantly in human neuroblastoma cells 12 hours after MPP^{+} treatment. Similarly, treatment of mice with **1** (24 mg/kg) increased levels of 8-hydroxyguanine, an indication that **1** led to the induction of DNA oxidative damage.[16]

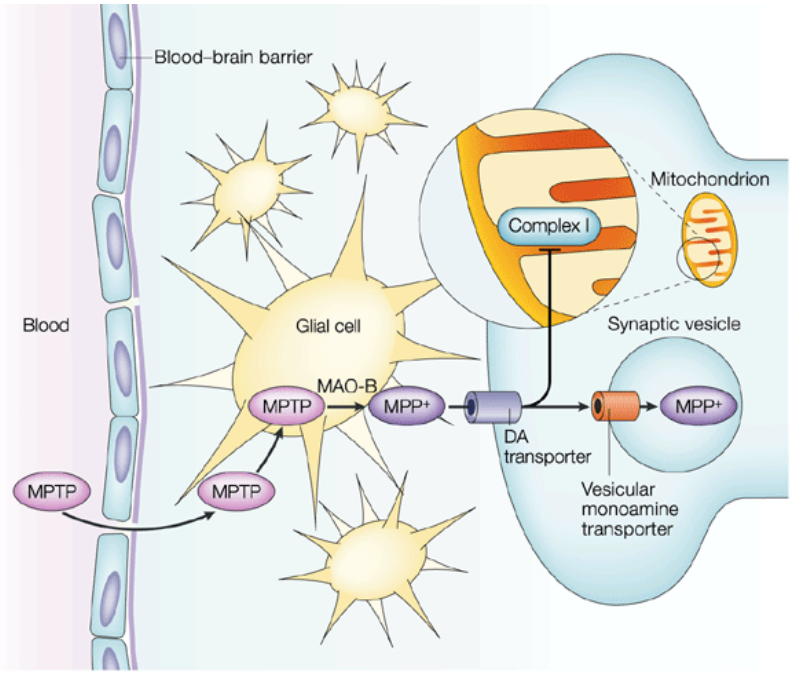

Figure 1-1. MPTP model of inhibiting mitochondrial function.[12] Reprinted by permission from Macmillan Publishers Ltd: Nature Review Neuroscience (Vila, M.; Przedborski, S., Targeting programmed cell death in neurodegenerative diseases. 2003, *4* (5), 365-75.), copyright (2003).*

A lower incidence of PD in smokers has been reported.[17] Furthermore, it has been shown that cigarette smoke inhibits the activity of MAO-A and MAO-B.[18] Chronic exposure to nicotine, however, showed no effects on the activity of these enzymes in rats.[19] Thus, the inhibition of MAO was not associated with the effect of nicotine.

* License agreement document shown in Appendix A.

In summary, PD is a growing global health problem. It is important to gain insight into the cause(s) of this disease. A detailed understanding of the MPTP model of PD could provide some clues relating to the etiology of idiopathic PD. Because there is little evidence to support a strong genetic link to PD,[20] it seems reasonable to assume that environmental insults must contribute to the ultimate loss of nigrostriatal neurons in those who develop PD. One important feature of the MPTP-induced degeneration of nigrostriatal neurons is its MAO-B catalyzed bioactivation. Although the MAO-B catalytic pathway has been a subject of study for decades, it remains poorly understood. In the present thesis, the oxidation of the pyrrolyl analog 1-methyl-4-(2-methylpyrrol-2-yl)-1,2,3,6-tetrahydropyridine [TMMP (**4**)] of **1** is examined (structures shown below) using models of FAD, the electron transporting co-factor of MAO-B.

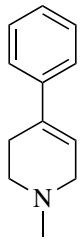

MPTP
1

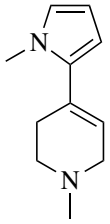

TMMP
4

1.2 Monoamine Oxidase – Function, Biochemistry and Role in Disease

1.2.1 Biochemistry of Monoamine Oxidase

Flavoenzymes, which are involved in important redox reactions, contain the cofactor flavin adenine dinucleotide (FAD) or mononucleotide (FMN).[21] Riboflavin (7,8-dimethyl-10-ribityl-isoalloxazine) is the central component of FMN and FAD; FAD consists of FMN and adenosine monophosphate as shown in Figure 1-2.[22]

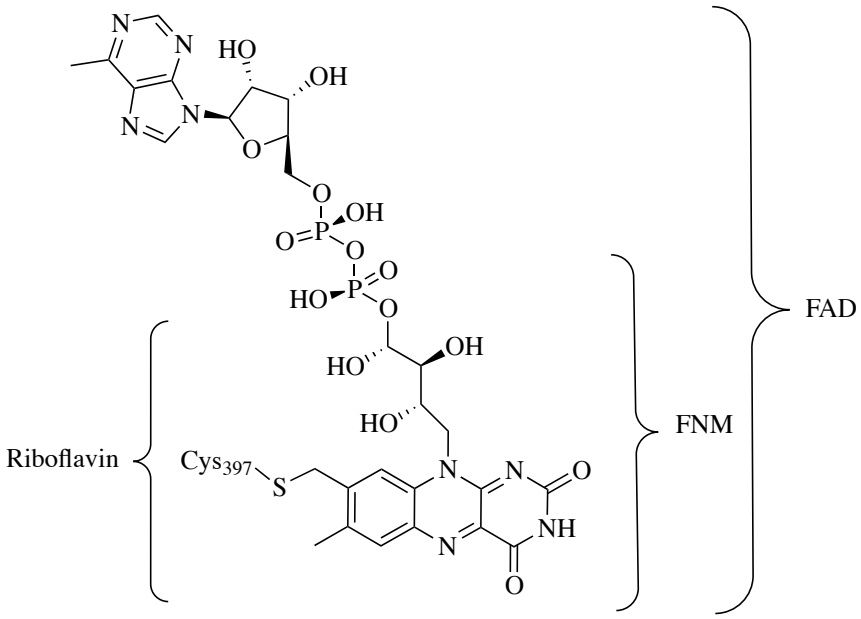

Figure 1-2. Structure of Flavin Adenine Dinucleotide.

The flavoenzymes MAO-A and MAO-B (EC 1.4.3.4; MAO) are outer-membrane mitochondrial proteins,[23] and are expressed in the majority of mammalian tissues.[5, 24] The A and B forms have approximately 70% sequence identity;[23] both forms contain the pentapeptide Ser-Gly-Gly-Cys-Tyr. The obligatory cofactor FAD is covalently attached at the 8α-position to an enzyme active site cysteinyl residue. The cysteinyl linkage of MAO-A is to Cys406 whereas the cysteinyl linkage of MAO-B is to Cys397.[25] The isoforms of these enzymes catalyze the oxidation of various biogenic amines in the brain and peripheral tissue.[5]

Differences in primary amino acid sequences suggest that the MAO-A and MAO-B are encoded by different genes.[26] The genes coding for these proteins are located on the X-chromosome and consist of 15 exons with identical intron-exon organization,[27] suggesting that both genes evolved from the same ancestral gene.[5]

Hence, because MAO-A and MAO-B are homologous, it is possible that the enzymes have similar chemical mechanisms for catalysis.[28] Their role in the oxidative metabolism of the biogenic amines dopamine, norepinephrine, epinephrine and serotonin is well documented.[24b] However, the oxidative metabolism of MPTP and MPTP derivatives has not been well

understood even though they are excellent substrates of MAO-B and precursors of the neurotoxins.

The catalytic pathway involves the net 2-electron oxidation of the substrate in a reaction that is coupled to the 2-electron reduction of the oxidized flavin (FAD) cofactor. The enzyme catalyzes the α-carbon oxidation of aminyl substrates and converts amines to the corresponding imines anaerobically.[29] The imines are then released from the enzyme and hydrolyzed to the corresponding aldehydes outside of the enzyme. Thus, MAOs are involved in the first 2-electron, α-carbon atom oxidation only; the hydrolytic step takes place outside of the enzyme.

Binda (2003) reported the X-ray crystal structure of MAO-B.[30] MAO-B has gained additional attention since it catalyzes the bioactivation of MPTP to its neurotoxic metabolite MPP^+ that mediates the degradation of dopaminergic neurons in the substantia nigra resulting in a parkinsonian syndrome closely resembling idiopathic Parkinson's disease. Efforts to develop selective inhibitors of MAO-A and MAO-B for the treatment of depression[31] and neurodegenerative disorders,[32] respectively, have been ongoing for decades.

1.2.2 Enzymatic Activity of MAO

The overall stoichiometry for the MAO-catalyzed oxidative deamination of a general aminyl substrate is shown in Scheme 1-2.[33] The cofactor FAD is reduced to $FADH_2$ as the aminyl substrate (**5**) is oxidized to produce the associated iminiumyl product (**6**). Subsequent hydrolysis of the iminiumyl product **6** yields the corresponding aldehyde and ammonium cation. When $FADH_2$ is re-oxidized to FAD, O_2 is reduced to H_2O_2, a potential ROS. In the next section of this review, proposed mechanisms of MAO catalysis for the oxidation of MPTP will be discussed.

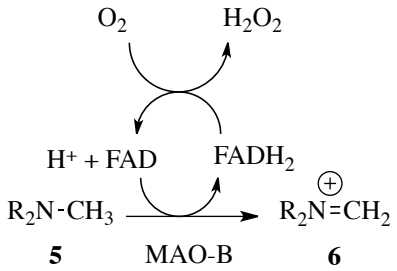

Scheme 1-2

1.3 Proposed Pathways of MAO Catalysis

1.3.1 Introducing the Proposed Pathways

Although the catalytic pathway for the MAO-catalyzed oxidation of amines has been studied for decades, the subject remains controversial. This topic remains relevant since selective inhibitors of MAO-A and MAO-B have the potential to develop into therapeutic agents to treat central and systemic disorders.

Three mechanisms have been proposed for the MAO-catalyzed oxidation of amines: (a) the single electron transfer (SET) pathway,[34] (b) the polar nucleophilic pathway,[35] and (c) the hydrogen atom transfer (HAT) pathway.[36] A fourth pathway, hydride transfer, recently has received some support but will not be considered here.[†]

1.3.1.1 Single Electron Transfer Pathway

The SET pathway for MAO catalysis was originally proposed by Silverman's group.[37] The central feature of this proposal is an initial single electron transfer (SET) reaction. Silverman's group proposed that MAO catalysis of monoamine oxidation involves two 1-electron transfers from the substrate to the flavin.[37] The SET pathway passes through an aminyl cation radical intermediate that is linked to the formation of the flavin semiquinone radical. It was proposed originally that the α-deprotonation of the aminyl radical cation is favored because the α-proton is acidic with an estimated pK_a of 10.[37b]

Scheme 1-3 shows the original SET pathway for MAO catalysis as proposed by Silverman in 1980.[37a] Single electron transfer from the nitrogen lone pair of the cyclopropylamine **7** to the oxidized flavin FAD is the initial step. This results in the generation of the aminyl radical cation $\mathbf{8}^{\bullet+}$ and the flavin semiquinone $FADH^{\bullet}$. Deprotonation of the α-carbon produces the α-aminyl radical ($\mathbf{9}^{\bullet}$)**.** In Pathway A, the iminium ion $\mathbf{11}^{+}$ and the flavin $FADH_2$ are produced from the α-amino radical $\mathbf{9}^{\bullet}$. In Pathway B, a covalent adduct **10** is present as an intermediate to generate the iminium ion $\mathbf{11}^{+}$ and $FADH_2$. This proposed pathway (Scheme 1-3) was supported by studies

[†] Orru R, Aldeco M, Edmondson DE. (2013) Do MAO A and MAO B utilize the same mechanism for the C-H bond cleavage step in catalysis? Evidence suggesting differing mechanisms. *J Neural Transm.* **120**, 847-51.

with *N*-benzylcyclopropylamine. Silverman *et al*. proposed that mechanism-based inactivation of MAO-B by *N*-benzylcyclopropylamine is initiated with generation of aminyl radical cations in an initial SET step.[34, 38]

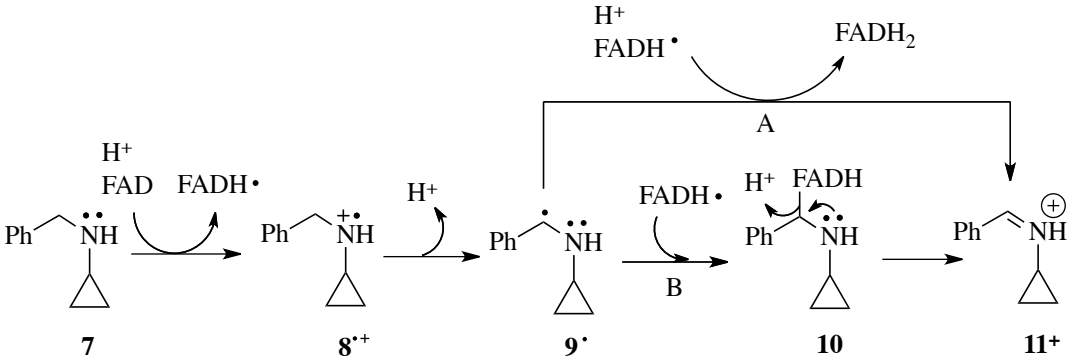

Scheme 1-3

In a later study, Silverman and his co-workers re-examined his proposed mechanism published in 1980 using *N*-(1-methylcyclopropyl)benzylamine [N-(1-Me)CBA](**12**).[34] If his proposed pathway (Scheme 1-4) were correct, the enzyme should not be inactivated because the corresponding aminyl radical cation (**13**$^{\bullet+}$) cannot undergo α-carbon deprotonation. To account for the observed enzyme inactivation, Silverman *et al*. proposed that the cyclopropylamine **12** undergoes a ring-opening process to give the corresponding distonic aminyl radical cation (**14**$^{\bullet+}$) that binds to the enzyme leading to inactivation (Scheme 1-4).

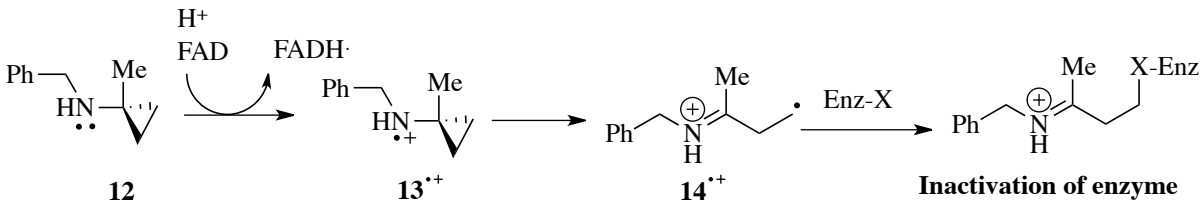

Scheme 1-4

The revised proposal for benzylcyclopropylamine includes a ring-opening step to form the distonic radical cation (**15**$^{\bullet+}$)(Scheme 1-5).[34] Covalent bond formation between **15**$^{\bullet+}$ and an unknown MAO radical species leads to the covalent adduct (**16**$^{+}$) and enzyme inactivation. In the

experiment, the investigators observed both inactivation of the enzyme via the covalent adduct **16**$^{+}$ and the formation of benzaldehyde (**18**). The partition ratio was found to be 1.0.[34] Single electron transfers from the nitrogen lone pair of the amine **7** to the oxidized flavin FAD is the proposed initial step. The resulting aminyl radical cation **8**$^{\bullet +}$ undergoes deprotonation to form the neutral carbon radical **9**$^{\bullet}$. Subsequent loss of the α-aminyl radical gives the iminium species (**11**$^{+}$) that undergoes hydrolysis to yield benzaldehyde (**18**). Thus, the aminyl radical cation (**8**$^{\bullet +}$) is the proposed obligatory intermediate for both of the proposed pathways, one leading to enzyme inactivation (ring opening) and the other to benzaldehyde (α-deprotonation). According to this proposal the rate of α-carbon deprotonation and ring opening of the cyclopropylaminyl radical cation must be comparable.

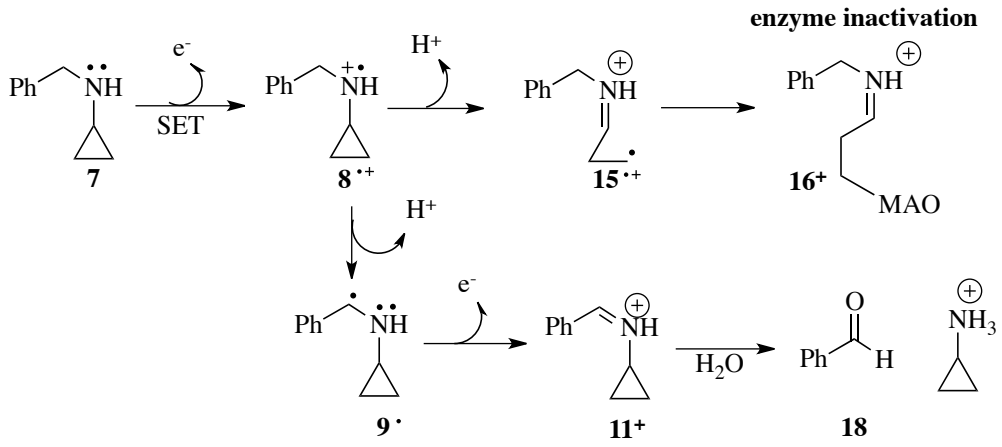

Scheme 1-5

More recently, another SET pathway was proposed by Rigby.[39] In this pathway, a phenoxyl radical plays a crucial role (Scheme 1-6).[39] In their experiment, reduction of MAO-A by sodium dithionite was examined using EPR spectroscopy and the formation of a phenoxyl radical was observed. Initial SET converts FAD (**19**) to flavosemiquinone (**20**) which, rather than undergoing deprotonation, abstracts a hydrogen atom from an intermediate radical cation. Also, a redox equilibrium is required between flavosemiquinone **20**$^{\bullet}$ and phenoxyl radical (**21**$^{\bullet}$) in the active site. Once the phenoxyl radical **21**$^{\bullet}$ is formed, one H$^{\bullet}$ transfers from the substrate to the flavin, followed by establishing the iminium ion and FADH^{-} (**22**$^{-}$). Finally, FADH^{-} (**22**$^{-}$) accepts one H^{+} from the iminium ion to form $FADH_2$ (**23**)

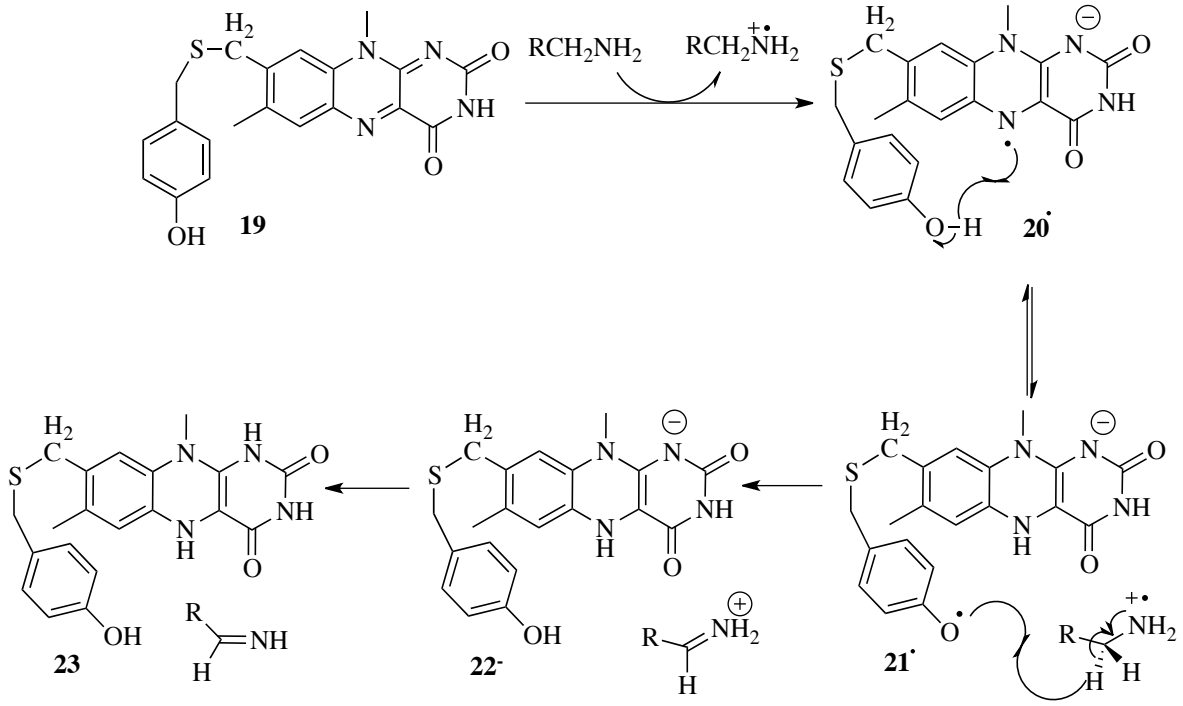

Scheme 1-6

Evidence both supporting and refuting an SET pathway for the MAO-catalyzed amine-oxidation mechanism has been reported subsequent to Silverman's initial proposal. For example, the X-ray crystal structure of the 4a-adduct formed between tranylcypromine and the FAD of MAO-B was obtained (Scheme 1-7).[30] In the study, inhibition of MAO-B with *trans*-2-phenylcyclopropylamine (**24**) was examined. The crystal structure of inhibited MAO-B revealed that the cyclopropyl group had undergone ring opening in the process of reacting with FAD to give the C4a flavin adduct **25** which supports the SET pathway.

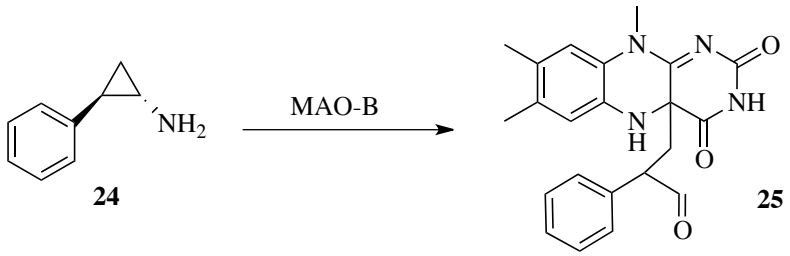

Scheme 1-7

Conversely, it has been argued that a one-electron transfer from the aminyl group to the flavin is thermodynamically unfavorable.[36a] Under anaerobic reductive half-reaction kinetic experiments performed with bovine liver MAO-B, spectral observations revealed no detectable formation of a flavin radical with a recorded absorbance. Also, the one-electron oxidation potential of primary amines examined with cyclic voltammetry (vs. the silver-silver ion reference electrode) was reported to be approximately + 1.02 eV,[40] while an estimation of flavin oxidation potential of flavin in MAO-B was reported as + 0.045 eV.[36a] This means that SET is highly disfavored, with ΔG^{o} = +22 kcal/mol.

Jurva (2005) examined the electrochemical oxidation of *N*-alkyl-4-phenyl-1,2,3,6-tetrahydropyridinyl derivatives using electrochemistry-electrospray mass spectrometry (EC/ESI-MS).[41] The mass spectrometry of the MPTP oxidation products showed that the ion intensity of the dihydropyridinium product **2** (*m/z* 172) increased as the ion intensity of MPTP (**1**) decreased (*m/z* 174) (Scheme 1-8). Interpretations of the data were consistent with the SET pathway as shown; the proposed oxidation mechanism proceeds via an aminyl radical cation (**26**$^{\bullet+}$) and an α-carbon radical (**27**$^{\bullet}$).

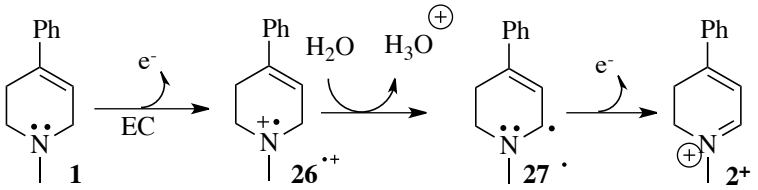

Scheme 1-8

Likewise, the results of the EC-ESI/MS with *N*-cyclopropyl-4-phenyl-1,2,3,6-tetrahydropyridine (**28**) were consistent with the SET pathway for the MAO-catalyzed reaction. These *N*-cyclopropyl analogs of MPTP are reported to be substrates for MAO-B and also are anticipated to be sensitive for single electron transfer. Following the electrochemical oxidation, the secondary amine **34**$^{+}$ (*m/z* 160) and the 4-phenyl-2,3-dihydropyridinium species **35**$^{+}$ (*m/z* 158) were obtained, indicating that the reaction proceeds via a cyclopropyl ring opening mechanism (Scheme 1-9).[41] The benzylic radical cation (**32**$^{\bullet+}$) and the corresponding inimium species (**33**$^{+}$) are obligatory intermediates for the formation of compounds **34**$^{+}$ and **35**$^{+}$.

However, when the *N*-cyclopropyl MPTP (**28**) analog was treated with MAO-B, the ring-closed form of its dihydropyridinium product **31**$^{+}$ was observed, via the proposed obligatory intermediate neutral radical species (**30**$^{\bullet}$).[17a] The partition ratio between the dihydropyridinium (**31**$^{+}$) and the inactivated enzyme was 17.0 to 1.0. Consequently, it is reasonable to assume that, unless enzyme active site bases are present, the rates of α-deprotonation of cyclopropylaminyl radical cations will be much slower than their rates of ring opening. In other words, the MAO-B catalyzed oxidation of the *N*-cyclopropyl MPTP analog **28** to the corresponding radical cation **29**$^{\bullet +}$ is unlikely to be the dominant pathway (SET pathway) as proposed by Silverman in this case.

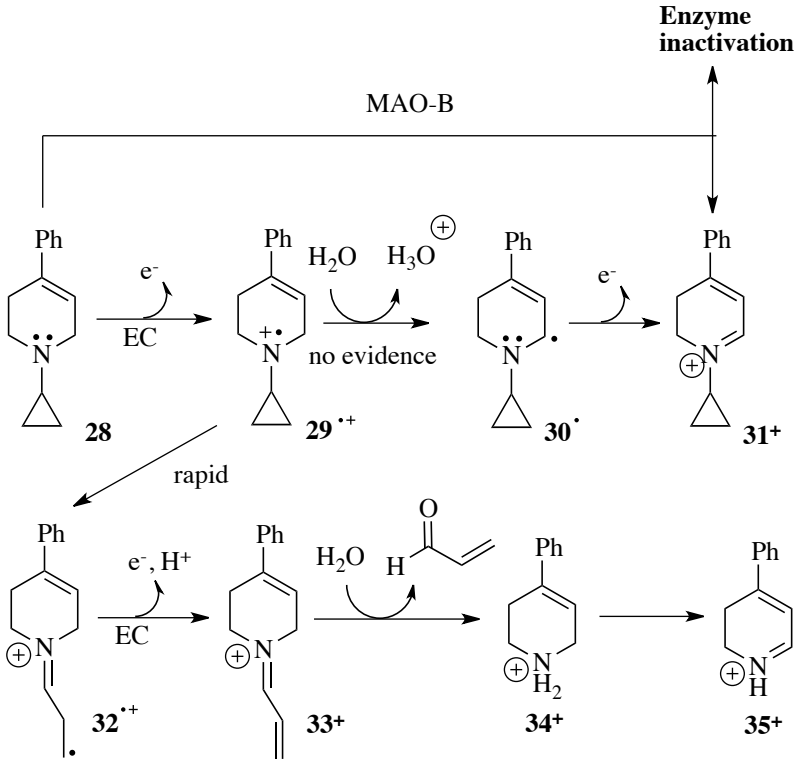

Scheme 1-9

Consistent with rapid ring opening rates of cyclopropylamines, some investigators have reported that formation of the ring-opened distonic radical cations may not pass through the corresponding radical cations.[42] This was argued when an energy minimum was not observed in the calculation for the conversion of cyclopropylamines to the ring-opened distonic radical cations.[41] Electron transfer and ring opening occur rapidly and may proceed by a concerted

mechanism. In brief, these data suggest that aminyl radical cations may not be obligatory intermediates for the MAO-catalyzed oxidation of MPTP and its analogs.

1.3.1.2 Polar Nucleophilic Pathway

A polar nucleophilic pathway was originally proposed by Brown *et al*. in 1970 for the oxidation of amines by MAO.[43] They proposed that the flavoenzyme-catalyzed dehydrogenations proceed via covalent attachment of the substrate to the flavin ring at the C4a position (**38**)(Scheme 1-10). The reaction is initiated by the C4a position of the flavin in the oxidized form (**36**) reacting with the lone pair on the nitrogen of benzylamine (**37**). The flavin in the reduced form (**39**) and benzylimine (**40**) are generated as final products. Evidence supporting this pathway came from studies on the mechanism of catalysis for D-amino acid oxidase.[44] This proposed mechanism has been further examined by different research groups.[35, 45]

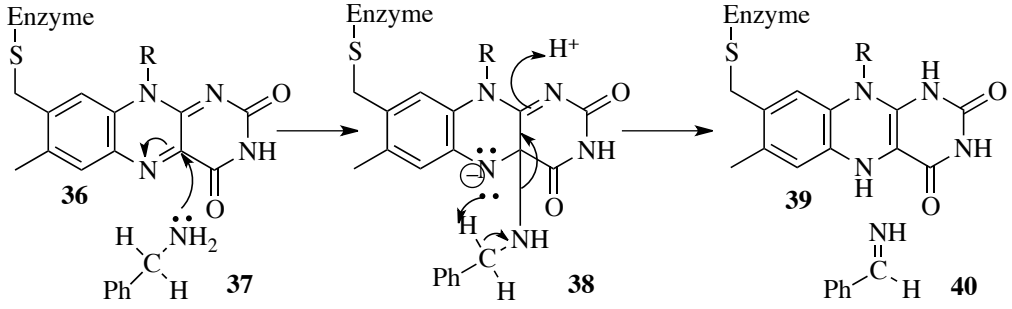

Scheme 1-10

For example, Mariano and co-workers used a flavin chemical model 5-ethyl-3-methyllumiflavinium perchlorate ($5Et3MLF^+ClO_4^-$) to study a polar nucleophilic reaction with benzylamine.[35] UV-visible results showed the disappearance of absorption bands at λ_{max} at 558 and 415 nm (markers of $5Et3MLF^+ClO_4^-$) and the appearance of an absorption band at λ_{max} 314 nm, which represents the C4a-benzylaminyldihydroflavinyl adduct (**41H$^+$**).

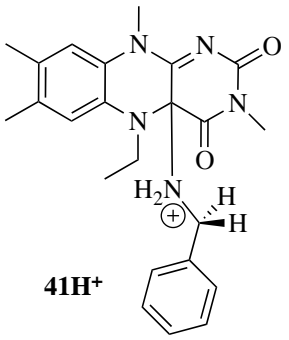

41H$^+$

Additionally, Bruice and his co-workers isolated C4a-adducts by reactions between 5Et3MLF$^+$$ClO_4^-$ and secondary amines in t-BuOH at 30 °C and observed the λ_{max} at 345 – 350 nm, such as 4a-FlEt-N$(C_4H_9)_2$, 4a-FlEt-N(isobutyl)$_2$, and 4a-F1Et-N$(CH_3)CH_2C_6H_5$.[46] Also, Mariano and co-workers examined reactions between 5Et3MLF$^+$$ClO_4^-$ and various amines in acetonitrile at 25 °C.[35, 45a, 47] The rates of oxidation were dependent on amine structure: in the order primary amine > secondary amine >> tertiary amine. No reaction was observed with the tertiary silylamine $PhCH_2NMeCH_2SiMe_3$ even after 6 days, presumably because of steric hindrance, implying a possible polar nucleophilic pathway involvement.[35] A polar nucleophilic mechanism may be sensitive to steric effects because that mechanism requires forming a covalent bond between two molecules.

However, this generalization may not apply to all MAO-catalyzed amine oxidations because MAOs act primarily on primary amines.[34, 48] Only few tertiary amines (see below) are known to be good substrates.[‡] Examples of tertiary amines oxidized by MAO are listed below, and the cyclic tertiary allylamines, such as MPTP **1** and TMMP **4**, are excellent MAO substrates. Those compounds might not be able to undergo a polar nucleophilic mechanism forming a covalent bond with the enzyme due to the steric interaction.

[‡] Silverman 1995 paper discusses *N*,α-dimethyl-*N*-(1-methylcyclopropy1)benzylamine is oxidized by MAO, and he cites his 1994 paper. And, in his 1994 paper, he states that the tertiary amine is an excellent inactivator of MAO. However, I failed to find any evidence of the tertiary amine being a substrate of MAO.

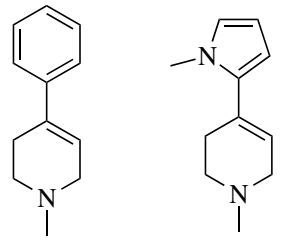

1 **4**

Accordingly, isotope effects on the reaction of 3-methyllumiflavin (3MLF) with $PhHCDNH_2$ were examined in 5 mM HCl in 2.5% H_2O-acetonitrile.[35] They compared reactions between the ground-state and excited-state (SET), using thermal (dark, 80 °C, 6 days) and photolytic ($\lambda > 320$ nm, 20 °C, 1h) conditions, respectively. Results showed a k_H/k_D of 4.3 (thermal) and 1.6 (photolysis). The ratio of k_H/k_D at 4.3 for the thermal reaction appears to be consistent with a primary isotope effect, suggesting a C-H bond breaking in the rate-determining step. On the other hand, the isotope effect of 1.6 for the photochemical reaction suggests either a primary or secondary isotope effect. When the transition state is not symmetrical, shifting to the right or left, the primary isotope effect can be relatively small. The isotope effect of 1.6 might suggest a hydrogen atom transfer process more than a deprotonation step. Because of the difference in isotope effects, Mariano and his co-workers concluded that these results were inconsistent with an SET mechanism for the reaction 3MLF with the primary amine.

However, their experimental conditions do not correspond to physiological pH and temperature. Also, their reaction did not proceed with tertiary amines. Therefore, their findings appear to be irrelevant to the mechanism of MAO-catalyzed oxidations of MPTP and its derivatives.

In a later study, the nature of the intermediate in the polar nucleophilic pathway was investigated by Edmondson and co-workers. The reaction rates and binding affinities of various *p*-substituted benzylamine analogues were examined with recombinant human MAO-A.[45b] The rate of flavin reduction showed a large positive ϱ value (~2.0), suggesting the development of a negative charge at the benzyl carbon position. The observed ϱ value for dideuterio substrates (1.8) was essentially the same as for the protio substrates (2.2), but the rate constants for the dideuterio substrates were lower with $k_H/k_D \approx 9.14$ (average). With the results found, Edmondson and co-workers proposed a concerted polar nucleopholic mechanism (Scheme 1-11).[49] In this modified polar nucleophilic pathway, the initial step involves nucleophilic attack of the lone pair on the

nitrogen of the aminyl substrate (**37**) at the C(4a) following which the N(5) anion of the flavin (**36**) serves as base to remove the benzylic α-C hydrogen atom of the adducted substrate (**38**) in the rate determining step.[49] In the second step, the iminium product (**40**) and the reduced flavin (**39**) separate from the intermediate complex (**38**), and the nitrogen at the N(11) position is protonated. Additional support for this mechanism has been reported in a computational study.[50] The semi-empirical PM3 method was used to examine the effects of the substituent electronic parameters on the rate of the proposed polar nucleophilic mechanism for MAO catalysis.[50] Calculations with PM3 revealed an increase in the reaction rate with electron-withdrawing groups at the *para* position of benzylamine. This computational model suggests the second step as the rate-determining step where the iminium product separates from the intermediate complex. The relationship between the log of rate constants and Hammett substituent parameter σ determined by PM3 method gave a ρ value of 1.0, which is similar in sign but lower in magnitude than the experimentally observed value of 2.0.

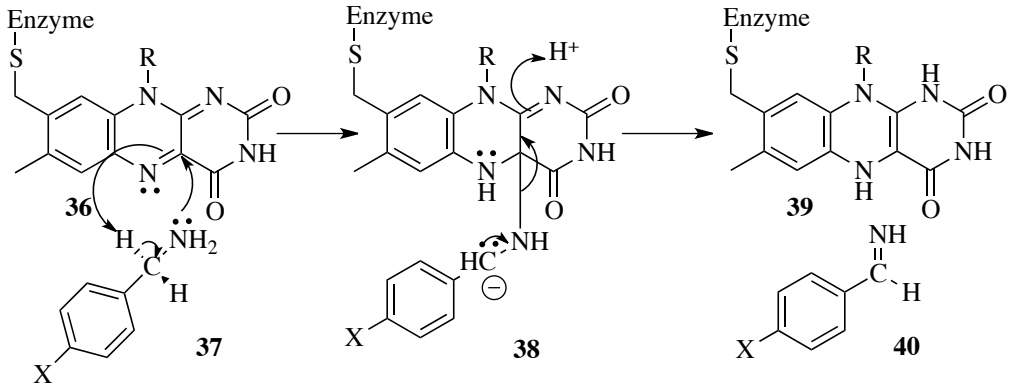

Scheme 1-11

In brief, a polar nucleophilic mechanism might be suitable for primary and secondary amines but not tertiary amines due to the steric effect because this mechanism requires covalent bond formation. On the other hand, tertiary amines, especially MPTP and its derivatives, are excellent MAO substrates. Thus, these previous findings suggest that the cyclic tertiary allylamines may undergo the MAO-catalyzed oxidation by another mechanism.

1.3.1.3 Hydrogen Atom Transfer Pathway

As shown above, neither the SET nor the polar nucleophilic pathway is consistent with all of the data observed. Thus, an HAT pathway for the MAO-catalytic α-carbon oxidation of MPTP was proposed by Castagnoli and co-workers[36b] and other investigators[51] The HAT pathway has been proposed for the oxidation of amines by cytochrome P450.[52] This pathway does not involve a radical cation intermediate but rather a direct hydrogen atom transfer step. For example, a comparison of the SET and HAT pathways was investigated for the α-carbon oxidation of 4-substituted 1-methyltetrahydropyridinyl analogues (MAO-B substrates).[51b] In this study, $[Phen]_3Fe](PF_6)_3$ was used as an electron acceptor for the SET pathway study while the *tert*-butoxyl radical was used as the hydrogen atom acceptor for the HAT pathway study. The isotope effects observed for the SET and HAT model pathways were similar, with k_H/k_D in the range of 1.65 – 2.30. Therefore, these models do not provide a means of distinguishing between these two pathways.

Scheme 1-12 shows the difference between the SET and HAT pathways proposed for the MAO catalyzed oxidation of MPTP (**1**).[53] The intermediate radical cation (**26**$^{\bullet+}$) is absent in the HAT pathway. The SET pathway includes the formation of an aminyl radical cation (**26**$^{\bullet+}$) followed by deprotonation to give an α-carbon radical (**27**$^{\bullet}$), whereas α-hydrogen transfer is involved in the HAT pathway. Finally, the intermediate $MPDP^+$ (**2**$^+$) is further oxidized into the pyridinium species MPP^+ (**3**$^+$).

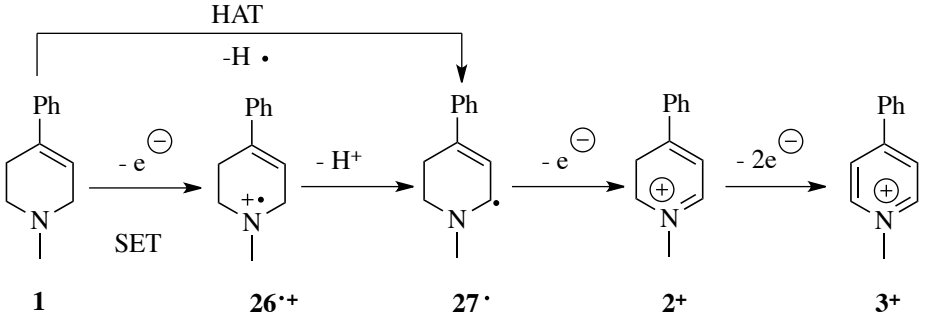

Scheme 1-12

1.4 Previous Work on the FAD Chemical Models

Figure 1-3 illustrates the FAD lumiflavin models, 3-methyllumiflavin [3MLF (**42**)] and 5-ethyl-3-methyllumiflavinium perchlorate [5Et3MLF^{+}ClO$_4^{-}$ (**43**$^{+}$ClO$_4^{-}$)]. Previously, both 3-MLF and 5Et3MLF^{+}ClO$_4^{-}$ have been used as chemical model oxidants to study MAO catalysis.[38, 47, 54] Investigators have examined the deamination of various amines with 3MLF and concluded that their findings support the polar nucleophilic pathway for MAO catalysis at least for primary and secondary amines. In regards to the oxidation of tertiary amines, the ground state 3MLF did not oxidize a tertiary amine,[35] presumably due to steric hindrance because interaction between the flavin chemical model and a tertiary amine would create the steric stain. This may be consistent with MAO catalysis since very few tertiary amines are known substrates.

A thorough search of the literature suggests that flavin chemical models for studying cyclic tertiary allylamines, such as MPTP and its derivatives, have not been investigated yet, although these amines are excellent MAO substrates. Mariano and his co-workers examined the flavin models using primary and secondary amines; however, the experimental conditions did not correspond to physiological pH or temperature. In addition, their research interest considered a silyl tertiary amine, which is not related to cyclic tertiary allylamines. Therefore, it is important to examine the α-carbon oxidation of tertiary allylamines with **42** and **43**$^{+}$ClO$_4^{-}$ as reported in this thesis.

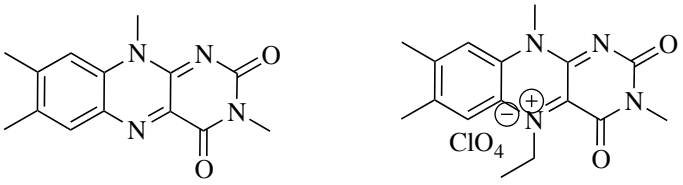

42 **43**$^{+}$**ClO**$_4^{-}$

Figure 1-3. 3-methyllumiflavin (left) and 5-ethyl-3-methyllumiflavinium perchlorate (right).

CHAPTER TWO

OBJECTIVES AND THESIS STATEMENT

2.1 Unique Reactivity of Tertiary Alkylamines and MAO

The enzyme MAO catalyzes the α-carbon oxidation of a variety of primary, secondary and teriary alkyl and arylalkyl amines. To accommodate this oxidation, the single electron transfer (SET), polar nucleophilic, and hydrogen atom transfer (HAT) pathways have been proposed. The proposed mechanisms are, however, based on studies mainly using primary and secondary amines, and my research interests, MPTP and MPTP derivatives, are allylic tertiary amines and known as excellent MAO-B substrates.

Formerly, Mariano and co-workers used FAD lumiflavin models, 3-methyllumiflavin [3MLF (**42**)] and 5-ethyl-3-methyllumiflavinium perchlorate [5Et3MLF$^+$ClO$_4^-$ (**43$^+$ClO$_4^-$**)] to study the MAO catalytic pathway and reported that primary and secondary amines underwent the polar nucleophilic pathway in the reaction with **43$^+$ClO$_4^-$**. However, they did not examine reactions between the flavin chemical models and allylic tertiary amines. MPTP and MPTP derivatives that are unlikely to interact with **43$^+$ClO$_4^-$** via the polar nucleophilic pathway because of the steric strain discussed in Chapter 1.

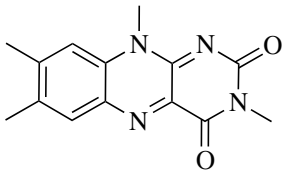

42

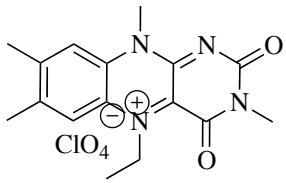

43$^+$ClO$_4^-$

2.2 Previous Work on the MPTP Chemistry

My research interest is to examine the FAD lumilfavin chemical models to mimic the MAO-catalyzed oxidation of α-carbon of cyclic tertiary-allylamines. MPTP (**1**) and MPTP derivatives have special properties that may make them susceptible to the oxidation by MAO-B. First, compound **1** has a π bond at C4 and C5 of the piperidinyl ring system, which may participate in homoallylic stabilization of the aminyl radical cation that would support the SET pathway.[55] After an electron is removed from the lone pair on the nitrogen of **1**, the resulting aminyl radical

cation (**26**$^{\bullet+}$) may be stabilized as shown by the homoallylic resonance form (the species on the right)(Scheme 2-1).

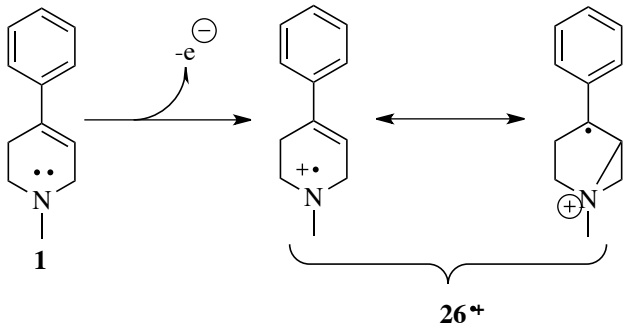

Scheme 2-1

Consistent with the argument, the corresponding saturated piperidinyl analog (**44**) does not undergo MAO-catalyzed oxidation while **1** does.[11b] This finding also supports the importance of the allylic π-bond in the MAO-catalyzed oxidation.

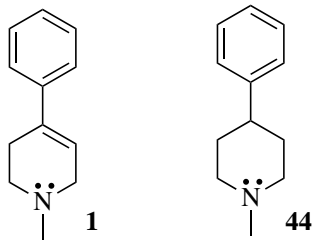

Also, the weaker BDE of the allylic C-H bond of **1** might facilitate a hydrogen atom transfer step as part of the overall α-carbon oxidation pathway. The BDE of the allylic C-H bond at C6 has been calculated to be 75 kcal/mol, which is a considerably weaker than the BDE (~ 90 kcal/mol) of the homoallylic C-H bond at C2.[56] The calculated BDEs for the various C-H bonds of **1** are shown below.

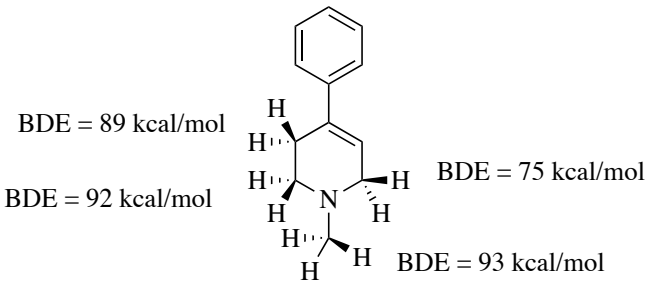

2.3 Objectives

The purpose of the present study is to examine FAD lumiflavin chemical models to mimic the MAO-B catalytic oxidation of cyclic tertiary-allylamines, such as MPTP and MPTP derivatives. To my knowledge, no such chemical model studies have been performed on this type of system even though those amines are good MAO substrates. In addition, current proposed mechanisms for the MAO-catalyzed oxidation are based on studies primarily using primary and secondary amines, but not tertiary amines. Therefore, in this thesis, FAD lumiflavin models of **42** and **43**$^{+}\mathbf{ClO_4}^{-}$ are examined with TMMP, an analog of MPTP that was chosen to study reactions with the lumiflavin chemical models because TMMP showed a similar reactivity to MAO-B[57] but has not been reported to be neurotoxic in mice[58] or humans.

CHAPTER THREE

INVESTIGATION OF 5-ETHYL-3-METHYLLUMIFLAVINIUM PERCHLORATE

3.1 Oxidation of Benzylamine in the Presence of 5-Etyl-3-methyllumiflavinium perchlorate

3.1.1 Introduction

The chemical FAD lumiflavin models, 3-methyllumiflavin [3MLF (**42**)] and 5-ethyl-3-methyllumiflavinium perchlorate [5Et3MLF$^+$ClO$_4^-$ (**43$^+$ClO$_4^-$**)], have been extensively investigated in the course of examining the mechanistic details involved in the MAO-catalytic oxidation of mainly primary amines.[45a, 46]

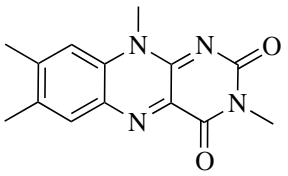

42

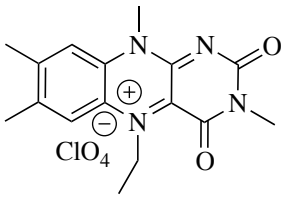

43$^+$ClO$_4^-$

Mariano and his co-workers had used forcing conditions when they studied the oxidation of benzylamine with **42**. For instance, **42** (10 mM) and benzylamine (**37**)(50 – 60 mM) were mixed together in acetonitrile containing 10 mM HCl, which was heated to 80 °C for 7 days.[35] About 30% of **37** were converted to *N*-benzylidenebenzylamine (**45**).

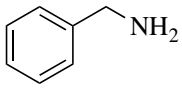

37

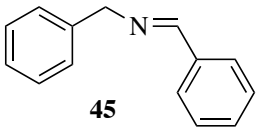

45

There were complications associated with the reaction condition; the amine nitrogen would be extensively protonated under such acidic conditions, and the nucleophilicity of **37** cannot be achieved when it is protonated. Because the nucleophilic properties of amines are necessary to study the amine oxidation, an activated FAD lumiflavin chemical model, **43$^+$ClO$_4^-$** was chosen for this compound of the project. Forcing conditions are not necessary for **43$^+$** to react with benzylamine. The flavinium salt **43$^+$ClO$_4^-$** is an activated form of **42** due to ethylation at the N5 position. This alkylation has made the C(4a) position of **43$^+$** more electrophilic, which makes the

species more receptive to nucleophiles. In preparation for the investigation of tertiary-allylamine chemistry using the aid of **43^{+}ClO$_4^{-}$**, the oxidation of benzylamine in the presence of **43^{+}ClO$_4^{-}$** was examined.

The analytical techniques used in the present study include UV/vis spectroscopy, nuclear magnetic resonance (NMR) spectroscopy, and accurate mass electrospray ionization mass spectrometry (ESI^{+}/MS). Each technique demonstrated strengths and weaknesses. First, it is easier to exclude air and water from the samples in UV/vis analysis. However, the overlap of chromospheres frequently reduces the effectiveness of quantitative analysis using UV/vis spectroscopy. Second, chemical shift values in NMR spectra show clearly resolved signals, yet it is more cumbersome to exclude air from the NMR samples. Finally, accurate-mass ESI^{+}/MS spectrometry provides strong evidence for mass per positive charge with clear signals, but sample preparations could affect the probability of excluding air and of contaminants.

3.1.2 Results and Discussion

3.1.2.1 Reaction Between 5-Ethyl-3-methyllumiflavinium perchlorate and Benzylamine

The reaction between **43^{+}ClO$_4^{-}$** and **37** was examined in considerable detail as described.[35] They reported an instant reaction between **43^{+}ClO$_4^{-}$** and **37** that was associated with adduct formation (**41**)(Scheme 3-1-1). Continuing the reaction, the adduct (**41**) was then heated at 60 °C for 40 hours in the presence of one mole of **37** under anaerobic conditions. This treatment led to **45** along with the spirohydantion **46** and the benzimidazolium salt **47^{+}** (Scheme 3-1-1).[35] The results reported by Kim 1993 indicated that the generation of **45** under thermal conditions, a subject that will be discussed later in this chapter.

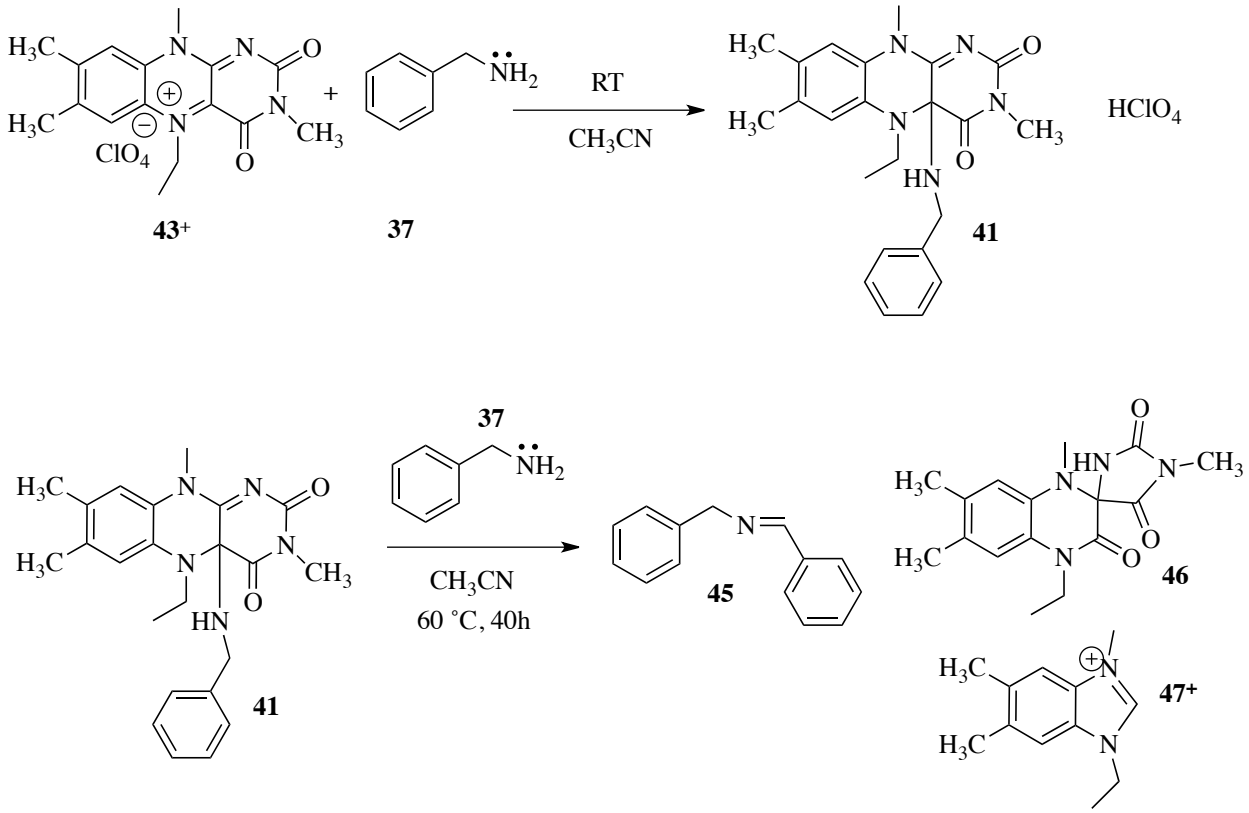

Scheme 3-1-1

The first step was to examine the reaction between $\mathbf{43^+ClO_4^-}$ (0.13 mM) and **37** (0.26 mM) in reagent grade acetonitrile at room temperature. Adduct formation appeared to take place rapidly following the addition of benzylamine since the purple color of $\mathbf{43^+ClO_4^-}$ immediately changed to yellow-green (Figure 3-1-1). Kim *et al*. (1993) also reported an instant color change from purple to green with the reaction of $\mathbf{43^+}$ (0.13 mM) with benzylamine (0.25 mM) in acetonitrile.[35]

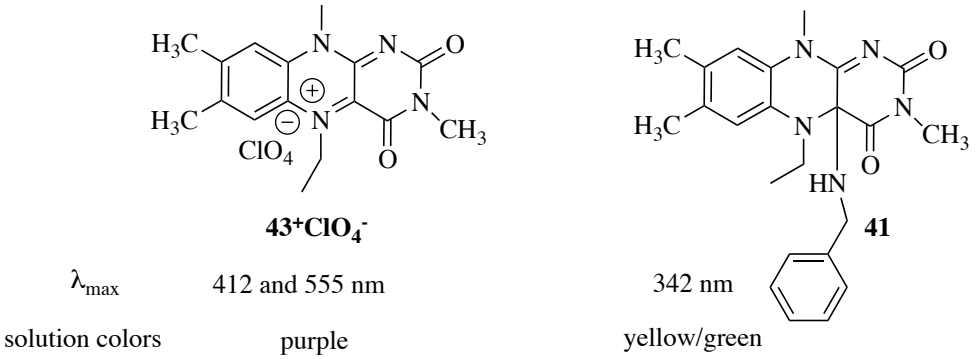

Figure 3-1-1. Lambda max and solution colors for the 5Et3MLF$^+$ClO$_4^-$ (left) and the 5Et3MLF-benzylamine adduct (right).[45a]

Next, a full UV/vis spectrum was taken every 15 sec for the first 15 min and every 30 sec for the second 15 min at room temperature. An UV/vis spectrum was recorded immediately after the addition of the benzylamine (Figure 3-1-2). The λ_{max} values of **43$^+$ClO$_4^-$** are at 412 and 555 nm, and those absorption bands disappeared with time after mixing. The absorbance at λ_{max} 342 nm, corresponding to the λ_{max} of **41**, developed with time. These results are consistent with the previous finding; the C4a adduct of **43$^+$ClO$_4^-$** has the λ_{max} value at 342 nm.[45a]

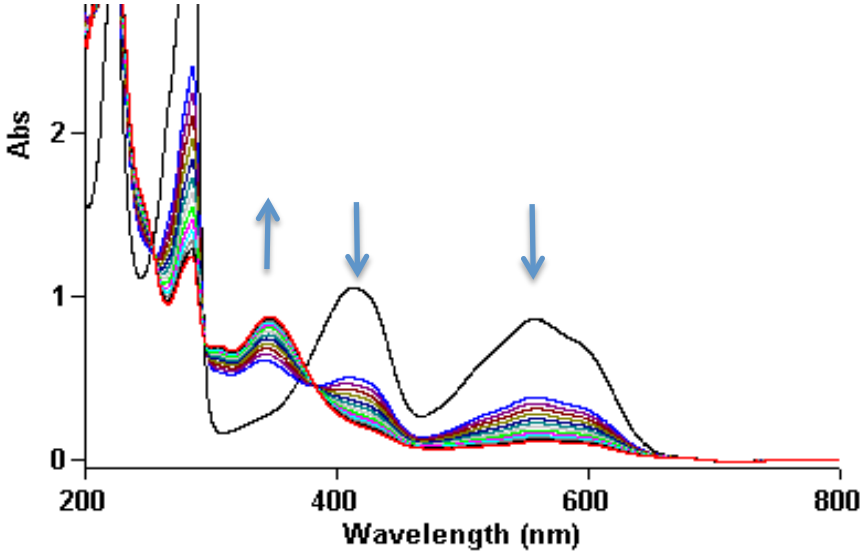

Figure 3-1-2. Time-dependent spectral changes in UV/vis spectra of the reaction mixture. The reaction between 5Et3MLF$^+$ClO$_4^-$ (0.075 mM) and benzylamine (0.15 mM) in acetonitrile was monitored at room temperature. Black, 5Et3MLF$^+$ClO$_4^-$ only; blue, 15 sec after mixing; purple, 30 sec after mixing; maroon, 45 sec after mixing. The reaction was monitored for 30 min.

Following the UV/vis analysis, the same reaction mixture was analyzed at t = 2 hours using accurate mass ESI$^+$/MS. The expected **41H$^+$** (MH$^+$) has an exact mass of 406.2238 amu. However, the detected masses were associated with peaks at *m/z* 299 and *m/z* 108.5, which were identical to exact mass values of the starting materials: **43$^+$ClO$_4^-$** (299.1503 amu) and protonated benzylamine (**37H$^+$**)(108.0808 amu). It is possible the expected adduct **41** reverted to starting materials under ESI$^+$ conditions (Scheme 3-1-2).

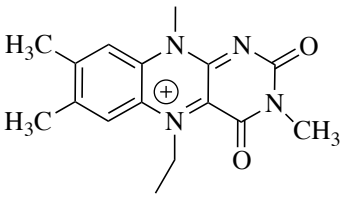

Exact Mass: 299.1503

43$^+$

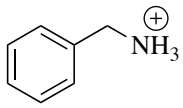

Exact Mass: 108.0808

37H$^+$

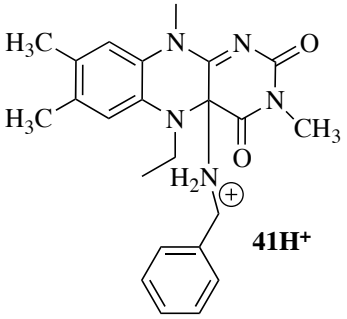

41H$^+$

Exact Mass: 406.2238

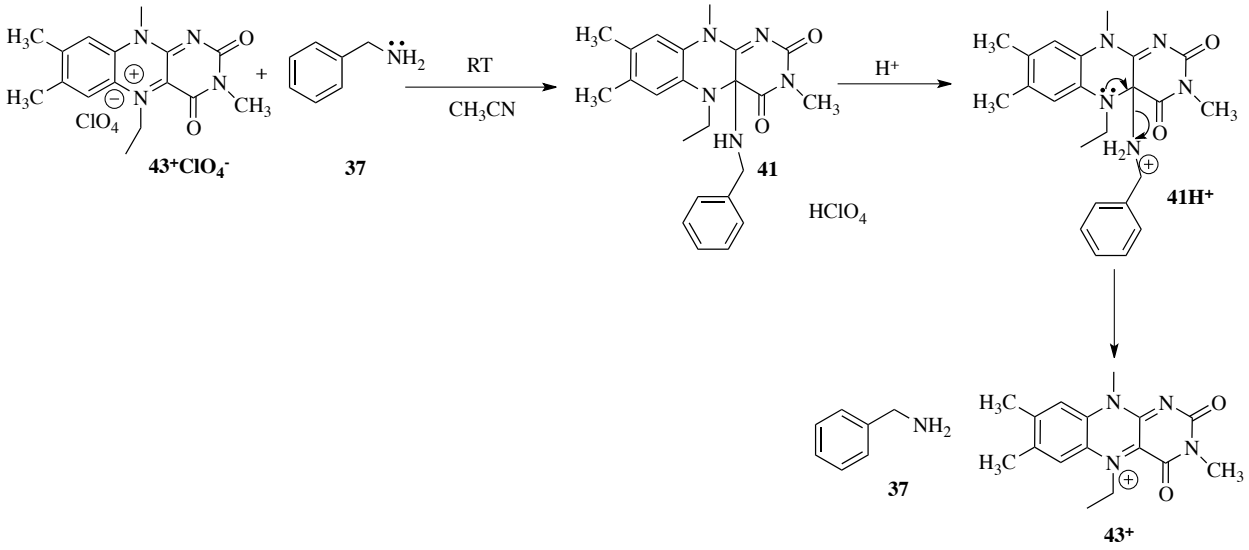

43$^+$ClO$_4^-$ **37** **41** **41H$^+$** **37** **43$^+$**

Scheme 3-1-2

The reaction mixture was futher analyzed by electron impact mass spectrometry (EI/MS). This EI method is different from ESI$^+$. While the ESI$^+$ method protonates species (M+H)$^+$, EI involves an ionization method with $M + e^- \rightarrow M^{+\bullet} + 2e^-$. Thus, the expected adduct (**41$^{\bullet+}$**) exact mass with the EI analysis was 405.2159 amu (Scheme 3-1-3).

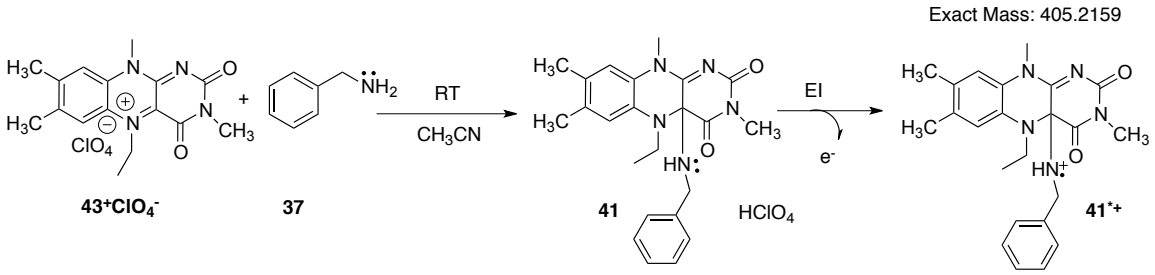

Scheme 3-1-3

For EI analysis, the orginal electron impact energy was 100 eV. However, compound **41** was reverted to the starting materials by the energy at 100 eV; thus, a lower electron impact energy was applied (70 eV) for this C4a-adduct analysis. Applying 70 eV successfully avoided fragmentation of the adduct and the adduct ion at *m/z* 405.2238 was observed in the mass spectrum (Figure 3-1-3).

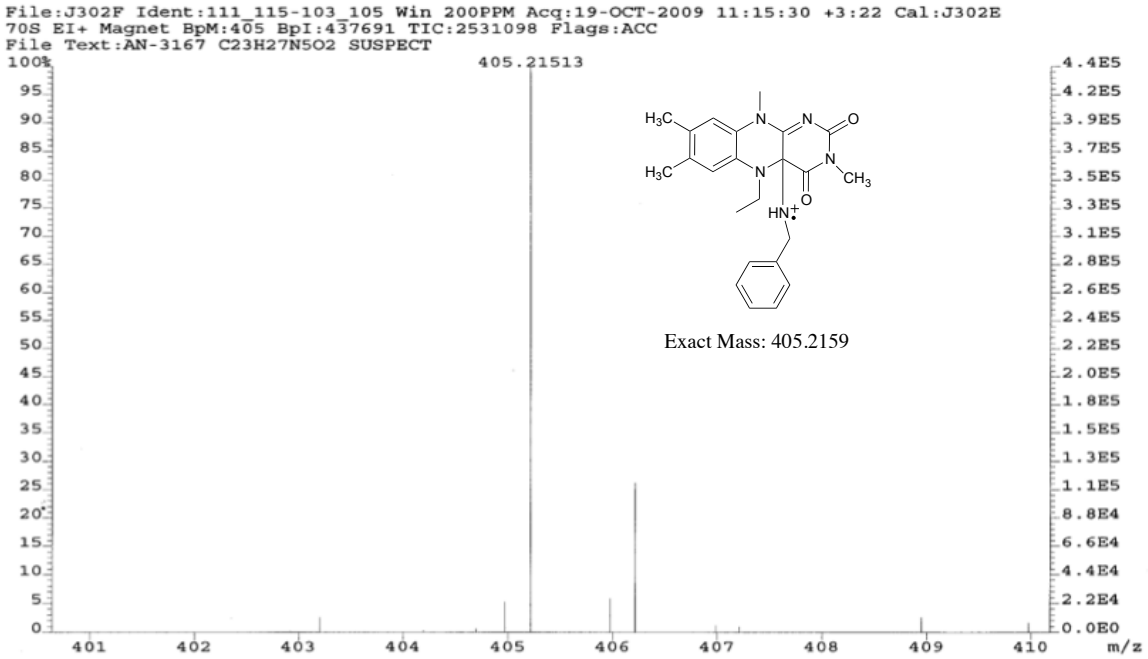

Figure 3-1-3. Electron impact mass spectrometry spectrum of the C4a adduct.[§] The mass spectrum shows the reaction mixture of 5Et3MLF$^+$ClO$_4^-$ (10 mM) and benzylamine (10 mM) (*x*-axis: *m/z*; *y*-axis: relative abundance), one to one molar ratio in commercial grade acetonitrile at room temperature.

[§] The spectrum was obtained by Kim Harich, Analytical Chemist Senior in Department of Biochemistry.

Additionally, a possible peak for one of the expected oxidative products, *N*-benzylidenebenzylamine (**45**$^{\bullet+}$), was observed in the EI spectrum (Figure 3-1-4). Recall that Mariano and his co-workers used thermal conditions (60 °C for 40 hours) to obtain the Schiff base from the reaction between **41** and **37** (as discussed earlier in Scheme 3-1-1).[35] The present results show that the formation of the Schiff base also occurs at room temperature. To confirm this possibility, the same reaction mixture was further analyzed using GC/MS.

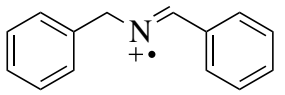

45$^{\bullet+}$

Chemical Formula: $C_{14}H_{13}N^{\bullet+}$
Exact Mass: 195.1043

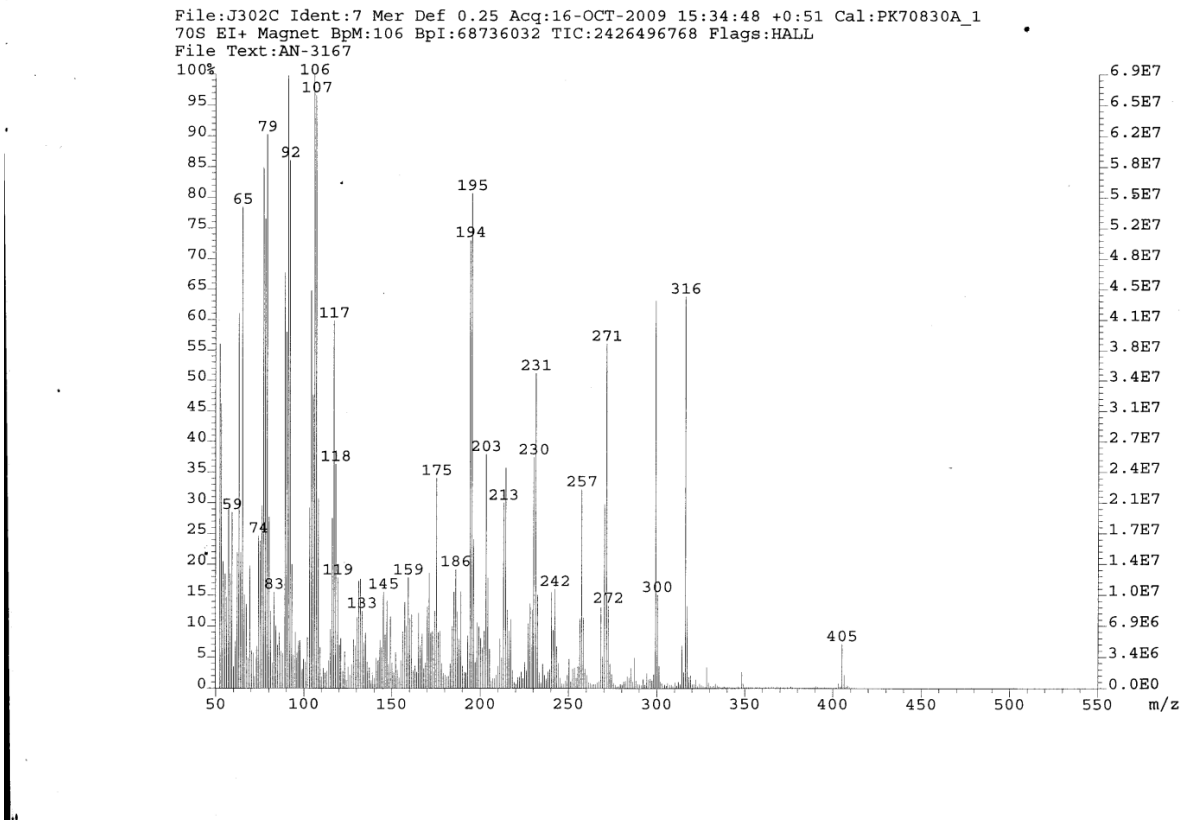

Figure 3-1-4. Electron impact mass spectrometry mass spectrum of the reaction mixture.[**] The mass spectrum (*x*-axis: *m*/*z*; *y*-axis: relative abundance) shows the reaction between 5Et3MLF^{+}ClO_4^{-} and benzylamine in commercial grade acetonitrile at room temprature.

[**] The spectrum was obtained by Kim Harich, Analytical Chemist Senior in Department of Biochemistry.

GC/MS analysis was used to detect products of the reaction between **43^{+}ClO$_4^{-}$** and **37**. GC/MS can be used to identify an unknown through analysis of the corresponding fragmentation pattern. Initially, the C4a adduct was formed by mixing **43^{+}ClO$_4^{-}$** (0.075 mM) and **37** (0.15 mM) at room temperature, which was prepared in the manner previously described.[35] Briefly, the two starting materials were mixed in commercial grade acetonitrile, and then the reaction mixture was concentrated *in vacuo*. Next, the product was extracted using $CHCl_3$ and analyzed with GC/MS. Table 3-1-1 summarizes the comparison of ionized fragments of the *m/z* ratio for the reaction mixture with a commercially available standard **45**; the retention times were 14.59 and 14.76 min, respectively, and the corresponding MS spectra are displayed in Figure 3-1-5. Ionized fragments of the *m/z* peaks are very similar in both cases, indicating that the extracted product is **45**.

Table 3-1-1. Comparison of *m/z* ratio values for ionized fragments of the *m/z* ratio: the reaction mixture of 5Et3MLF^{+} (0.075 mM) and benzylamine (0.15 mM) with 14.59 min retention time and commercially available *N*-benzylidenebenzylamine with 14.76 min retention time. The peak intensity was reported as abundance in Figure 3-1-4. The solvent was commercial grade acetonitrile.

	Retention Time	*m/z* (peak intensity in Abundance)
Reaction mixture (Figure 3-1-4 A)	14.59 min	196 (10,000) and 92 (5,000)
N-benzylidenebenzylamine (Figure 3-1-4 B)	14.76 min	196 (17,000) and 92 (7,000)

A

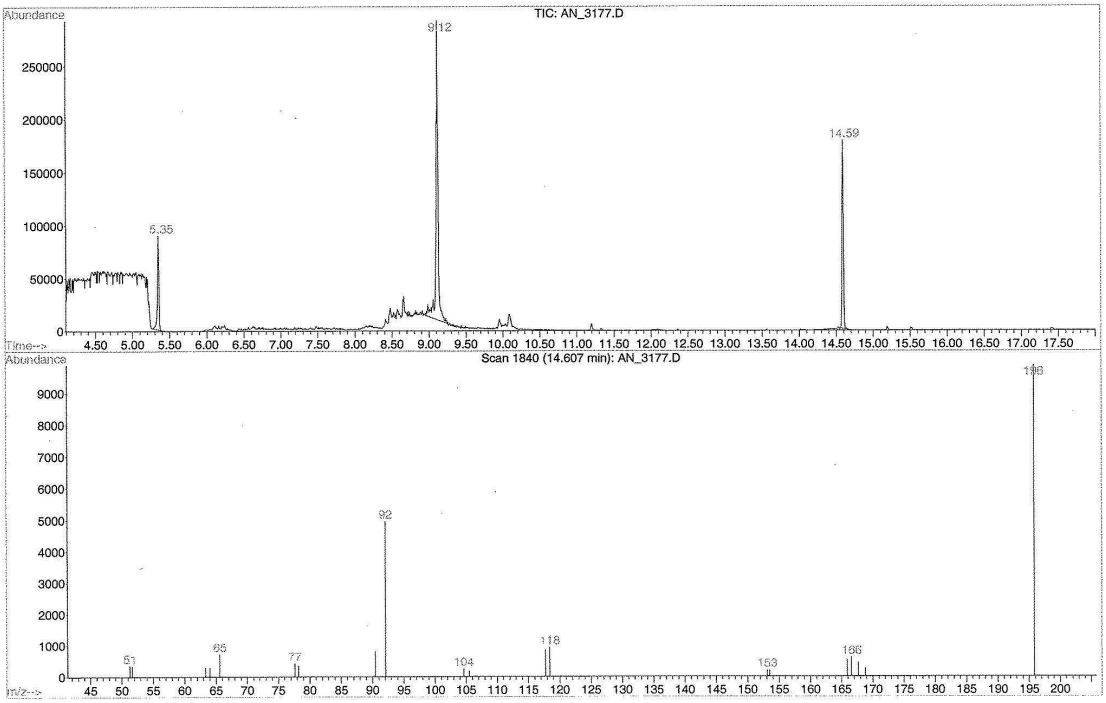

B

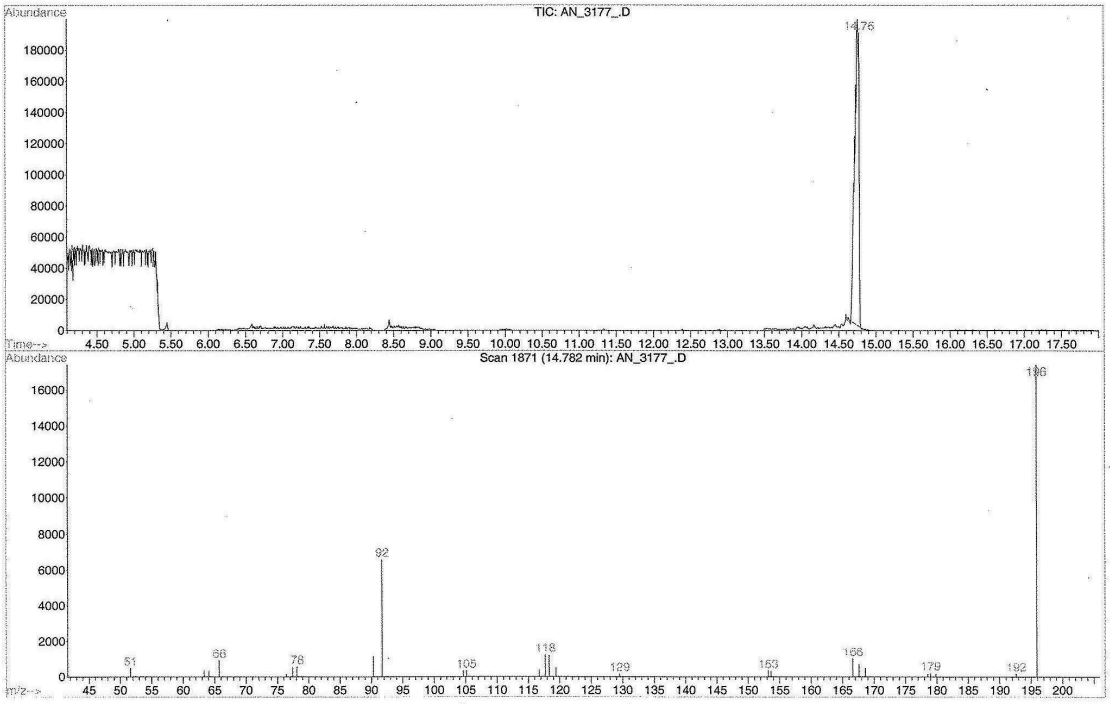

Figure 3-1-5. Comparison of GC/MS data between the reaction mixture and *N*-benzylidenebenzylamine. The reaction mixture [5Et3MLF^{+}ClO$_4^{-}$ (0.075 mM) and benzylamine (0.15 mM), reagent grade acetonitrile at room temperature (A) and commercially available *N*-benzylidenebenzylamine (the corresponding Schiff base to benzylamine; B). The mass spectra show a peak intensity (abundance) vs. *m/z* (mass-to-charge ratio).

Thereafter, a time-dependent examination of the reaction mixture was conducted using GC/MS. Spectra of the reaction mixture (**43**$^{+}$**ClO**$_4^{-}$ 0.075 mM and **37** 0.15 mM) at room temperature were recorded at t = 0, 6, 19, and 24 hours. The solvent was commercial grade acetonitrile, and chlorobenzene (0.15 mM) was used as an internal standard.

At t = 0 min, chlorobenzene and benzylamine are present in the spectrum with retention times at 7.21 min and 9.13 min, respectively; a wide and broad peak with *m/z* 196 (retention time 15 to 15.50 min) is evident in Figure 3-1-6 A. This peak sharpens and narrows at t = 6 h (Figure 3-1-6 B). At t = 6 h, the presence of *N*-benzylidenebenzylamine (**45**) was evident on the tracing at 14.61 min, and this peak was subsequently confirmed using the MS. The height of the peak remains constant at t = 19 h (Figure 3-1-6 C) and t = 24 h (Figure 3-1-6 D). The GCMS results suggest that the formation of the Schiff base at room temperature reaches the plateau approximately six hours after mixing **43**$^{+}$**ClO**$_4^{-}$ and **37** in commercial grade acetonitrile. Unfortunately, an attempt to perform quantitative analysis failed because of the poor chromatographic behavior of the internal standard signal (chlorobenzene).

A

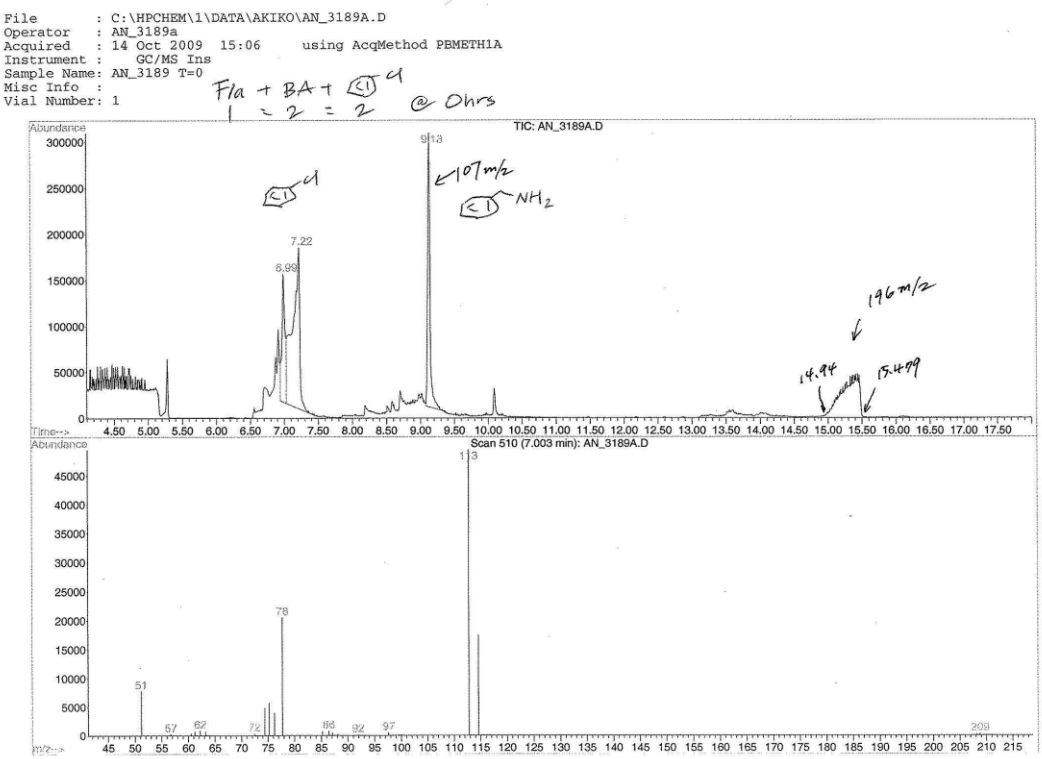
File : C:\HPCHEM\1\DATA\AKIKO\AN_3189A.D
Operator : AN_3189a
Acquired : 14 Oct 2009 15:06 using AcqMethod PBMETH1A
Instrument : GC/MS Ins
Sample Name: AN_3189 T=0
Misc Info :
Vial Number: 1
Fla + BA + Cl
1 : 2 : 2 @ 0hrs
TIC: AN_3189A.D
9.13
107m/z
7.22
6.99
196m/z
14.94
15.409
Scan 510 (7.003 min): AN_3189A.D
113
78
51

B

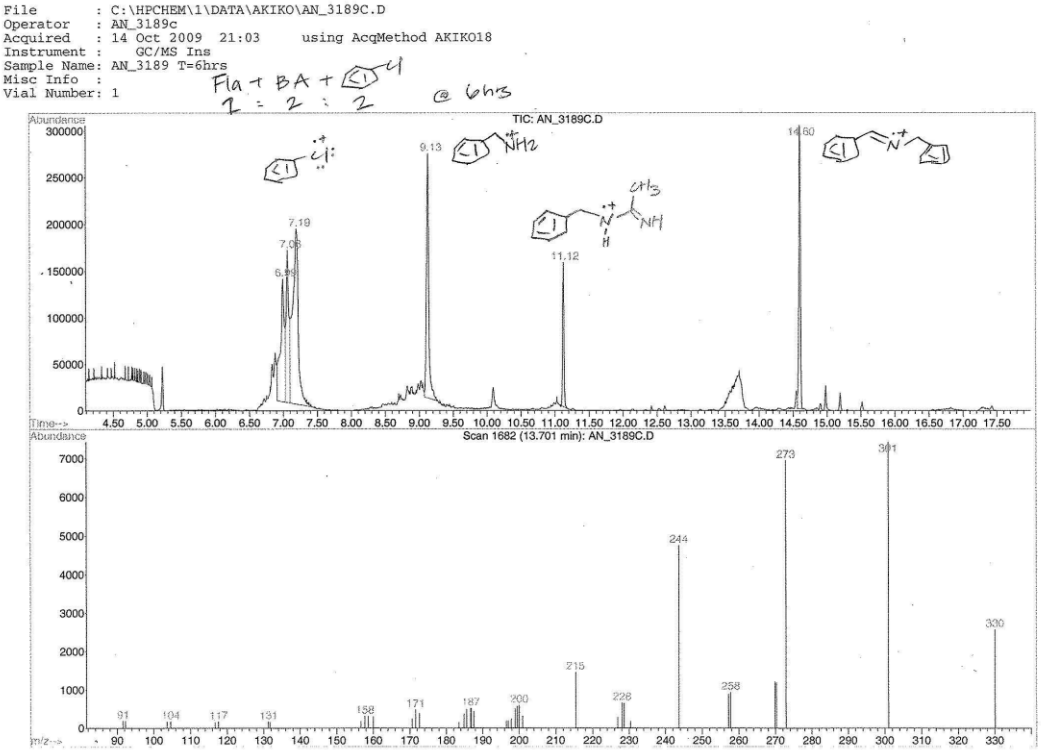
File : C:\HPCHEM\1\DATA\AKIKO\AN_3189C.D
Operator : AN_3189c
Acquired : 14 Oct 2009 21:03 using AcqMethod AKIKO18
Instrument : GC/MS Ins
Sample Name: AN_3189 T=6hrs
Misc Info :
Vial Number: 1
Fla + BA + Cl
1 : 2 : 2 @ 6hrs
TIC: AN_3189C.D
9.13
14.60
7.19
7.06
6.89
11.12
Scan 1682 (13.701 min): AN_3189C.D
273
301
244
330
215
258

C

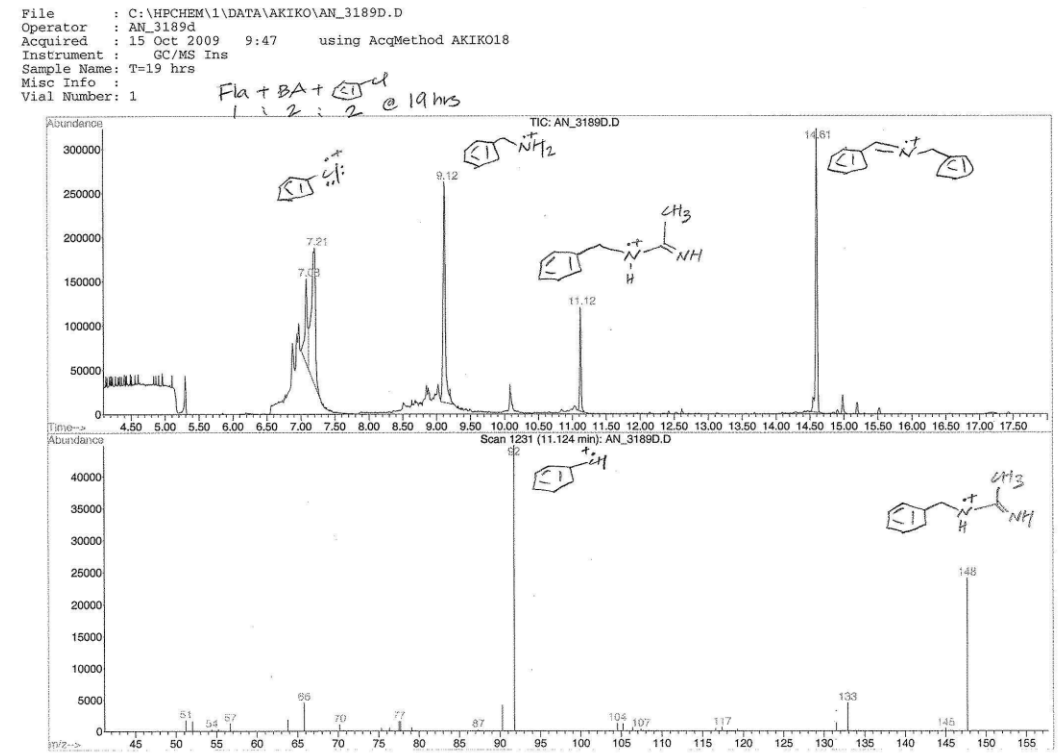

D

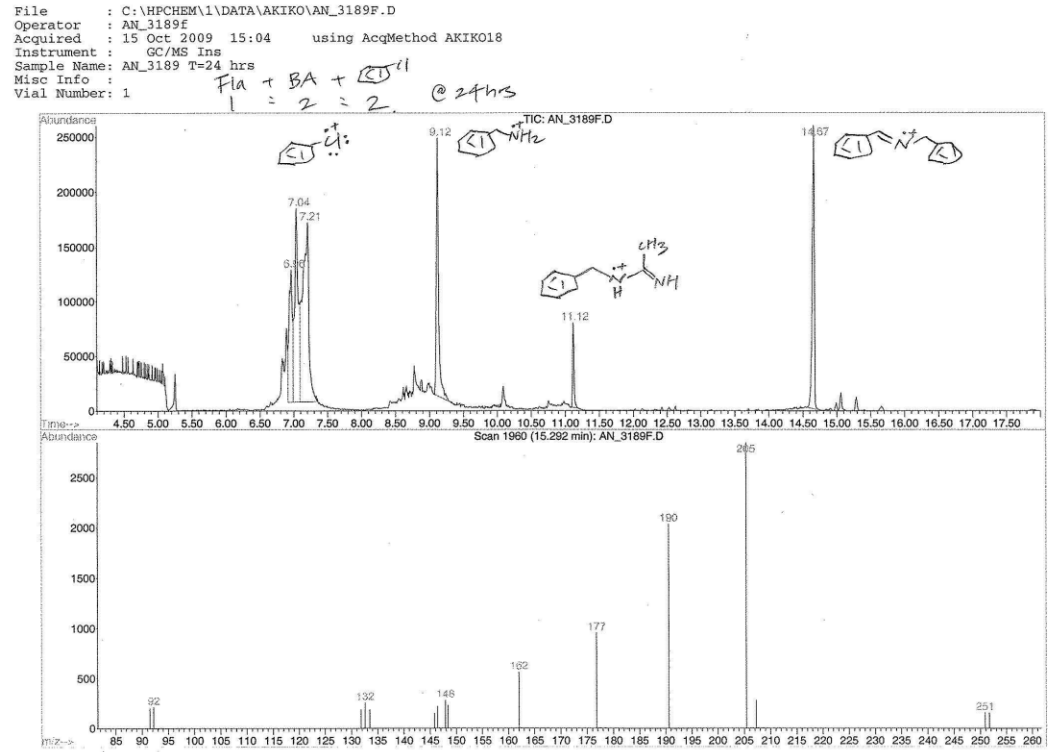

Figure 3-1-6. Time-dependent spectral changes in GC/MS data. Representative GC/MS data of the reaction mixture 5Et3MLF^{+}ClO$_4^{-}$ (0.075 mM) and benzylamine (0.15 mM) in commercial grade acetonitrile at room temperature at T = 0 min (A), 6 h (B), 19 h (C), and 24 h (D). Chlorobenzene (0.15 mM) was used as an internal standard.

In addition, one unknown peak appeared at *m/z* 148 (retention time 11.12 min) at t = 6 h and remained high at t = 19 h and 24h. The species at *m/z* 148 may result from solvolysis, a reaction between **37** and the solvent, acetonitrile, forming *N*-benzylacetimidamide radical cation (**48**$^{\bullet+}$) with the exact mass of 148.100 amu (Scheme 3-1-4).

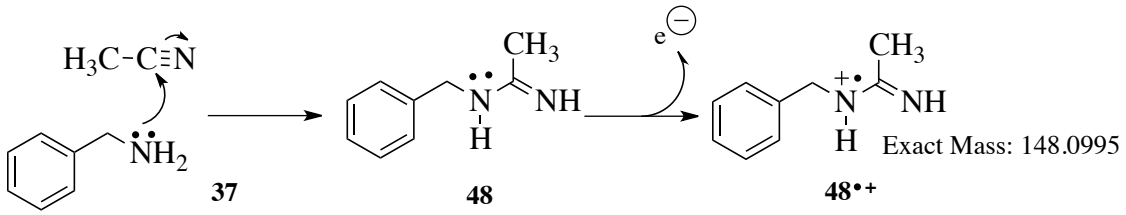

Scheme 3-1-4

The above results indicated that the oxidation of **37** in the presence of **43**$^{+}$**ClO**$_4^{-}$ gives the Schiff base (**45**) via the intermediate C4a adduct (**41**). In order to confirm the GC/MS results, the C4a adduct was identified using NMR. First, the ^{1}H NMR spectra of **43**$^{+}$**ClO**$_4^{-}$ and **37**, each on its own, in CD_3CN were recorded as standards. The complete assignments of **43**$^{+}$**ClO**$_4^{-}$ and **37** chemical shifts are illustrated in Figure 3-1-7. The triplet signal for the methyl protons of **43**$^{+}$**ClO**$_4^{-}$ is centered at δ 1.80 ppm. The methylene signals are complex (the non-equivalence is due to hindered rotation about the N-CH_2 bond) and appears as the broad (geminal and vicinal coupled) peaks centered at δ = 6.09 and 5.05 ppm. For **37**, the signal for the benzyl protons occurs at δ 1.57 ppm, and the signals for the aromatic protons appear as multiple peaks at δ 7.12 and 7.32 ppm.

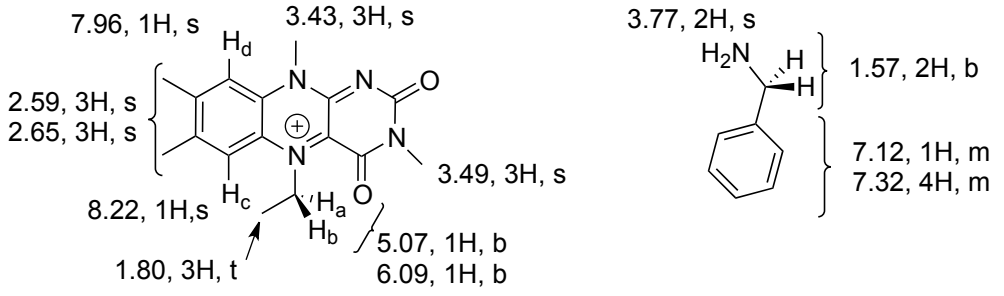

Figure 3-1-7. ^{1}H NMR signal assignments: 5Et3MLF^{+} (left) and benzylamine (right)(500 MHz, CD_3CN).

After analyzing the starting materials, compounds **43^{+}ClO$_4^{-}$** and **37** were mixed in acetonitrile-d_3 for NMR analysis. A couple of hours after mixing, greenish white solids precipitated out of solution in an NMR tube. Thus, the greenish white solids were purified using column chromatography (solvent system: ethyl acetate and hexane at 1 to 1 ratio) and analyzed using NMR (Figure 3-1-8). The ^{1}H NMR signals are consistent with the NMR results assigned by Kim *et al*.[35] The triplet for the NCH$_2$*CH$_3$* signal (δ 1.80 ppm) of **43^{+}ClO$_4^{-}$** shifted upfield to δ 0.85 ppm. Note that the methylene peaks (centered at δ 6.09 and 5.05 ppm) of **43^{+}ClO$_4^{-}$** are shifted downfield to δ 3.06 and 3.15 ppm in the adduct. It should be mentioned that the methylene protons at N5-*CH$_2$*CH$_3$ are diastereotopic, thus non-equivalent in the adduct; the signals for the N*CH$_2$*CH$_3$ show up as two doublets of the quartet at the center δ 3.06 and 3.15 ppm. Since these protons are non-equivalent, the simple triplet observed for the NCH$_2$*CH$_3$* protons may indicate that the coupling constants for the non-equivalent methylene protons are very similar.

A

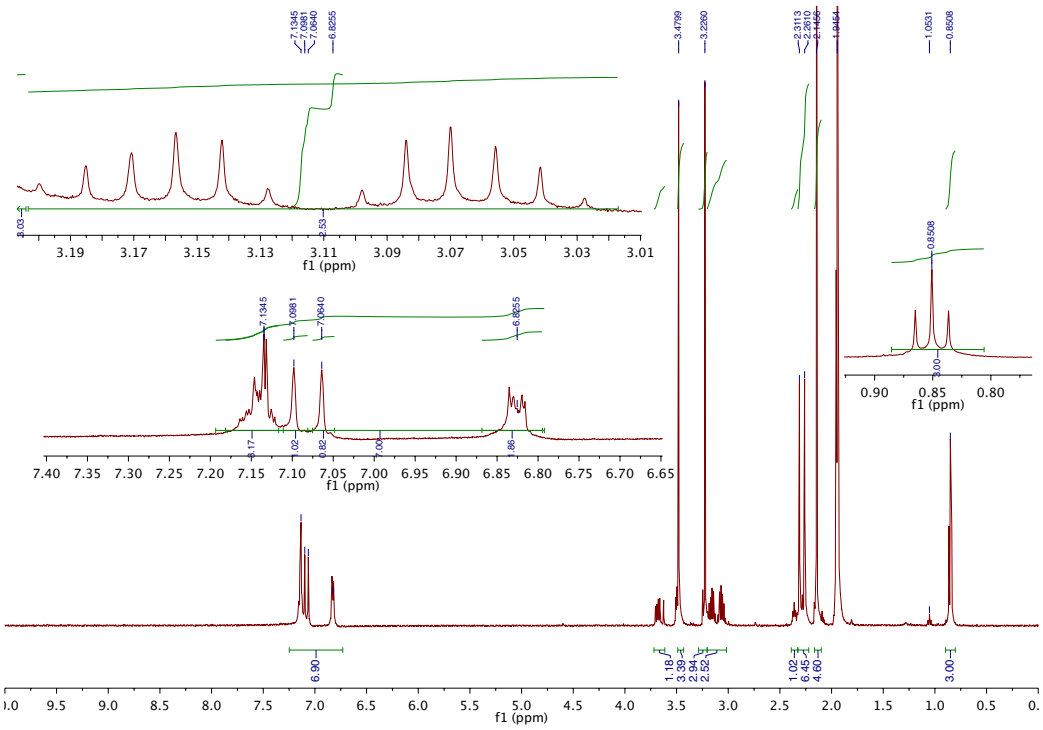

B

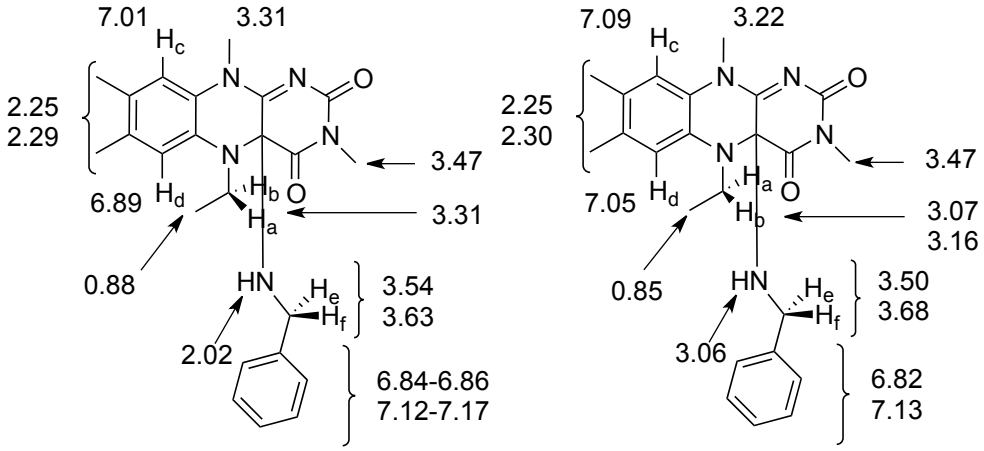

Figure 3-1-8. [1]H-NMR data of the C4a adduct in acetonitrile-d_3. (A)[1]H-NMR spectrum of the C4a adduct in acetonitrile-d_3 (500 MHz) and (B) the comparison of chemical shifts for published data (left)[35] and the present study (right)(B).

Subsequently, the C4a adduct (**41**) was isolated as a single crystalline product and identified using X-ray diffraction (Figure 3-1-9). The adduct (**41**), which is structurally rigid, contains stereocenters at N(5) and C(4a), and thus the methylene protons are diastereotopic. According to the synthetic procedure for the C4a adduct, both diastereomeric products were possible. The

crystal structure, however, demonstrates that the *cis* diastereomer cannot form on account of steric effects. For the *trans* diastereomer, the tetrahedral geometry of N(4) and C(4a) cause puckering of the ring system. As a result, there is essentially no steric interaction between the N(5)-ethyl group and the N-benzyl group, as is evident from the dihedral angle of 162.5°. This torsion change from the planar to non-planarity may contribute to the reaction for flavoenzymes involving polar pathways. The single crystalline product chosen for the X-ray diffraction had the chiral space group $P4_12_12$. Interestingly, Bijvoet pair analysis indicated that the racemic mixture from solution spontaneously resolved into an enantiomerically pure crystal.

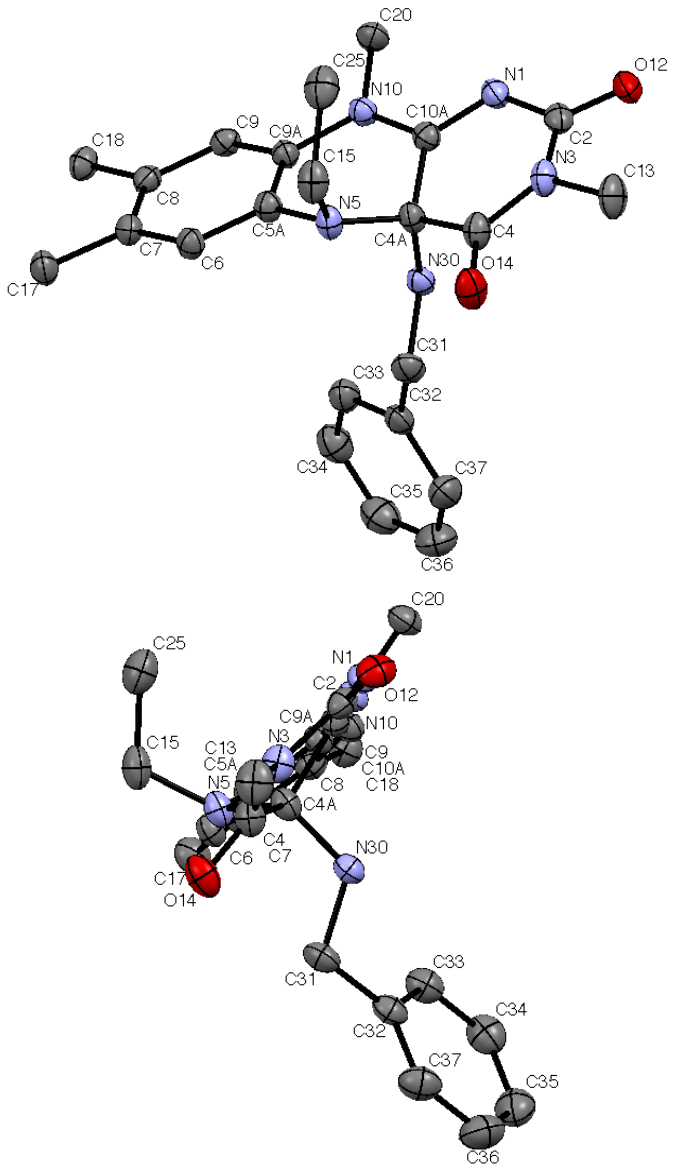

Figure 3-1-9. X-ray crystal images of the C4a-benzyl adduct. Thermal ellipsoid plot of the molecular structure of the C4a-benzylaminyldihydroflavinyl adduct at 50 % probability.

Further characterization of the reaction between **43^{+}ClO$_4^{-}$** and **37** at the molar ratios of 1 to 1 (25 mM each) and 1 to 2 (25 mM to 50 mM), respectively, was examined using NMR spectroscopy. The reaction was monitored by NMR, which does not involve heat. This experiment was to examine whether two moles of **37** to one mole of **43^{+}ClO$_4^{-}$** are required to give one mole of the Schiff base (**45**). The reaction was monitored at room temperature for 96 hours (at intervals according to t = 0, 1, 2, 3, 4, 5, 6, 24, 48, 72, and 96 hours). The C4a adduct (**41**) was observed in both reaction mixtures (1 to 1 and 1 to 2 molar ratios) immediately after mixing the two starting materials, **43^{+}ClO$_4^{-}$** and **37** (Figure 3-1-10 A).

Following the generation of **41**, evidence indicating the presence of the corresponding Schiff base (**45**) was observed over time. The relative integrations of peaks at δ 4.78 ppm (benzylic proton, 2H) and 8.44 ppm (benzylic and vinylic proton, 1H) were monitored as the marker of **45**. The formation of **45** was only found with the 1 to 2 molar ratio reaction because a second mole of **37** is necessary to form **45** according to Kim *et al*.[35] The NMR signals for **45** appeared by t = 24 hours (Figure 3-1-10 B) and developed with time (Figure 3-1-10 C).

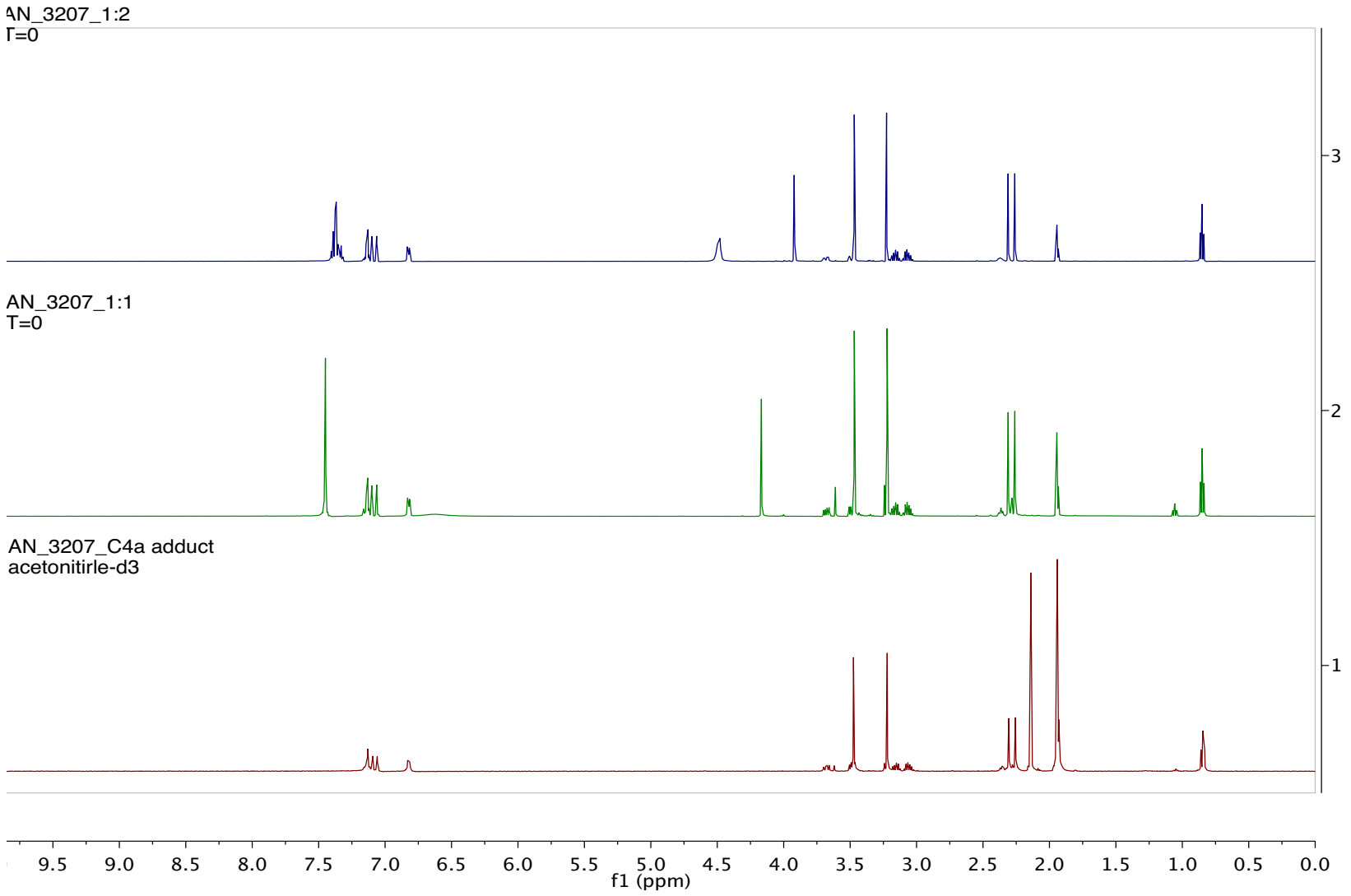

Figure 3-1-10 A. ^{1}H-NMR spectrum of the reaction product of 5Et3MLF^{+}ClO$_4^{-}$ with benzylamine at t = 0 min.

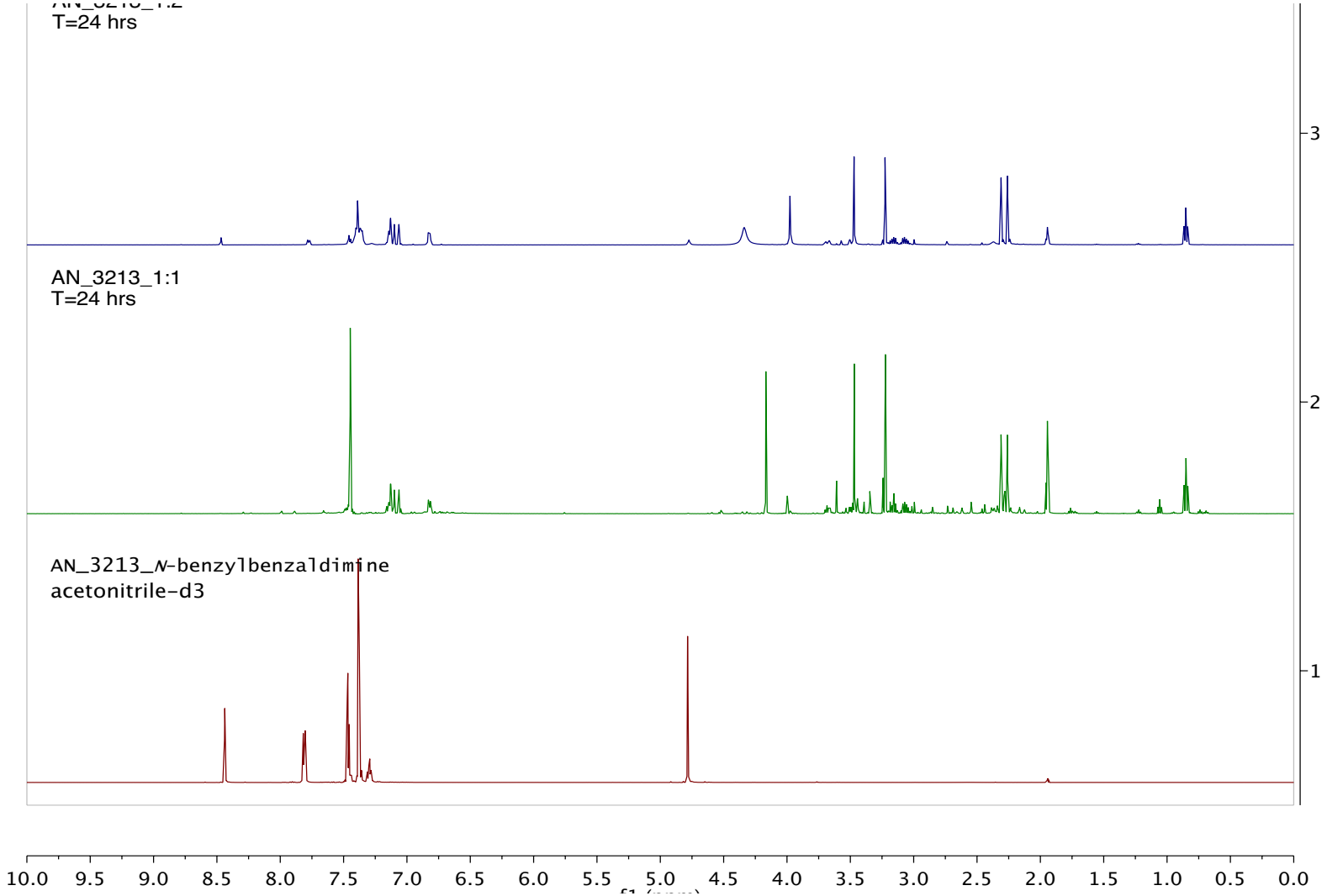

Figure 3-1-10 B. ^{1}H-NMR spectrum of the reaction product of 5Et3MLF^{+}ClO$_4^{-}$ with benzylamine at t = 24 hours.

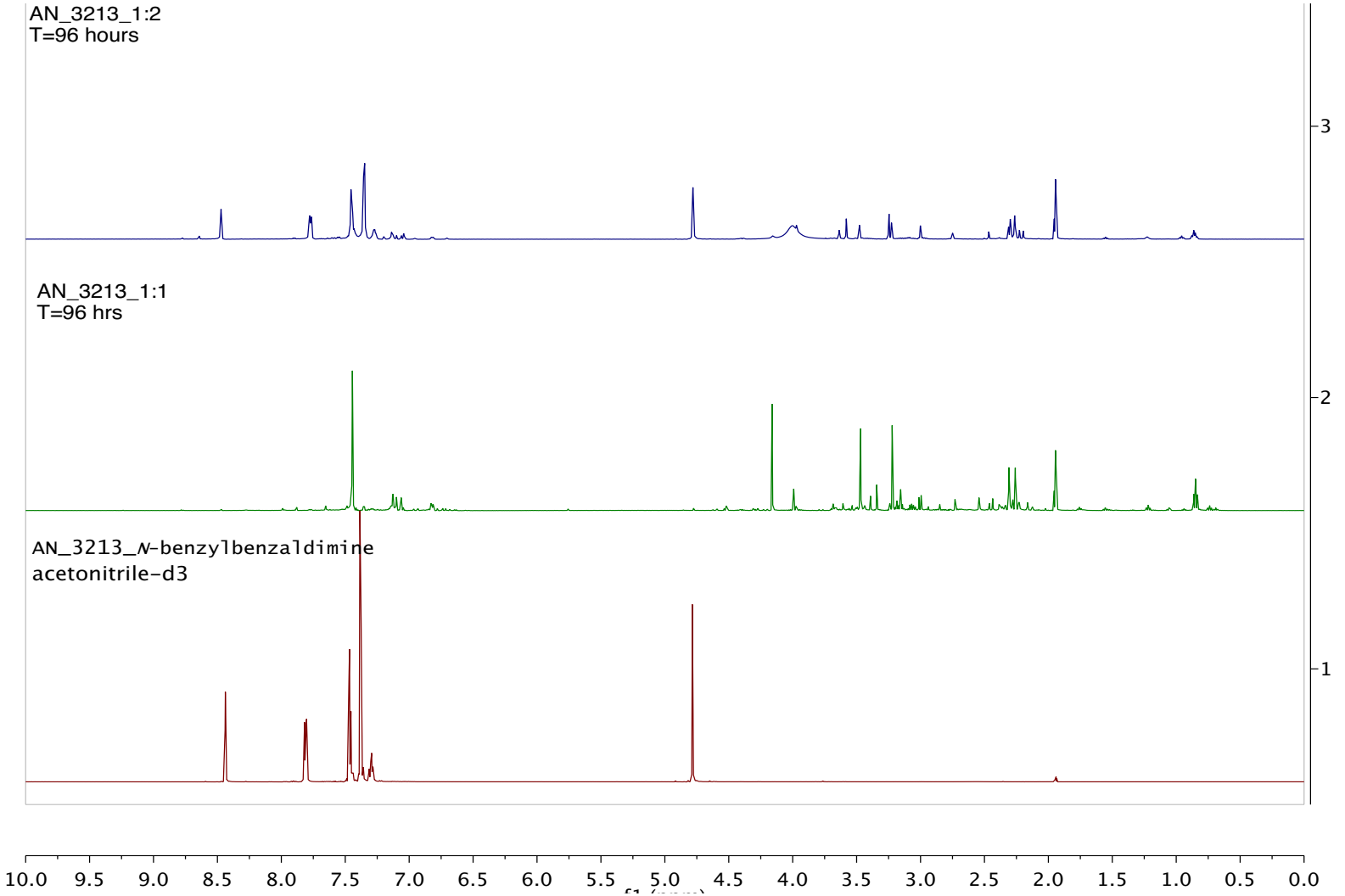

Figure 3-1-10 C. ^{1}H-NMR spectrum of the reaction product of 5Et3MLF^{+}ClO$_4^{-}$ with benzylamine at t = 96 hours.

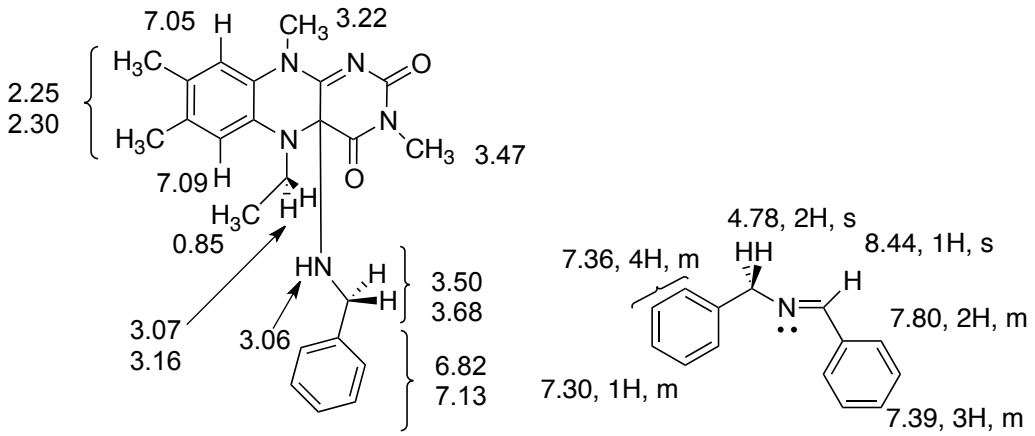

Figure 3-1-10 D. NMR signals assignments for the C4a-adduct (left) and *N*-benzylidenebenzylamine (right). Superimposed images of 1 to 1 (blue) and 1 to 2 (green) molar ratios at t = 0 min (A), 24 hours (B), and 96 hours (C) (500HMz, CD_3CN). Spectra recorded at t = 0 min were compared to the spectrum of C4a adduct. Spectra recorded at t = 24 and 96 hours were compared to the spectrum of *N*-benzylidenebenzylamine.

In summary, the results of GC, GC/MS, and NMR analyses show the time-dependent effect on the formation of the Schiff base with **43**$^{+}$**ClO**$_4^{-}$ and **37** by one to two molar ratio reactions at room temperature. Recall that the formation of **45** was previously reported under forced conditions (60 °C and 40 hours).[35] Results from the work described in this thesis establish for the first time the detection of **45** in a reaction mixture **37** and **43**$^{+}$**ClO**$_4^{-}$ at room temperature. To form the adduct intermediate, the reaction between **37** and **43**$^{+}$**ClO**$_4^{-}$ appears to proceed via a nucleophilic polar pathway.

3.1.2.2 Effect of Dioxygen on the Oxidation of Benzylamine

MAO-B catalyzes the oxidation of benzylamine (**37)** by a dioxygen-independent pathway. Dioxygen is required for catalysis. Thus, whether the oxidation of **37** in the presence of 5Et3MLF^{+}ClO$_4^{-}$ (**43^{+}ClO$_4^{-}$**) requires dioxygen was examined using NMR spectroscopy. A time-dependent study of the reaction between **43^{+}ClO$_4^{-}$** (25.12 mM) and **37** (50.24 mM) in dried acetonitrile-d_3 was monitored over time. The solvent acetonitrile-d_3 was dried over CaH_2 for 2 days and de-gassed/distilled immediately before use, and the two starting materials were mixed in a glove box. Thus, the samples under anaerobic conditions also were anhydrous. Upon mixing the two starting materials, the C4a adduct (**41**) was formed under both aerobic (Figure 3-1-11 A) and anaerobic conditions (Figure 3-1-12 A) at t = 0 min. As expected, the initial nucleophile polar mechanism was not dioxygen dependent.

Twenty-four hours later, the effect of dioxygen was apparent. Examination of the NMR spectra suggests that the reaction between the Schiff base and benzylamine is water dependent. The underlying rationales will be discussed later in this section. For aerobic samples, NMR peaks corresponding to the Schiff base (final product) appeared and increased with time while the peaks corresponding to **41** (intermediate) decreased as the reaction progressed (Figure 3-1-11 B) up to 120 hours (Figure 3-1-11 C). There was no significant difference in the relative integration for **45** in the aerobic samples between t = 120 hours and 240 hours; hence, the formation of **45** nearly reached the plateau by 120 hours. Conversely, the signals corresponding to **45** were not observed in the reaction mixture under argon even at t = 120 hours (Figure 3-1-11 C). Therefore, NMR results suggest that the conversion of **41** into **45** at room temperature is dependent on water.

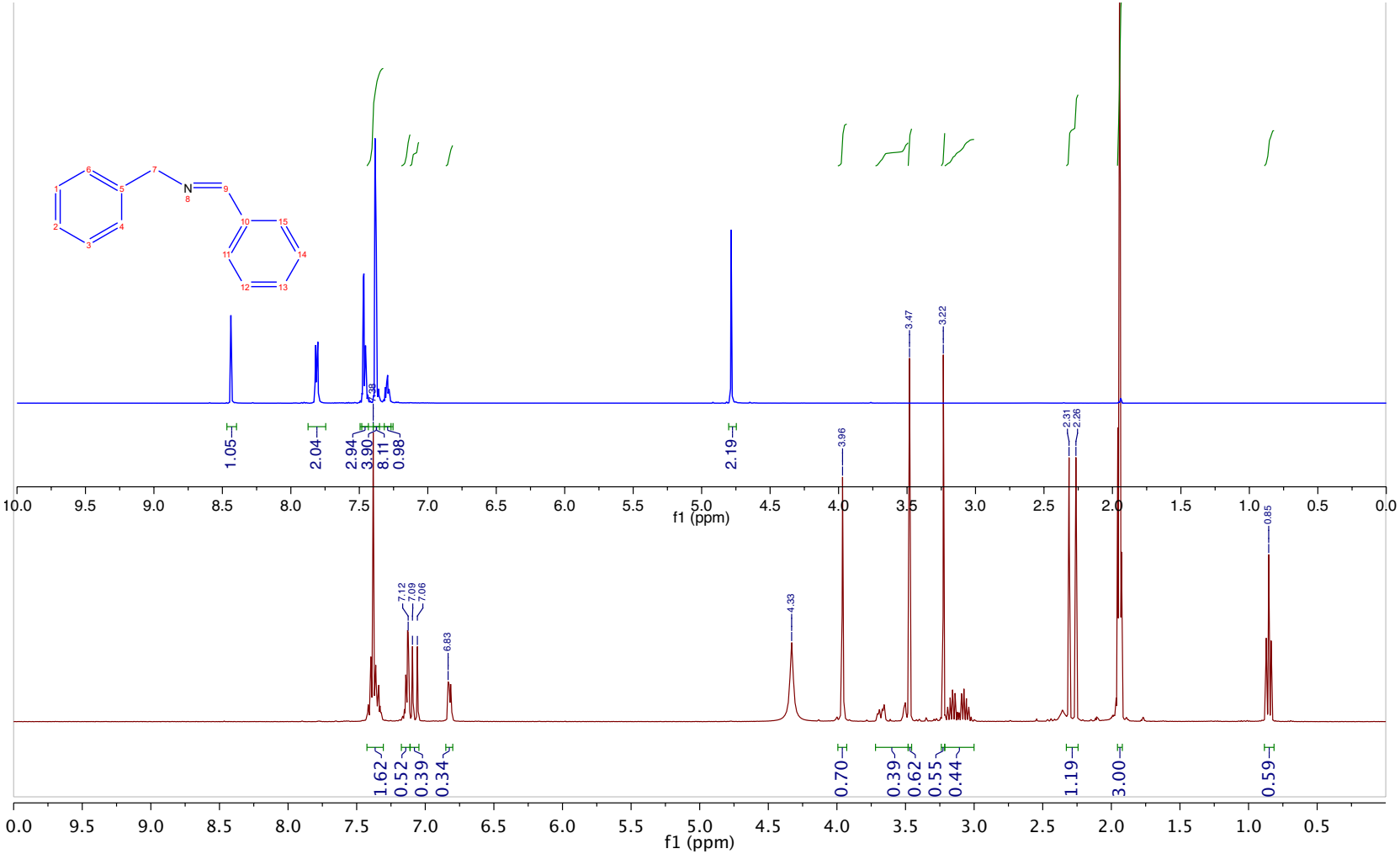

Figure 3-1-11 A. Comparison of ^{1}H-NMR spectra between the reaction mixture at t = 0 min and *N*-benzylidenebenzylamine. The spectra were recorded after mixing 5Et3MLF^{+}ClO$_4^{-}$ (25 mM) and benzylamine (50 mM) (500 MHz, CD_3CN) in air in dried acetonitrile-d_3. The solvent peak at 1.94 ppm was integrated as 3.00. The peak assignments were listed in Figure 3-1-6.

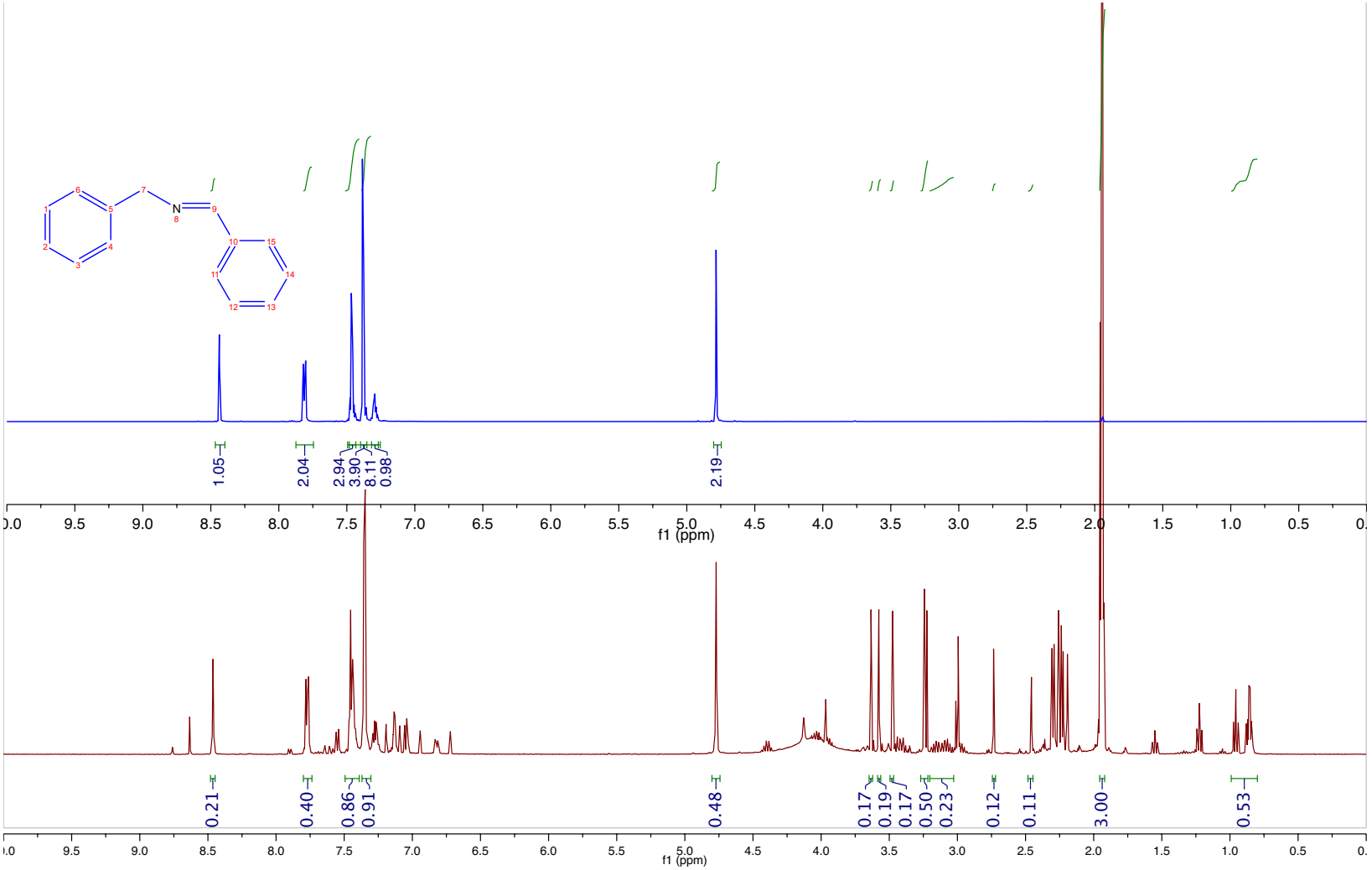

Figure 3-1-11 B. Comparison of ^{1}H-NMR spectra between the reaction mixture at t = 48 hours and *N*-benzylidenebenzylamine. The spectra were recorded after mixing 5Et3MLF^{+}ClO_4^{-} (25 mM) and benzylamine (50 mM) (500 MHz, CD_3CN) in air in dried acetonitrile-d_3. The solvent peak at 1.94 ppm was integrated as 3.00. The peak assignments were listed in Figure 3-1-6.

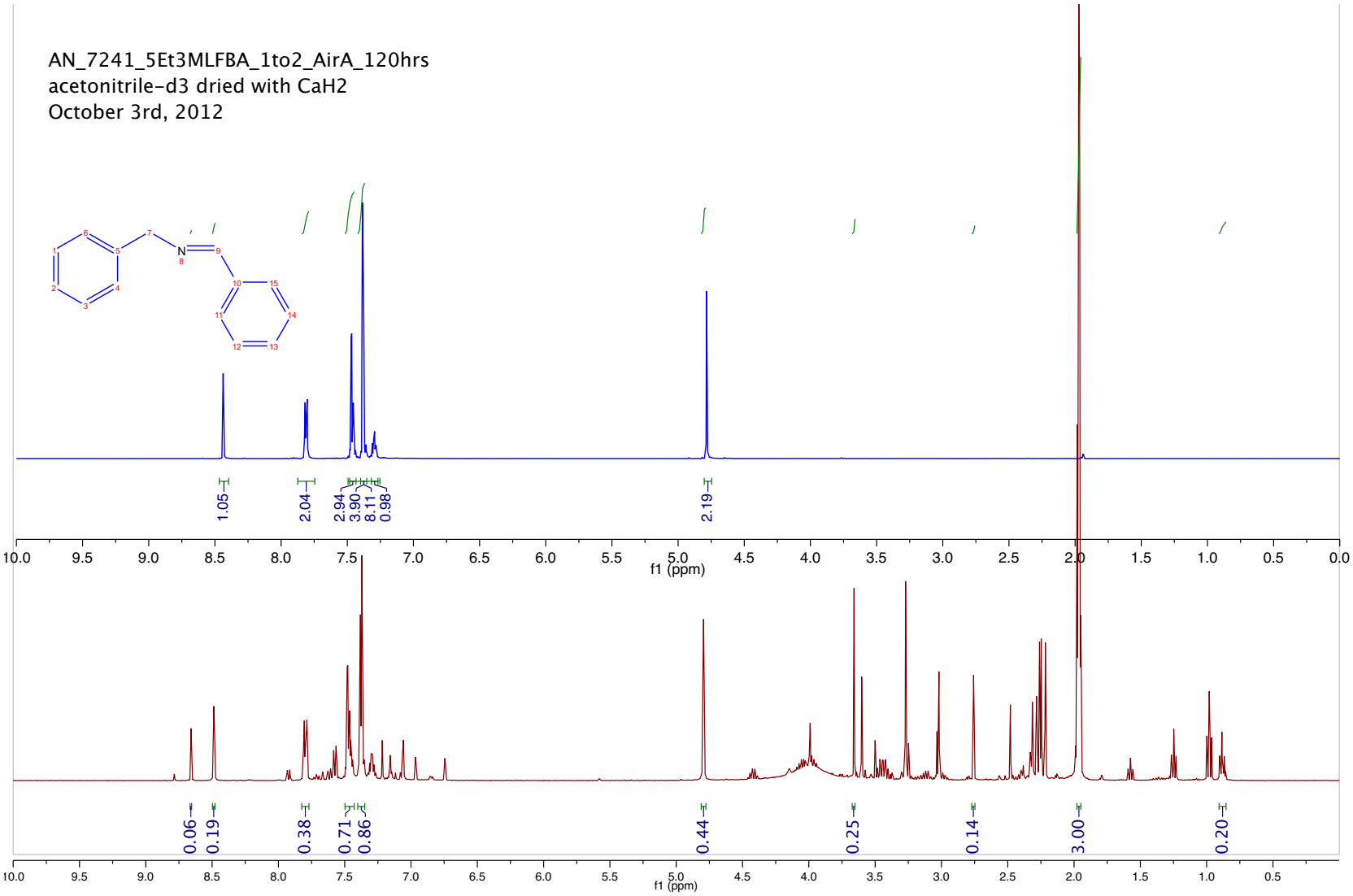

Figure 3-1-11 C. Comparison of ^{1}H-NMR spectra between the reaction mixture at t = 120 hours and *N*-benzylidenebenzylamine. The spectra were recorded after mixing 5Et3MLF^{+}ClO_4^{-} (25 mM) and benzylamine (50 mM) (500 MHz, CD_3CN) in air in dried acetonitrile-d_3. The solvent peak at 1.94 ppm was integrated as 3.00. The peak assignments were listed in Figure 3-1-6.

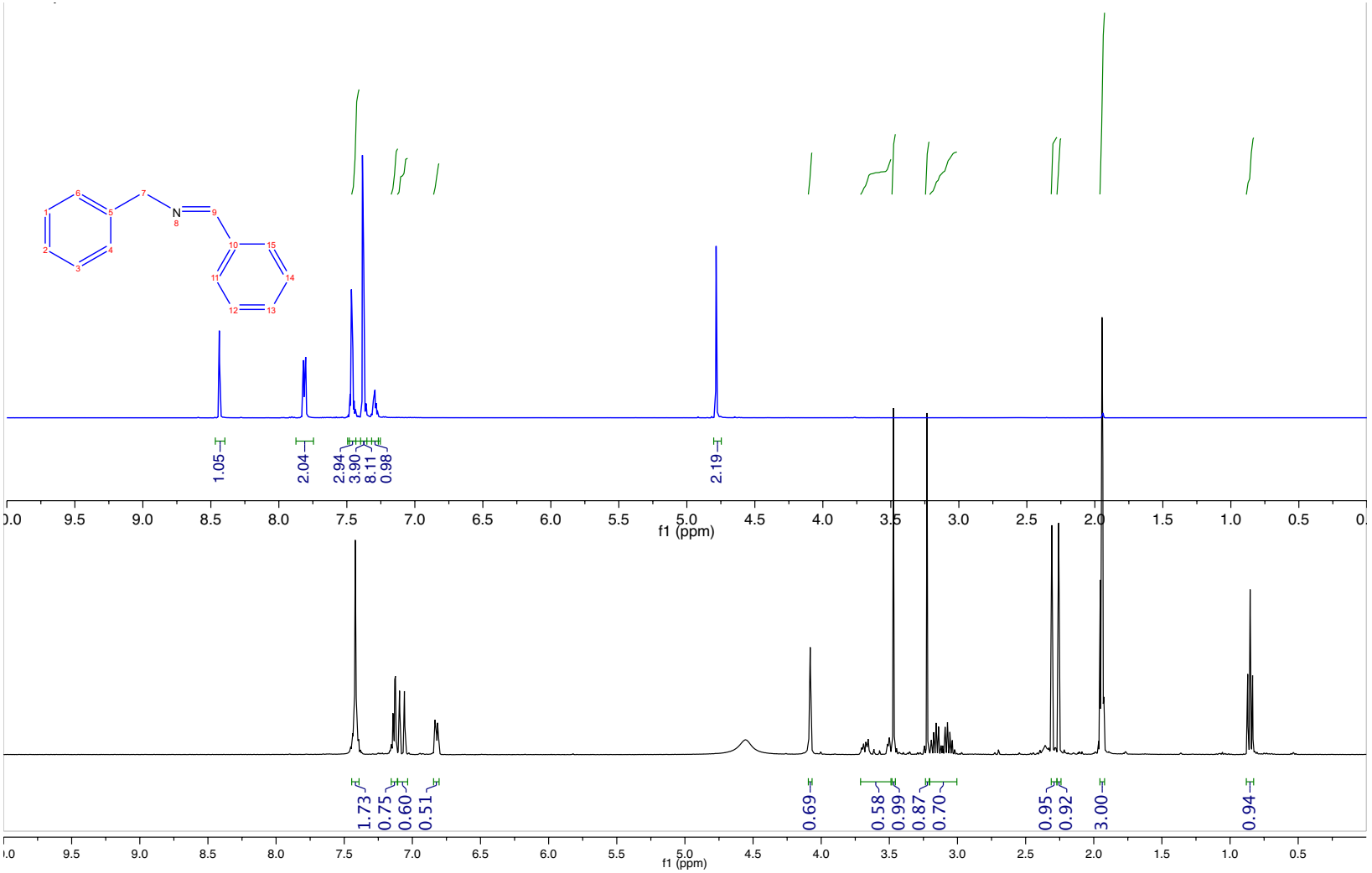

Figure 3-1-12 A. Comparison of ^{1}H-NMR spectra between the reaction mixture at t = 0 min and *N*-benzylidenebenzylamine. The spectra were recorded after mixing 5Et3MLF^{+}ClO$_4^{-}$ (25 mM) and benzylamine (50 mM) (500 MHz, CD_3CN) in air in dried acetonitrile-d_3. The solvent peak at 1.94 ppm was integrated as 3.00. The peak assignments were listed in Figure 3-1-6.

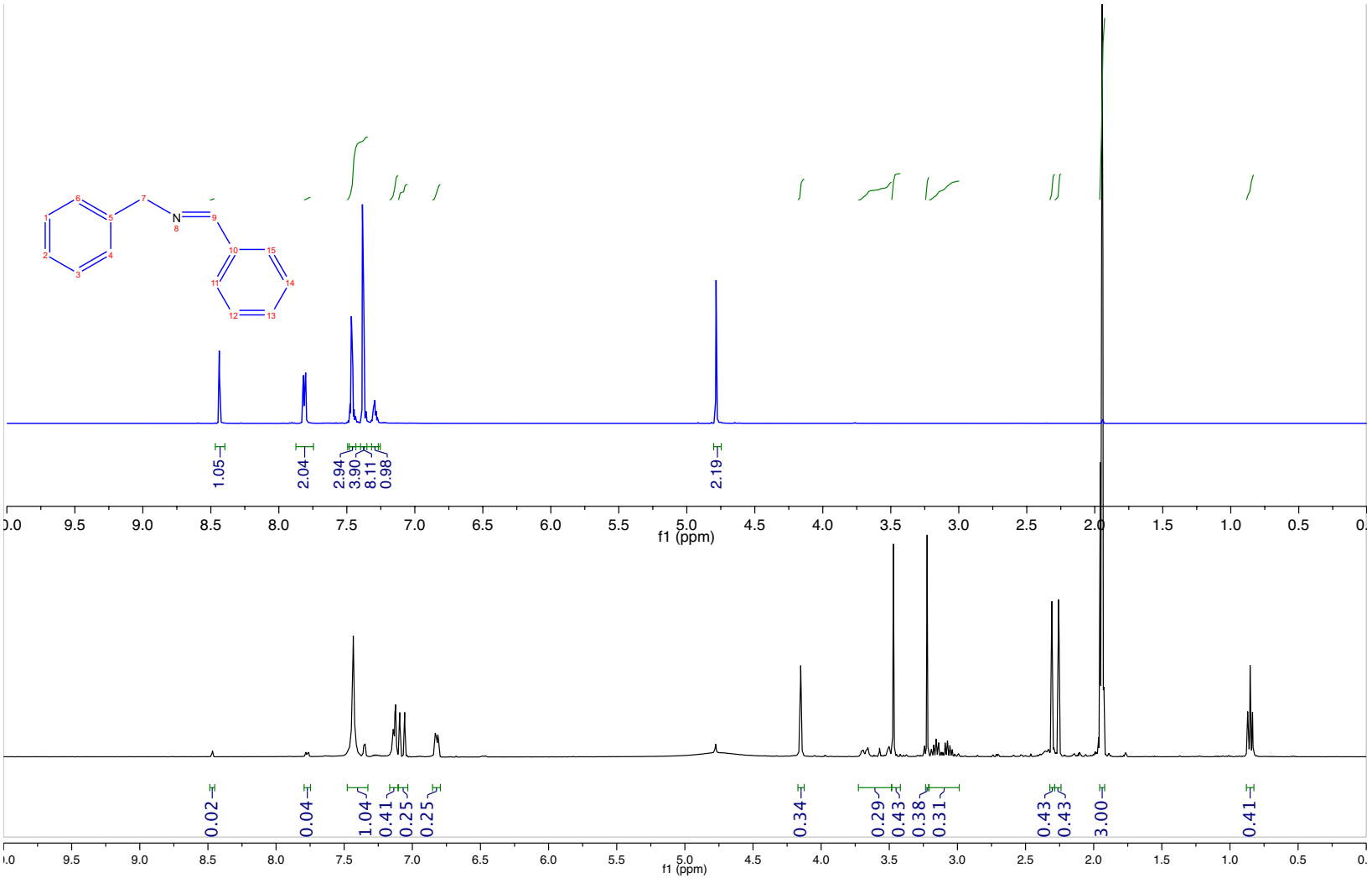

Figure 3-1-12 B. Comparison of ^{1}H-NMR spectra between the reaction mixture at t = 48 hours and *N*-benzylidenebenzylamine. The spectra were recorded after mixing 5Et3MLF^{+}ClO_4^{-} (25 mM) and benzylamine (50 mM) (500 MHz, CD_3CN) in air in dried acetonitrile-d_3. The solvent peak at 1.94 ppm was integrated as 3.00. The peak assignments were listed in Figure 3-1-6.

C

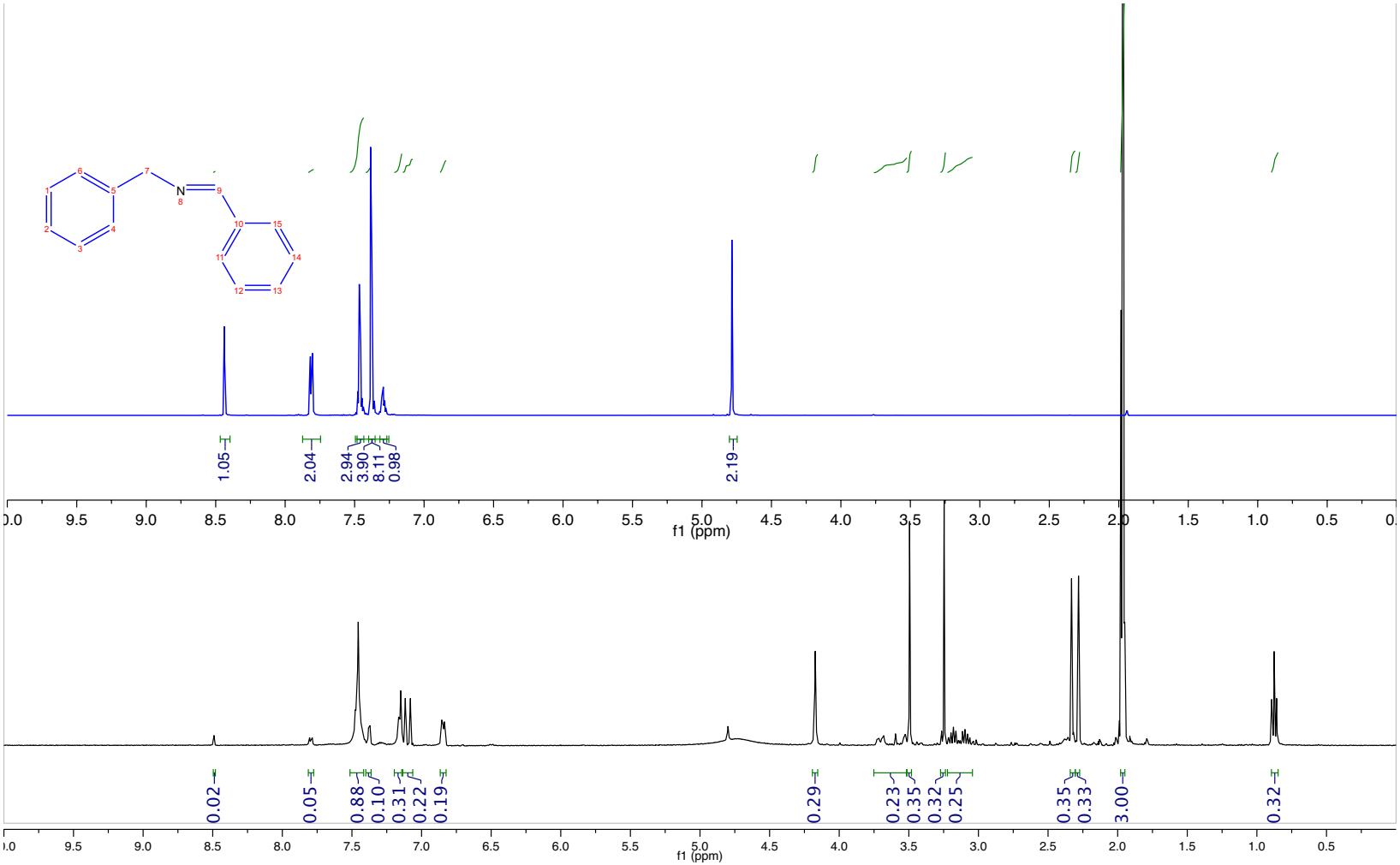

Figure 3-1-12 C. Comparison of ^{1}H-NMR spectra between the reaction mixture at t = 120 hours and *N*-benzylidenebenzylamine. The spectra were recorded after mixing 5Et3MLF^{+}ClO_4^{-} (25 mM) and benzylamine (50 mM) (500 MHz, CD_3CN) in air in dried acetonitrile-d_3. The solvent peak at 1.94 ppm was integrated as 3.00. The peak assignments were listed in Figure 3-1-6.

Next, to determine if the reaction between **37** and **41** requires dioxygen and/or water, the same reaction mixture at t = 48 hours was subjected to accurate-mass ESI^+/MS analysis. To dilute samples, commercial grade acetonitrile that contains trace water was purged with argon prior to use. Hence, moisture was introduced to the anaerobic samples, while these samples still remained air-free. The MS data demonstrated that there was not much difference between the aerobic (Figure 3-1-13 A) and anaerobic samples (3-1-13 B). The expected final product **45H$^+$** (MH^+) has an exact mass of 196.1121 amu, and this ion was observed on both MS spectra. These findings suggest that the reaction between **37** and **41** requires water. The ion at *m/z* 189 will be discussed later in this section.

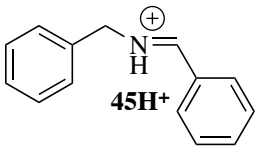

45H$^+$

Exact Mass: 196.1121

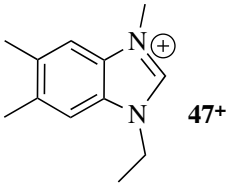

47$^+$

Exact Mass: 189.1386

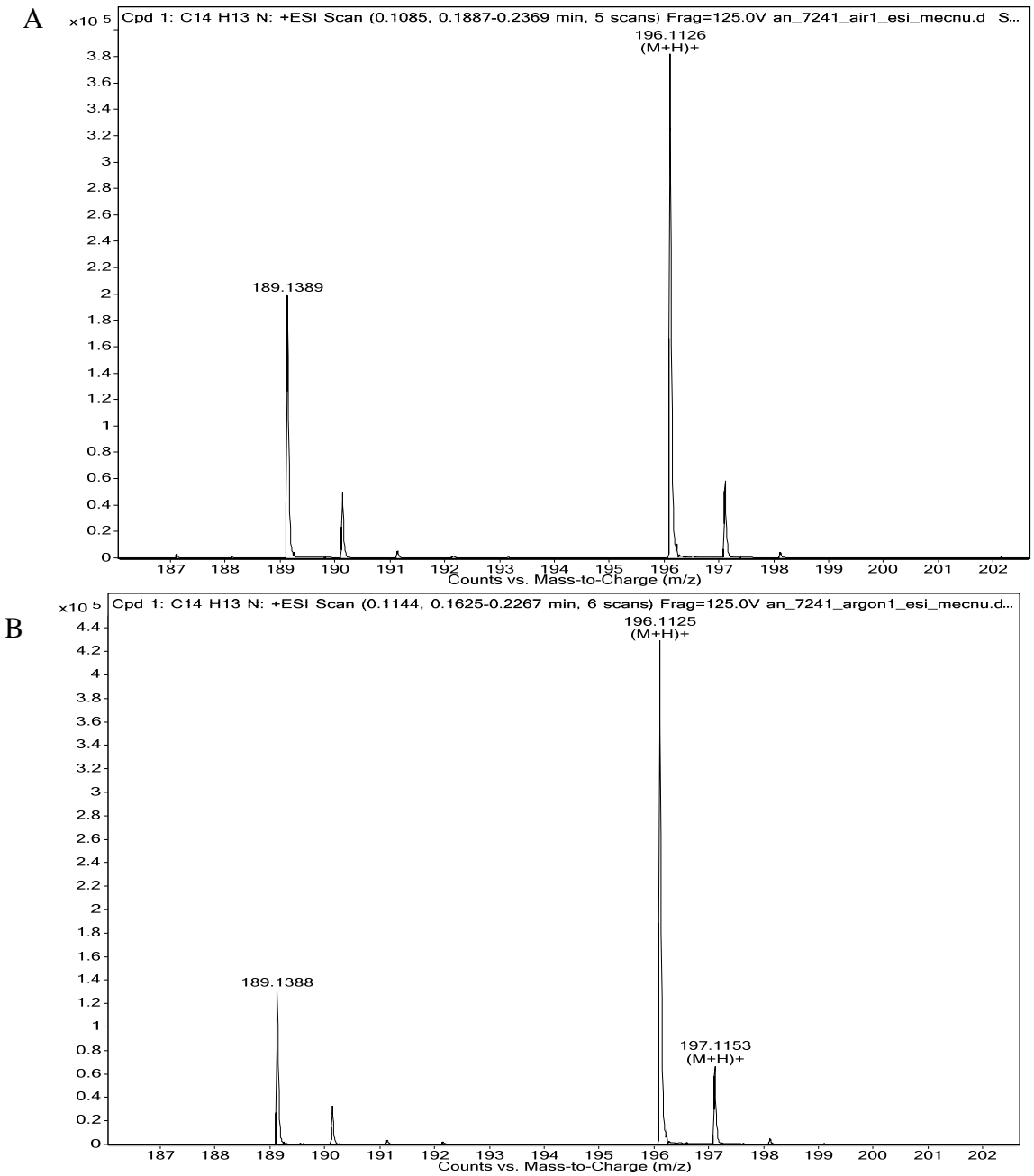

Figure 3-1-13. Accurate-mass ESI^+ mass spectra of the reaction mixture. The reaction between $5Et3MLF^+ClO_4^-$ (25 mM) and benzylamine (50 mM) underwent air (A) and under argon (B) at t = 48 hours.

Scheme 3-1-6 illustrates a proposed mechanism for the reaction between the C(4a) adduct (**41**) and benzylamine (**37**) in the presence of water at room temperature. The reduced 5Et3MLF ($\mathbf{43H_2}$) and benzylideneamine (**77**) arose from the C(4a) adduct (**41**), followed by the hydrolysis of **77** forming benzaldehyde (**56**). Finally, the reaction between the protonated benzaldehyde

56H⁺ and **37** undergoes the formation and an adduct, subsequently generating the final product of the Schiff base (**45**).

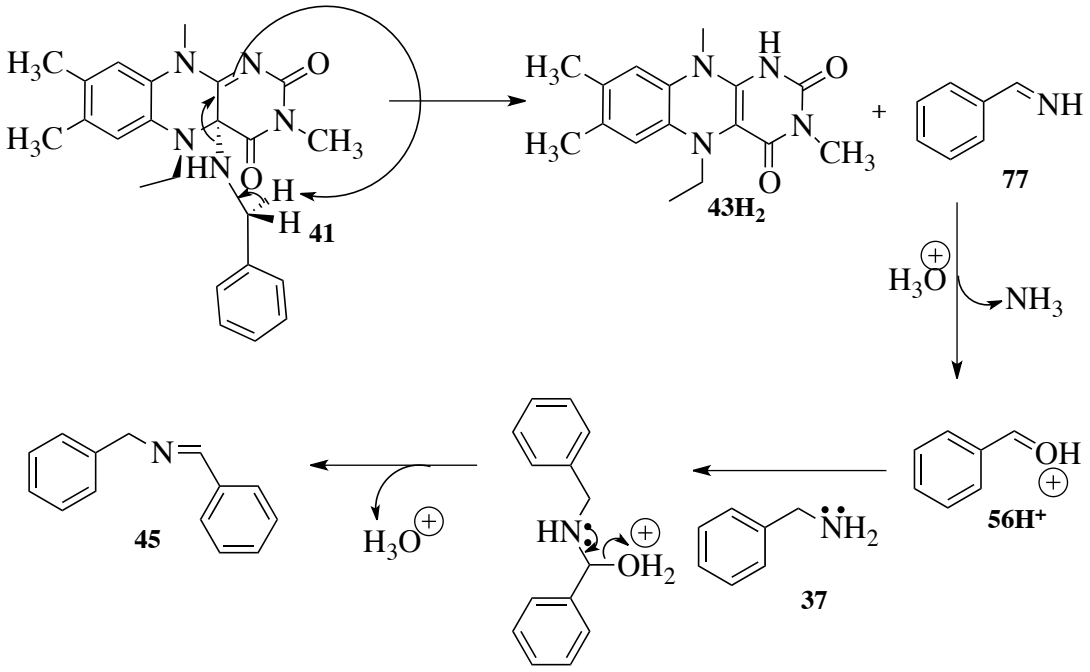

Scheme 3-1-6

Lastly, to confirm the ESI⁺/MS data, the NMR spectrum of an aerobic sample at t = 48 hours was compared with the ^{1}H NMR spectrum of synthetic 1-ethyl-3,5,6-trimethyl-1*H*-benzo[*d*]imidazol-3-ium iodide [imidazolium iodide (**47⁺I⁻**)]:[††] δ 4.40 (quartet, 2H, N*CH*$_2$CH$_3$), 4.00 (singlet, 3H, N-CH3), 2.46 (singlet, 6H, Ar-CH$_3$), and 1.57 (triplet, 3H, NCH$_2$*CH*$_3$)(Figure 3-1-14). The most downfield proton (9.16 ppm) of synthetic **47⁺I⁻** is shifted more upfield (8.76 ppm) in the reaction mixture. This signal shifting will be discussed in the next section. The imidazolium species (**47⁺**) is one of the degradation products of the 5Et3MLF salt, which will be discussed in detail in Chapter 5.

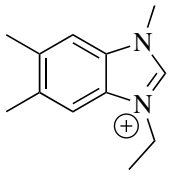

47⁺

[††] Prepared by reaction of 5,6-dimethylbenzimidazole with iodomethane followed by treatment of the resulting trimethyl product with iodoethane. Detailes will be reported separately.

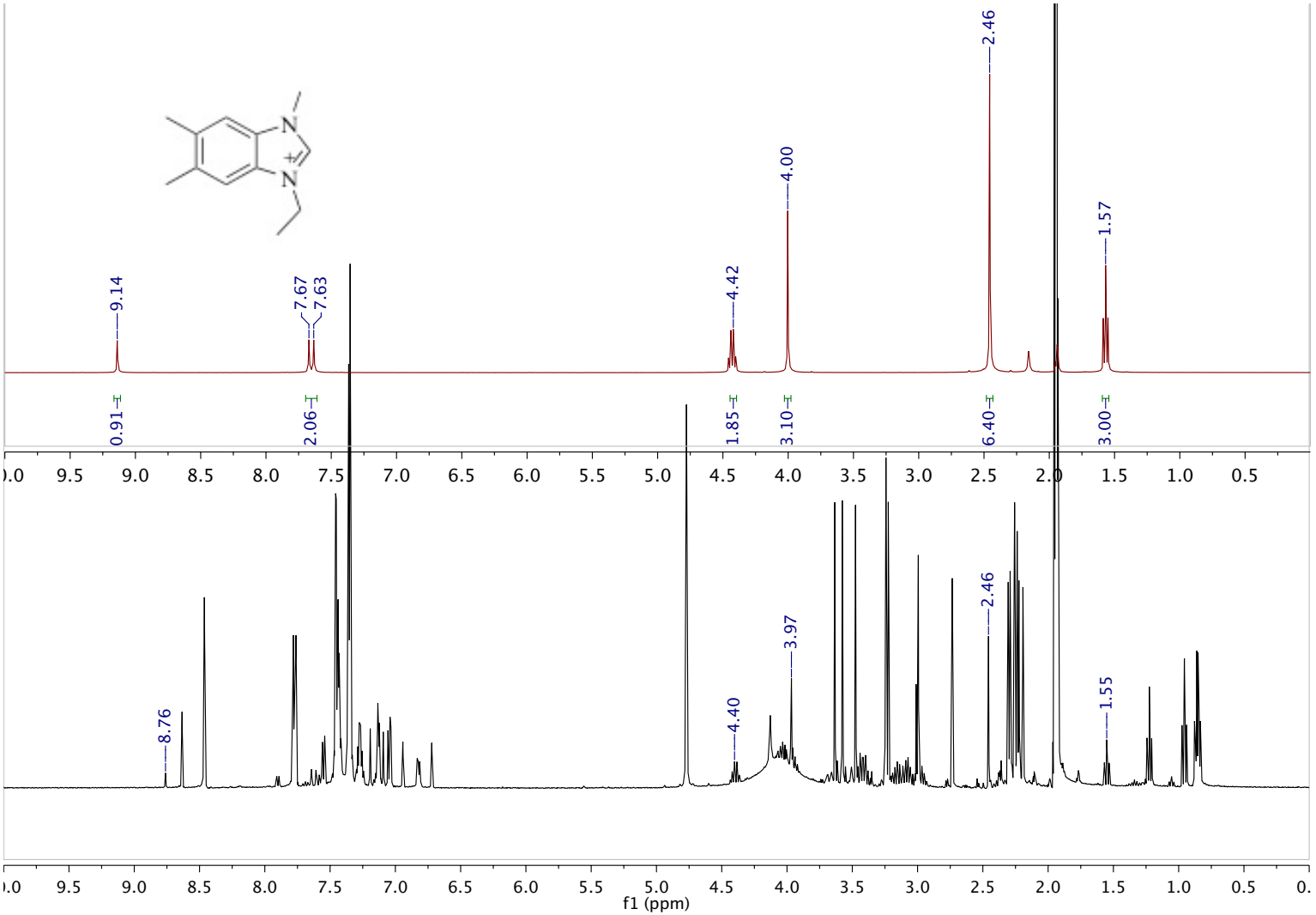

Figure 3-1-14. Comparison of ^{1}H NMR spectra of the authentic imidazolium and the reaction mixture in the air. ^{1}H NMR spectra show the authentic imidazolium (top) and the reaction mixture of 5Et3MLF^{+}ClO$_4^{-}$ (25 mM) and benzylamine (50 mM) in air (bottom) at t = 48 hours.

3.1.3 Conclusions

These findings provide unambiguous evidence for the conversion of **37** to **45** in the presence of **43$^+$ClO$_4^-$** at room temperature. Scheme 3-1-7 summarizes the observations on the reaction (it is not a stoichiometrically balanced equation because of uncertainty about the fate of the **43$^+$ClO$_4^-$** salt). The peak corresponding to **45** developed with time while the peak corresponding to compound **37** disappeared by t = 96 h. Also, the addition reaction to form the intermediate **41** proceeds along a nucleophilic polar pathway, which occurs instantly when **43$^+$ClO$_4^-$** and **37** are mixed together. The oxidation of the intermediate **41** to give eventually the Schiff base **45** may require presence of water.

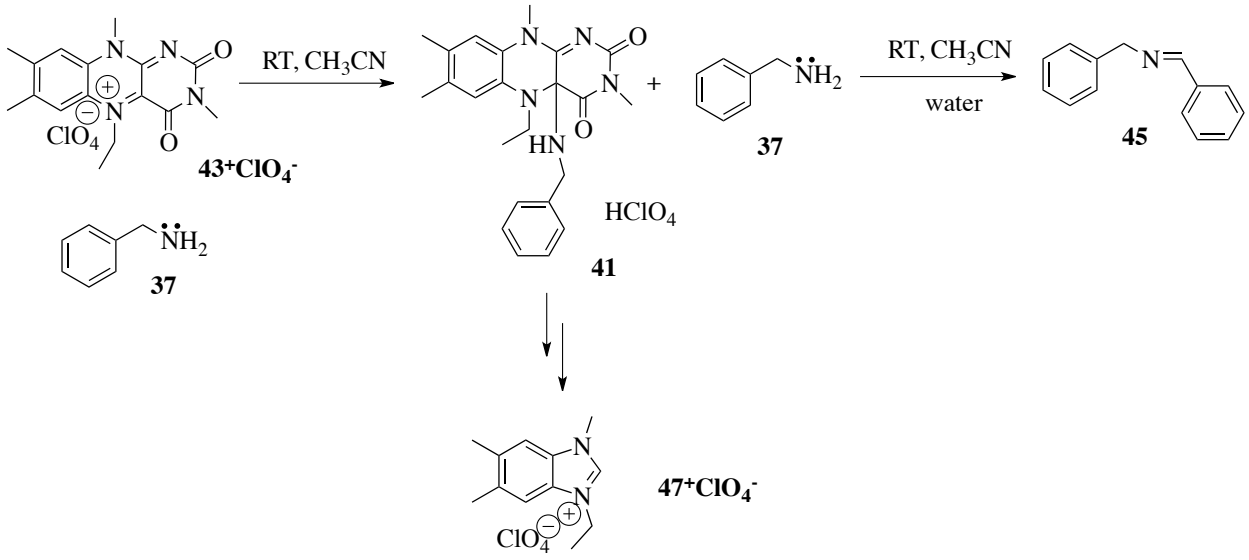

Scheme 3-1-7

3.2 Oxidation of 1-Methyl-4-(1-methyl-1*H*-pyrrol-2-yl)-1,2,3,6-tetrahydropyridine in the Presence of 5-Ethyl-3-methyllumiflavinium Perchlorate

3.2.1. Introduction

The flavoenzyme MAO-B catalyzes the α-carbon oxidation of multiple neurotransmitters, such as dopamine and serotonin, and the neurotoxin precursor MPTP and its derivatives. One of the MPTP derivatives, 1-methyl-4-(1-methyl-1*H*-pyrrol-2-yl)-1,2,3,6-tetrahydropyridine [TMMP (**4**)], was examined in the present study. Previous work explored the oxidation of **4** by MAO-A and MAO-B (Scheme 3-2-1),[59] and demonstrated that **4** was in fact a substrate for both MAO-A and MAO-B. The $V_{max.app}$ of the MAO-B-catalyzed oxidation of **4** was 30-fold greater than that observed with the MAO-A-catalyzed oxidation of **4**. In addition, compound **4** exposure to mice caused dopamine depletion, similar to that observed with MPTP (**1**).[59a] The oxidation of **4** to 1-methyl-4-(methylpyrrol-2-yl)pyridine [MMP^+ (**50^+**)] in the presence of MAO-B appears to proceed via an obligatory intermediate, the 2,3-dihydro-1-methyl-4-(methylpyrrol-2-yl)pyridinium species [DHP^+ (**49^+**)].[60]

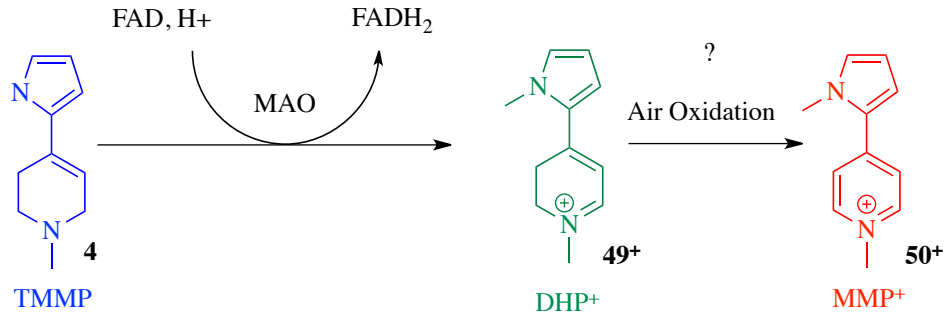

Scheme 3-2-1

Formerly, researchers had used 5-ethyl-3-methyllumiflavinium perchlorate [$5Et3MLF^+ClO_4^-$ (**$43^+ClO_4^-$**)] as a chemical model oxidant to study MAO catalysis. Their findings indicate that **$43^+ClO_4^-$** acts principally on primary and secondary amines.[35, 38, 47] However, cyclic tertiary allylamines, such as MPTP (**1**) and **4**, are excellent MAO substrates. The oxidation of the cyclic tertiary allylamines in the presence of **$43^+ClO_4^-$** has never been reported. The present study seeks to investigate the oxidation of **4** with the chemical model **$43^+ClO_4^-$**.

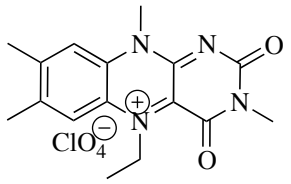

$43^{+}ClO_4^{-}$

The section addresses the following items:

1) The oxidation of **4** to the pyridinium species **50^{+}** by the flavin chemical model **$43^{+}ClO_4^{-}$** is reported. Also addressed is the detection of the dihydropyridinium intermediate **49^{+}** in the reaction. (Section 3.2.2)

2) The formation of **50^{+}** in the reaction mixture of **4** and **$43^{+}ClO_4^{-}$** is reported. (Section 3.2.3)

3) The second oxidation of the **49^{+}** to **50^{+}** is examined to determine if **$43^{+}ClO_4^{-}$** is involved in the second oxidation as well as the first 2-electron α-carbon oxidation. (Section 3.2.4)

4) The possible contribution of disproportionation in the second oxidation is considered. The concept addressed is whether the second oxidation is caused by dioxygen and/or disproportionation. (Section 3.2.5)

5) The variables that affect the reaction between **$43^{+}ClO_4^{-}$** and **4** are explored in order to determine whether the reaction is dioxygen dependent. (Section 3.2.6)

6) The fate of the chemical model **$43^{+}ClO_4^{-}$** is discussed. (Section 3.2.7)

Difficulty in obtaining and handling dried acetonitrile has proved to be major issues in this research. To avoid any confusion, it is necessary to distinguish between commercial grade acetonitrile (e.g., 99.9% anhydrous acetonitrile AcroSeal™ , CAS# 75-05-8), which is referred to as "commercial grade acetonitrile" and truly anhydrous acetonitrile (treated with CaH_2 and distilled immediately before use), which is referred to in this thesis as "dried acetonitrile".

Commercial grade acetonitrile was used for the UV/vis and accurate-mass ESI^{+}/MS analyses. This commercial product was chosen because it provides protection from air via a three-layer spectrum (inner silicone layer and double outer rubber septum with one side Teflon coated). It was checked for re-closure of any puncture hole. However, results demonstrated that commercial grade acetonitrile was not truly anhydrous or became wet with time regardless of the special septum.

For NMR analysis, a new vial (1 mL) of commercial grade acetonitrile-d_3 (Cambridge Isotope Laboratories, Inc.) was opened for each investigation unless described otherwise. The company literature indicates that the deuterated acetonitrile was dried with CaH_2 and distilled under N_2 or argon before being packed into each glass vial. Thus, it was expected to have been dried in the course of its preparation. However, despite all efforts, NMR spectra showed a water peak at 2.13 ppm, indicating that there was moisture contamination in the solvent, or that handling of the solvent lead to the introduction of water. The effect of water on the reaction between **43**$^{+}$**ClO**$_4^{-}$ and **4** is discussed in Chapter 5 in considerable detail.

3.2.2 Results and Discussion

3.2.2.1 Oxidation of TMMP by the Flavin Chemical Model 5Et3MLF$^+$ClO$_4^-$

The principal objective was to determine whether the flavin chemical model **43**$^+$**ClO**$_4^-$ was capable of oxidizing **4**, a known substrate of the MAOs. The synthesis of **43**$^+$**ClO**$_4^-$ was accomplished by the multi-step reaction sequence as previously described.[61] Details of the synthesis and characterization of **43**$^+$**ClO**$_4^-$ will be considered in Chapter 6.

At first, the stabilities of **43**$^+$**ClO**$_4^-$ and **4** were examined by NMR, UV/vis and accurate-mass ESI$^+$/MS analyses. TMMP in commercial grade acetonitrile proved to be stable for at least two weeks at room temperature. The flavinium salt **43**$^+$**ClO**$_4^-$ in commercial acetonitrile-d_3 also appeared to be stable for at least a week.

Initially, the reaction between **43**$^+$**ClO**$_4^-$ (12.5 mM) and **4** (25 mM) in commercial grade acetonitrile was followed by UV/vis spectrophotometry. The reaction mixture was constantly stirred under acetonitrile-saturated air at room temperature.[‡‡] The sample tube was covered with aluminum foil to avoid light. For each sample reading, 3.3 μL of the reaction mixture was removed from the system using a syringe, which was then dissolved into two mL of commercial grade acetonitrile (a 600 fold dilution) for the UV/vis analysis.

As soon as TMMP was added to the purple-colored solution of **43**$^+$**ClO**$_4^-$ in commercial grade acetonitrile, the color changed to a green hue; after 2 hours, the reaction mixture had transformed into an orange yellow color.

Figure 3-2-1 shows the principal spectral changes that were observed over the first 45 min. The UV spectrum of **50**$^+$**I**$^-$ displayed a peak with λ_{max} = 370 nm and molar esinction coefficient of 34125 (Appendix B). The absorbance bands for **43**$^+$**ClO**$_4^-$ (412 nm and 555 nm) were lost rapidly following the addition of TMMP. A new peak appeared with λ_{max} 350 nm (1 – 15 min). This peak shifted to λ_{max} 366 nm (15 min – 2 h), corresponding to that of **50**$^+$.[62] Published data indicated that λ_{max} 350 nm may correspond to either a C(4a)-hydroxyl adduct (**51**) or C(4a)-

[‡‡] The air was passed through acetonitrile before being passed over the headspace of the flask to avoid evaporation.

hydroperoxyl adduct (**52**),[63] suggesting the reaction of water and/or dioxygen with **43$^+$ClO$_4^-$**. Then, over the course of time, the peak shifted to a new chromophore with λ_{max} 366 nm when the solution had become orange/yellow. This peak continued to increase over the first 45 min. As mentioned, this absorbance band corresponds to that of the pyridinium species, **50$^+$**.[62] The immediate color change from purple to green probably misleading in that it seemed to indicate an initial reaction between **43$^+$ClO$_4^-$** and **4** when the most likely the process involved addition of water to the 4a position.

Because their stock solution of (but not other stock solutions) TMMP contained a small amount of MMP$^+$ contamination (absorbance 0.05 at λ_{max} 366 nm), it was subtracted from experimental measurements before calculating the concentrations of MMP$^+$. This stock solution of TMMP had been stored in the freezer over two month. For the final reading, the absorbance of λ_{max} 366 nm was 0.64 (0.69 – 0.05) at t = 2 hours. According to the UV/vis results, the formation of **50$^+$** is 11.32 mM, and this might suggest the contribution of overlapping chromophores to the 366 nm absorbance.

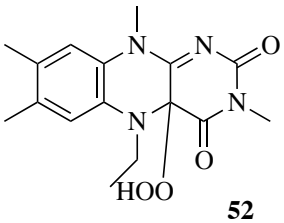

52

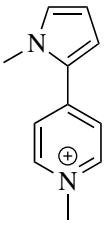

50

λ_{max} of principal species	350 nm	366 nm
Color of solution	green	orange/yellow

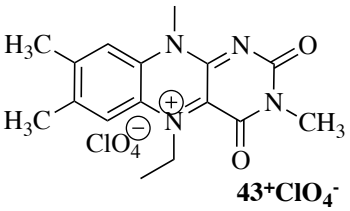

43$^+$ClO$_4^-$

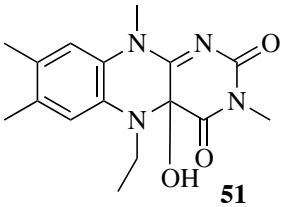

51

λ_{max} of principal species	412 nm and 555 nm	350 nm
Color of solution	purple	green

A

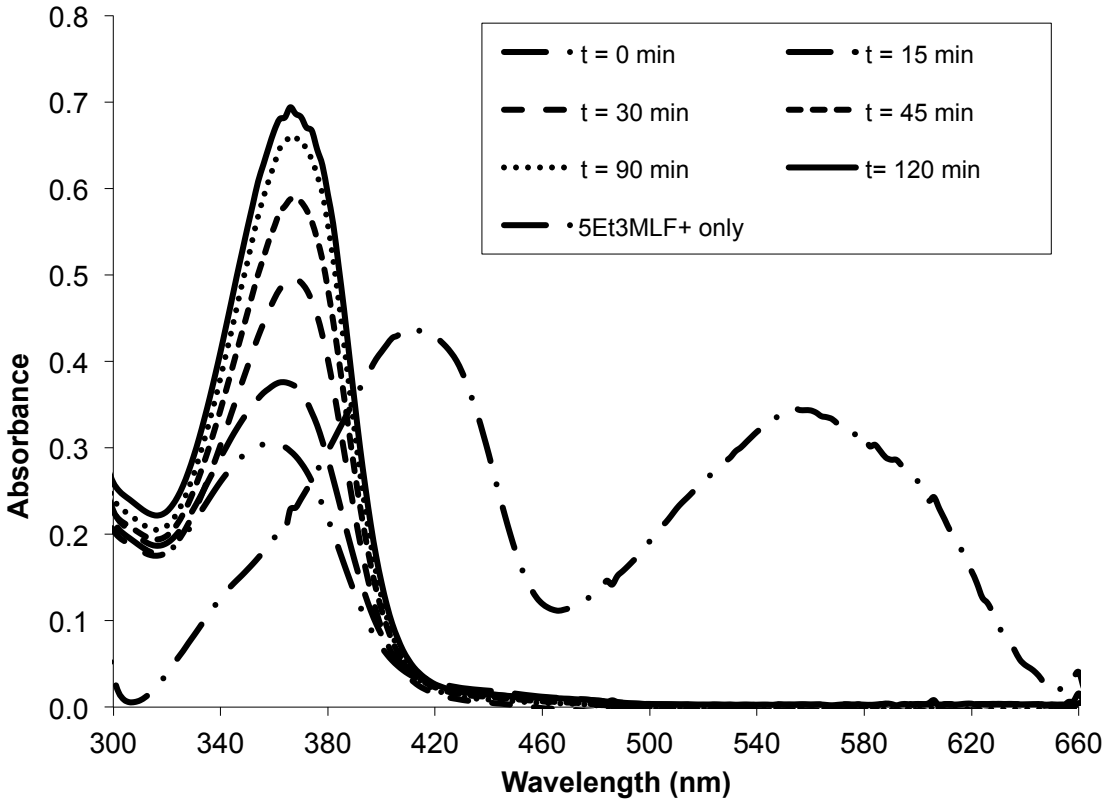

B

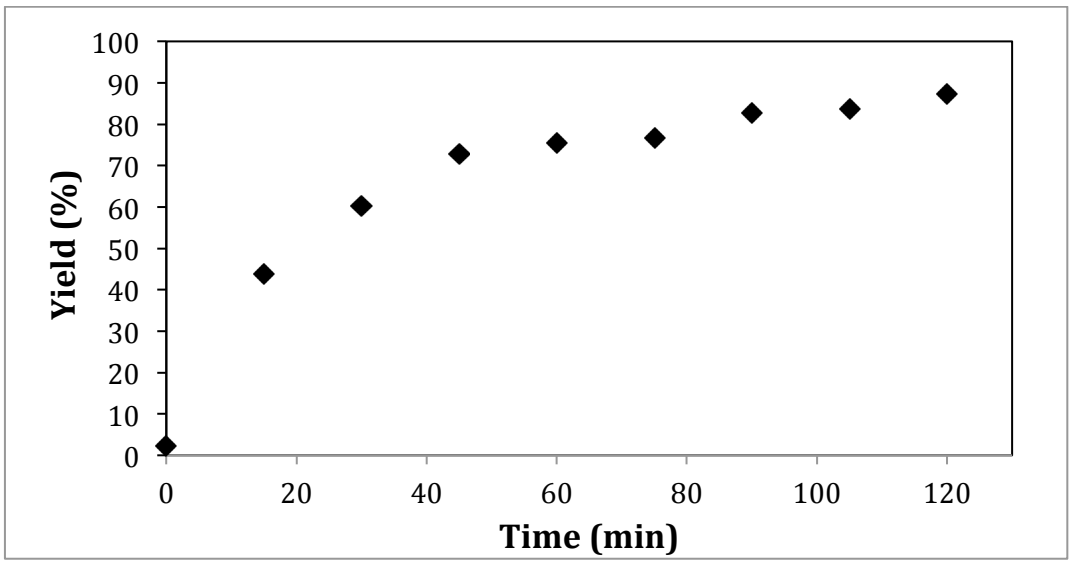

Figure 3-2-1. Formation of the oxidation product MMP^+ in the reaction mixture. The concentrations of MMP^+ was monitored in the presence of air of $5Et3MLF^+ClO_4^-$ (25 mM) and TMMP (50 mM) (molar ratio of 1 to 2) in commercial grade acetonitrile: (A) UV/vis spectra of the reaction for 2 hours (long dash dot, $5Et3MLF^+ClO_4^-$ alone; long dash dot dot at t = 0 min; long dash at t = 15 min; dash at t = 30 min; square dot at = 45 min; round dot t = 90 min; solid at t = 120 min) and (B) increment of % yield with time.

As noted previously, the results indicated the possible water contamination in commercial grade acetonitrile used in the reaction mixture. Moisture also would have been introduced from the air that had not been dried. To introduce air into the reaction mixture, house air was bubbled through the commercial grade acetonitrile. The house air was not dried before use.

To isolate the pyridinium species (**50**$^+$) from the reaction mixture of **43**$^+$**ClO**$_4^-$ (25 mM) and **4** (50 mM) in commercial grade acetonitrile, a small sample had been removed at t = 2 hours. Prior to this experiment, the salt **4H**$^+$**ClO**$_4^-$ was freshly converted to the free base **4**, and results indicated no contamination with **50**$^+$. The reaction mixture was extracted with D_2O to isolate polar products. Figure 3-2-2 shows the superimposed images of ^{1}H-NMR spectra in D_2O —the top tracing shows the spectrum of the D_2O reaction mixture extract, and the bottom tracing depicts the spectrum of a synthetic sample of **50**$^+$.[62] The presence of all of the signals for **50**$^+$ in the D_2O extract confirms the conversion of **4** to **50**$^+$ in the reaction mixture.

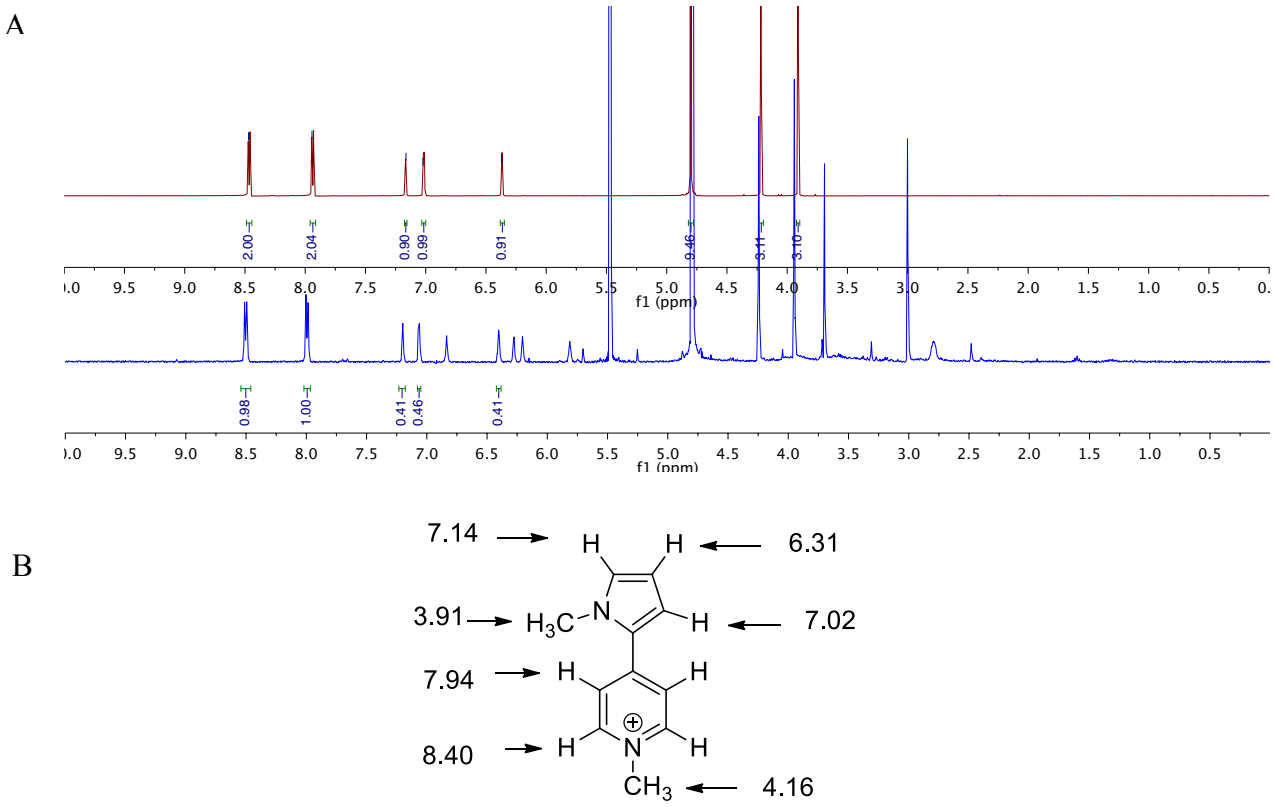

Figure 3-2-2. Superimposed image of ^{1}H NMR spectra (500 MHz, D_2O). A: Comparison of the authentic MMP$^+$ClO$_4^-$ (maroon, top) and the product extract (blue, bottom) and in D_2O, and B: NMR chemical shifts of authentic MMP$^+$ in D_2O.

Following the UV/vis and NMR studies, the same reaction mixture (**43**$^{+}$**ClO**$_4^{-}$, 25 mM and **4**, 50 mM) at t = 24 hours was analyzed using high resolution ESI^{+} mass spectrometry (Figure 3-2-3). The molecular composition of the intense ion at *m/z* 173.1073 corresponds to **50**$^{+}$ (δ 0.0 mDa). The less intense ion at *m/z* 177.1393 is due to the starting material TMMP [MH^{+} at *m/z* 177.1313 (δ 1.3 mDa)]. Note that the ion at *m*/z 242.2845 is a background peak (the tetrabutylammonium species). The second intense ion (*m/z* 189.1382) in this spectrum proved to be an imidazolium species. This subject will be explored more thoroughly in Section 3-2-7, which discusses the possible fate of the flavinium species in this reaction.

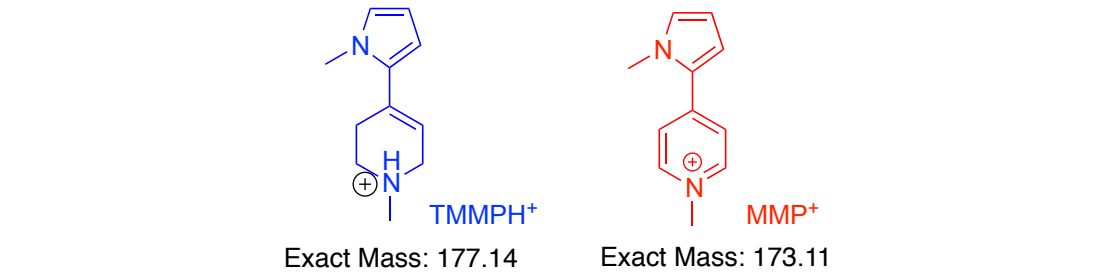

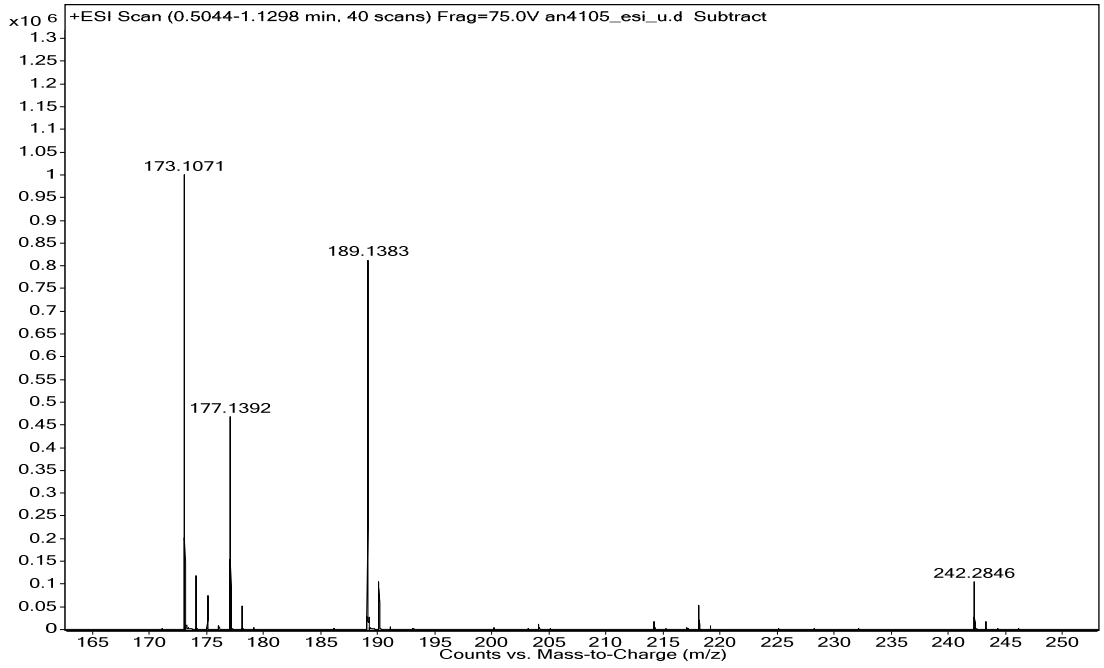

Figure 3-2-3. Positive ion electron spray ionization mass spectrum of MMP^{+} formation. The spectrum (*x*-axis: *m/z*; *y*-axis: relative abundance) shows the reaction product of 5Et3MLF^{+}ClO$_4^{-}$ (12.5 mM) with TMMP (50 mM) in commercial grade acetonitrile (t = 24 hours). The reaction mixture was constantly stirred in the dark at room temperature while acetonitrile-saturated air was introduced. An expansion of the spectrum from *m/z* 160 to *m/z* 260 is shown.

To monitor the formation of **50⁺**, ^{1}H NMR was used for quantitative analysis. Figure 3-2-4 displays the time-dependent formation of MMP^+ in aerobic condition in dried acetonitrile-d_3 at room temperature. A known concentration of an internal standard hexamethyldisiloxane (HMDSO) was added to the reaction mixture at t = 24 hours to calculate the concentration of the final product, MMP^+. A sample calculation for MMP^+ concentrations is shown in Appendix C. HMDSO was chosen because its peak appears at δ 0.06 ppm, and it does not overlap with other peaks in the reaction mixture. Addition of HMDSO was waited until t = 24 hours because the reaction involves radical formations at the initial stage. All NMR spectra were integrated relative to the solvent peak (acetonitrile) at δ 1.94 ppm, and the concentration of **50⁺** was estimated from the integration of MMP^+ peaks (Appendix D). At t = 24 hours, the percent yield was 91 %.

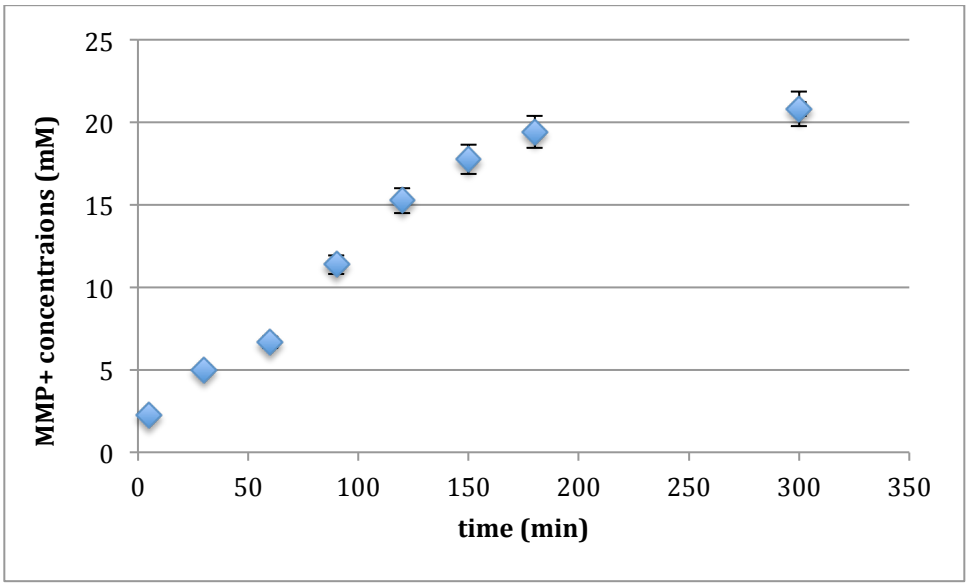

Figure 3-2-4. Time-dependent development of MMP^+ concentrations. The concentration of MMP^+ was calculated from ^{1}H NMR analysis of the reaction between $5Et3MLF^+ClO_4^-$ (25 mM) with TMMP (50 mM)(500 MHz, acetonitrile-d_3). The reaction underwent in dried acetonitrile-d_3 in air at room temperature, expressed in MMP^+ concentrations relative to 1H NMR peak integration compared to the internal standard (hexamethyldisiloxane) at t = 0 to 350 min. The values are the average of triplicate samples with the standard deviation.

Therefore, UV/vis, NMR, and accurate-mass ESI^+/MS analyses all revealed the formation of **50^+** with the oxidation of **4** in the presence of **$43^+ClO_4^-$**. Qualitative analyses were performed using NMR and accurate-mass ESI^+/MS, and data from both techniques indicated the generation of **50^+**. Quantitative analysis of **50^+** using NMR analysis showed a quantitative yield (91%) at t = 300 min. The fate of **$43^+ClO_4^-$** will be discussed separately in Chapter 5.

3.2.2.2 Detection of the 1-Methyl-4-(1-methylpyrrol-2-yl)-2,3-dihydropyridinium Species

The next effort focused on determining if the production of MMP^+ (**50^+**), resulting from the reaction between $5Et3MLF^+ClO_4^-$ (**$43^+ClO_4^-$**) and TMMP (**4**), proceeds via the intermediate dihydropyridinium species DHP^+ (**49^+**), the expected initial 2-electron oxidation product of **4**. Castagnoli and his co-workers have reported the identification of the corresponding dihydropyridinium species in the MAO-B catalyzed oxidation of MPTP.[60] They also found the corresponding dihydropyridinium species formed from the reaction between MAO-B and TMMP.[60]

Figure 3-2-5 displays an accurate-mass ESI^+ mass spectrum of the product resulting from the reaction between **$43^+ClO_4^-$** (12.25 mM) with **4** (25.5 mM) at room temperature in commercial grade acetonitrile. At t = 30 min, a small amount of the reaction mixture (2 μL) was removed, and the mixture was diluted by a factor of 1000 for accurate-mass ESI^+/MS analysis. Samples were stored at 4 °C and read within 2 hours.

As shown earlier, the peaks at *m/z* 177.1380 and 173.1064 correspond to **$4H^+$** and **50^+**, respectively (structures shown below). The signal at *m/z* 178.1411 is the ^{13}C-satelite peak of 50^+. The weaker ion at *m/z* 175.1231 (δ 0.1 mDa) corresponds to the dihydropyridinium species **49^+**, which is the predicted intermediate.

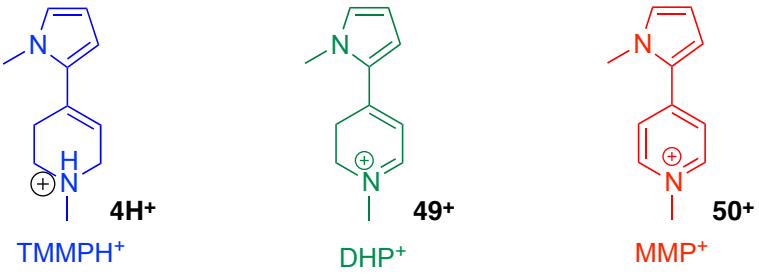

Exact Mass: 177.1386 Exact Mass: 175.1230 Exact Mass: 173.1073

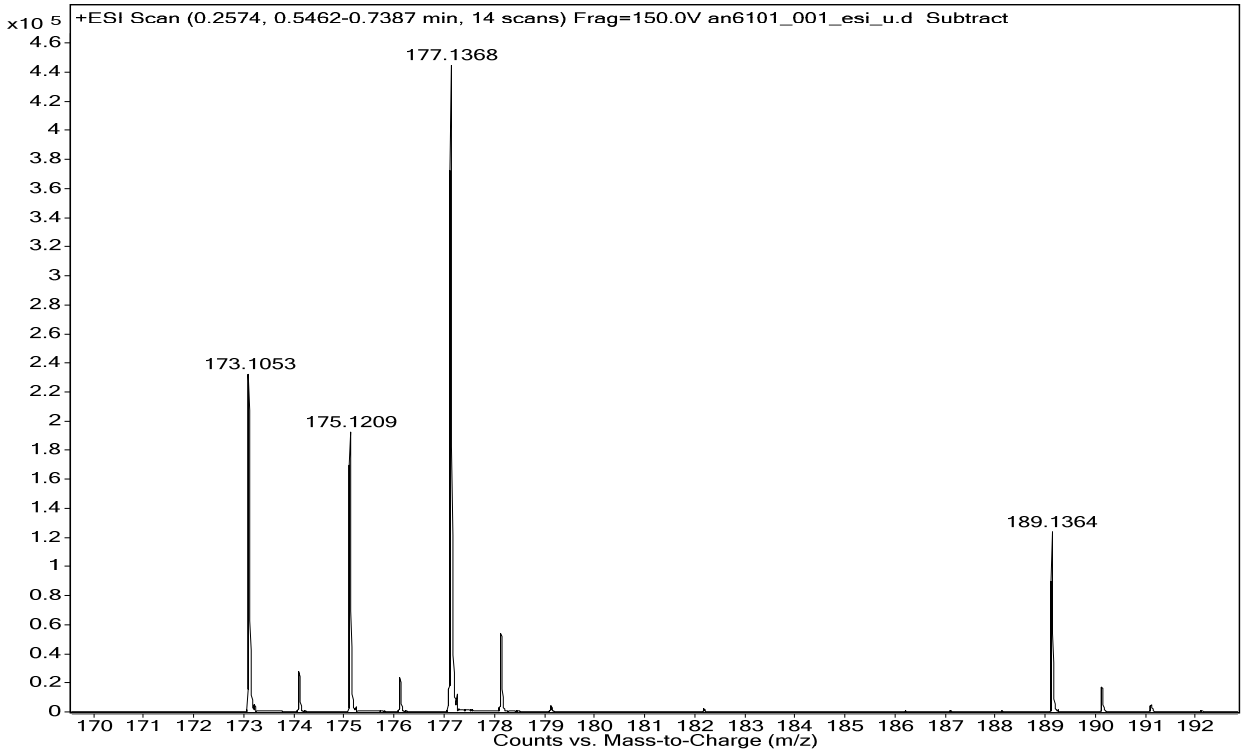

Figure 3-2-5. Accurate-Mass ESI$^+$ mass spectrum of the reaction products. The reaction of 5Et3MLF$^+$ClO$_4^-$ with TMMP proceeds in air. An expansion of the spectrum from *m/z* 170 to *m/z* 200 is shown.

In order to examine further the oxidation of **4** by **43$^+$ClO$_4^-$**, 25 mM of **4** was combined with 50 mM of **43$^+$ClO$_4^-$**, in commercial grade acetonitrile-d_3. Figure 3-2-6 presents the NMR data from this experiment. The expected dihydropyridinium intermediate (**49$^+$**) was also detected using NMR in the reaction mixture examined at t = 120 minutes. Results suggest that the second oxidation to give **50$^+$** occurs more rapidly than the initial 2-electron oxidation since **50$^+$** does not accumulate in the reaction mixture.

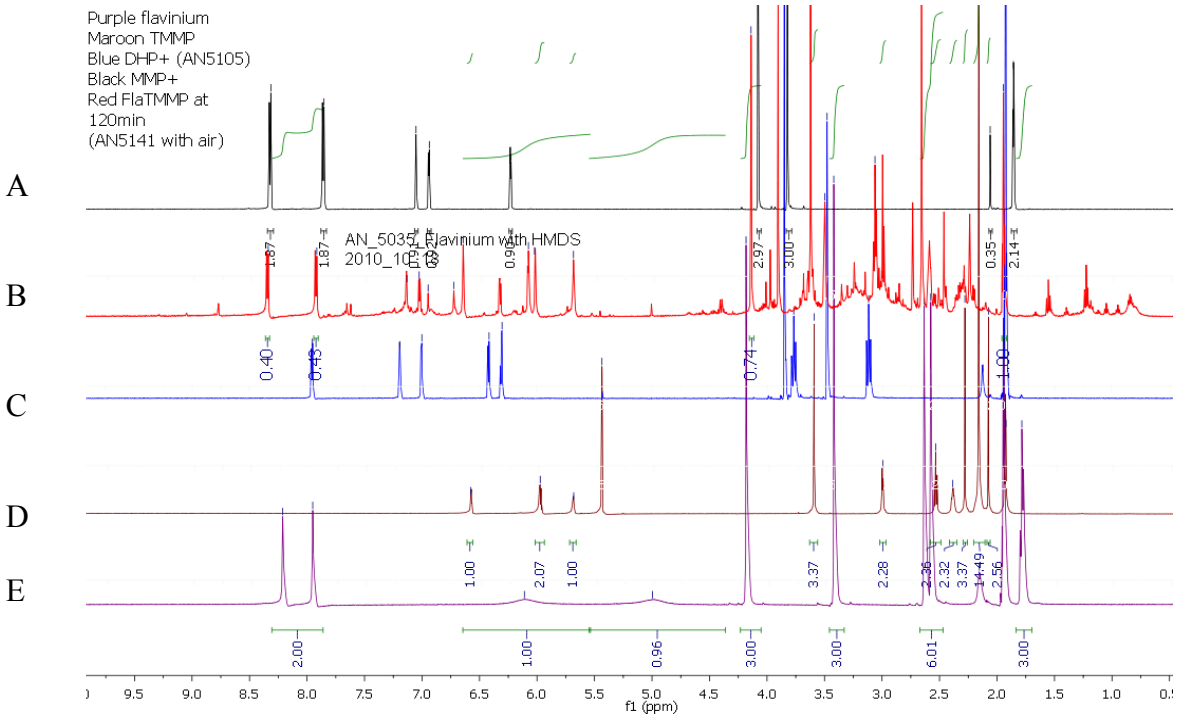

Figure 3-2-6. Comparison of ^{1}H NMR spectra between the reaction mixture and standards. Superimposed images of ^{1}HNMR spectra (500HMz, CD_3CN) of the reaction product of $5Et3MLF^{+}ClO_4^{-}$(12.25 mM) with TMMP (25.5 M): A, authentic $MMP^{+}ClO_4^{-}$; B, the reaction mixture at 2 h; C, authentic $DHP^{+}ClO_4^{-}$; D, TMMP; E, $5Et3MLF^{+}ClO_4^{-}$.

In summary, as shown in Scheme 3-2-3, the oxidation of **4** with **$43^{+}ClO_4^{-}$** leads initially to **49^{+}** that undergoes a second 2-electron oxidation to give the pyridinium species **50^{+}**. The second 2-electron oxidation may be an autoxidation process.

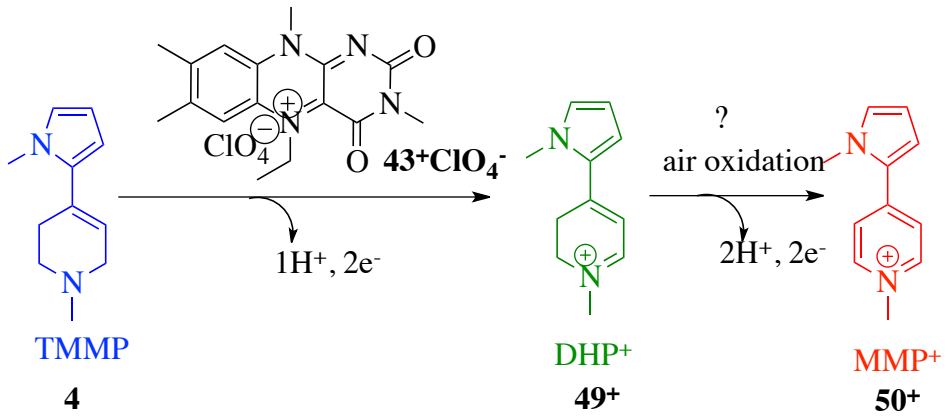

Scheme 3-2-3

3.2.2.3 Investigation of Oxidation of the DHP^+ with $5Et3MLF^+ClO_4^-$

The next objective was to examine whether $5Et3MLF^+ClO_4^-$ (**$43^+ClO_4^-$**) is involved in the second oxidation, the conversion of the obligatory intermediate DHP^+ (**49^+**) to MMP^+ (**50^+**). A working hypothesis, based on stoichiometric consideration, was that the second oxidation proceeds independently of **$43^+ClO_4^-$**. To test this hypothesis, the flavinium salt **$43^+ClO_4^-$** (25 mM) and the synthetic **49^+**[62] (50 mM) were mixed in commercial acetonitrile-d_3. The reaction was monitored using NMR. Even after 90 min, no peaks corresponding to the chemical shifts for **50^+** were observed in the NMR spectra. There was no difference in the NMR spectra between t = 5 min and 90 min. In addition, the effect of dioxygen on the oxidation of **49^+** was examined with the solutions treated under either air or argon. Argon was purified of traces of oxygen and moisture by passage through

a supported-copper oxygen scavenger (BASF) and anhydrous calcium sulfate in a sealed glass column. Both ends of the column were stuffed with glass wool. Argon was purged through the column before being applied to the samples. Figure 3-2-7 shows the comparison between the reaction in air (Figure 3-2-7 A) and under argon (Figure 3-2-7 B). The NMR results suggested the oxidation of DHP^+ does not occur regardless of the presence of dioxygen.

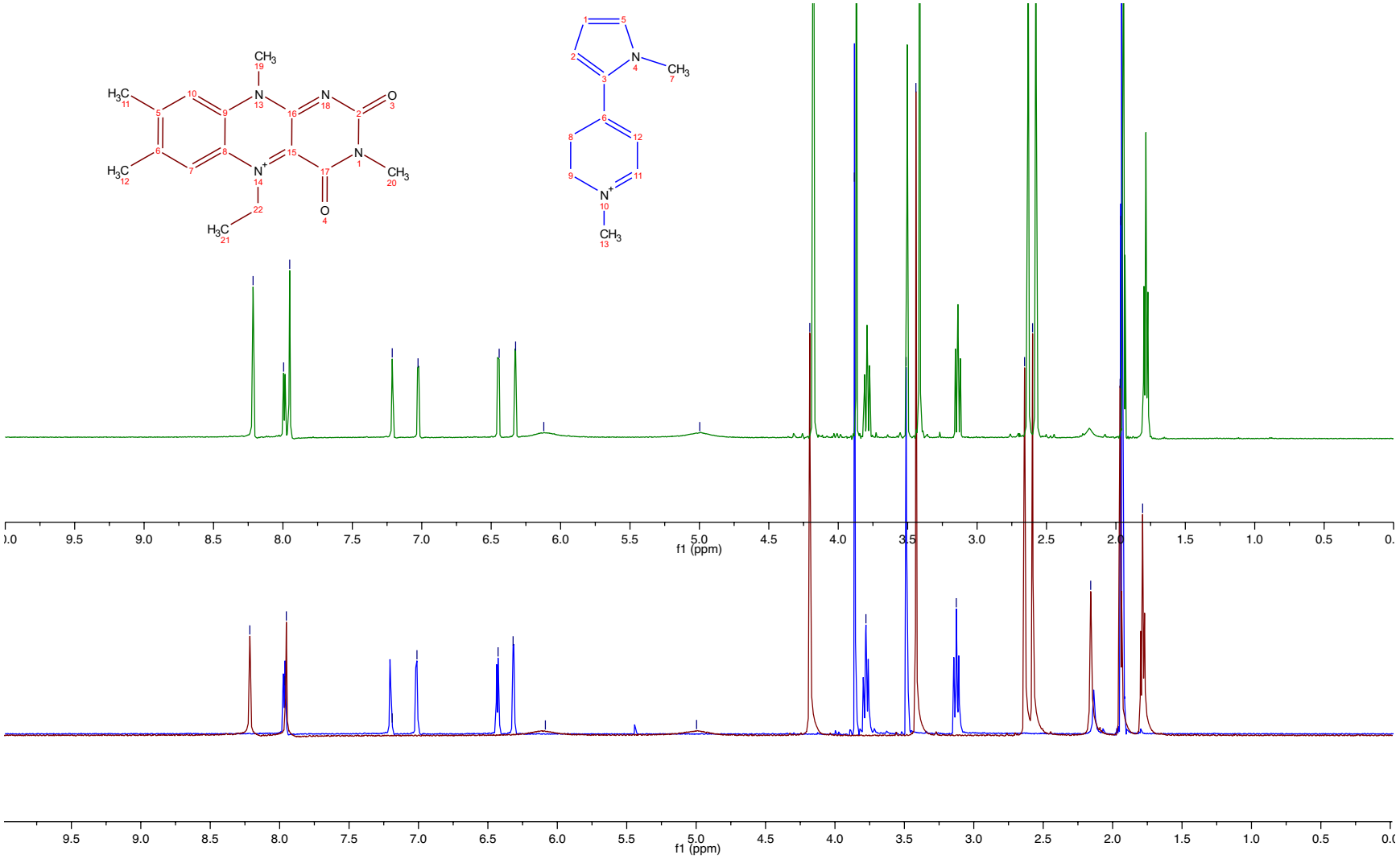

Figure 3-2-7 A. Comparison of ^{1}H NMR spectra in air at t = 90 min. Superimposed image of ^{1}H NMR spectra of individual 5Et3MLF^{+}ClO$_4^{-}$ (maroon, botom) and DHP^{+} (blue, bottom spectrum), compared to the actual reaction mixture of 5Et3MLF^{+}ClO$_4^{-}$ with DHP^{+} (green, top spectrum) in air at t = 90 min (500 MHz, CD_3CN).

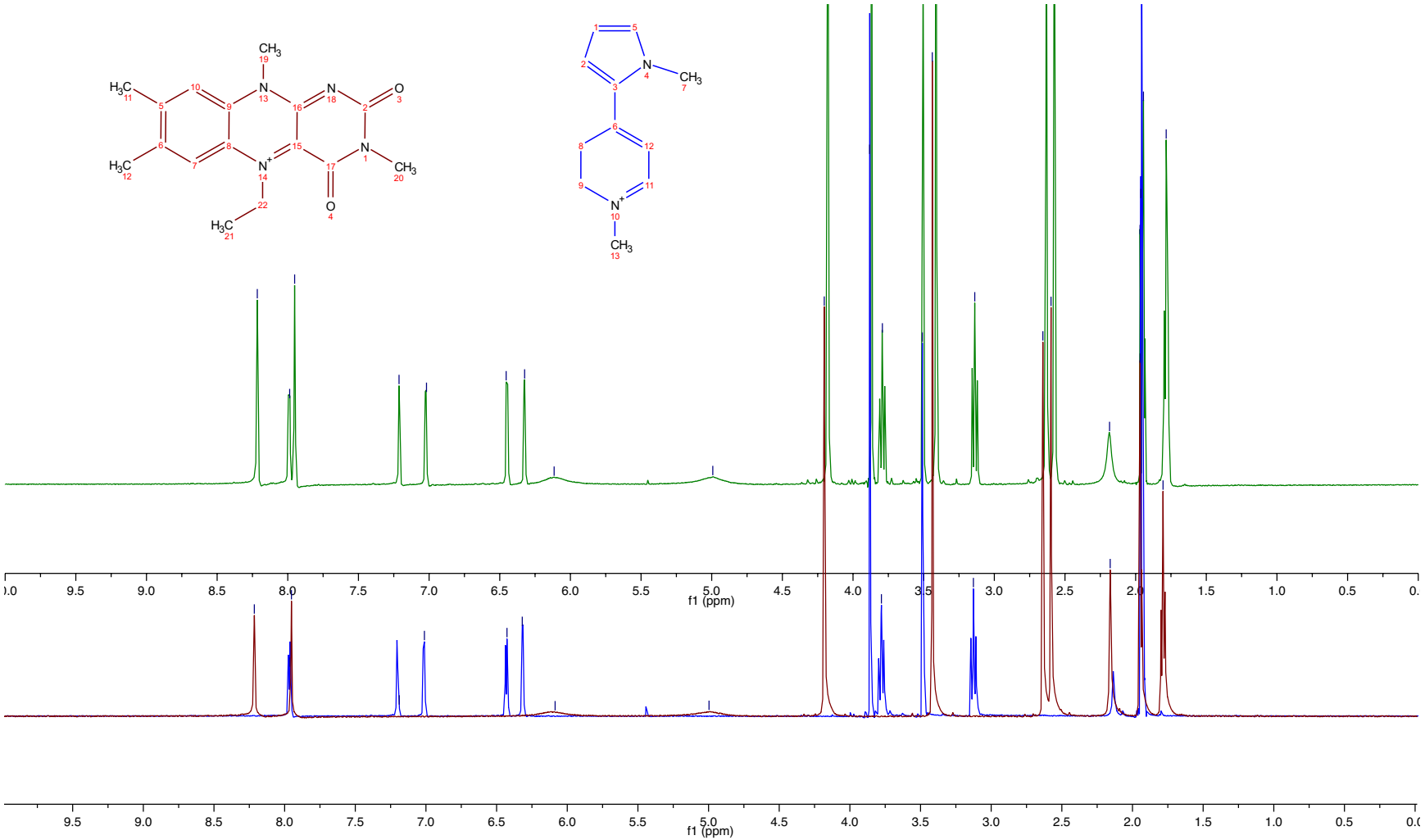

Figure 3-2-7 B. Comparison of ^{1}H NMR spectra under argon at t = 90 min. Superimposed image of ^{1}H NMR spectra of individual 5Et3MLF^{+}ClO$_4^{-}$ (maroon, botom) and DHP^{+} (blue, bottom spectrum), compared to the actual reaction mixture of 5Et3MLF^{+}ClO$_4^{-}$ with DHP^{+} (green, top spectrum) under argon at t = 90 min (500 MHz, CD_3CN).

Those NMR data suggested that **43**$^{+}$**ClO**$_4^{-}$ is not responsible for the oxidation of **49**$^{+}$. The solution of **49**$^{+}$ also did not undergo air oxidation either; **49**$^{+}$ in commercial grade acetonitrile was stable in the presence of air over days. Note that it is difficult to remove electrons from a positively charged species, and the oxidation of **49**$^{+}$ to **50**$^{+}$ involves the net loss of 2-electron. Therefore, the conversion of **49**$^{+}$ to its corresponding free base **54** might be an obligatory step for further oxidation. A remaining question is whether **43**$^{+}$**ClO**$_4^{-}$ oxidizes the DHP free base (**54**). Previously, the oxidation of MPDP^{+} (**2**$^{+}$) to MPP^{+} (**3**$^{+}$) at pH 7.4 was reported, indicating the oxidation of **2**$^{+}$ requires the presence of a base because the oxidation proceeds via the free base **2**.[64] The oxidation may proceed via disproportionation, a process that does not require the presence of air (Scheme 3-2-4).[64]

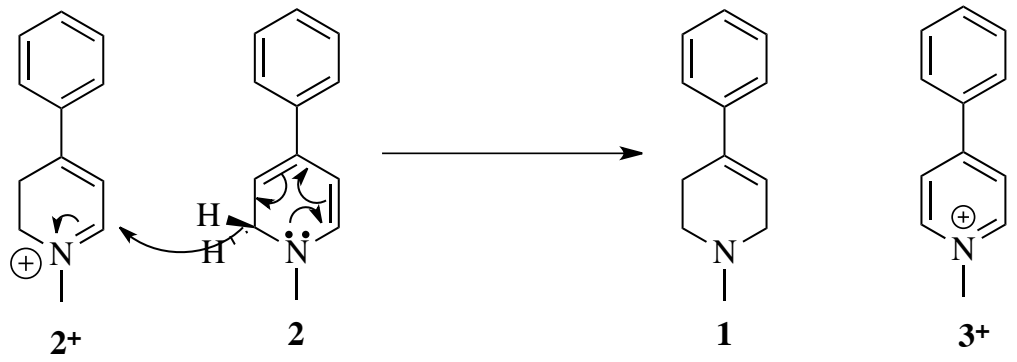

Scheme 3-2-4

Therefore, the next goal was to investigate whether DHP (**54**) is involved in the oxidation of DHP^{+} (**49**$^{+}$) to MMP^{+} (**50**$^{+}$) for the second 2-electron oxidation.

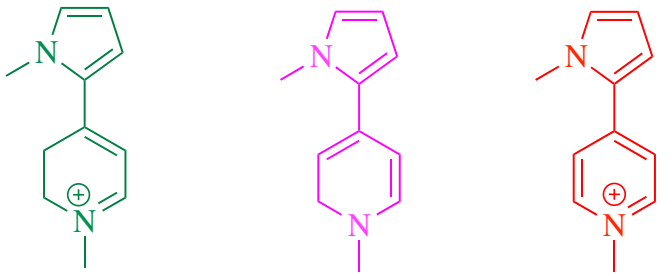

DHP^{+} DHP MMP^{+}

49^{+} **54** **50**$^{+}$

3.2.2.4 Disproportionation and Dioxygen Effects on the Conversion from the Intermediate DHP^+ to Oxidation Product MMP^+

To examine whether the conversion of DHP^+ (**49**$^+$) to its free base DHP (**54**) is required to occur prior to the second oxidation, a solution of authentic **49**$^+$**ClO**$_4^-$ was incubated in the presence of triethylamine [Et_3N (**53**)] but in the absence of **43**$^+$**ClO**$_4^-$. At first, authentic **49**$^+$**ClO**$_4^-$ was dissolved in commercial grade acetonitrile and then Et_3N was added to the solution of **49**$^+$**ClO**$_4^-$. The mixture was monitored by UV/vis, which indicated the generation of MMP^+ (**50**$^+$) in the presence of dioxygen over time. The results demonstrated that the presence of a base was obligatory for the conversion of **49**$^+$ into **50**$^+$ consistent with the understanding that the oxidation proceeds via the free base **54**. Scheme 3-2-5 illustrates a proposed disproportionation mechanism from one mole of **53** and two moles of **49**$^+$ to form protonated Et_3N (**53**H$^+$), **50**$^+$, and **4**. It was expected that if the disproportionation reaction made a major contribution to the formation of **49**$^+$ then compound **4** would be generated in a 1:1 molar ratio in the presence of **50**$^+$ as illustrated in Scheme 3.2.5.

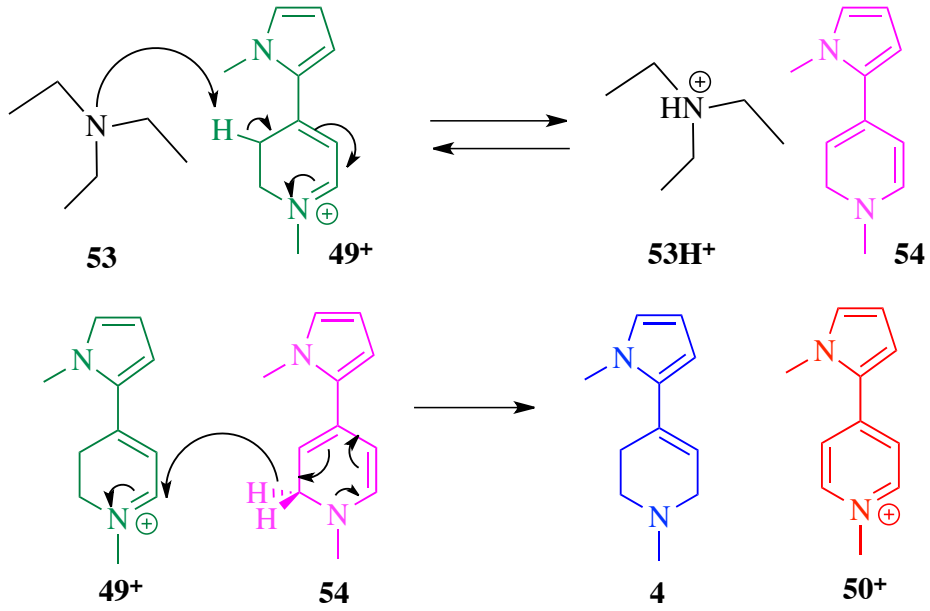

Scheme 3-2-5

The above results raised another question: Does the conversion from **49$^+$** to **50$^+$** proceed via air oxidation and/or disproportionation, and is the reaction dioxygen dependent? To examine these questions, a reaction mixture of **49$^+$ClO$_4^-$** (0.2 mM) and **53** (1.8 mM) in commercial grade acetonitrile was incubated either under argon or in air. The reaction mixtures were analyzed by UV/vis, NMR and accurate-mass ESI$^+$/MS.

In the past, excluding air during sample preparation was problematic because reaction mixtures needed to be diluted prior to sample readings when absorbances were measured using a 1 cm path length probe for UV/vis analysis. Thus, a shorter path length probe (0.2 cm) was used for this experiment, so that absorbance can be read without diluting samples, and air exposure can be minimized.

Both anaerobic and aerobic samples were protected from light and incubated for five days, which was chosen because it requires that long to nearly reach quantitative yield using a 0.2 cm path length probe. The anaerobic samples were capped and stored in an argon chamber at room temperature. After five days of incubation, absorbances were recorded without diluting the samples. To minimize air exposure, the anaerobic samples were purged with argon during measurements. UV/vis results indicated the reactions under both conditions generated the oxidation product **50$^+$** (Figures 3-2-7). When the reaction mixture was run under argon, the formation of **50$^+$** presumably occurred via disproportionation. The UV/vis results also demonstrated that the yield of MMP$^+$ (λ_{max} at 370) was greater under aerobic rather than anaerobic condition.

Under the aerobic conditions, quantitative yield was nearly reach while the percent yield was 62% for the reaction under aerobic conditions. The reason why no evidence of the dihydropyridinium starting material [authentic DHP$^+$ClO$_4^-$ (**49$^+$ClO$_4^-$**)] at 420 nm might be as a result of all **49$^+$ClO$_4^-$** being deprotonated by **53** by day 5 and **49$^+$** being in the process of the conversion to the product **50$^+$**.

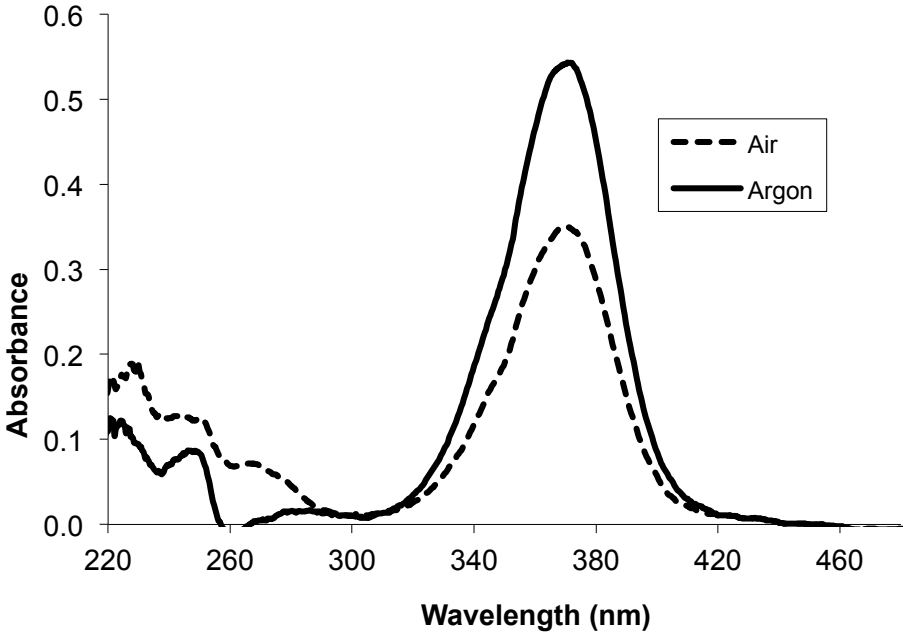

Figure 3-2-8. Comparison of UV/vis spectra. Superimposed image of the reaction mixture of authentic $DHP^+ClO_4^-$ (0.2 mM) and triethylamine (1.8 mM) in commercial grade acetonitrile after 5-days incubation under either anaerobic or aerobic conditions. Absorbances display the average of three samples. All samples were protected from light, and anaerobic samples were stored in an argon chamber.

The previous reaction mixtures were also examined using an accurate-mass ESI^+/MS analysis (Figure 3-2-9). Analysis of control samples (authentic $DHP^+ClO_4^-$ alone in commercial grade acetonitrile, incubated either in air or under argon) detected the ion corresponding to DHP^+ (**49$^+$**) at *m/z* 175, demonstrating that DHP^+ is stable in commercial grade acetonitrile over the five-day period in both conditions (Figure 3-2-9 A). On the other hand, when **49$^+$ClO$_4^-$** was incubated with Et_3N (**53**), the ion corresponding to MMP^+ (**50$^+$**) at *m/z* 173 was observed in both conditions (Figures 3-2-9 B and C).

Therefore, the combination of UV/vis and accurate-mass ESI^+/MS results suggests that authentic **49$^+$ClO$_4^-$** is capable of being oxidized into MMP^+ (**50$^+$**) *only in the presence of a base*. As proposed in Scheme 3-2-5, for the conversion of DHP^+ (**49$^+$**) to MMP^+ (**50$^+$**) via disproportionation, a step to form the conjugate base DHP (**54**) derived from DHP^+ (**49$^+$**) is obligatory. This finding is consistent with the previous finding (Scheme 3-2-4).[64]

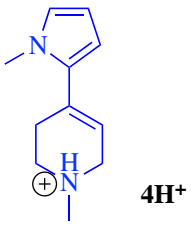

4H⁺

Exact Mass: 177.14

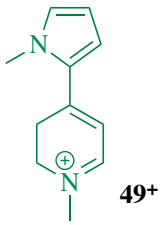

49⁺

Exact Mass: 175.12

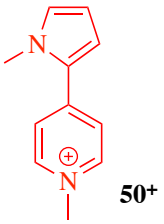

50⁺

Exact Mass: 173.11

A

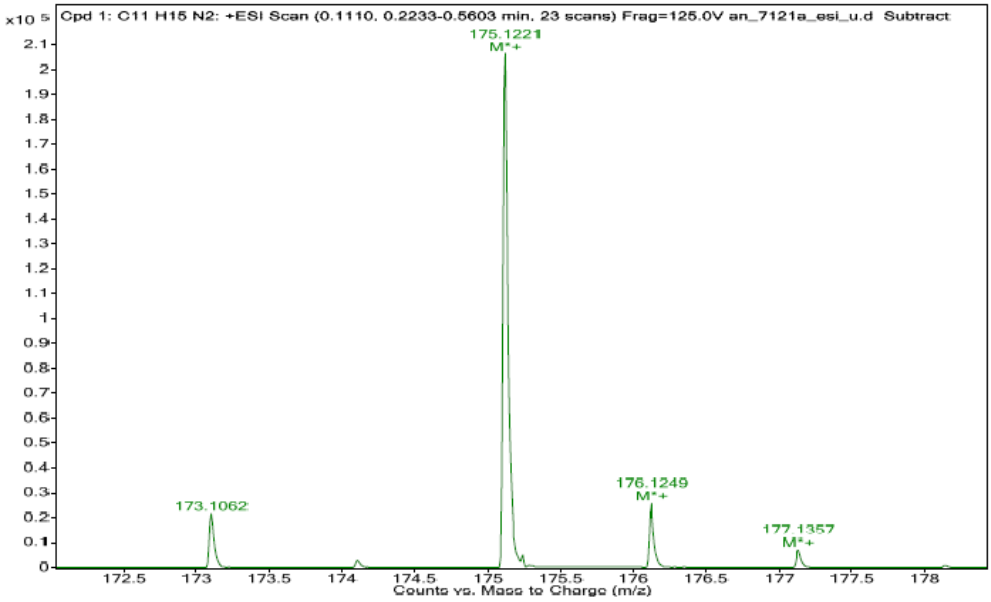

B

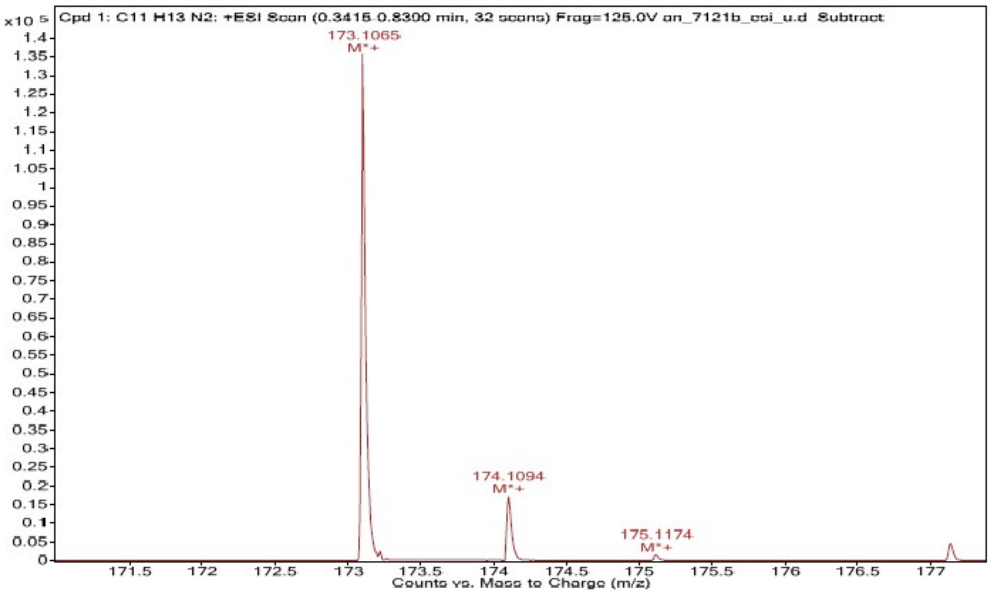

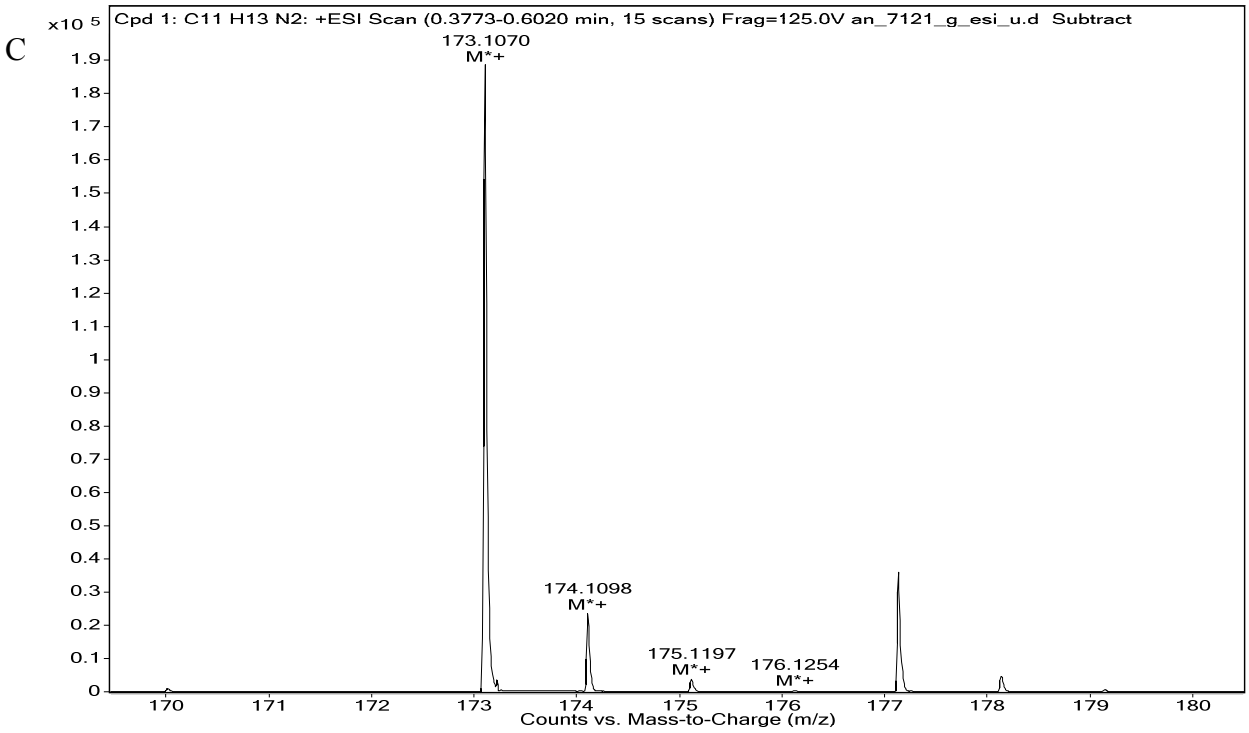

Figure 3-2-9. Accurate-Mass ESI$^+$ mass spectrum of the reaction product. The mixtures of authentic DHP$^+$ClO$_4^-$ (0.2 mM) and triethylamine (1.8 mM) were submitted after 5-days incubation in commercial grade acetonitrile. An expansion of the spectrum from *m/z* 170 to *m/z* 180 is shown. A, authentic DHP$^+$ClO$_4^-$ only; B, reaction in air; C, reaction under argon.

The same samples also were analyzed using NMR. To prepare for NMR analysis, the solvent (acetonitrile) was evaporated from the reaction mixtures by purging with dried argon, followed by the dissolution of the remaining species in acetonitrile-d_3. Figures 3-2-10 show that the peaks corresponding to the TMMP chemical shift were observed with the reaction under anaerobic (Figure 3-2-10 B) but not aerobic conditions (Figure 3-2-10 A). Recall that the disproportionation conversion involves the production of TMMP from the reaction between Et_3N (**53**) and DHP$^+$ (**49$^+$**) under argon (Scheme 3-2-5). The accurate-mass ESI$^+$/MS results identified the MMP$^+$ (**50$^+$**) generation occurred under anaerobic and aerobic conditions, whereas **4** was detected only under anaerobic conditions. Only the reaction proceeding via disproportionation can generate **4** (Figure 3-2-10 B).

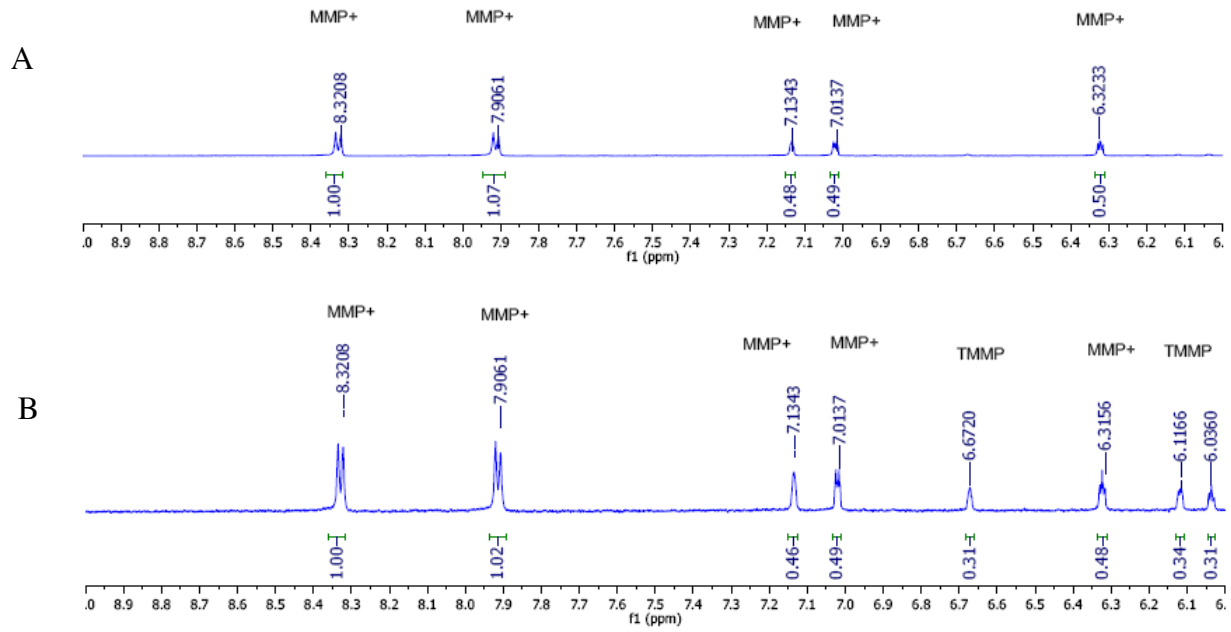

Figure 3-2-10. Comparison of ^{1}H NMR spectra between the reaction in air and under argon. ^{1}H-NMR spectra (500 MHz, CD_3CN) of the reaction mixture authentic $DHP^+ClO_4^-$ and triethylamine: A in air and B under argon.

In summary, the conversion of the intermediate DHP^+ (**49$^+$**) into MMP^+ (**50$^+$**) requires the presence of a base as **49$^+$** must be converted into DHP (**54**) prior to the generation of **50$^+$**. The sequence of reactions described in this section is illustrated in Scheme 3-2-6. The reaction between authentic $DHP^+ClO_4^-$ (**49$^+$ClO$_4^-$**) and Et_3N (**53**) requires five days to reach nearly quantitative yield. In respect to the mechanism, both air oxidation and disproportionation are likely responsible for the conversion. Under aerobic conditions, the oxidation product **50$^+$** was formed in a nearly quantitative yield compared to 67% under anaerobic conditions. This suggests that this reaction is air sensitive; when dioxygen is available, the conversion from **54** to **50$^+$** will most likely proceeds by air oxidation. With regards to the rate of the MMP^+ formation, the disproportionation may not be negligible in the presence of air. In order to produce one mole of the final product **50$^+$**, two moles of the starting material **4** are required since the intermediate **49$^+$** must be deprotonated by a base in order to initially be converted to **54**, followed by the generation of **50$^+$**.

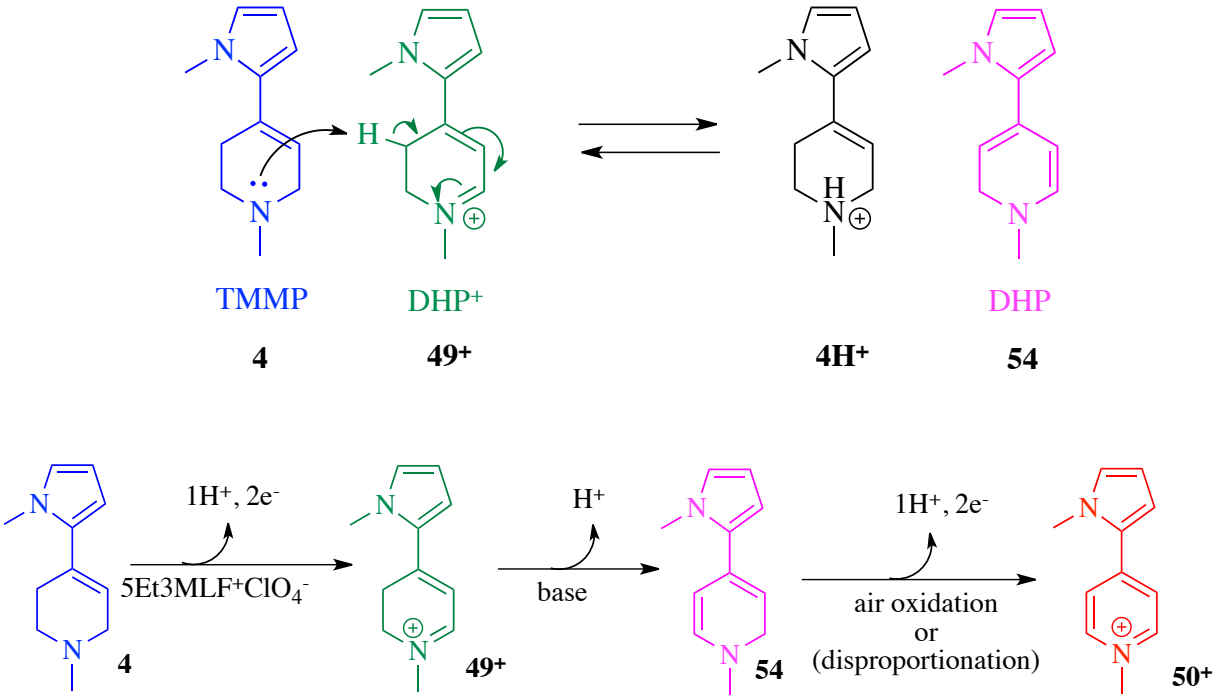
TMMP
DHP+
DHP
4
49+
4H+
54
1H+, 2e-
5Et3MLF+ClO4-
H+
base
1H+, 2e-
air oxidation
or
(disproportionation)
4
49+
54
50+

Scheme 3-2-6

3.2.2.5 Effect of Dioxygen on TMMP Oxidation with 5Et3MLF$^+$ClO$_4^-$

Because the second part of the TMMP oxidation was oxygen dependent, the next goal was to determine whether the first 2-electron oxidation was also air sensitive. To examine the effect of dioxygen on the reaction between 5Et3MLF$^+$ClO$_4^-$ (**43$^+$ClO$_4^-$**) (25 mM) and TMMP (**4**)(50 mM), these two starting materials were mixed in dried acetonitrile-d_3 (pre-treated with CaH_2 and then distilled under argon) in a glove box to avoid any oxygen-contamination. Prior to the experiment, compounds **43$^+$ClO$_4^-$** and **4** were shown to be pure by UV/vis and NMR. A total of four NMR samples were prepared anaerobically for this experiment. To clarify the difference between aerobic and anaerobic samples, reaction times are presented as T_{air} (reaction time in air) and T_{ag} (reaction time under argon) in this chapter.

As soon as the starting materials were mixed in a glove box, the solution's color changed from purple to bluish/green. This observation suggests an instant reaction between **43$^+$ClO$_4^-$** and **4**, because each starting material is stable in acetonitrile. Also, the color change may indicate a single electron transfer to the flavinium salt **43$^+$ClO$_4^-$** because violet-blue color is reported as 5Et3MLF neutral radical [5Et3MLF$^\bullet$ (43$^\bullet$)].[63] This difference in colors of **43$^+$ClO$_4^-$** and the reported 5Et3MLF neutral radical [5Et3MLF$^\bullet$ (43$^\bullet$)] is shown in Figure 3-2-11.

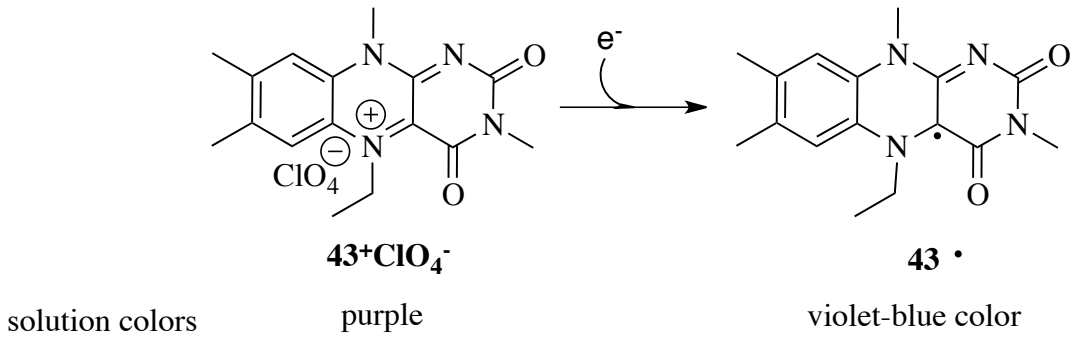

Figure 3-2-11. Solution colors of 5Et3MLF$^+$ClO$_4^-$ and the 5Et3MLF neutral radical in acetonitrile.[65]

The color change indicated that the initial reaction does not require oxygen and that **43^{+}ClO$_4^{-}$** and **4** interacted quickly. A ^{1}H NMR spectrum of anaerobic samples obtained immediately after mixing these starting materials is shown in Figure 3-2-12 (T_{ag} = 0 min).

One of the most obvious features of the NMR spectrum at T_{ag} = 0 min was that any signals corresponding to **43^{+}ClO$_4^{-}$** as well as **43^{+}** derived intermediates were absent. The signals that do appear in the spectra (Figure 3-2-12) are tentatively assigned to **4H^{+}.** It is not clear how much TMMP was converted **4H^{+}** and how much of TMMP underwent the oxidation with **43^{+}ClO$_4^{-}$**. Quantification has been one of the challenges throughout the project. Because the formation of radicals and silent NMR are involved, addition of an internal standard has never been particularly successfully especially at the earlier stages of this reaction. Because the stoichiometry was 1 to 2, in favor of TMMP, it might be logical to suggest that one mole of TMMP reacted the flavinium salt and the other mole of TMMP was protonated as **4H^{+}** during the course of reaction. This "silent NMR" behavior is attributable to the formation of radicals, and the flavin radical was detected by EPR under these conditions (Figure 3-2-18). The fate and structure of TMMP-derived radicals were not detected by EPR.

Another important observation with the reaction under argon was that NMR signals, which are potentially associated with flavinium-derived intermediates, appeared after dioxygen was re-introduced to the reaction mixture, suggesting that unpaired electron formation (radical formation) occurs immediately after mixing the two starting materials, and dioxygen comes in to play afterwards.

The "NMR silence" behavior was observed immediately after two starting materials were mixed under argon, and the behavior was continuously observed until the air was re-introduced. Developing NMR signals of the product (MMP) were then observed afterward (followed by the re-introduction of air).

The signals associated with the pyridinium ring of TMMP shifted from downfield to upfield during the course of the reaction after the air was re-introduced, while the signals associated with the pyrrol did not shift on the NMR spectra. For example, the N-methyl signal in the pyridinium

ring shifted from 2.62 ppm (reaction under argon) to 2.40 ppm (24 hours after the air was re-introduced), whereas the N-methyl signal in the pyrrol ring occurred at the region of 3.60 ppm during the course of the reaction. Please see Appendix E for more details. It is likely that this chemical shift changed due to characteristics of spectator anions (intermediates).

The NMR results indicated a small amount of MMP^+ (**50**$^+$)(δ = 8.33, 7.91, 7.13 and 7.02 ppm) immediately after mixing **43**$^+$**ClO**$_4^-$ and **4** in degassed/dried acetonitrile-d_3 inside a glove box. Hence, this reaction must occur quickly.

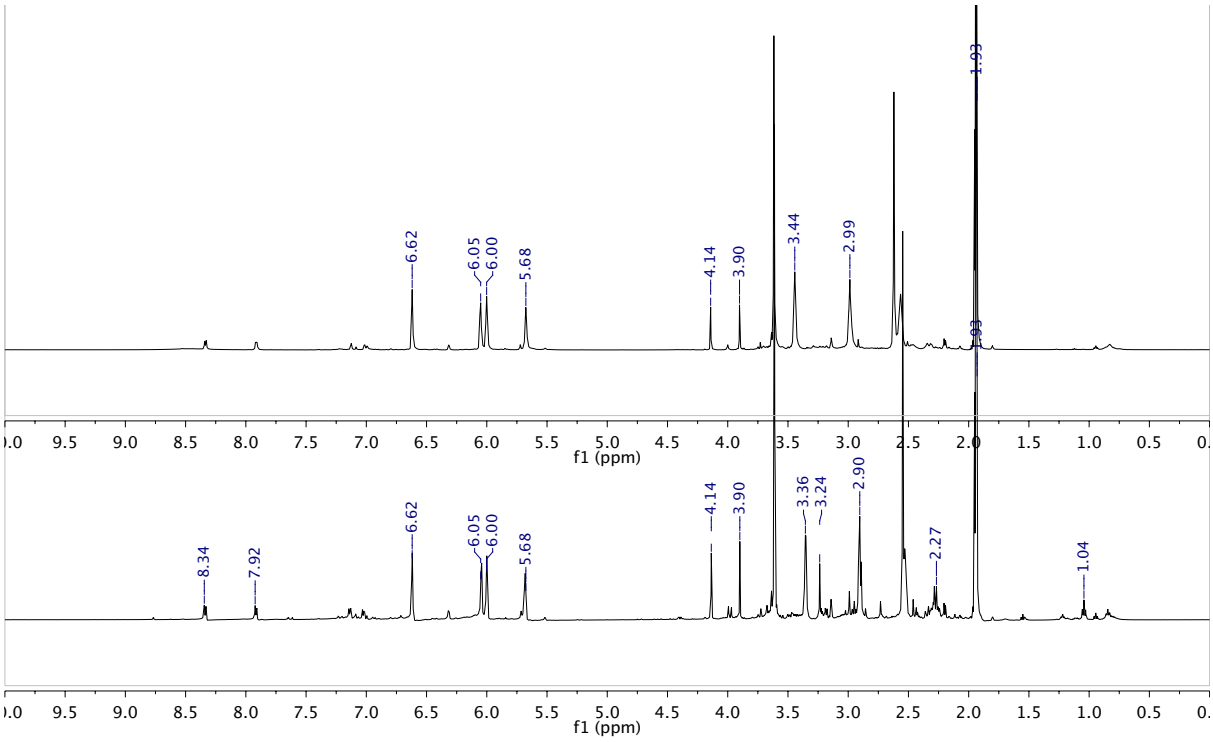

Figure 3-2-12. Comparison of ^{1}H NMR spectra. ^{1}H NMR (500 MHz, CD_3CN) spectra of the reaction product of 5Et3MLF$^+$$ClO_4^-$ (25 mM) with TMMP (50 mM) in dried acetonitrile-d_3 under argon obtained immediately after mixing (top, T_{ag} = 0 min) and immediately after air exposure (bottom, T_{air} = 0 min)

After recording the NMR spectrum of anaerobic samples immediately after mixing **43**$^+$**ClO**$_4^-$ and **4** at T_{ag} = 0 min, aerobic samples were generated by adding dried air to the anaerobic samples, while the other two samples remained under argon (two aerobic samples and two anaerobic samples). Immediately after air was introduced, another NMR spectrum was recorded for the

aerobic samples; this spectrum is shown at T_{air} = 0 min (Figure 3-2-11, bottom). The aerobic samples were kept away from dioxygen for approximately 15 – 20 min. The samples were protected from light and stored in the dark, and the reaction was monitored using NMR.

The NMR data show that the protons in the tetrahydropyridinyl group of **4** are shifted in the anaerobic reaction mixture compared to that with the TMMP free base. Figure 3-2-13 shows the comparison of the signals in the ^{1}H NMR spectra between authentic $\mathbf{4H^+ClO_4^-}$ alone[62] and the reaction mixture of $\mathbf{43^+ClO_4^-}$ and **4** at T_{air} = 0 min in acetonitrile-d_3. The NMR results indicated that the signals of the three hydrogens and N-methyl protons in the tetrahydropyridinium group were deshielded in the reaction mixture, compared to the authentic $\mathbf{4H^+ClO_4^-}$ alone. This observation may be due to $\mathbf{4H^+}$ having a different counterion in the reaction mixture.

Also, the signal of the N-methyl protons in the tetrahydropyridinium group at δ 2.54 ppm appear as a weaker intensity in the reaction mixture, compared to the N-methyl protons in the pyrrol group (Figure 3-2-13, bottom). Also, the chemical shift of the signals in the tetrahydropyridinium group moves to the upfield as the reaction progresses. This might suggest formation and consumption of intermediates during the reaction.

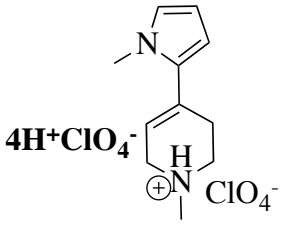

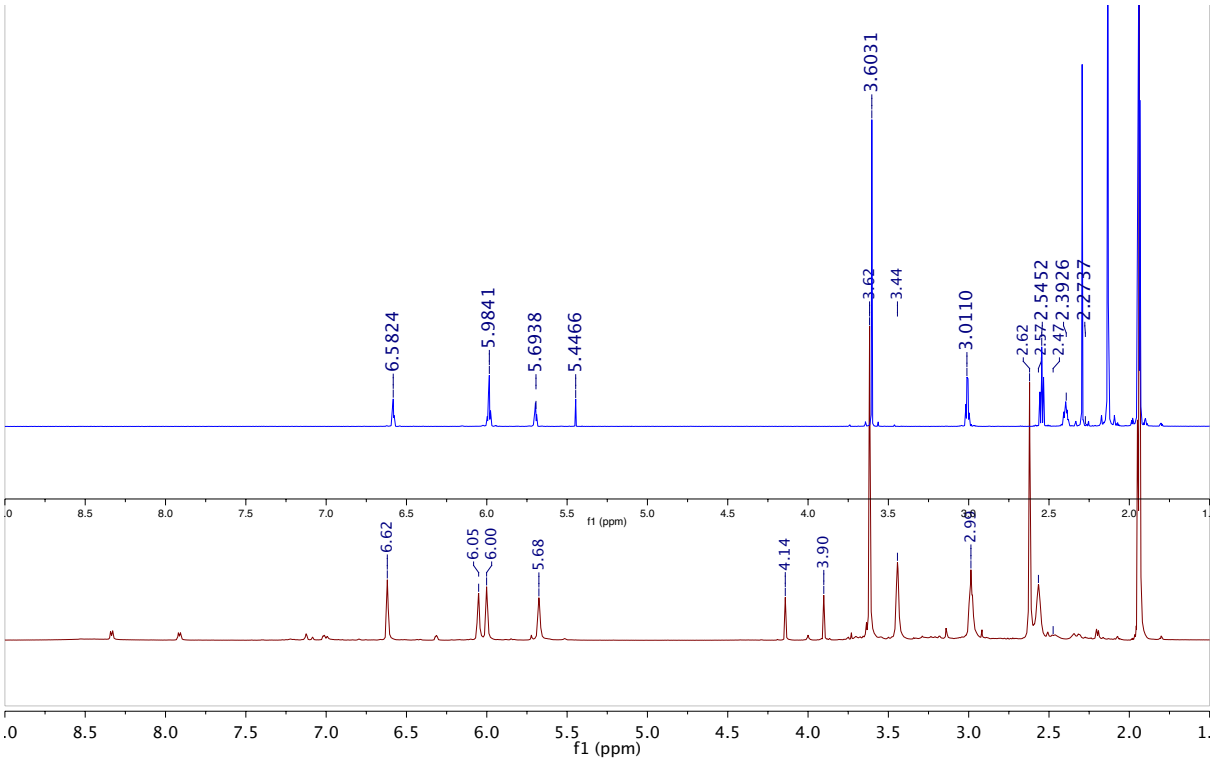

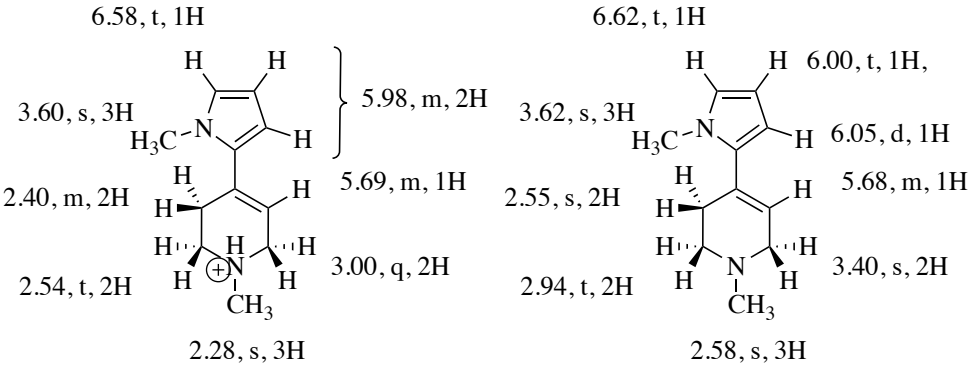

Figure 3-2-13. Comparison of ^{1}H NMR spectra between TMMP and the reaction mixture. ^{1}H NMR spectra show TMMP (blue) and the reaction product (maroon) of 5Et3MLF^{+}ClO$_4^{-}$ (12.25 mM) with TMMP (25.5 mM) in dried acetonitrile-d_3 under argon (T_{ag} = 0 min) (500 MHz, CD_3CN). Assignments of ^{1}H NMR chemical shifts of TMMP in acetonitrile-d_3: TMMPH^{+}ClO$_4^{-}$ (left) and TMMP with the presence of 5Et3MLF^{+}ClO$_4^{-}$ at T_{ag} = 0 min (right). The peak at δ 5.45 ppm in TMMP solution (blue line) represents CH_2Cl_2 from preparation. It was evaporated and removed prior to the reaction experiment.

Next, the NMR sample solutions were also analyzed using accurate-mass ESI$^+$/MS on day 3. Figures 3-2-14 A and B show mass spectra of the anaerobic and aerobic samples. The anaerobic samples were transferred and diluted in a glove box. In the aerobic reaction mixture (control condition), the molecular composition of the intense ion at *m/z* 173.1074 corresponds to the oxidation product **50$^+$** (δ 0.0 mDa). The key difference between the aerobic and anaerobic reactions was that the main peak under aerobic conditions corresponds to **50$^+$** at *m/z* 173. 1074, while the main peak under anaerobic condition corresponds to TMMP [MH$^+$ at *m/z* 177.1383] and a mass accuracy of -1.69 ppm (0.3 mDa). The less intense ion at *m/z* 175 corresponds to the intermediate dihydropyridinium species. Conversely, the accurate-mass ESI$^+$/MS data for the anaerobic reaction are difficult to interpret. No explanation can be offered for the ion at *m/z* 187.1223 at this time. However, this ion has been constantly observed in argon samples. Additionally, the second intense ion at *m/z* 189.1385 in this spectrum may be assigned to the imidazolium species, which will be discussed in Section 3-2-7.

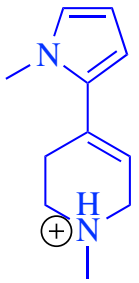

4H$^+$

Exact Mass: 177.1386

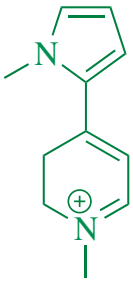

49$^+$

Exact Mass: 175.1230

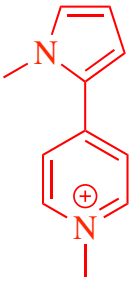

50$^+$

Exact Mass: 173.1073

A

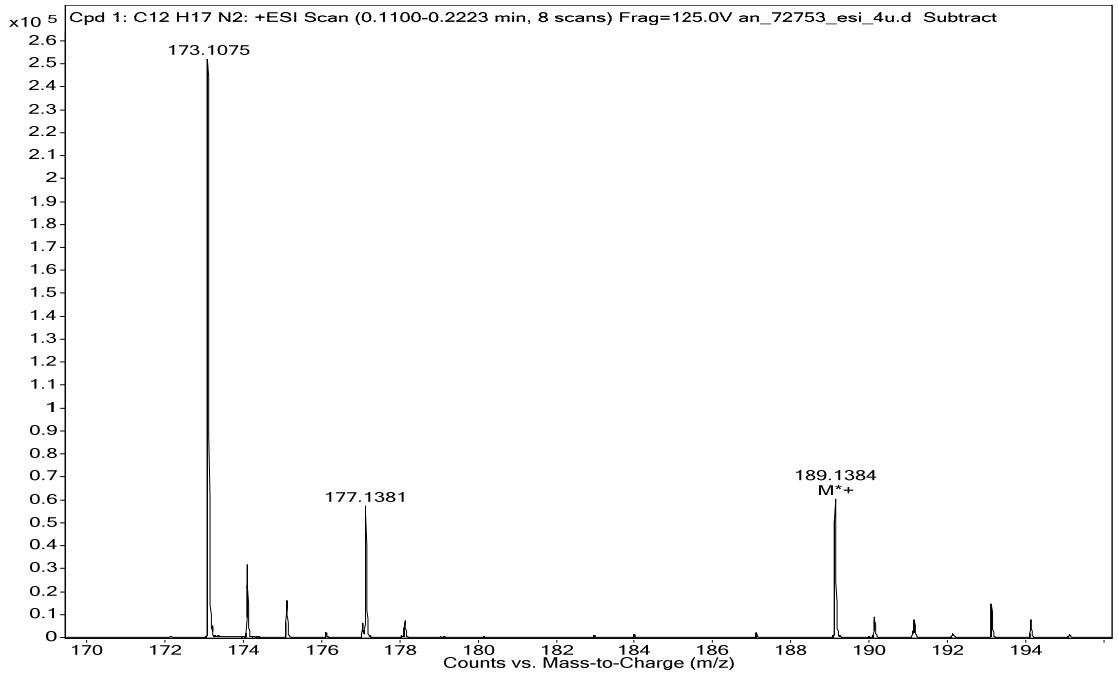

B

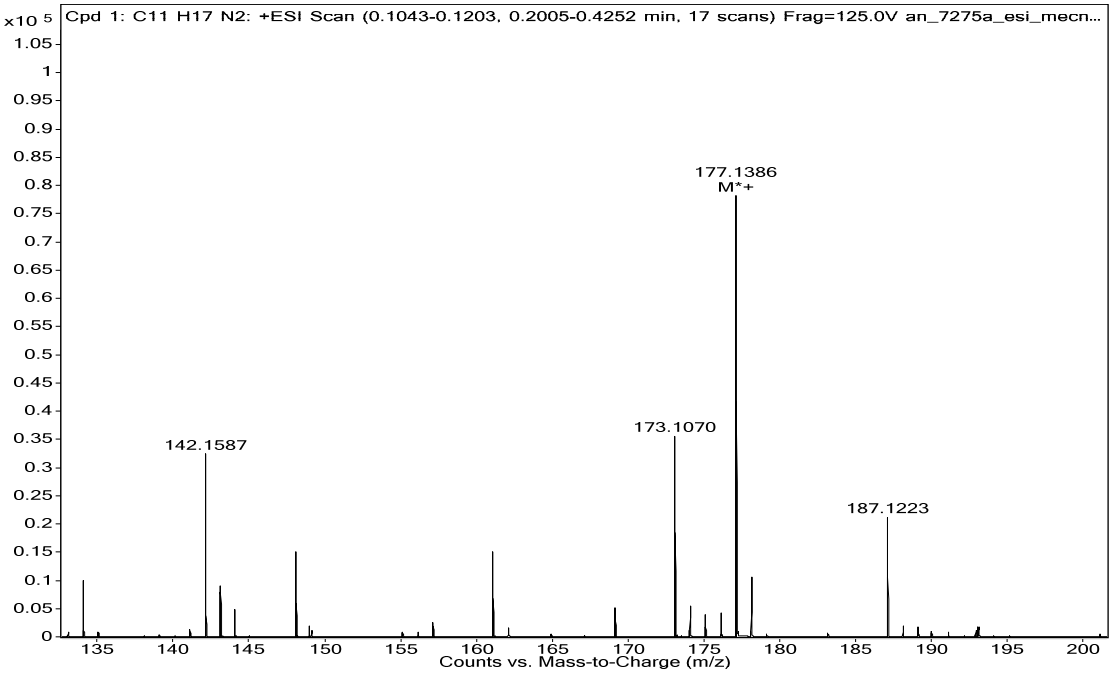

Figure 3-2-14. Accurate-mass ESI$^+$ mass spectra of the reaction product. Mass spectra show the reaction of 5-ethyl-3-methyllumiflavinium perchlorate (12.25 mM) with 1-methyl-4-(1-methylpyrrol-2-yl)-1,2,3,6- tetrahydropyridine (25.5 mM) in dried acetonitrile under aerobic conditions (A) and under anaerobic conditions (B). An expansion of the spectrum from *m/z* 130 to *m/z* 200 is shown.

Following the NMR and ESI$^+$ analyses, the same reaction mixture (**43$^+$ClO$_4^-$** and **4**, 12.25 mM and 25.5 mM) was further analyzed on day 3 using the UV/vis spectroscopy. Only the aerobic samples generated significant concentrations of the oxidation product **50$^+$** (Figure 3-2-15 A), which is consistent with the NMR and accurate-mass ESI$^+$/MS data. The absorbance at λ_{max} of 368 nm (marker of **50$^+$**) was 1.10 for the aerobic sample (Figure 3-2-15 A), and the concentration of **50$^+$** at day 3 is 19.01 mM (dilution factor 500), indicating something else overlaps at the 368 nm region.

There was a significant difference between aerobic and anaerobic reaction mixtures in UV/vis spectra (Figures 3-2-15 A and B). The UV/vis spectrum in the anaerobic reaction mixture showed a wide peak at 500 nm to 700 nm and also other peaks at 490 nm, 450 nm, and 370 nm.

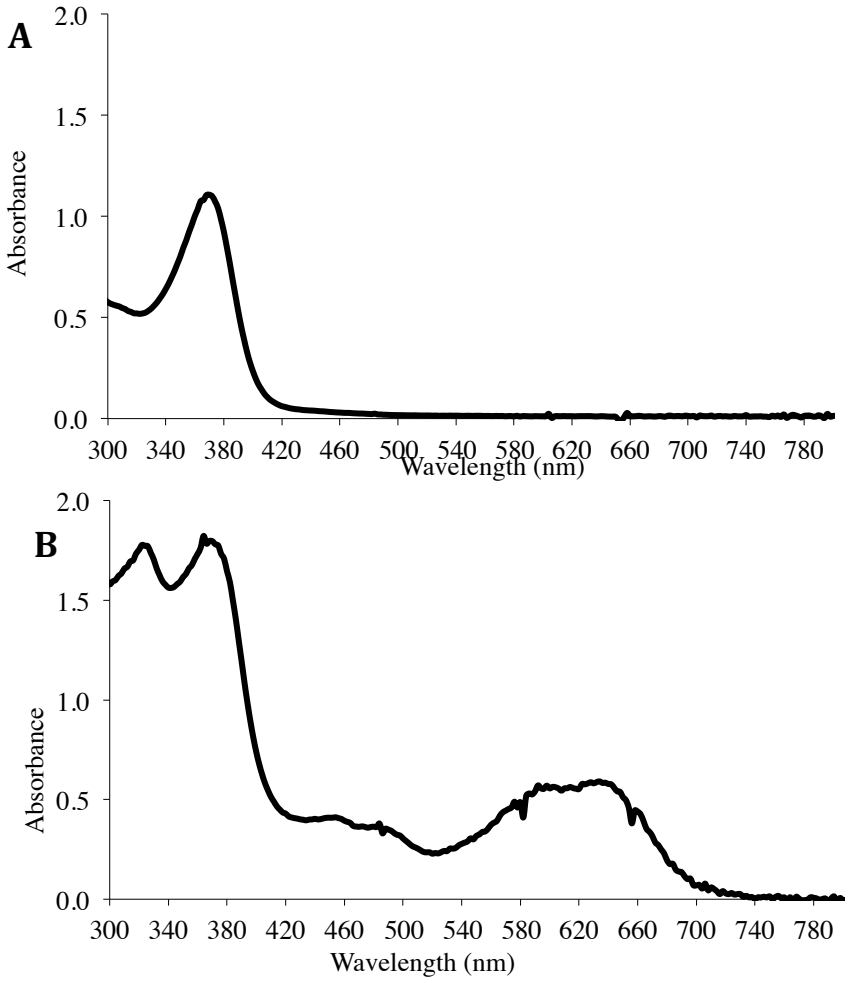

Figure 3-2-15. UV/vis spectra of the reaction mixture. The reaction of 5Et3MLF$^+$ClO$_4^-$ (25 mM) and TMMP (50 mM) in dried acetonitrile: aerobic sample (A) and the anaerobic sample (B) at room temperature.

A similar UV/vis spectrum in the anaerobic reaction mixture (Figure 3-2-15 B) was reported previously (Figure 3-2-16).[66] Their reported λ_{max} (ε) data of the 5Et3MLF neutral radical in acetonitrile as 631 (6000), 600 (5700), 486 (3500), 456 (3400), 379 (7700), and 324 nm (8600). According to their reported ε values, the concentration of the 5Et3MLF neutral radical in the reaction mixture of **43^{+}ClO$_4^{-}$** and **4** and under anaerobic conditions was 12.5 mM using the absorption at 600 nm, 12.1 mM at 456 nm, and 27.6 mM at 379 nm (dilution factor 125)[nearly a half of quantitative conversion of **43^{+}ClO$_4^{-}$** to the 5Et3MLF radical (**43•**)].

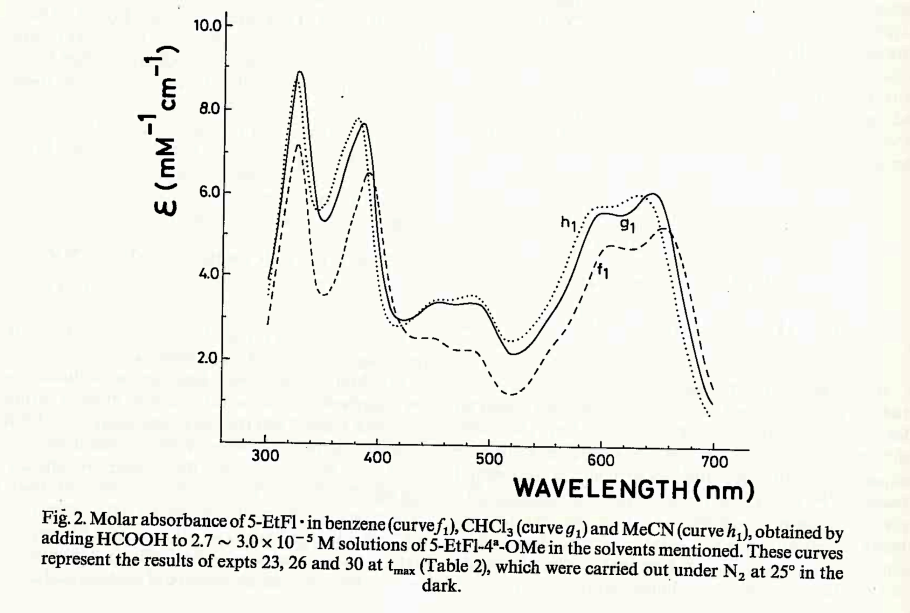

Fig. 2. Molar absorbance of 5-EtFl · in benzene (curve f_1), $CHCl_3$ (curve g_1) and MeCN (curve h_1), obtained by adding HCOOH to 2.7 ~ 3.0 × 10^{-5} M solutions of 5-EtFl-4^a-OMe in the solvents mentioned. These curves represent the results of expts 23, 26 and 30 at t_{max} (Table 2), which were carried out under N_2 at 25° in the dark.

Figure 3-2-16. Published UV/vis spectra of the flavinium radicals. Curve h1 is in acetonitrile.[66§§] Reprinted from Electron transfer-II: Accumulation of 5-ethyl-3-methyllumiflavin radical by spontaneous conversions of 5-ethyl-3- methyllumiflavinium salts, 41/1, Mager H.I.X. and Addink, R., Tetrahedron, 183-190, Copyright (2013), with permission from Elsevier.

The UV/vis spectrum of the anaerobic sample (Figure 3-2-15 B) is similar to the reported 5Et3MLF radical spectrum (Figure 3-2-16).[66] Other researchers also reported **43•** with their findings also consistent with this study's reaction spectrum.[67] In short, the findings support the radical formation in the reaction mixture between **43^{+}ClO$_4^{-}$** and **4.**

§§ License agreement document shown in Appendix F.

The next objective was to record the UV/vis spectrum of the 5Et3MLF neutral flavin radical (**43•**). A particular challenge for obtaining the UV/vis spectrum of the neutral flavin radical was to overcome the unstability of **43•**. The yield of the flavin radical (•FlH) is only 2% of the total flavin present in solution because the equilibrium favors the right, due to the disproportionation [$2FlH^{\bullet} \rightleftharpoons Fl + FlH_2$].[68] According to Muller (1987), the addition of non-redox active metal ions to a "half-reduced" flavin solution (**42** and **42H$_2$**) at neutral pH stabilizes the flavin radical (**42H•**) and leads to a considerable increase in radical concentration because of shifting of the equilibrium in favor of the flavin-metal complex (**42H•M$^+$**)(Scheme 3-2-9).[68b]

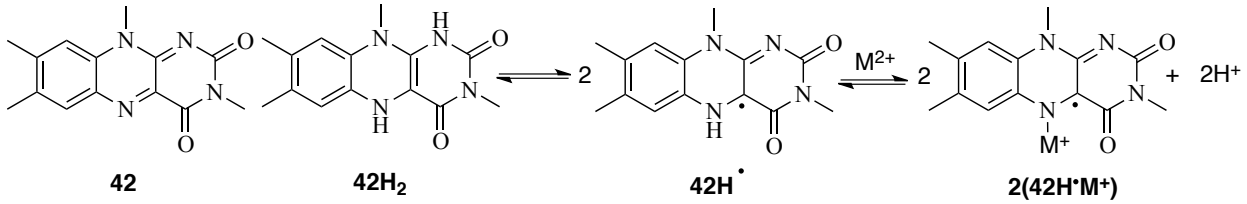

Scheme 3-2-9

Therefore, a formation of the neutral flavin radical was attempted by treating **43$^+$ClO$_4^-$** and $Na_2S_2O_4$ (1 to 1 ratio) with $ZnCl_2$ in commercial grade acetonitrile at room temperature (Scheme 3-2-10).

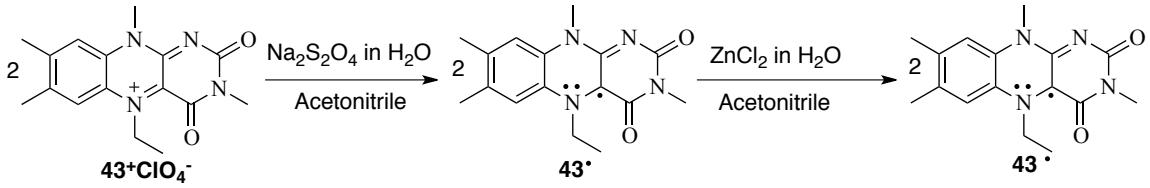

Scheme 3-2-10

To obtain the neutral flavin radical, the flavinium salt **43$^+$ClO$_4^-$** was dissolved in commercial grade acetonitrile (Solution 1), and a few drops of deionized H_2O with the reducing agent $Na_2S_2O_4$ added to the 5Et3MLF solution (Solution 2). Lastly, several drops of deionized H_2O

with $ZnCl_2$ were added to the reduced 5Et3MLF solution in order to stabilize the neutral flavin radical (Solution 3).

Figure 3-2-17 displays a comparison of the UV/vis spectra from the $5Et3MLF^+ClO_4^-$ (**$43^+ClO_4^-$**) combined with the neutral flavin radical in solution. The dashed line shows **$43^+ClO_4^-$** alone (**$43^+ClO_4^-$** in acetonitrile), and the chromophores are found at λ_{max} 420 nm and 520 nm. The long dash dot line displays the reduced 5Et3MLF solution, prepared by mixing **$43^+ClO_4^-$** in acetonitrile with a few drops of H_2O with $Na_2S_2O_4$; a relatively sharp peak at 350 nm and a wide range peak at 555 nm are visible. Reported absorbances of the fully reduced 5Et3MLF are reported as chromophores at λ_{max} of 345 nm and 245 nm at pH 5.[61a]

The solid line demonstrates the neutral flavin radical (flavosemiquinone), which was prepared by adding the non redox active metal ion (Zn^{2+}) to the reduced 5Et3MLF solution. The UV/vis spectrum of the neutral flavin radical that showed a wide region of a high wavelength peak was recorded (λ_{max} 540 nm - 680 nm). Recall that a similar high wavelength peak (λ_{max} 540 nm - 680 nm) was also observed with the reaction mixture of **$43^+ClO_4^-$** with **4** under anaerobic conditions (Figure 3-2-17B). Conversely, the reduced 5Et3MLF peaks were not observed on the UV/vis spectra of the reaction mixture in air or under argon.

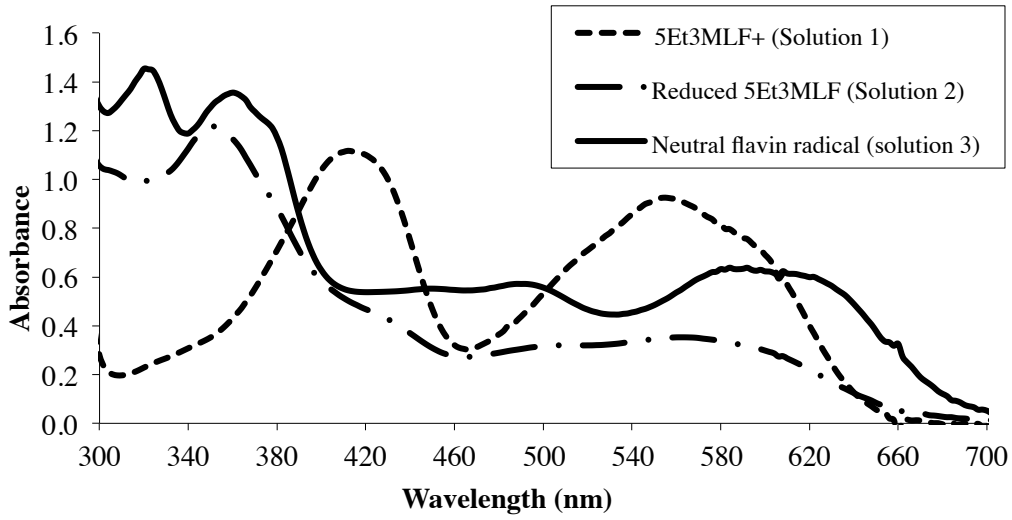

Figure 3-2-17. Comparison of the UV/vis spectra. The spectra show the comparison of the $5Et3MLF^+ClO_4^-$ and the neutral flavin radical: the $5Et3MLF^+ClO_4^-$ solution in commercial grade acetonitrile (dashed line), the reduced 5Et3MLF solution (long dash dot), and neutral flavin radical (solid) at room temperature.

Accordingly, since the neutral flavin radical (solid line in Figure 3-2-17) and the reaction mixture under argon (Figure 3-2-15B) are almost identical, the reaction mixture was examined further using EPR analysis. The EPR analysis detected radicals in the reaction mixture (Figure 3-2-18A), and the spectrum was almost identical to the neutral 5Et3MLF radical (**43•**) reported by Muller 1972 (Figure 3-2-18B). Figure 3-2-18A suggests that **43•** is delocalized over the entire framework and not localized on a single atom (Scheme 3-2-11). If it were only present on the nitrogen, one would expect to see far fewer lines. In addition, the EPR spectrum was recorded on Day 12 after mixing $\mathbf{43^{+}ClO_4^{-}}$ and **4** in acetonitrile, which suggests that **43•** are stable in the solution for at least 12 days.

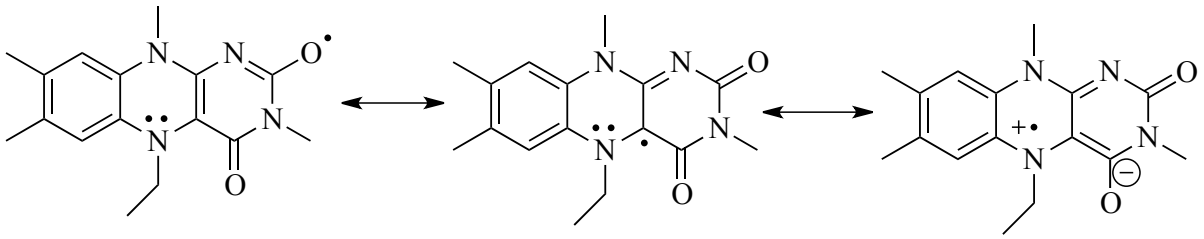

43 •

Scheme 3-2-11

A

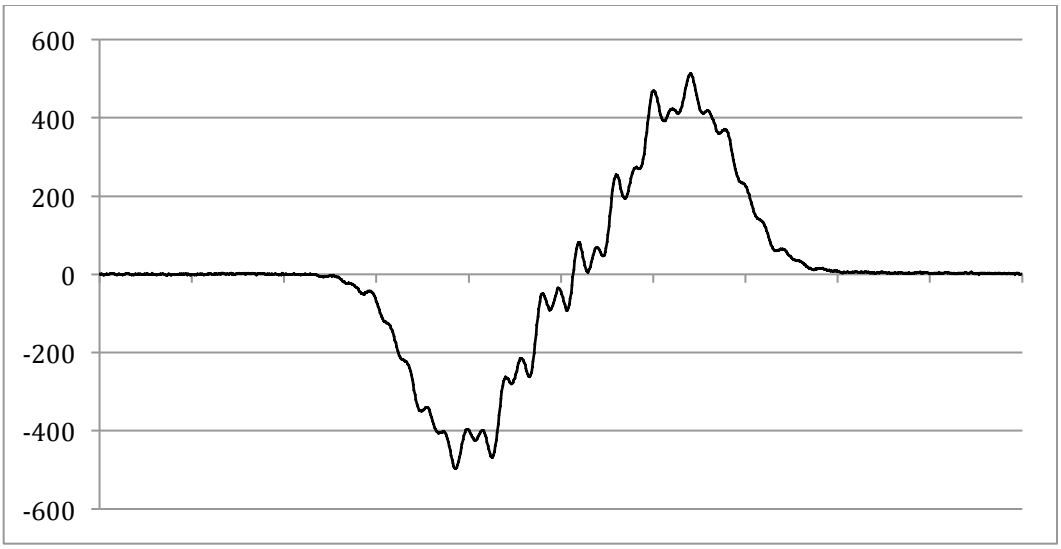

B

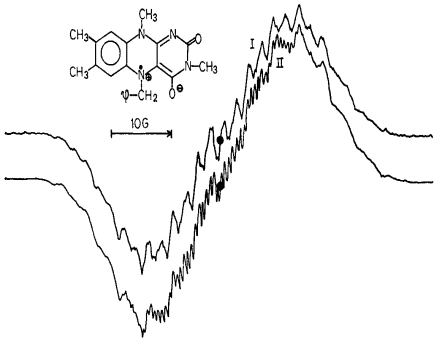

Fig. 4. *Electron-spin-resonance signals obtained from 3-methyl-5-benzyl-monohydrolumiflavin, prepared by air oxidation of the 1,5-monohydro-analog [13] in 50% methanolic phosphate buffer pH 7 (I), in the absence and (II) in the presence of 1 M ammonium benzoate under the same conditions of measurement.* The additional superhyperfine splitting due to benzoate association is of the order of 1 gauss

Figure 3-2-18. Comparison of EPR spectra between the reaction mixture and published flavin radicals. The spectra show the reaction of 5Et3MLF^{+}ClO$_4^{-}$ 12.25 mM and TMMP 25.5 mM in dried acetonitrile-d_3 under argon at t = day 12 (A) and a published spectrum of the neutral 5Et3MLF radical (B).[67b] Reprinted by permission from John Wiley and Sons: [FEBS JOURNAL](Mller, F. *et al*., Light-absorption studies on neutral flavin radicals. 1972, 25 (3), 573-580), DOI:10.1111/j.1432-1033.1972.tb01730.x, copyright (2005)[***]

The next goal was to determine whether the reduced 5Et3MLF (**43H$_2$**) was formed in the course of the reaction from **43^{+}ClO$_4^{-}$** and **4**. It has been previously reported that the flavinium salt **43^{+}ClO$_4^{-}$** is first fully reduced to form **43H$_2$**. And, **43H$_2$** now reacts with dioxygen to generate the 4a-hydroperoxyl adduct of 5Et3MLF (**52**) (Scheme 3-2-13)[69].

[***] License agreement document shown in Appendix G.

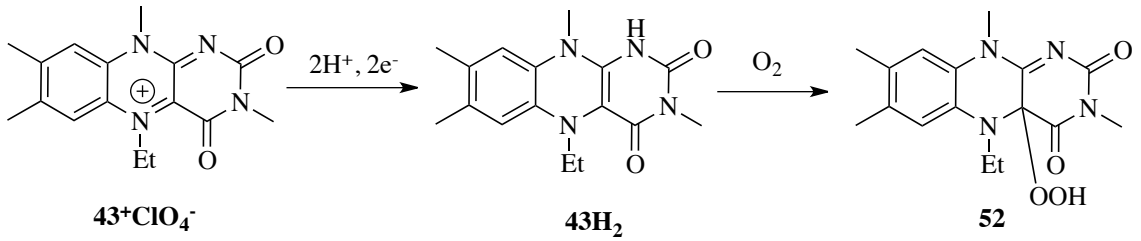

43⁺ClO₄⁻ **43H₂** **52**

Scheme 3-2-13[69a]

However, the ^{1}H-NMR spectrum of the reaction mixture (**43⁺ClO₄⁻** and **4**, 1 to 2 molar ratio) does not indicate the reduced form of 5Et3MLF (**43H₂**). Figure 3-2-19 displays the ^{1}H NMR spectrum of **43H₂**, synthesized by mixing **43⁺ClO₄⁻** in acetonitrile-d_3 and a couple of drops of D_2O containing $Na_2S_2O_4$: δ = 6.66 and 6.57 ppm (s, Ar-H, 2H), 3.22 – 3.16 ppm (q, CH_2CH_3, 2H), 3.13 and 3.12 ppm (s, N-CH_3, 6H), 2.14 and 2.10 ppm (s, Ar-CH_3, 6H), and 0.98 ppm (t, CH_2CH_3, 3H).

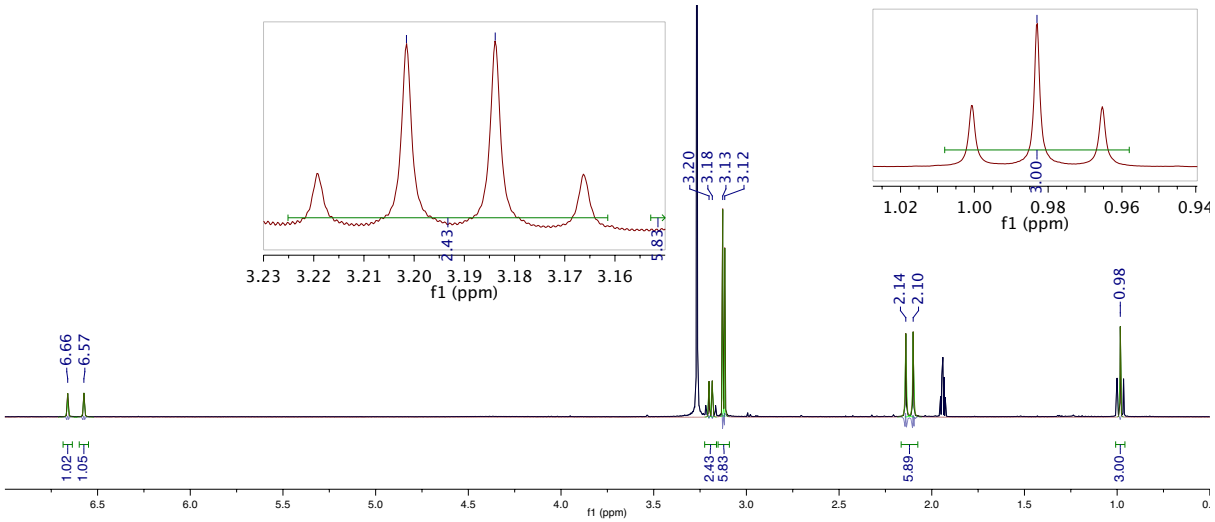

Figure 3-2-19.^{1}H NMR spectrum of the reduced 5Et3MLF (500 MHz, CD_3CN).

The ^{1}H NMR spectrum of the reduced 5Et3MLF (**43H₂**)(Figure 3-2-20) was compared with the ^{1}H-NMR spectrum of the reaction mixture under argon at t = 30 min. No comparable peaks for **43H₂** were observed on the ^{1}H-NMR spectrum of the reaction mixture under argon at t = 30 min. Hence, the flavinium salt **43⁺ClO₄⁻** might not fully get reduced with the oxidation of **4** under argon.

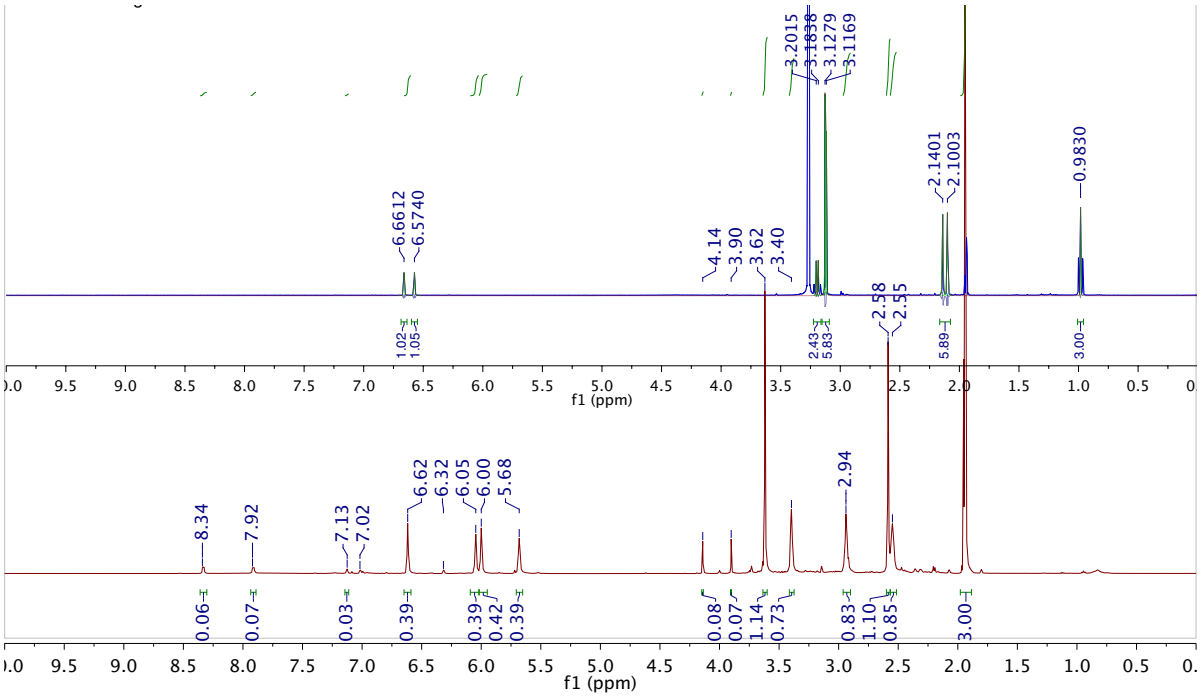

Figure 3-2-20. Comparison of ^{1}H-NMR spectra between the reduced 5Et3MLF and reaction mixture under argon. ^{1}H-NMR (500 MHz, CD_3CN) spectra show the reduced 5Et3MLF (top, blue) and anaerobic reaction mixture at t = 30 min (bottom, maroon). The reaction product of $5Et3MLF^{+}ClO_4^{-}$ (12.25 mM) with TMMP (25.5 mM) in dried acetonitrile-d_3 under argon is shown here.

Next, the ^{1}H NMR spectrum of **43H$_2$** (Figures 3-2-21) was compared with the ^{1}H NMR spectra of the reaction mixture (1 to 2 molar ratio) in air at t = 30 min (Figure 3-2-21A) and t = 300 min (Figure3-2-21B). Peaks corresponding to **43H$_2$** were not observed in the ^{1}H-NMR spectra of the reaction mixture. Therefore, the results suggest that **43H$_2$** is not formed during the course of the reaction either under argon or air.

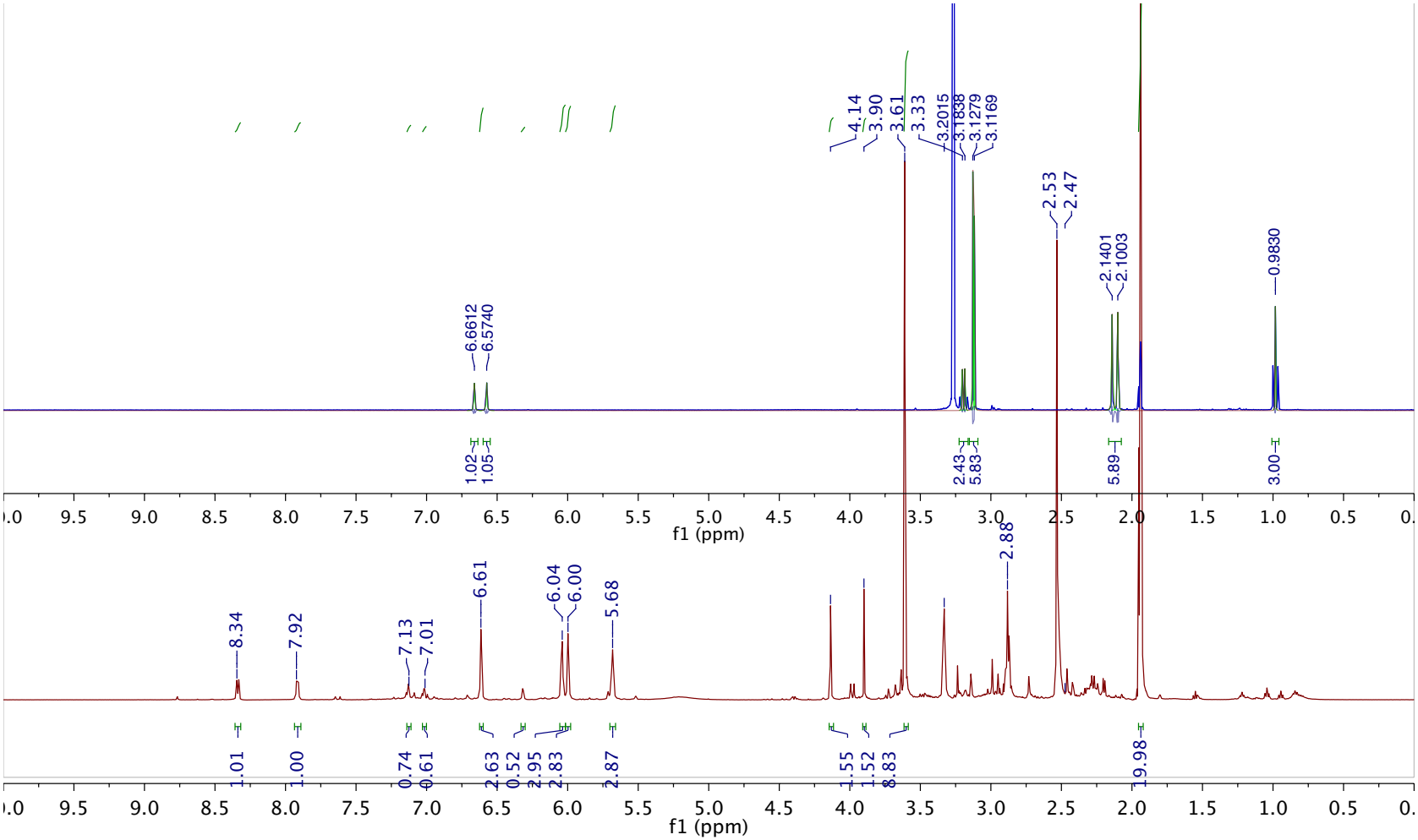

Figure 3-2-21 A. Comparison of ^{1}H-NMR spectra between the reduced 5Et3MLF and reaction mixture in air at t = 30 min. Spectra show the reduced 5Et3MLF (top, blue line) and the reaction mixtures (bottom, maroon). ^{1}H-NMR (500 MHz, CD_3CN) spectra of the reaction product of $5Et3MLF^{+}ClO_4^{-}$ (12.25 mM) with TMMP (25.5 mM) in dried acetonitrile-d_3 in air at t = 30 min.

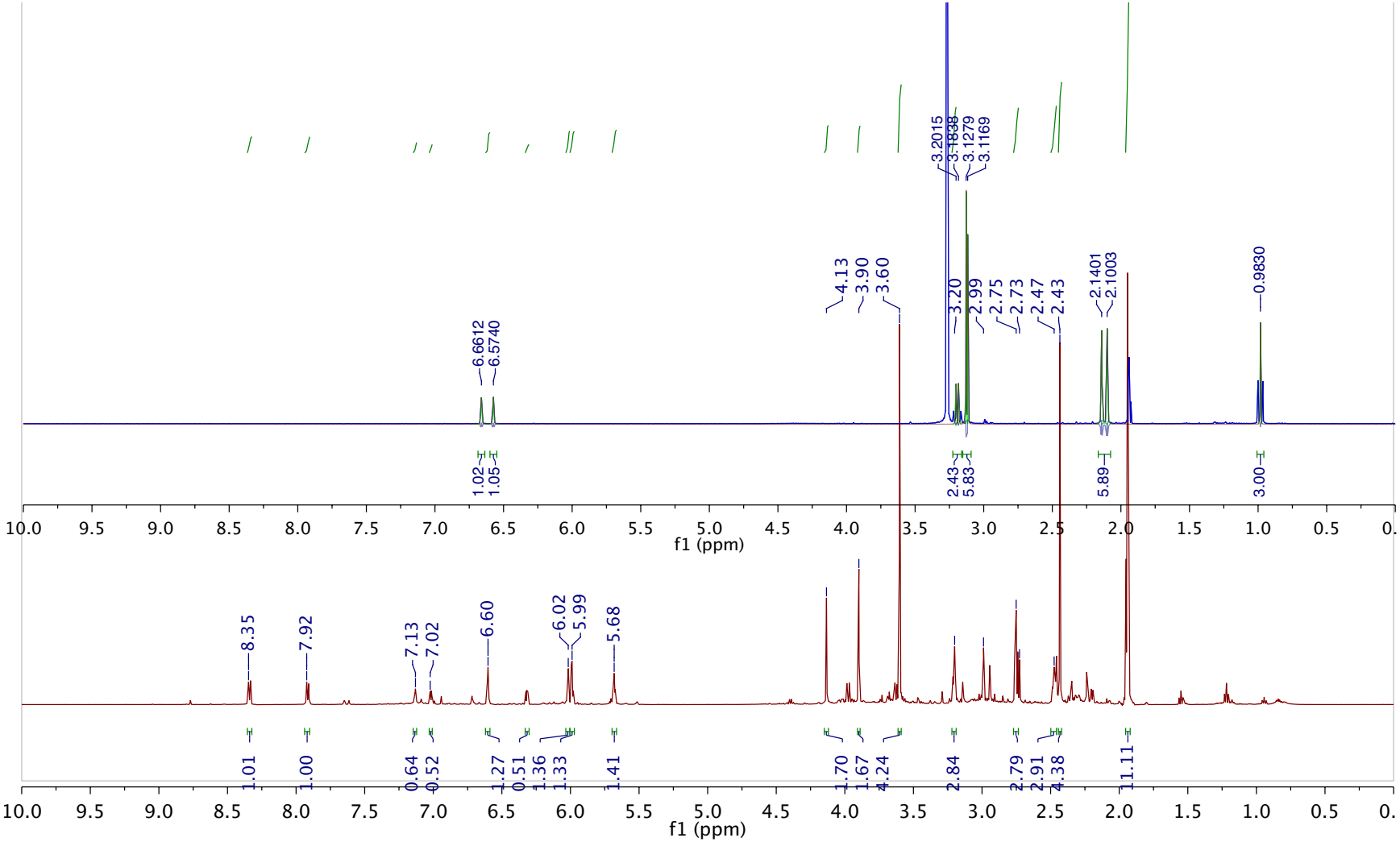

Figure 3-2-21 B. Comparison of ^{1}H-NMR spectra between the reduced 5Et3MLF and reaction mixture in air at t = 300 min. Spectra show the reduced 5Et3MLF (top, blue line) and the reaction mixtures (bottom, maroon). ^{1}H-NMR (500 MHz, CD_3CN) spectra of the reaction product of $5Et3MLF^{+}ClO_4^{-}$ (12.25 mM) with TMMP (25.5 mM) in dried acetonitrile-d_3 in air at t = 300 min.

Instead of the production of the reduced 5Et3MLF (**43H$_2$**), the C(4a)-hydroxyl adduct or C(4a)-hydroperoxyl adduct of 5Et3MLF (**52**) may be formed in the reaction mixture. According to the UV/vis results (Figure 3-2-1), a compound corresponding to the peak at λ_{max} of 350 nm was formed with the reaction in air [5Et3MLF$^+$ClO$_4^-$ (12.25 mM) with TMMP (25.5 mM]. These C(4a) adducts have a chromophore at λ_{max} of 350 nm also. Figure 3-2-22 depicts the NMR images of the reaction mixture under argon (top) and immediately after air introduction (bottom). Notice that new peaks at 3.25 ppm, 2.25 ppm, 2.27 ppm, and 1.04 ppm appeared as the reaction mixture was exposed to air. Those peaks may correspond to the C(4a)-hydroxyl adduct (**51**) and/or C(4a)-hydroperoxyl adduct (**52**). Recall that the reaction mixture was made in dried/distilled acetonitrile, and the air was dried with drierite (anhydrous calcium sulfate with indicator). Thus, the C(4a)-OH adduct (**51**) would not likely be formed. Therefore, the adduct **52** might be an intermediate of the oxidation of **4** in the presence of **43$^+$ClO$_4^-$**.

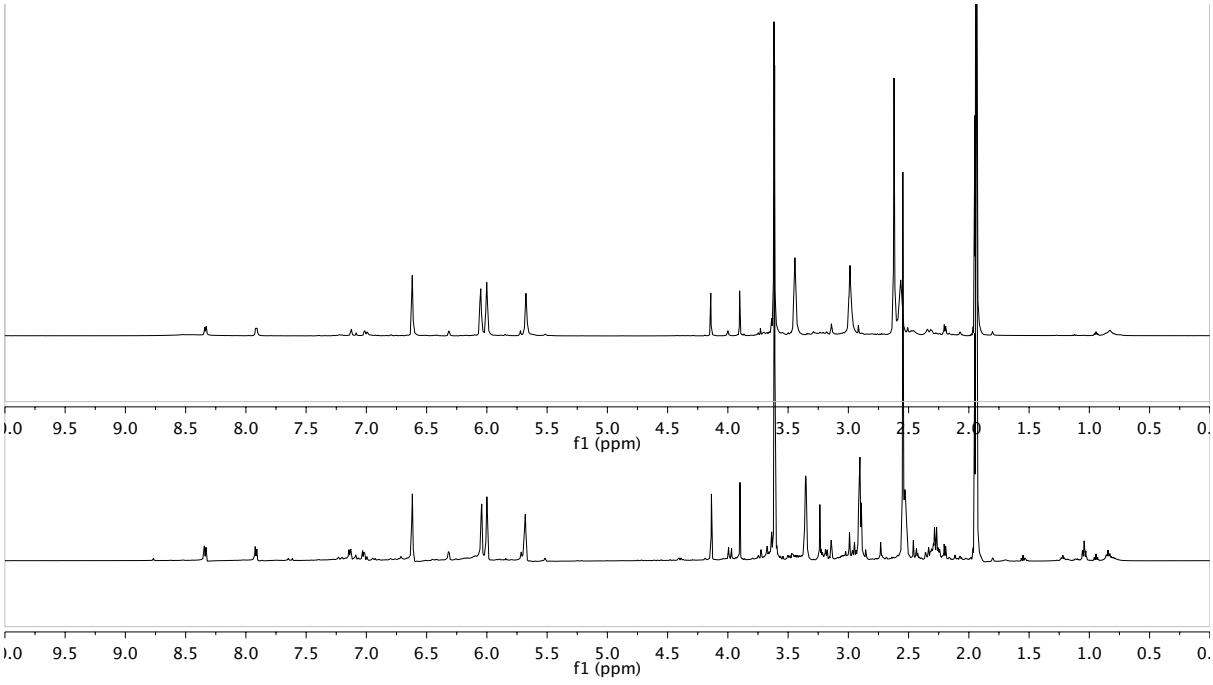

Figure 3-2-22. Comparison of ^{1}H-NMR spectra between the reaction mixture under argon and immediately after air-exposure. The reaction product of 5Et3MLF$^+$ClO$_4^-$ (12.25 mM) with TMMP (25.5 mM) in dried acetonitrile-*d*$_3$ (500 MHz, CD$_3$CN).

In summary, these results indicated that the initial step in the reaction between **43$^+$ClO$_4^-$** and **4** proceeded via a SET pathway, which results in the formation of the flavin radical (Scheme 3-2-14). After proceeding via the initial SET pathway, dioxygen is required since the flavin radical

did not react further under argon. Under aerobic conditions, the obligatory intermediate DHP$^+$ (**49**$^+$) was formed in the presence of **43**$^+$**ClO**$_4^-$, which was then converted to the free base **49**. Finally, the formation of **50**$^+$ appears to proceed via air oxidation. In the scheme below, the counter ions are not included. Fates of the flavinium salt **43**$^+$**ClO**$_4^-$ will be discussed in Chapter 5.

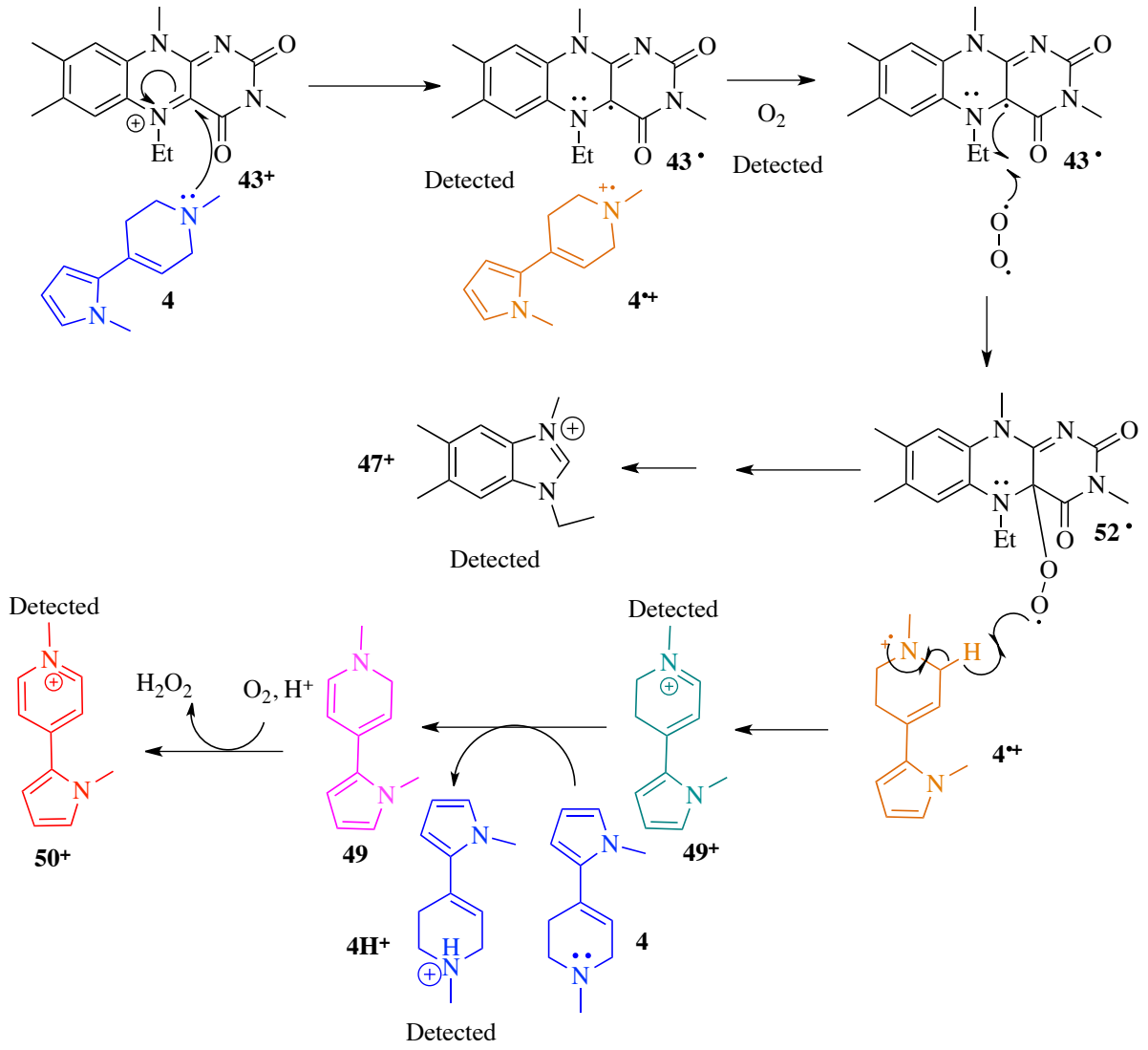

Scheme 3-2-14

3.2.2.6 Fates of 5Et3MLF$^{+}ClO_4^{-}$ with the Oxidation of TMMP

The results described above involve a 189 species (exact mass of 189.1386 Da) as a component of the reaction mixture of 5Et3MLF$^{+}ClO_4^{-}$ (**43**$^{+}$**ClO**$_4^{-}$) and TMMP (**4**) in acetonitrile. Mager (1979) reports on the decomposition of **43**$^{+}$**ClO**$_4^{-}$ in anhydrous media to the benzoimidazoliumyl species **47**$^{+}$.[70] However, the Mager group did not fully characterize the compound; thus, characteristics of **47**$^{+}$ were examined in greater detail in the course of this research project.

It is worth mentioning that vitamin B_{12} contains an analog of **47**$^{+}$, 5,6-dimethylbenzimidazole [DMB (**78**)] that is biosynthesized from the reduced flavin $FMNH_2$ (Figure 3-2-23).[71] DMB becomes a part of cobalamin in vitamin B_{12}. This biosynthesis of the dimethyl-benzoimidazole moiety appears to involve a 4a-hydroperoxide adduct of FMN; however, the mechanism of the biosynthetic pathway remains unclear.

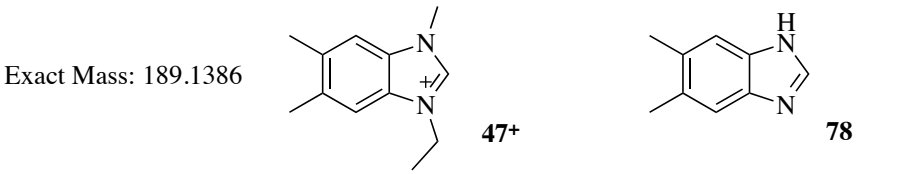

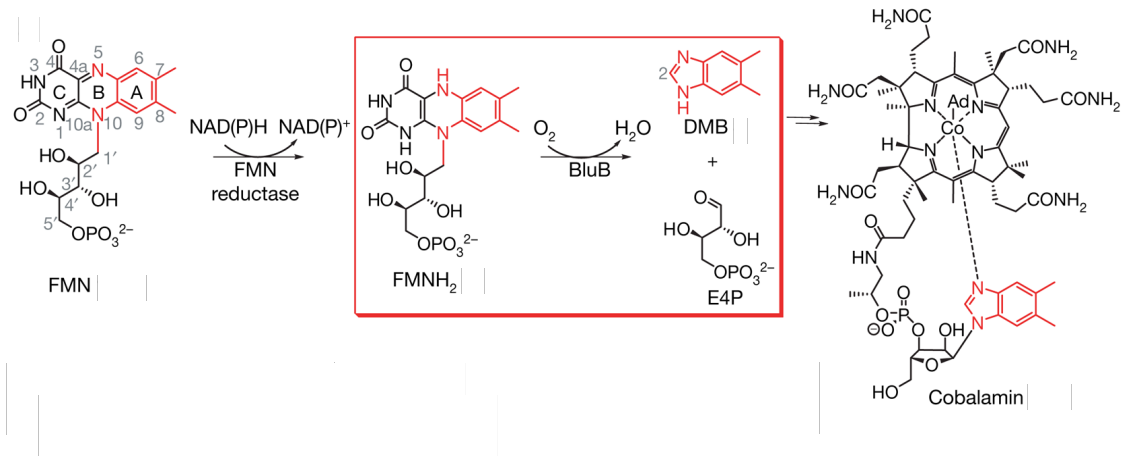

Figure 3-2-23. Biosynthesis of 5,6-dimethylbenzimidazole (DMB) and its involvement in vitamin B_{12}.[71] Reprinted by permission from Macmillan Publishers Ltd on behalf of Cancer Research UK: Nature, advance online publication, 2007 March 22; 446(7134): 449–453(doi:10.1038/nature05611.[†††]

[†††] License agreement in Appendix H.

In the present work, the initial structure assignment for the peak at *m*/z 189 was the protonated form of the lactam (exact mass of 189.1022)(**55H$^+$**) since the corresponding lactam (**56H$^+$**) is a known metabolite of MPTP that presumably arises from the oxidation of the intermediate pyridinium species. The observed accurate mass of **47$^+$** (189.1382), however, differs from the exact mass of the lactam by 36.1 mDa.

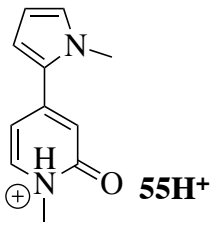

55H$^+$

Exact Mass: 189.10

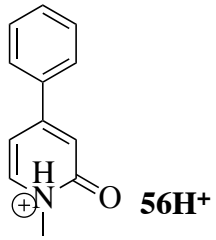

56H$^+$

Exact Mass: 186.09

The next suspected compound was the ethyl-3,5,6-trimethyl-1*H*-benzimidazolium spectra since Mager (1979) reported the fate of **43$^+$ClO$_4^-$** following the formation of the C(4a)-OR adduct (R = H, OH, or Me): spirohydantoin (**57**) and benzoimidazolium salt (**47$^+$**).[70] As shown in Figure 3-2-3, the exact mass of **47$^+$** was consistent with the observed mass (δ 0.3 mDa) in the accurate-mass ESI$^+$ mass spectrum of the reaction product of **43$^+$ClO$_4^-$** (12.5 mM) and **4** (50 mM) in commercial grade acetonitrile (t = 24 hours).

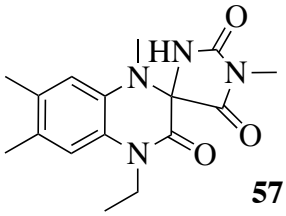

57

Chemical Formula: $C_{16}H_{20}N_4O_3$
Exact Mass: 316.1535

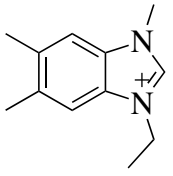

47$^+$

Chemical Formula: $C_{12}H_{17}N_2^+$
Exact Mass: 189.14

To my knowledge, NMR data for **47$^+$** have never been published. Also, the synthesis of this compound has not been published previously. Therefore, the next goal was to synthesize **47$^+$** and to obtain an NMR spectrum for identification. N-methylation of commercially available 5,6-dimethyl-1*H*-benzo(d)imidazole with iodomethane gave the corresponding 1,5,6-trimethyl species which upon treatment with iodoethane gave the iodide salt of **47$^+$**. After the synthetic product was isolated and purified, an NMR spectrum of **47$^+$** was recorded in acetonitrile-d_3 (Figure 3-2-24, top) and the X-ray crystallography data (Figure 3-2-24, bottom) confirmed the structure.

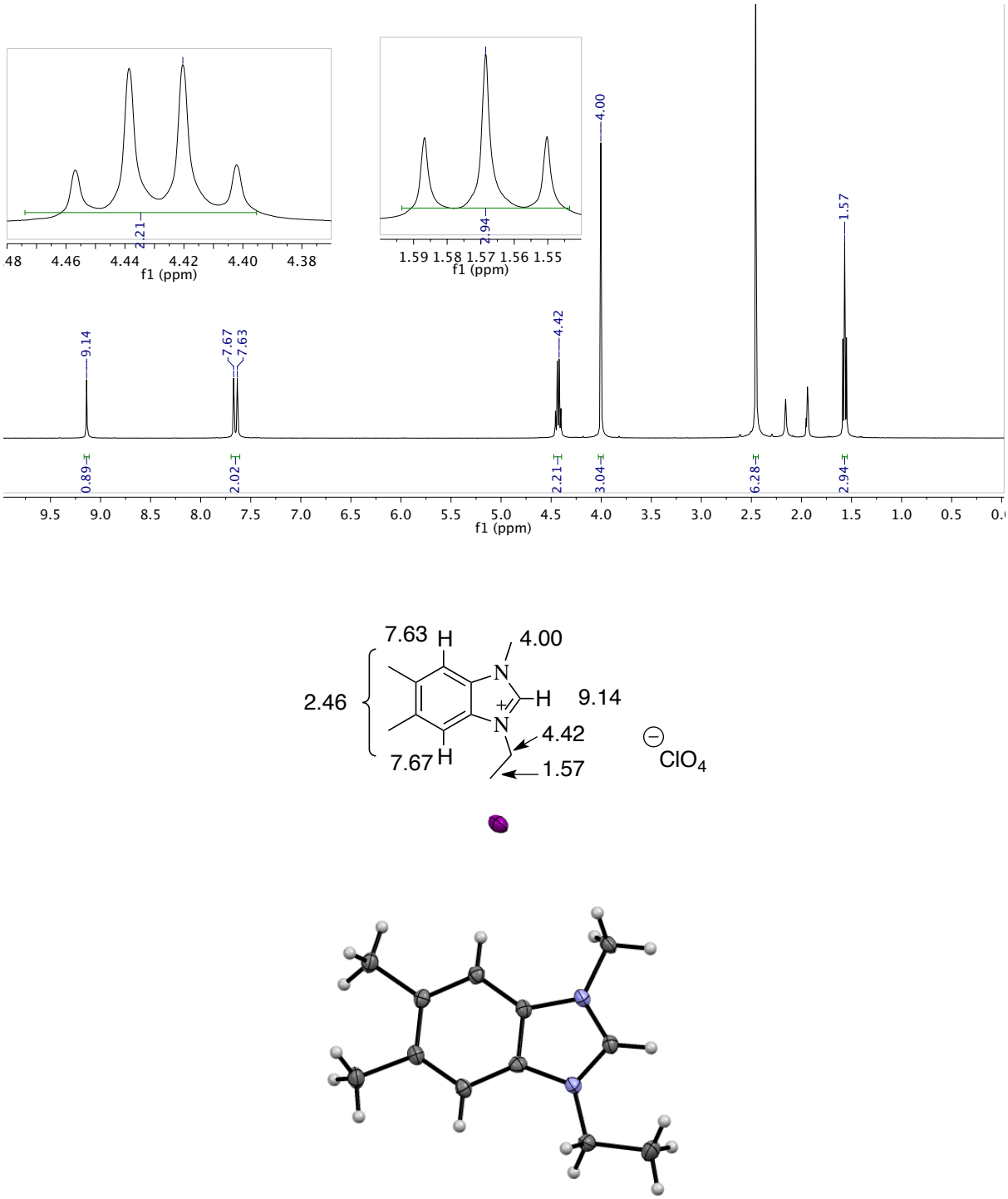

Figure 3-2-24. Identification of the benzoimidazoliumyl compound. Top: ^{1}H-NMR (500 MHz) spectrum and assignments of the benzoimidazoliumyl compound in acetonitrile-d_3 (δ = 1.57 (3H, t), 2.46 (6H, s), 4.00 (3H, s), 4,42 (2H, q), 7.63 (1H, s), 7.67 (1H, s), and 9.14 (1H, s). Bottom: Thermal ellipsoid plot of the molecular structure of benzoimidazolium iodide at 50 % probability. The spectator ion (iodide) is shown in purple.

The corresponding 1,5,6-trimethyl species (the precursor of the iodide salt of **47**$^{+}$)(**79**) and compound **47**$^{+}$ were examined by elemental analysis: Anal. Calcd for $C_{11}H_{14}N_2$: C, 75.82; H, 8.10; N 16.08. Found: C, 75.83; H, 7.94; N, 16.08 and Anal. Calcd for $C_{12}H_{17}N_2I$: C, 45.58; H, 5.42; N 8.86. Found: C, 45.58; H, 5.34; N, 8.72. Thus, elemental analysis data further supported that these are the valid structures. Results of the elemental analysis are shown in Appendix I. The chemical names and melting points of these compounds are listed below.

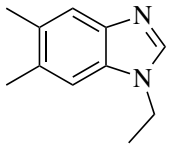

79

1-ethyl-5,6-dimethyl-1*H*-benzo[*d*]imidazole
Chemical Formula: $C_{11}H_{14}N_2$
Elemental Analysis: C, 75.82; H, 8.10; N, 16.08
Melting point: 240 - 241˚C

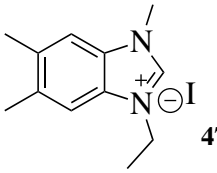

47^{+}**I**$^{-}$

3-ethyl-1,5,6-trimethyl-1*H*-benzo[*d*]imidazol-3-ium iodide
Chemical Formula: $C_{12}H_{17}IN_2$
Elemental Analysis: C, 45.58; H, 5.42; I, 40.14; N, 8.86
Melting point: 72-73 ˚C

Next, the reaction mixture of **43**$^{+}$**ClO**$_4^{-}$ and **4** on day 12 was analyzed using NMR. That spectrum was compared with the authentic benzoimidazolium iodide (**47**$^{+}$**I**$^{-}$)(Figure 3-2-25). The superimposed images of that aerobic reaction mixture (bottom) and the synthetic benzoimidazole (top) are displayed in Figure 3-2-25A. The expansion images of those NMR spectra (synthesized **47**$^{+}$ on the top and reaction mixture at the bottom) are shown in Figure 3-2-25 B. Although compound **47**$^{+}$ appears to have slightly different chemical shifts compared to that of the reaction mixture (Figure 3-2-25A), the peaks for N-*CH*$_2$CH$_3$ (q) and N-CH$_2$*CH*$_3$ (t) have the same coupling constant in the reaction mixture (bottom) and the synthetic benzoimidazole (Figure 3-2-25B). This evidence clearly support the formation of **47**$^{+}$**I**$^{-}$ in the reaction mixture of **43**$^{+}$**ClO**$_4^{-}$ and **4** in the presence of air.

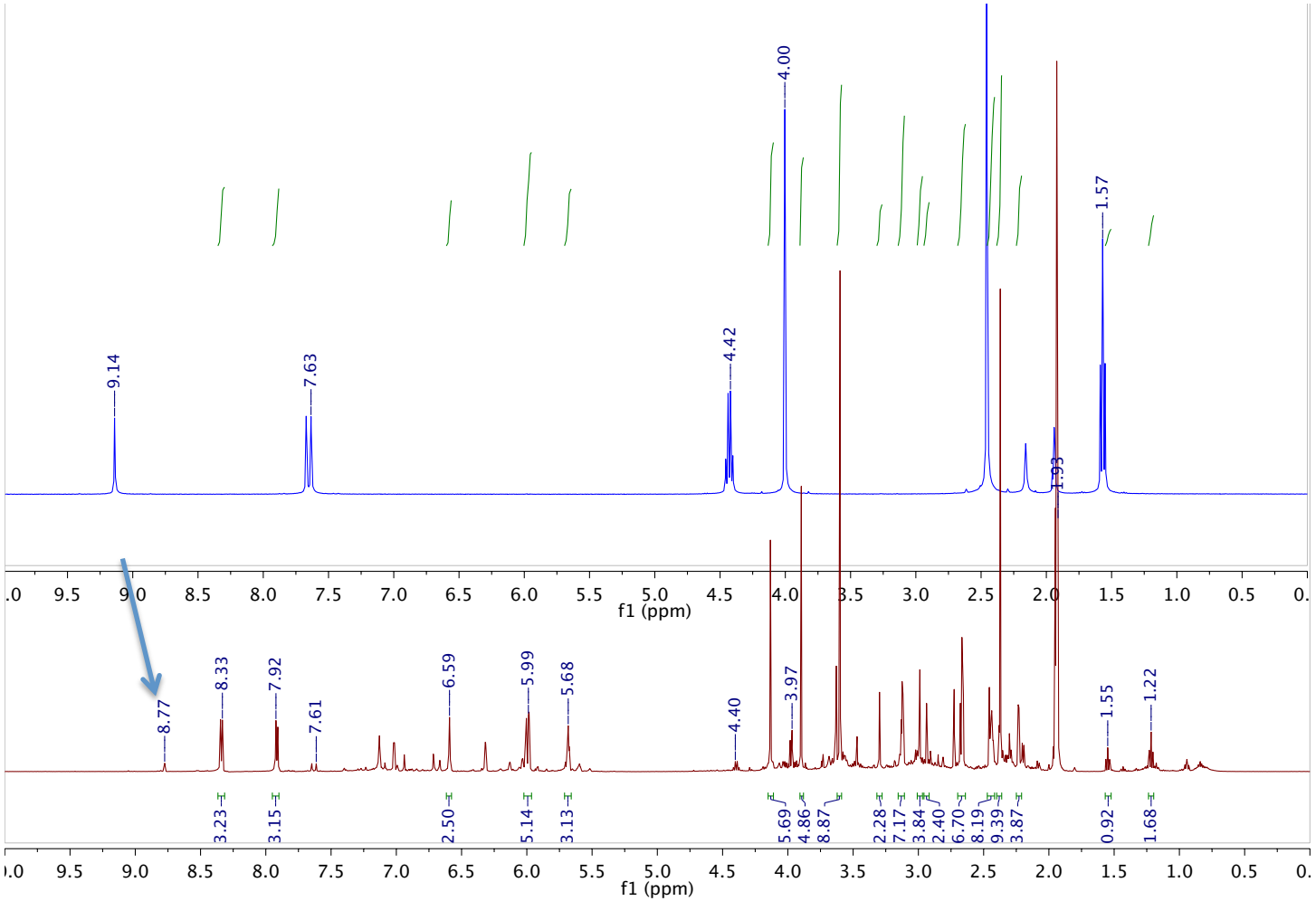

Figure 3-2-25 A. Superimposed image of ^{1}H NMR spectra of the reaction mixture and the authentic benzoimidazole. The reaction mixture between 5Et3MLF^{+}ClO_4^{-} (25 mM) and TMMP (50 mM) in the aerobic condition (bottom) on day 12 and the synthetic benzoimidazole (top)(A)

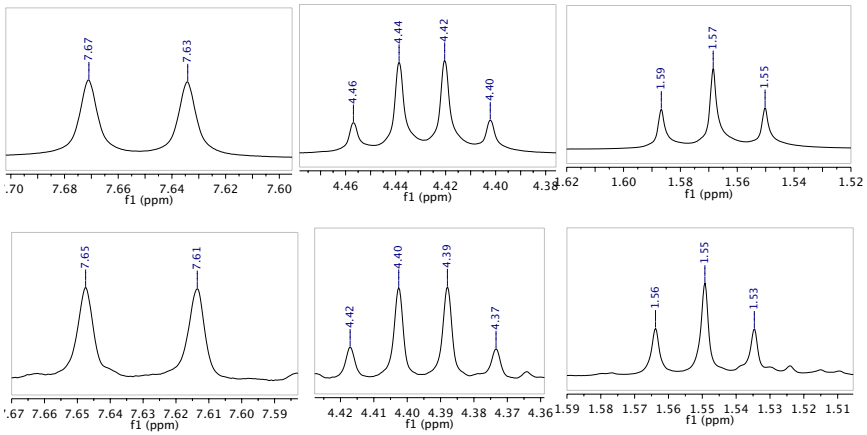

Figure 3-2-25 B. Expansion images of ^{1}H NMR signals of the reaction mixture and the authentic benzoimidazole. Top three images show synthetic benzoimidazole, and bottom three images show aerobic reaction mixture: right, $NCH_2\mathit{CH}_3$; middle, $N\mathit{CH}_2CH_3$; left, Ar-H's (500 MHz, CD_3CN).

Figures 3-2-26 A and B (spectrum of the reaction mixture under aerobic conditions) contains all signals belonging to **47**$^{+}$ except the signal at 9.14 ppm. Instead, a new signal at 8.77 ppm was observed in the reaction mixture (see below). Thus, the next goal was to determine whether the signal at 8.77 ppm in the reaction mixture belongs to the proton next to the N with positive charge in **47**$^{+}$. To address that question, a 2D HMBC (Heteronuclear Multiple Bond Correlation) spectrum of the reaction mixture was obtained (Figures 3-2-26 A and B). An *HMBC* experiment correlates chemical shifts of two types of nuclei separated from each other with two or more chemical bonds. According to the HMBC results, both signals at 7.65 and 8.77 ppm correlate to each other and those protons belong to one compound. It may be possible that the positive charge at the N likely with a compound in the reaction mixture to make that proton to shift upfield (8.77 ppm).

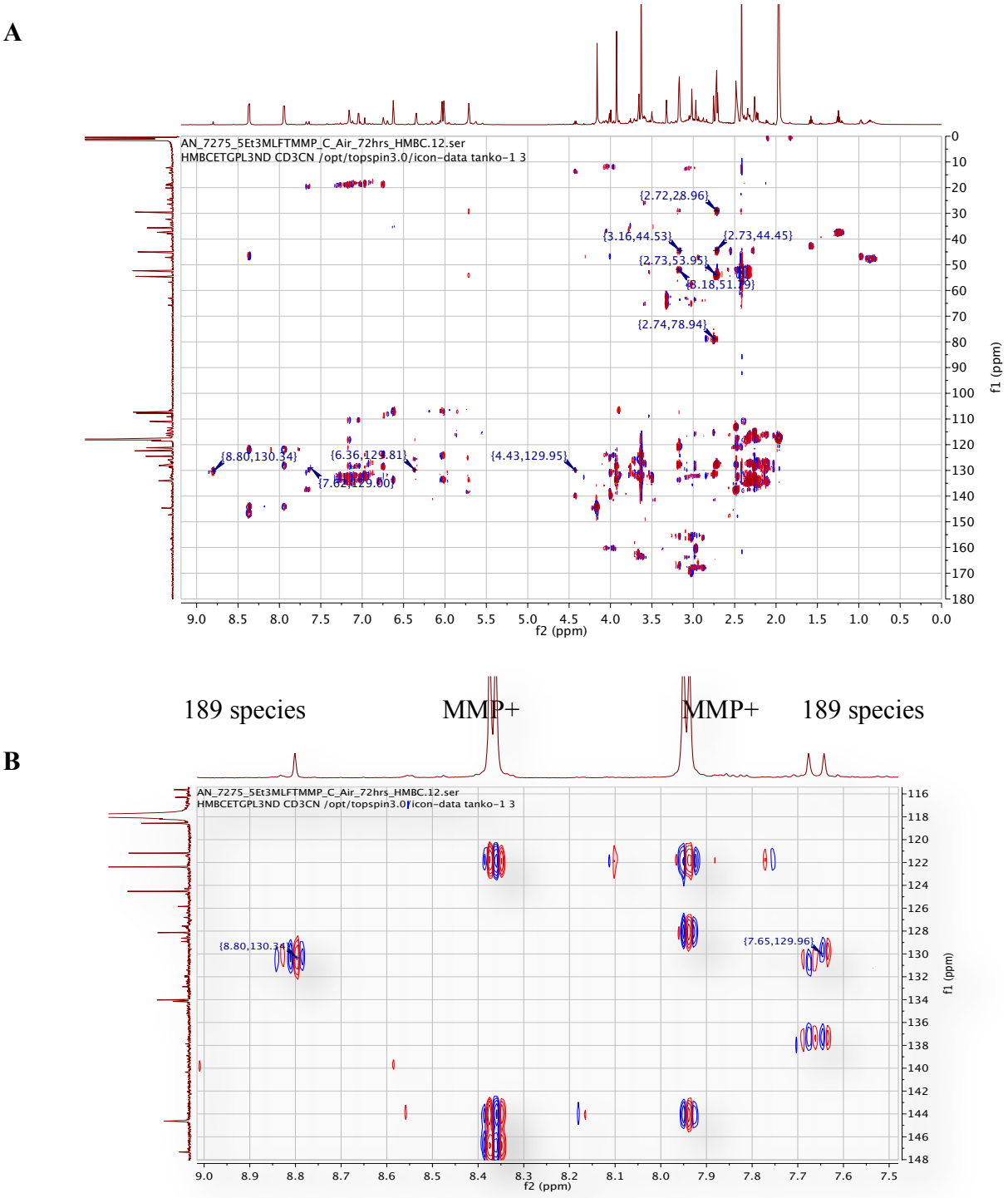

Figure 3-2-26. 2D HMBC NMR spectra of the reaction mixture in air (A) and the magnified region at 7.5, 116 ppm - 9.0, 148 ppm (B). The signals at δ 7.67 (s), 7.63 (s), and 8.77 (s) belong to the benzoimidazoliumyl species whereas the signals at δ 7.93 (d) and 8.39 (d) belong to the oxidation product MMP^+ (500 MHz, CD_3CN).

To test the hypothesis, the NMR spectrum of authentic **47**$^{+}$**I**$^{-}$ in D_2O and examined (Figure 3-2-27). In the D_2O NMR spectrum, the signal for the most downfield proton vanish, which indicates that the most downfield proton is acidic, and thus its shift is sensitive. The proton is easily exchanged on account of the N positive charge. Thus, it is possible that the proton might be shifted more upfield from 9.14 ppm to 8.77 ppm in the reaction mixture.

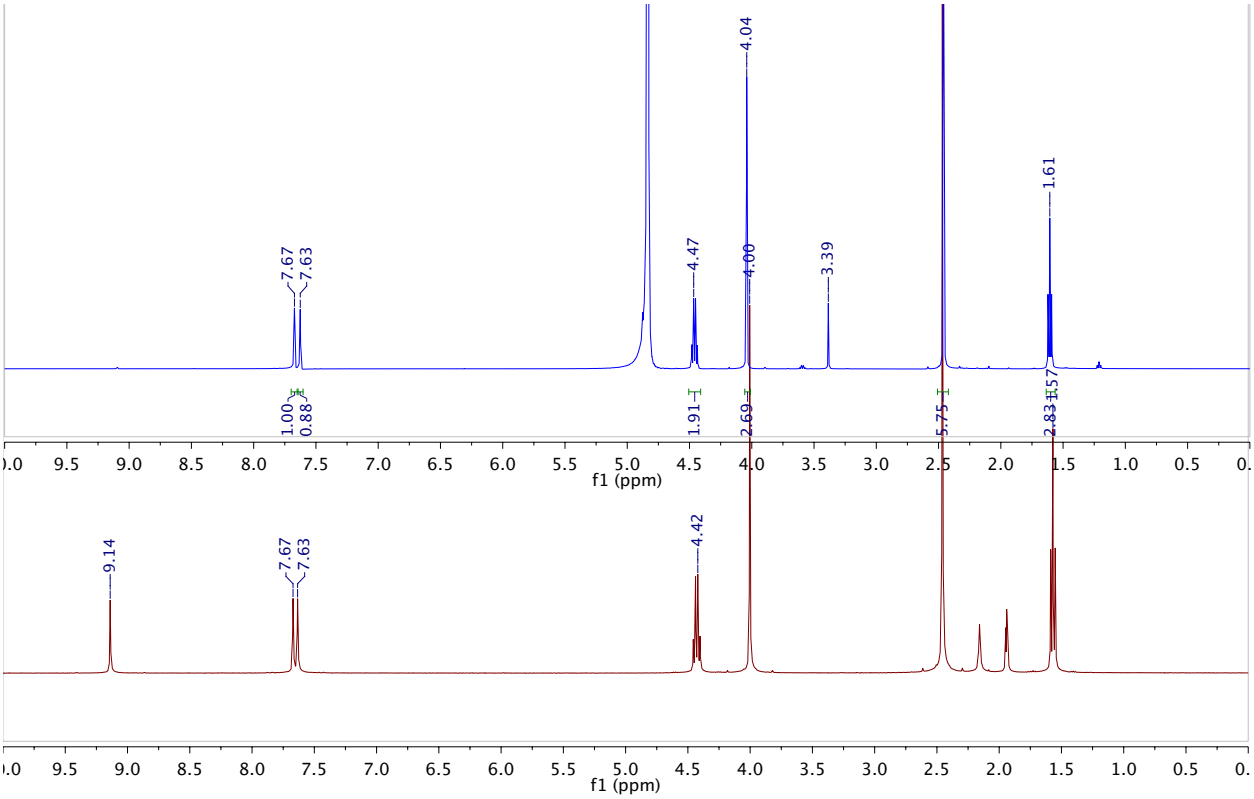

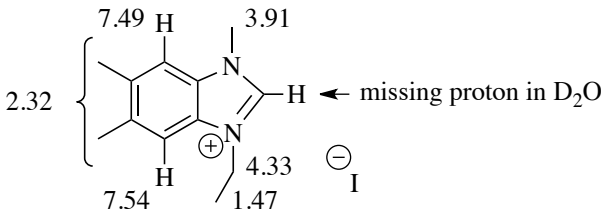

Figure 3-2-27. ^{1}H NMR spectra of the benzoimidazoliumyl compound with D_2O addition. The bottom spectrum (maroon) was recorded in CD_3CN, while the top spectrum (blue) was recorded in D_2O: δ = 1.47 (3H, t), 2.32 (6H, s), 3.91 (3H, s), 4,33 (2H, q), 7.49 (1H, s), and 7.54 (1H, s)(400 MHz).

Next, to further investigate if the most downfield proton signal (δ 8.77 ppm) in the reaction mixture belongs to compound **47$^+$**, a small amount of the authentic **47$^+$I$^-$** was added to the reaction mixture (NMR spiking experiment). First, a ^{1}H NMR spectrum of the reaction mixture of 5Et3MLF$^+$ClO$_4^-$ (25 mM) and TMMP (50 mM) was recorded (Figure 3-2-28, bottom). Next, a small spoon full of the authentic **47$^+$I$^-$** was dissolved in acetonitrile-d_3, which was then added to the same reaction mixture, and another ^{1}H NMR spectrum was recorded afterward (Figure 3-2-28, top). Result demonstrated that the most downfield proton signal at δ 8.77 ppm increased as the authentic compound was added to the reaction mixture, along as other signals associated with **47$^+$I$^-$**, suggesting that the authentic **47$^+$I$^-$** and the imidazolium species **47$^+$** in the reaction mixture are the same compound.

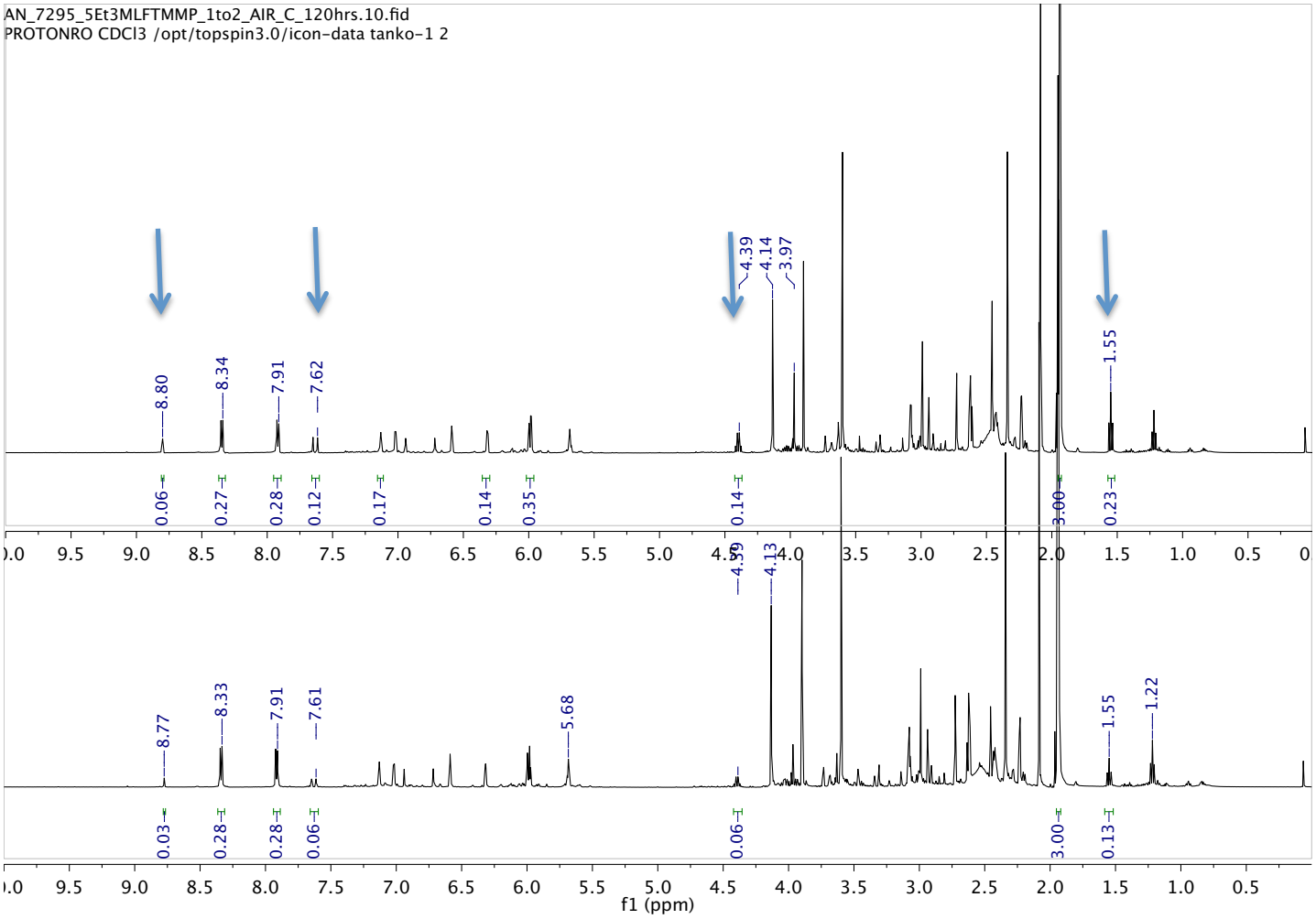

Figure 3-2-28. ^{1}H NMR spiking experiment. Superimposed image of ^{1}H NMR spectra of the reaction mixture of 5Et3MLF^{+}ClO$_4^{-}$ (25 mM) and TMMP (50 mM) in dried acetonitrile-d_3 in air at t = 120 hours before (bottom) and after (top) addition of the authentic MMP^{+}I^{-} to the reaction mixture (500 MHz, CD_3CN).

In the reaction mixture, the positive charge on the N may interact with a constituent of the mixture to cause that proton to appear to be more upfield (8.77 ppm); when the authentic compound **47^{+}I^{-}** was examined, the signal was more downfield (9.16 ppm) due to the positive charge. Scheme 3-2-15 displays my proposal for a possible interaction between **47^{+}** and the neutral flavin radical (**43$^{\bullet}$**).

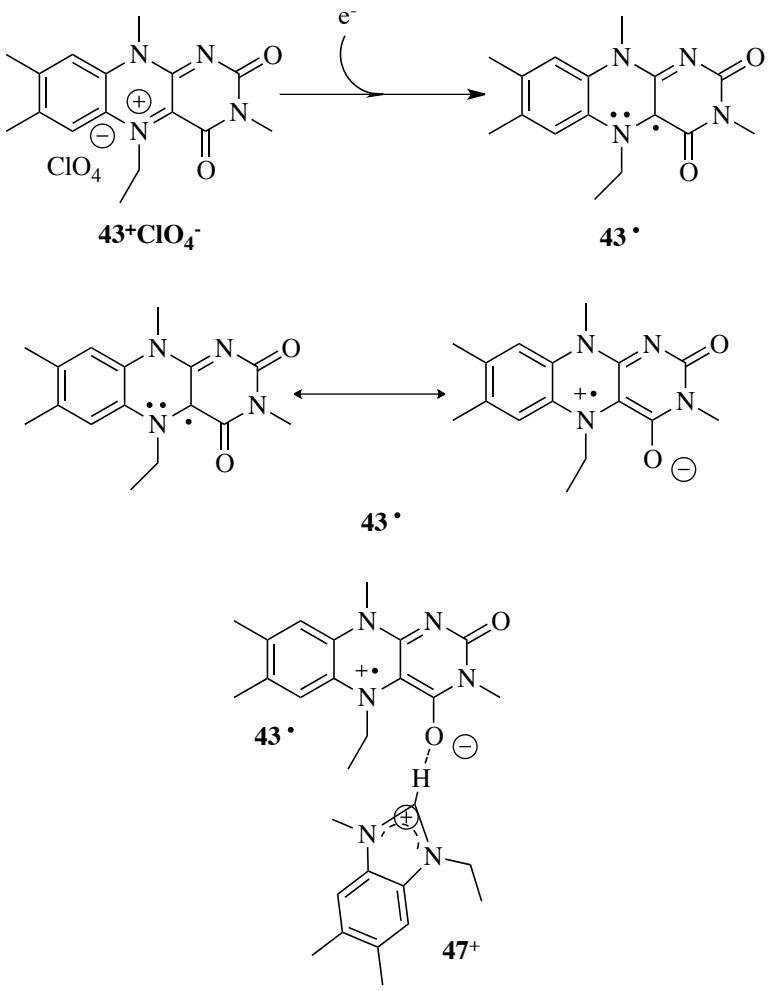

Scheme 3-2-15

In addition, the reaction mixture was also examined with the TLC system. However, it was hard to see **47^{+}** on the TLC because of its low concentration in the reaction mixture.

To summarize, the benzoimidazoliumyl compound (**47$^+$**)(exact mass of 189. 1386 Da) was detected in the reaction mixture between **43$^+$ClO$_4^-$** and **4** under aerobic conditions (NMR and accurate-mass ESI$^+$/MS analyses). This compound is one of the ultimate products of reactions involving **43$^+$**. A proposed mechanism involving **47$^+$** is shown in Chapter 5 (the effect of water on flavinium chemistry).

To have a better understanding of formation of the imidazolium compound, the reaction between **43$^+$ClO$_4^-$** and the reducing agent $Na_2S_2O_4$ (1 to 1 molar ratio) in commercial grade acetonitrile and water was examined using accurate-mass ESI$^+$/MS. Initially, **43$^+$ClO$_4^-$** was dissolved in acetonitrile, and deionized water containing $Na_2S_2O_4$ was added to this solution. These solutions were mixed at room temperature and analyzed using accurate-mass ESI$^+$/MS analysis. Aside from the 189 species **47$^+$**, protonated 3MLF (**42H$^+$**)(MH^+) was observed at *m/z* 271.1190 (δ 0.0 mDa)(Figure 3-2-29). The 232.1440 species that corresponds to **58$^+$** may be a fragment of the intermediates in the fate of **43$^+$ClO$_4^-$** (δ 0.4 mDa).

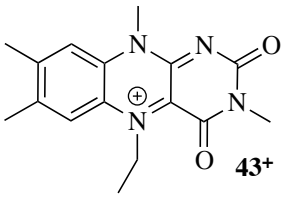

43$^+$

Chemical Formula: $C_{16}H_{19}N_4O_2^+$
Exact Mass: 299.1503

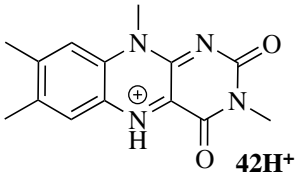

42H$^+$

Chemical Formula: $C_{14}H_{15}N_4O_2^+$
Exact Mass: 271.1190

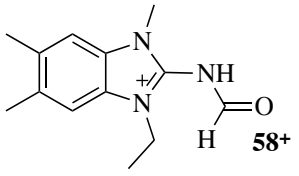

58$^+$

Chemical Formula: $C_{13}H_{18}N_3O^+$
Exact Mass: 232.1444

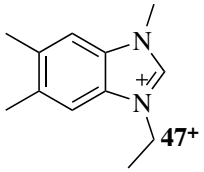

47$^+$

Chemical Formula: $C_{12}H_{17}N_2^+$
Exact Mass: 189.1386

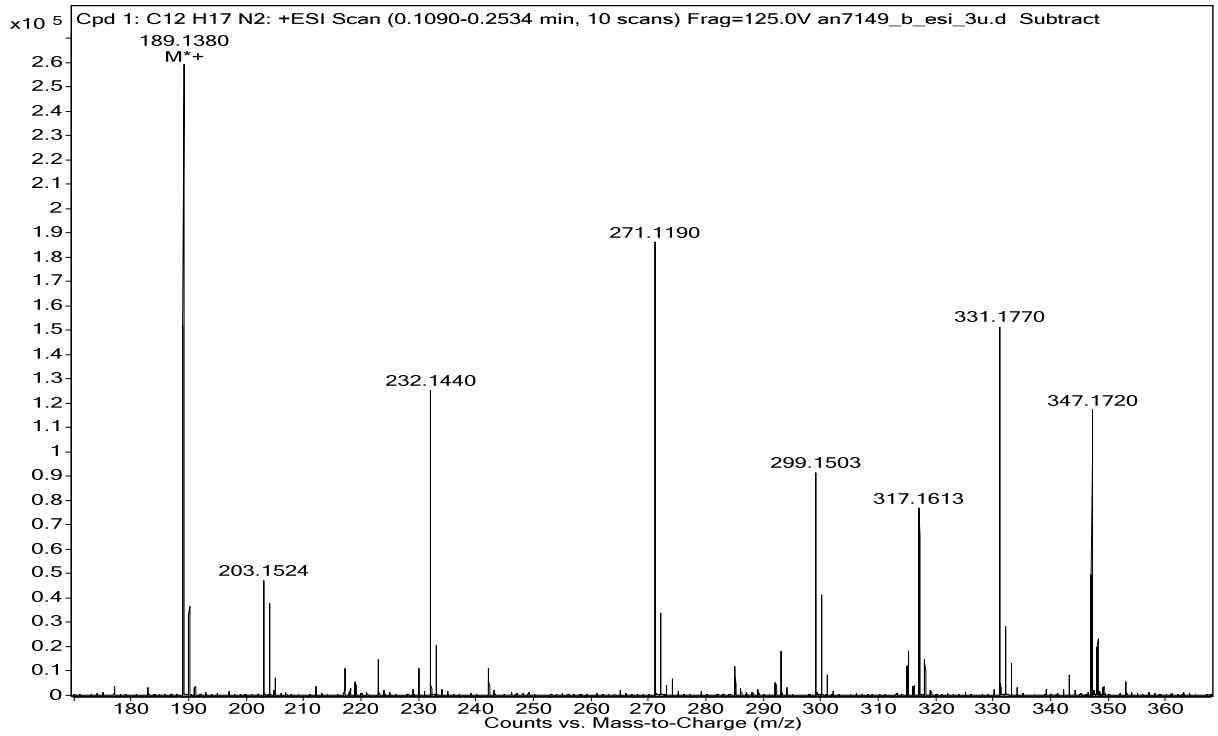

Figure 3-2-29. Accurate-Mass ESI$^+$ mass spectrum of the reduction of 5Et3MLF$^+$$ClO_4^-$. The mixture of 5Et3MLF$^+$$ClO_4^-$ with the reducing agent $Na_2S_2O_4$ (1 to 1 molar ratio) in commercial grade acetonitrile. An expansion of the spectrum from *m/z* 180 to *m/z* 360 is shown.

3.2.3 Conclusions

Therefore, in brief, the FAD chemical model **43$^+$$ClO_4^-$** oxidizes **4** in commercial grade acetonitrile in the presence of air. The oxidation of **4** proceeds via the obligatory intermediate **49$^+$**, which is converted to the corresponding free based species **54**; finally, **54** is converted to **50$^+$** via air oxidation (Scheme 3-2-16). The conversion of **49$^+$** into **54** may undergo either disproportionation or air oxidation, but air oxidation is the primary pathway. The flavinium salt **43$^+$$ClO_4^-$** is involved in the first 2-electron oxidation of **4**, involving the conversion of **4** into **49$^+$**, but may not be responsible for the second oxidation from **49$^+$** to **50$^+$**. The initial step involves an SET pathway, which results in the generation of the neutral flavin radical **43$^\bullet$** followed by an air-sensitive reaction.

These findings in this section revealed that **43$^+$$ClO_4^-$** is a good chemical model to study a SET pathway with the oxidation of **4** under normal conditions (not acid-catalyzed at room

temperature). However, it probably not a good model for MAO that does not require dioxygen to oxidize monamines. Formerly, Mariano and his co-workers reported that **43**$^{+}$**ClO**$_4^-$ oxidized primary and secondary amines but not tertiary amines. This research, however, demonstrated that **43**$^{+}$**ClO**$_4^-$ does oxidize the cyclic tertiary allyl amine **4** via an SET pathway. This research project demonstrates for the first time that the oxidation of a tertiary allyl amine with a FAD chemical model. Therefore, **43**$^{+}$**ClO**$_4^-$ is a possible chemical model to study both SET and nucleophilic polar mechanisms for oxygen-dependent flavoenzymes, other than MAO's.

In addition, one of the side reactions involved the formation of **51** results from the reaction between **43**$^{+}$**ClO**$_4^-$ and water. Adduct formation could inactivate **43**$^{+}$**ClO**$_4^-$; therefore, the effect of water may need to be considered when research is conducted using **43**$^{+}$**ClO**$_4^-$.

Finally, decomposition of **43**$^{+}$**ClO**$_4^-$ by a still to be determined pathway generates the imidazolium under reducing conditions. Thus, the oxidation of **4** by **43**$^{+}$**ClO**$_4^-$ may be not catalytic is unlikely to be catalytic.

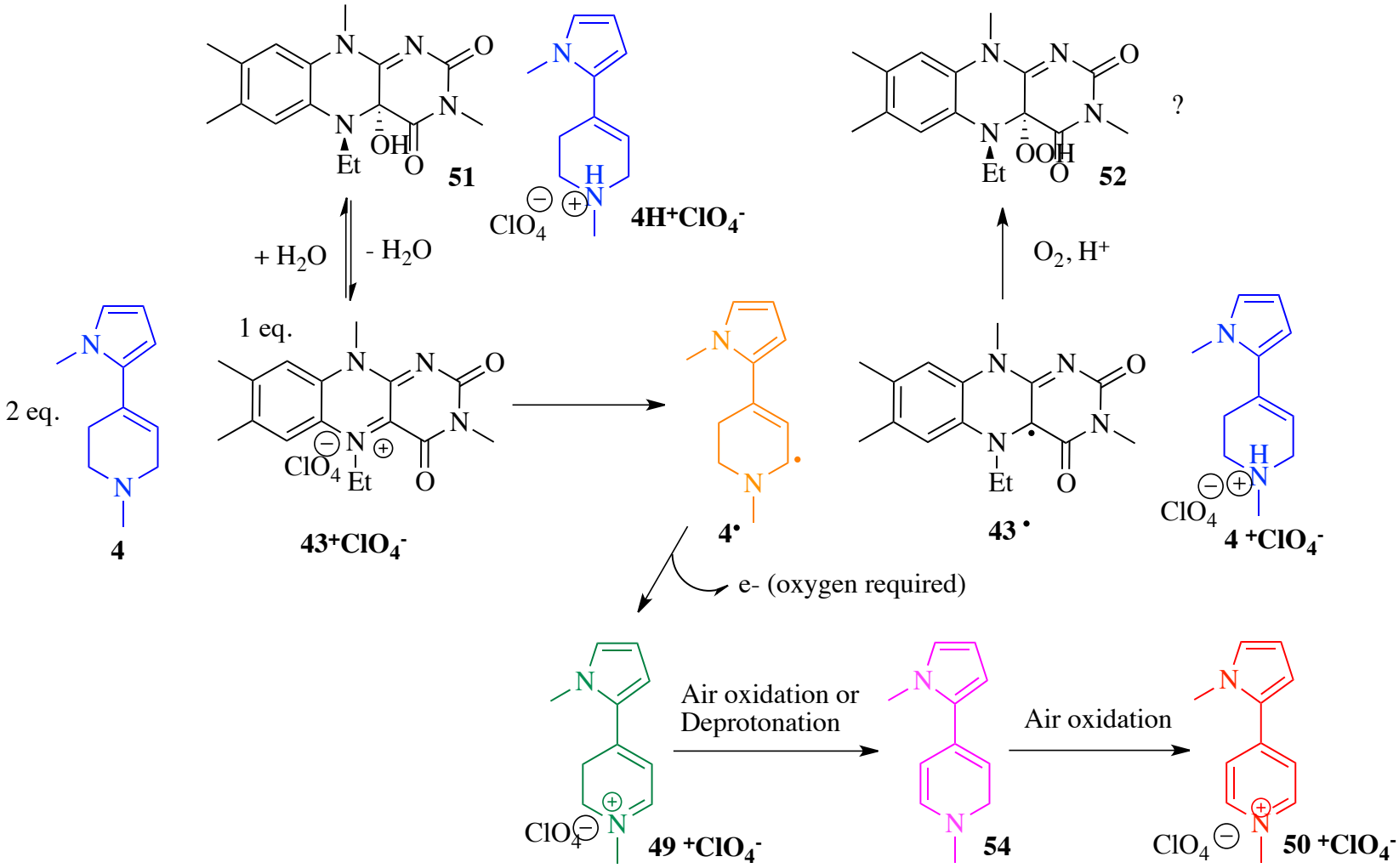
51
4H+ClO4-
52
?
+ H2O
- H2O
O2, H+
2 eq.
1 eq.
4
43+ClO4-
4•
43 •
4 +ClO4-
e- (oxygen required)
Air oxidation or
Deprotonation
Air oxidation
49 +ClO4-
54
50 +ClO4-

Scheme 3-2-1

CHAPTER FOUR

INVESTIGATION OF REACTION BETWEEN 3-METHYLLUMIFLAVIN AND TMMP

4.1 Introduction

In early efforts, acid-catalyzed reactions of 3-methyllumiflavin [3MLF (**42**)] with amines were examined and steric hindrance appeared to contribute to the outcomes.[35, 45a] Mariano and his co-workers proposed a polar mechanism for the α-carbon oxidation of primary and secondary amines by **42**. This nucleophilic polar mechanism was thought to be initiated with the addition of an amine (**61**) to the C(4a)-position of the flavin ring system **42** to give **62**. A subsequent intramolecular redox reaction led to the reduced form of 3MLF [$3MLF_{red}$ (**$42H_2$**)] and an imine, **62**, the products of the proposed the α-carbon oxidation pathway (Scheme 4-1).[35, 43]

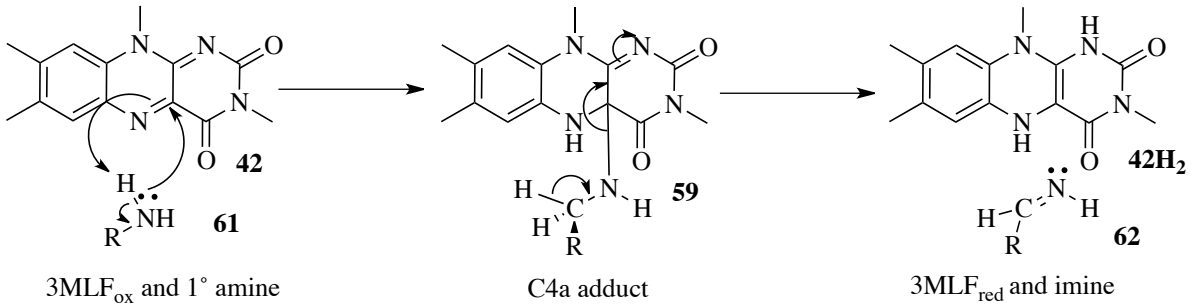

Scheme 4-1

Few other reports have investigated the oxidation of amines using ground-state flavin models. Previous work indicated that the ground state of **42** is not involved in the oxidation of tertiary amines. Relatively few tertiary amines have been reported to be good substrates for MAO-A and MAO-B.[35, 45a] However, MPTP and its derivatives are excellent MAO substrates, and steric hindrance may not affect MAO oxidation.[29] The reaction between **42** and tertiary allylamines has never been investigated. The present study seeks to explore this issue by examining the reaction between **42** and 1-methyl-4-(1-methyl-1*H*-pyrrol-2-yl)-1,2,3,6-tetrahydropyridine [TMMP (**4**)].

The oxidation of **4** in the presence of 5Et3MLF$^+$ClO$_4^-$ (**43$^+$ClO$_4^-$**) has been observed as described in Chapter 3. The conversion of **4** into MMP$^+$ (**50$^+$**) was demonstrated. The flavinium salt **43$^+$ClO$_4^-$** is an N5-ethylated analog of **42** and the C4a position of **43$^+$ClO$_4^-$** is more electrophilic compared with the C4a position of **42**.

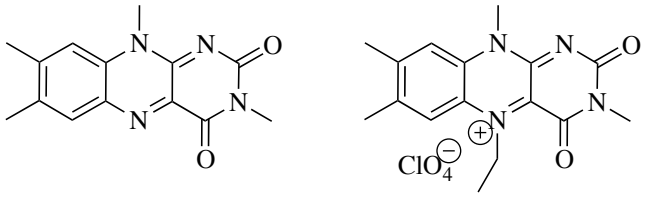

42 **43$^+$ClO$_4^-$**

This chapter describes efforts to determine if **42** oxidizes **4** under mild conditions (room temperature in the absence of acid). This is an important question because the FAD in MAO-B is not alkylated at the N5 position. Therefore, **42** is more structurally related to the flavin in the FAD than is to 5Et3MLF$^+$. First, stability of **42** in acetonitrile was examined using NMR and ESI$^+$ analyses. TMMP in commercial grade acetonitrile had already shown to be stable (Chapter 3). The flavin model **42** in commercial acetonitrile-*d*$_3$ also appeared to be stable for at least two months at room temperature.

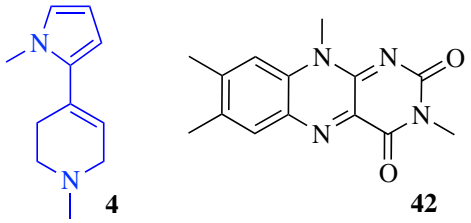

4 **42**

4.2 Results and Discussion

4.2.1 Oxidation of TMMP in the Presence of 3MLF

Initially, the reaction of **42** (3.7 mM) and **4** (13 mM)(1 to 3.5 molar ratio) at room temperature was monitored using UV/vis spectroscopy (Figure 4-1). The solvent used in the present research was commercial grade acetonitrile (anhydrous acetonitrile 99.9 %, AcroSeal catalog # 61022-0010), unless described otherwise. The reaction mixture was stirred constantly and was exposed

to acetonitrile-enriched air.[‡‡‡] This reaction was monitored over the course of six weeks. Chromophores for **42** were found at λ_{max} of 268 nm, 340 nm and 440 nm in acetonitrile, as reported previously (Sikorska 2004). The chromophore for **4** in acetonitrile is found at λ_{max} of 260 nm. The absorbance band at λ_{max} of 366 nm corresponds to an absorption feature of **50⁺**, the 4-electron oxidation product of **4**. After mixing **42** with **4**, the chromophore at λ_{max} of 366 nm (**50⁺** marker) over time increased, while the corresponding chromophores of **42** remained constant (see Table 4-1 and Figure 4.1) The absorbance at λ_{max} of 366 nm was 1.22 at t = 2 weeks and 1.40 at t = 3 weeks (Table 4-1). To calculate the percent yield for the putative product **50⁺**, the absorbance for **42** at 366 nm (absorption 0.38) was subtracted from the product absorbance at λ_{max} of 366 nm (absorption 1.68) before adjustment for **42** since the absorbance of **42** did not change during the reaction. The chromophore at λ_{max} of 440 nm remains constant during the course of the reaction (Figure 4-1), indicating that the spectrum of **42** overlaps with the spectra of the reaction mixture. According to this calculation, using ε = 28,928 for **50⁺** and dilution factor 100, the percent yield was 123%, suggesting that **42** oxidizes **4** catalytically. However, reaction byproducts might have also contributed to the absorbance at 366 nm. Thus, there is the possibility of a lower percent yield with the reaction.

Table 4-1. UV/vis absorption of the product formation of MMP^+. The spectrum of 3MLF (absorbance 0.38 at λmax 366 nm) was subtracted from the spectra of the reaction mixture at t = 2 to 6 weeks.

Time	2 wks	3 wks	4 wks	5 wks	6 wks
Absorbance at 366 nm	0.84	1.02	1.18	1.23	1.32

[‡‡‡] To prevent evaporation of the reaction mixture, in-house air was first passed through acetonitrile and then used to flush the reaction system.

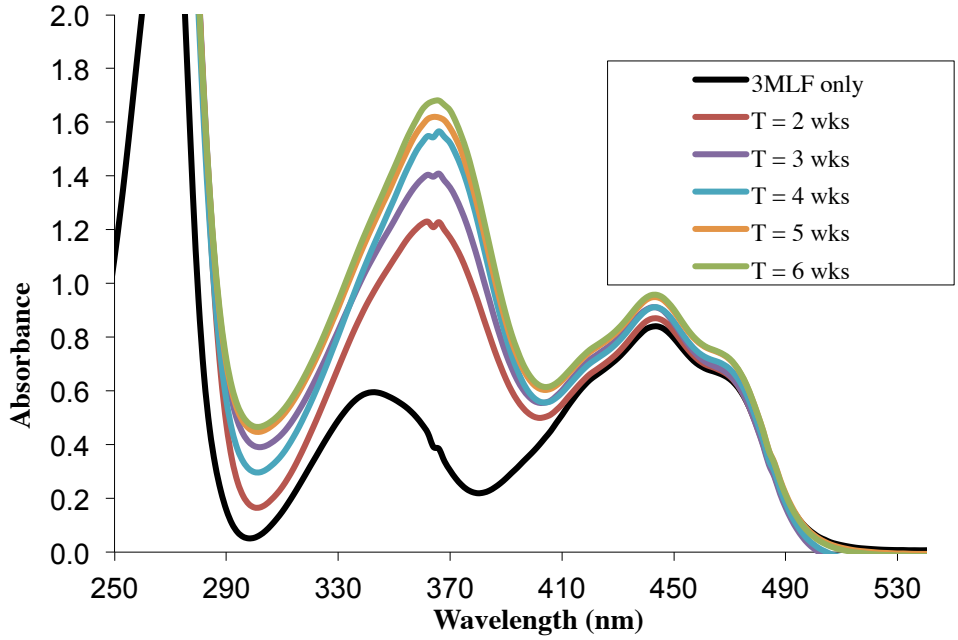

Figure 4-1. UV/vis spectra of a reaction mixture of 3MLF and TMMP. Spectra show the time-dependent formation of MMP^+ with the reaction between 3MLF (3.7 mM) and TMMP (13 mM)(1 to 3.5 molar ratio) in reagent grade acetonitrile at room temperature in darkness.

To confirm the formation of **50**$^+$, the reaction mixture (**42** 3.7 mM and **4** 25 mM) was examined in commercial grade acetonitrile using accurate-mass ESI^+/MS analysis. Figure 4-2 displays the starting material **4** (δ 5.0 mDa)($M+H^+$), whereas the ion peak at *m/z* 173.1074 corresponds to the final product **50**$^+$ (δ 0.1 mDa). See the bottom spectrum of Figure 4-3 (closer view around 170 – 180 *m/z* regions) for the 173 ion peak. Also, the expected intermediate dihydropyridinium species was observed at *m/z* 175.1233 (δ 0.3 mDa). Results (shown in the bottom spectrum) indicated the conversion from **4** to **50**$^+$ in the presence of **42**, and this reaction proceeds via the intermediate DHP^+. In addition, a small amount of crystalline separated from the solution at t = 48 hours; X-ray crystallography data revealed that the particles were **42**.

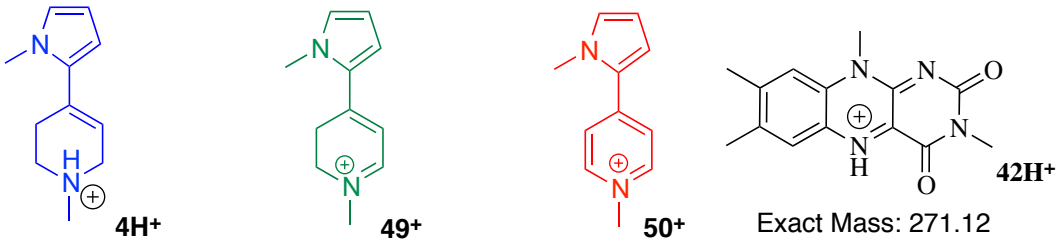

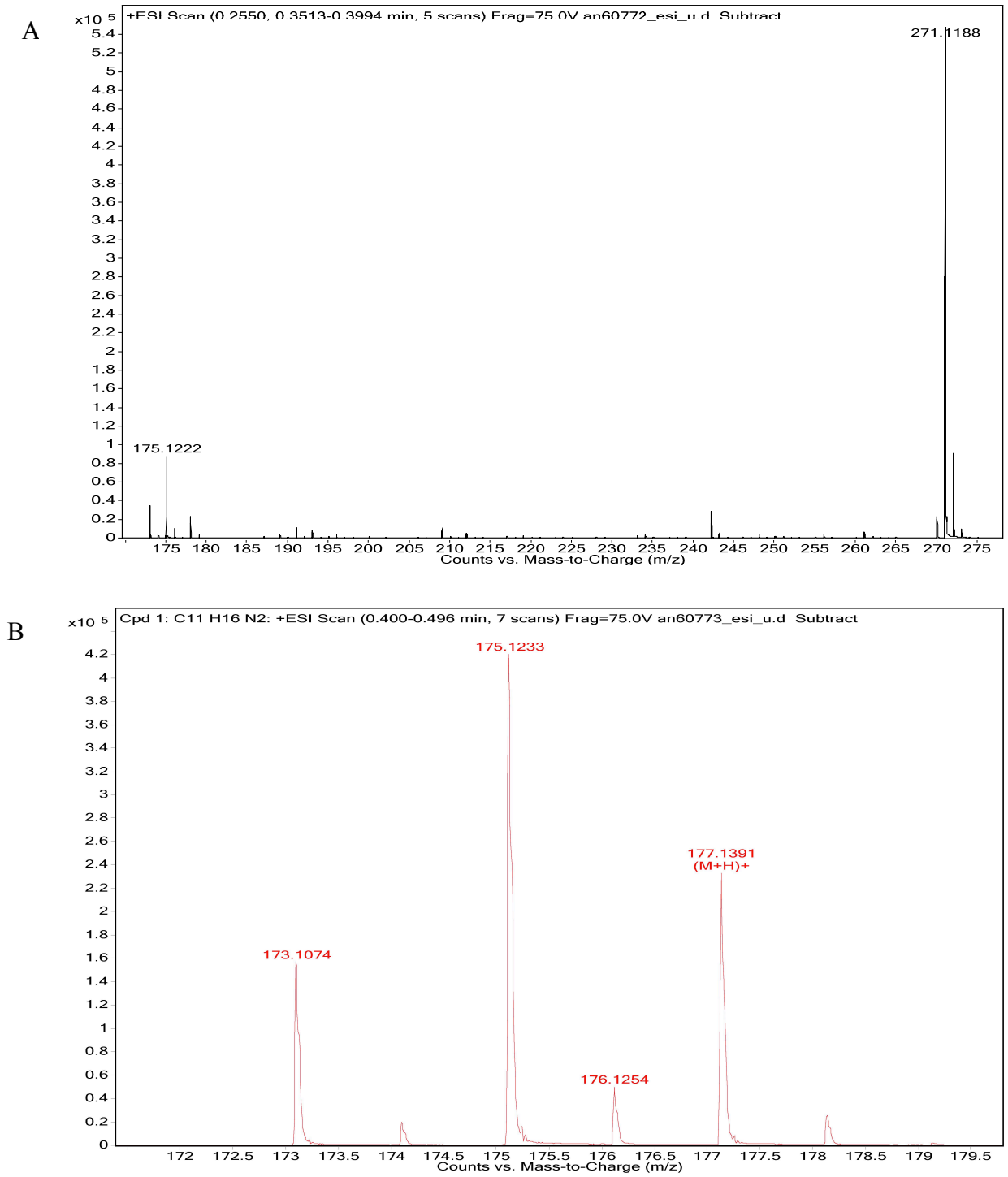

Figure 4-2. Accurate masse ESI$^+$ mass spectra of the reaction product. The reaction mixture of 3MLF (3 mM) with TMMP (13 mM) in commercial grade acetonitrile was examined at t = 48 hours (*x*-axis: *m*/*z*; *y*-axis: relative abundance): the protonated TMMP, the intermediate DHP$^+$, and the product MMP$^+$ (left)[closer view around 170 – 275 *m*/*z* (A, top) and around 170 – 180 *m*/*z* regions (B, bottom)].

The reaction mixture **42** (3.7 mM) and TMMP (25 mM) was monitored using NMR. The solvent was acetonitrile-d_3, and the 1 mL vial was opened immediately before use (Cambridge Isotope Laboratories, Inc.). The reaction mixture was stored in the dark at room temperature. Figures 4-3 and 4-4 show the ^{1}HNMR spectra of the starting materials, **42** and **4**. Figure 4-5 displays the NMR spectrum of **50$^+$**, the oxidized product of **4**.

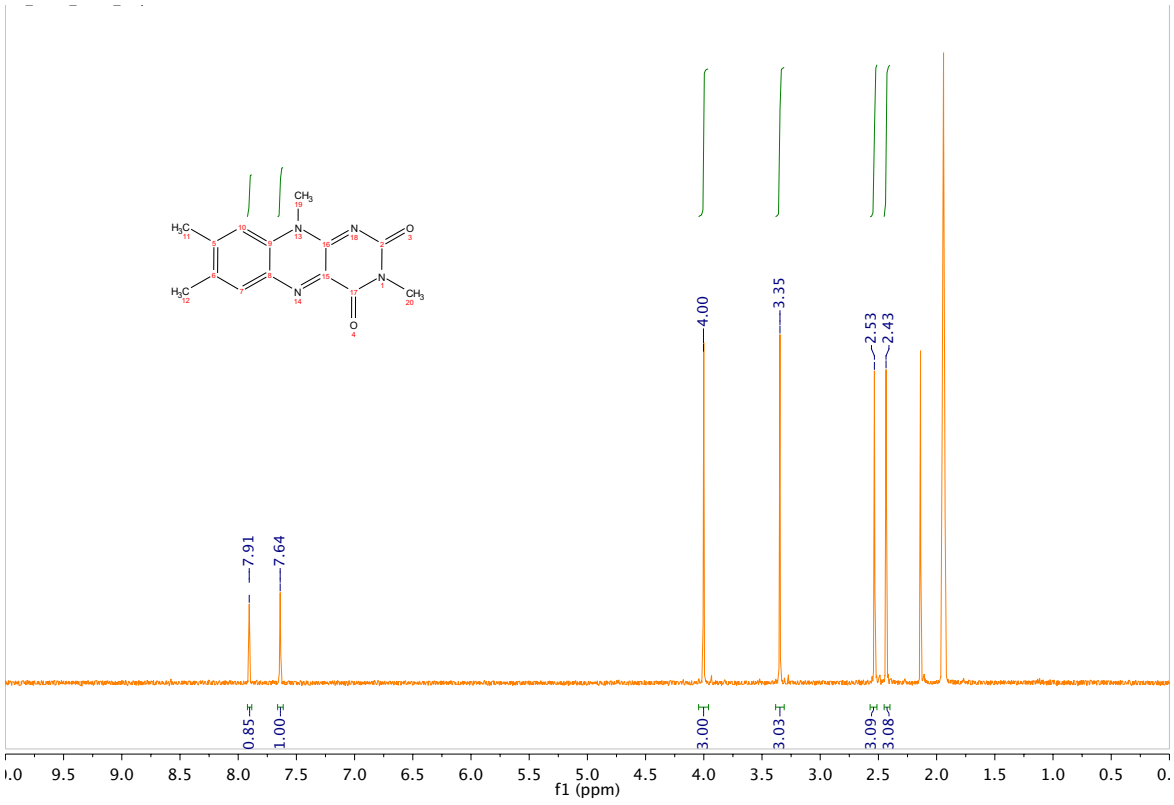

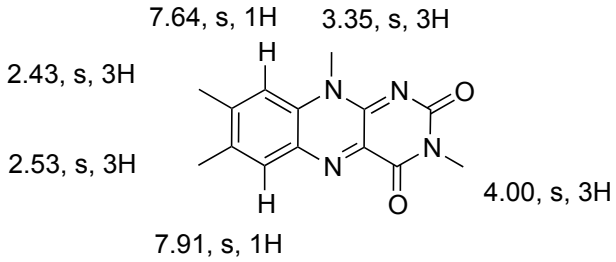

Figure 4-3. ^{1}H-NMR spectrum of 3-methyllumiflavin in acetonitrile-d_3 and chemical shift assignments (500MHz).

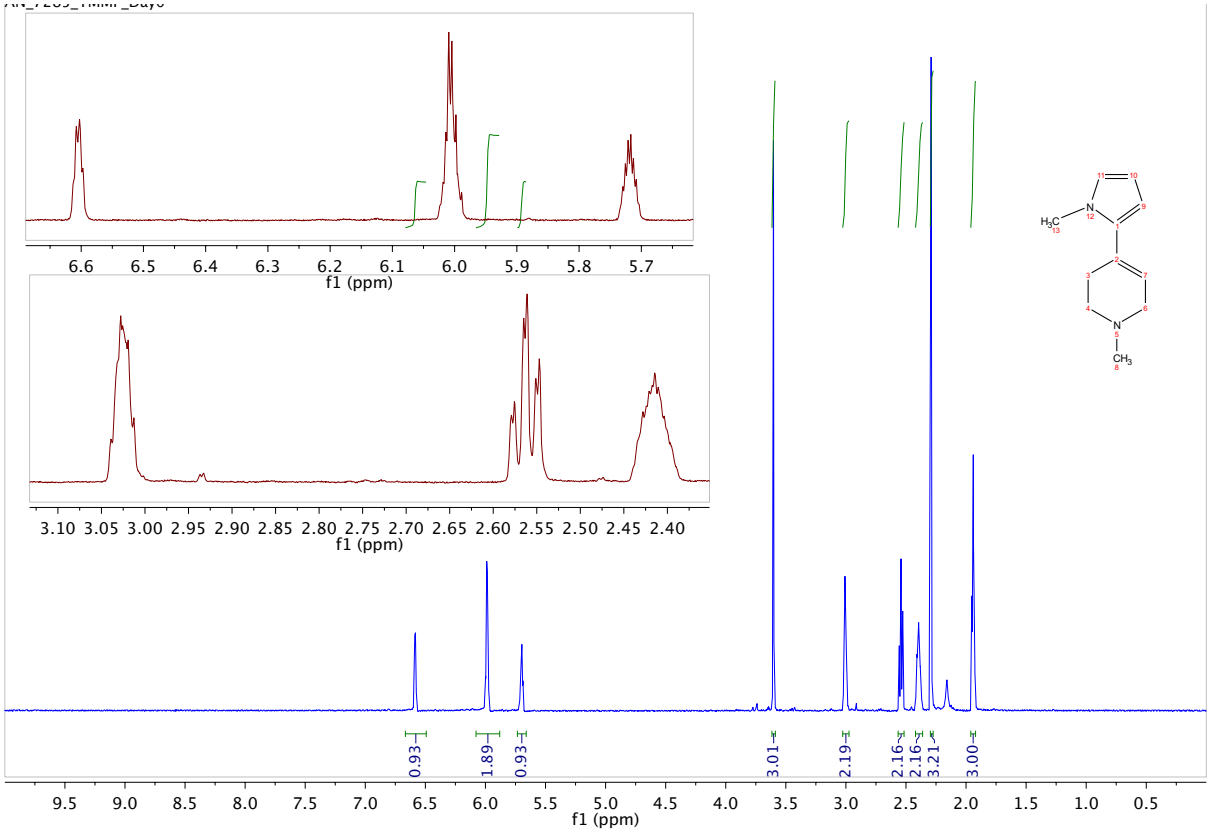

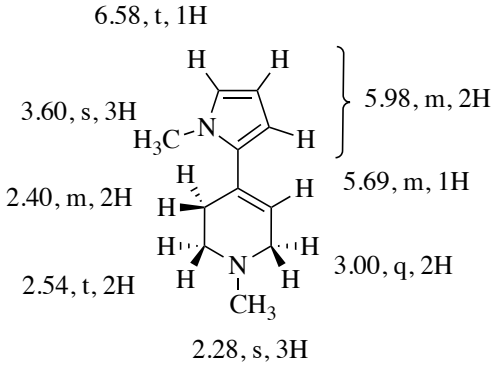

Figure 4-4. [1]H-NMR spectrum of TMMP chemical shift assignments (500MHz, CD_3CN).

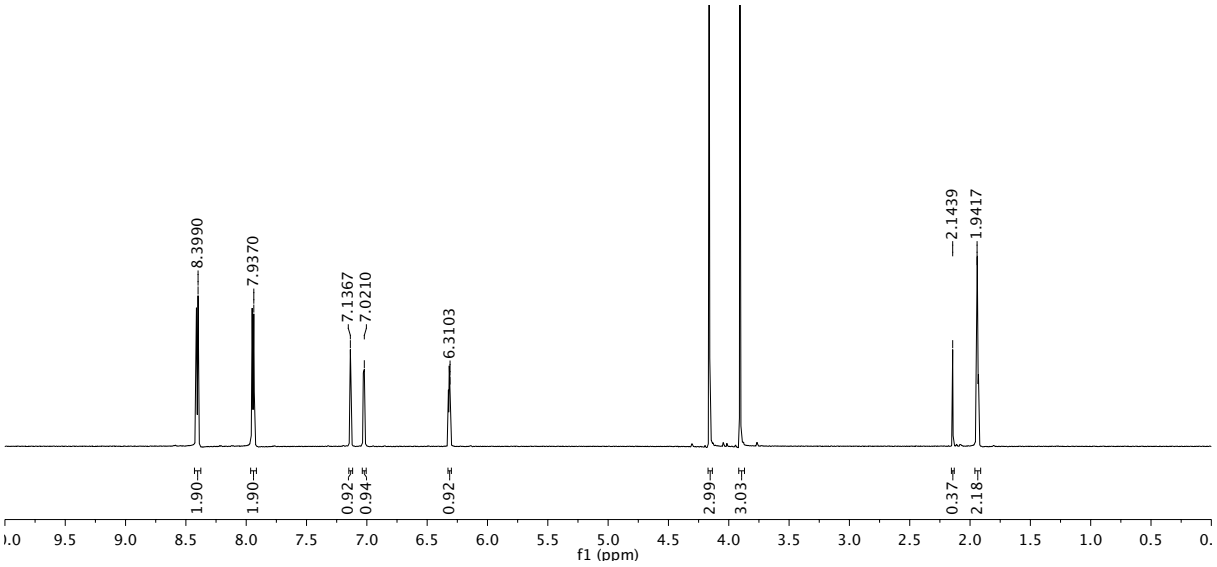

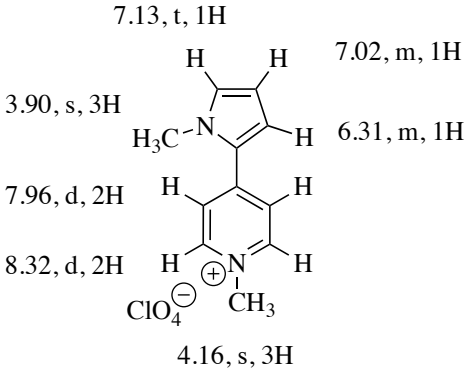

Figure 4-5. ^{1}H-NMR spectrum of MMP^{+} and chemical shift assignments (400MHz, CD_3CN).

For quantitative analysis, the solvent peak (CH_3CN) at 1.94 ppm was integrated as 3.00 (Figure 4-5). The areas under the curves for the various signals were integrated as a measure of concentrations. The reaction between **42** (3.7 mM) and **4** (25 mM) in acetonitrile-d_3 in the presence of air was monitored using NMR over the course of 1300 hours. The samples were stored in the dark at room temperature. The NMR tubes were capped, and the capped area was wrapped in parafilm, so that the solvent did not evaporate during the course of the reaction. The spectra of the reaction mixture at = 0, 24, 96, 192, 480, 1300 hours are presented in Appendix J.

Signals at 3.99 and 7.63 ppm (**42**), 5.70 and 5.98 ppm (**4**), and 4.14 and 8.33 ppm (**50^{+}**) were chosen as markers because they do not overlap with other signals. The experiment was run in

duplicate and the concentrations were calculated from the average intensity of signals for each peak. Because this reaction proceeds slowly, the concentration of **4** at t = 0 min was assumed to correspond to 25 mM. The concentrations of $\mathbf{50^+}$ and **42** were calculated by ratio analysis based on the integrated intensities of the TMMP peaks.

The results established that the concentration of **42** did not change throughout the experiment. As the reaction progressed, the TMMP concentration decreased while the concentrations of $\mathbf{50^+}$ increased. At t = 24 hours, the concentrations of **4** and $\mathbf{50^+}$ were 22.5 mM and 1.08 mM. At t = 120 hours, the concentrations were 21.08 mM and 2.42 mM, respectively. At t = 480 hours, the concentrations were 15.01 mM and 4.73 mM, respectively. Note that the total of the **4** and $\mathbf{50^+}$ concentrations totaled less than 25 mM as the reaction progressed. It is possible that evidence of an intermediate(s) might not be resolvable in the NMR spectra. At t = 840 hours, the concentration of $\mathbf{50^+}$ was 6.12 mM (165 % yield). This result suggests that the oxidation of **4** in the presence of **42** occurs at room temperature. Both the UV/vis and NMR data support the catalytic-oxidation characteristics of **42**.

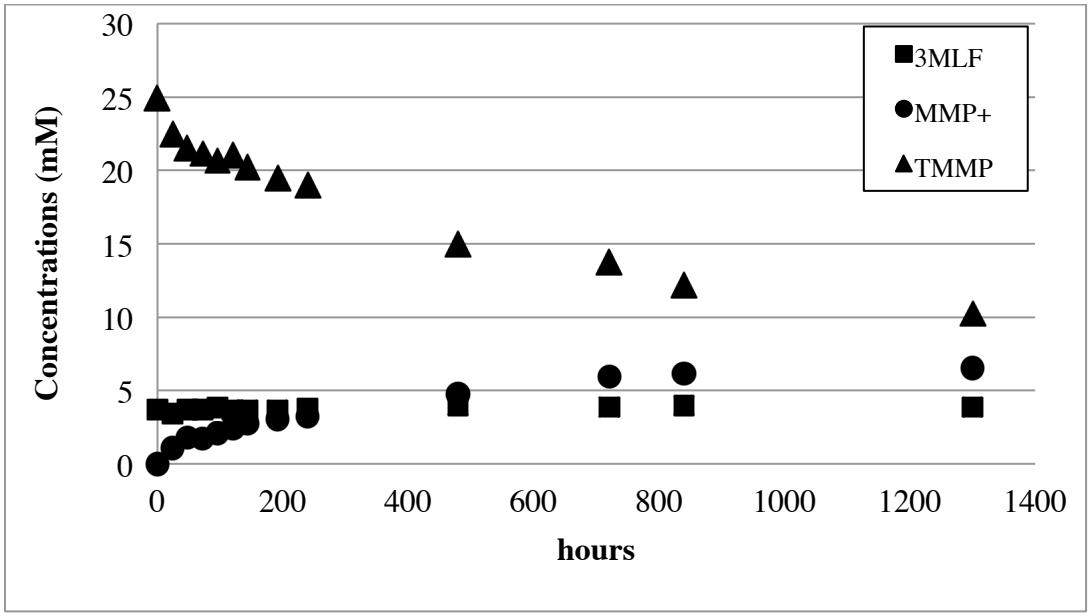

Figure 4-6. Comparison of concentrations of the starting materials and product. Reaction of 3MLF (3.7 mM) and TMMP (25 mM) at 1 to 6 molar ratio reaction in acetonitrile-d_3 in the dark at room temperature. The values are the average of duplicated samples.

4.2.2 The Effect of Dioxygen and Water

The effect of dioxygen on the reaction between **42** and **4** was also examined. The reaction between **42** (12.25 mM) and **4** (25.12 mM) was monitored using NMR spectroscopy under argon or in air (duplicate samples for each). The solvent (acetonitrile-d_3) was pre-treated with CaH_2 for two days prior to the experiment, degassed, and then distilled under argon. A valved NMR tube was used for this experiment because it is designed to improve the safety of sample handling for volatile, air-sensitive compounds. Initially, **42** was placed in valved NMR tubes, and the pre-treated acetonitrile-d_3 was vacuum-transferred to the valved NMR tubes containing **42**. Then, the 3MLF solution was warmed to 70 °C in order to dissolve all 3MLF crystals. Once the 3MLF solution cooled down, the NMR tubes were transferred to a glove box where **4** was added to the NMR tubes anaerobically. After mixing the two starting materials (**42** and **4**), the sample tubes were taken to the NMR room and a time-dependent experiment was initiated. All four samples were prepared under anaerobic conditions, and the NMR spectra of the reaction mixture were recorded immediately after mixing **42** and **4** (T_{ag} = 0 min). Next, two sample solutions were exposed to the air after recoding the NMR spectra (aerobic samples), and the other two samples remained under argon (anaerobic samples). For quantitative analysis, hexamethyldisiloxane (18 protons, signal at 0.06 ppm) was used as an internal standard in the aerobic samples on Day 10.

When the two substrates were mixed in the glove box, no color change was observed. The solvent peak (CH_3CN) at 1.94 ppm was integrated as 3.00. Signals at 3.99 and 7.63 ppm (**42**), 5.70 and 5.98 ppm (**4**), and 4.14 and 8.33 ppm (**50$^+$**) were used as markers. Both aerobic and anaerobic samples were monitored by ^{1}HNMR for 38 days. However, formation of **50$^+$** was not observed to any significant extent under either condition. Figure 4-7 displays the NMR spectra of the reaction in air, and the signals for **50$^+$** (4.14 and 8.33 ppm) were not particularly evident even by Day 23. The failure to observe **50$^+$** was puzzling because it had been detected in previous experiments.

Recall that acetonitrile-d_3 was pre-treated with CaH_2 for two days, degassed, and then distilled under argon immediately before mixing with **4** and **42** for the NMR experiment. Also, valved NMR tubes were used to hold the sample solutions, and valved NMR tubes are reliable for excluding air or moisture. Consequently, exposure to water was not significant in the reaction

mixture; the oxidation of **4** with **42** may require water, presumably for proton transfers, for the reaction mechanism to proceed. The absence of NMR signals in the presence of radicals is discussed in Chapter 3-2.

Since MMP^+ (50^+) was not evident in the NMR spectrum by day 23 (Figure 4-7, middle), D_2O was then added to the aerobic samples, and again these samples were further monitored using NMR spectroscopy. However, the generation was less than expected (Figure 4-7, bottom). Addition of D_2O slightly increased the intensity of MMP^+ peaks on ^{1}HNMR spectra; the concentration of $\mathbf{50^+}$ was 4.5 mM at t = 360 hours. It is possible that an intermediate(s) had degraded before the addition of D_2O.

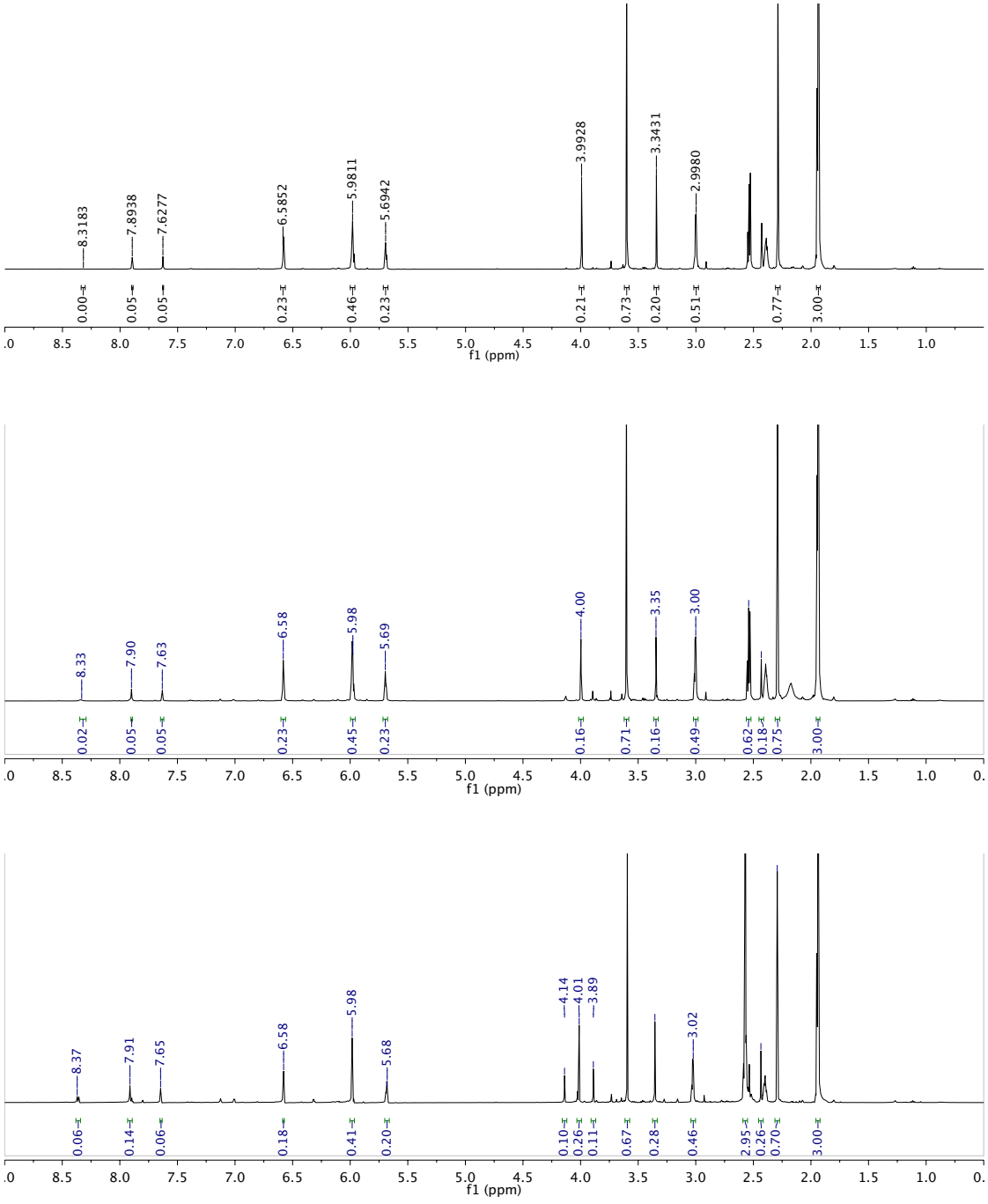

Figure 4-7. ^{1}H NMR spectra of the reaction mixture in air in pre-gassed/distilled acetonitrile-d_3 (500 MHz). Samples (3MLF 25 mM and TMMP 50 mM) were prepared in a glove box. Top: t = 0 min, immediately after mixing 3MLF and TMMP; middle: t = 23 days after mixing the two substrates; and bottom: t = 360 hours after the addition of D_2O. Samples were stored in darkness at room temperature. These were integrated based on the solvent peak as 3.00.

Next, the effect of air on the oxidation reaction was examined by NMR. Figure 4-8 shows the reaction mixture **42** (12.25 mM) and **4** (25.12 mM) immediately after mixing them under argon (t = 0 min) and later at t = 24 hours (anaerobic samples). There was not a significant difference between these ^{1}H NMR spectra at t = 0 min and t = 24 hours; the spectrum appeared as if it were a superimposed image of the two starting materials (Figure 4-8, top). However, alterations were found after 24 hours. Notice that the peaks corresponding to **42** disappeared by this time, which were located at δ = 7.62 (1H), 7.88 (1H), 3.98 (3H), 3.40 ppm (3H)(Figure 4-8, bottom).

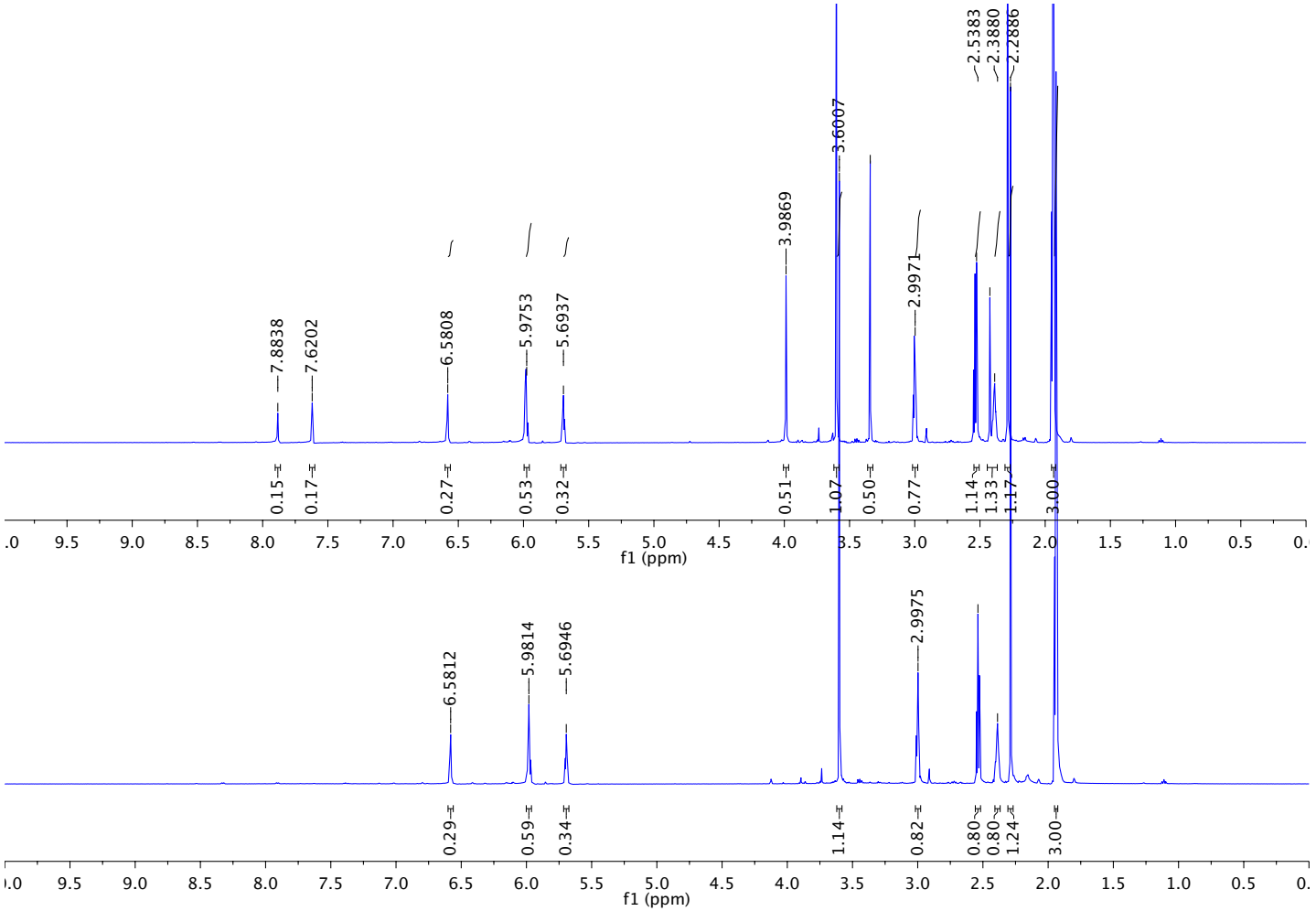

Figure 4-8. [1]H NMR spectra of the reaction mixture under argon in pre-gassed/distilled acetonitrile-d_3 (500 MHz). The sample was prepared in a glove box. Top: t = 0 min, immediately after mixing 3MLF (12.25 mM) and TMMP (25.50 mM), and bottom: t = 24 hours after mixing the two substrates. Samples were stored in the dark at room temperature. These were integrated based on the solvent peak as 3.00.

Figures 4-9 shows the effect of dioxygen on the reaction mixture **42** (12.25 mM) and **4** (25.50 mM). Before adding the air to the reaction mixture, the signals for **42** could not be detected (Figure 4-9, top). However, immediately after air introductions, the signals for 3MLF re-appeared (Figure 4-9, bottom). This result indicates the effect of dioxygen on the reaction, but it is not clear if the dioxygen is involved in the oxidation of **4** or in the conversion of the reduced 3MLF (**42H$_2$**) to oxidized 3MLF (**42**).

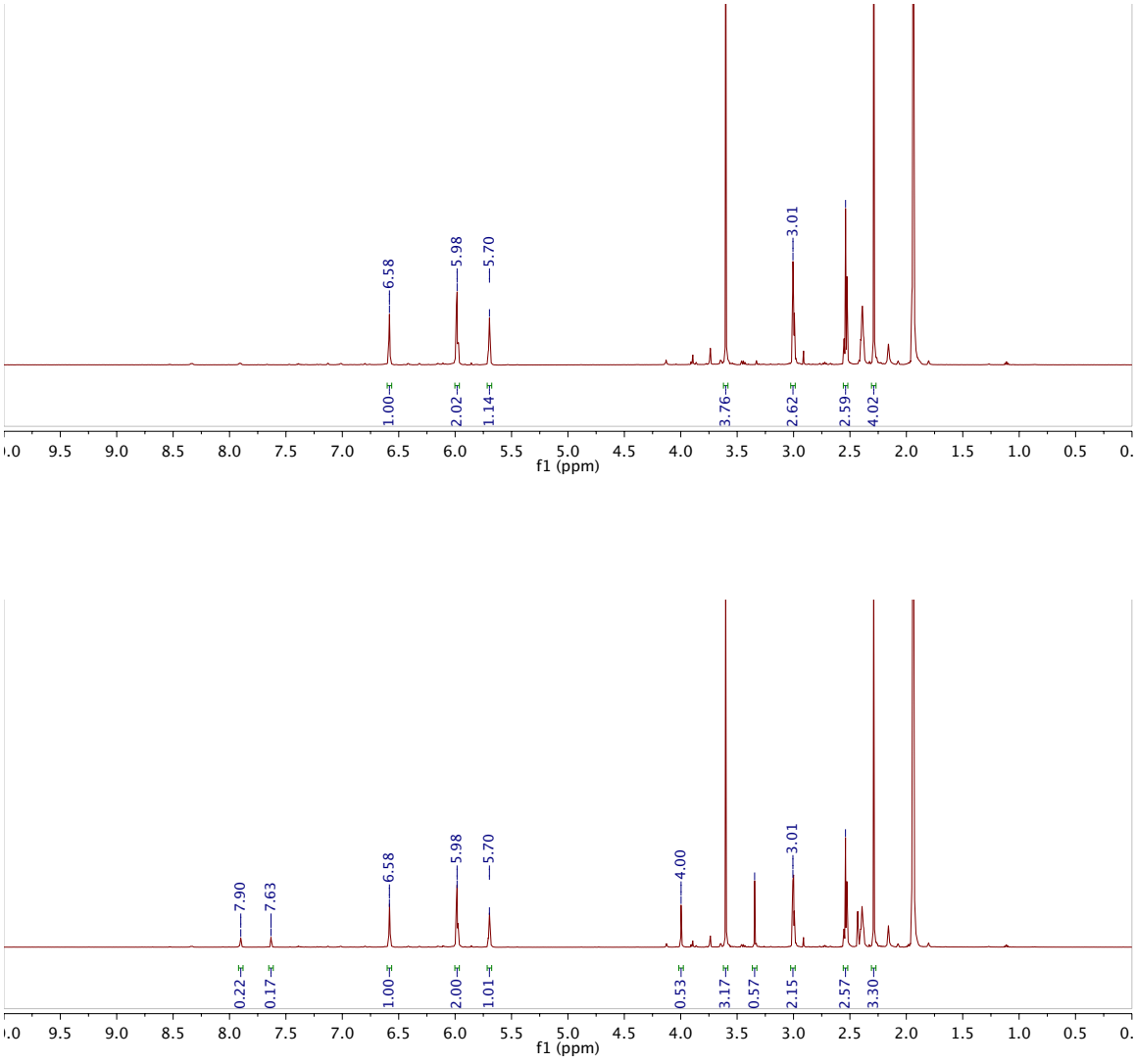

Figure 4-9. ^{1}H NMR spectra of the reaction mixture under argon in pre-gassed/distilled acetonitrile-d_3 (500 MHz). The sample was prepared in a glove box: t = 10th day after mixing 3MLF (25 mM) and TMMP (50 mM)(top) and immediately after addition of air to the reaction mixture. Samples were stored in the dark at room temperature (bottom).

Similar to these findings, the absence of NMR signals was observed in the ^{1}H NMR spectra of the reaction between **43**$^+$**ClO**$_4^-$ and **4** under argon, as reported in Chapter 3. EPR data discussed in Chapter 3 (Figure 3-2-19) indicated the formation of radicals in that reaction mixture. Therefore, my next attempt was to analyze the reaction mixture between **42** and **4** by EPR.

Figure 4-11 displays the EPR spectrum of the reaction mixture prepared in dried acetonitrile in argon on Day 14. To my knowledge, an EPR spectrum of the 3MLF radical anion had not been published before. The EPR data support the formation of radicals in the reaction mixture, **42** and **4** (1 to 2 molar ratio), which suggest SET involvement in the reaction mechanism. Also, because the reaction mixture may contain a mixture of radicals, the spectrum displays complicated pattern, and interpretation is difficult.

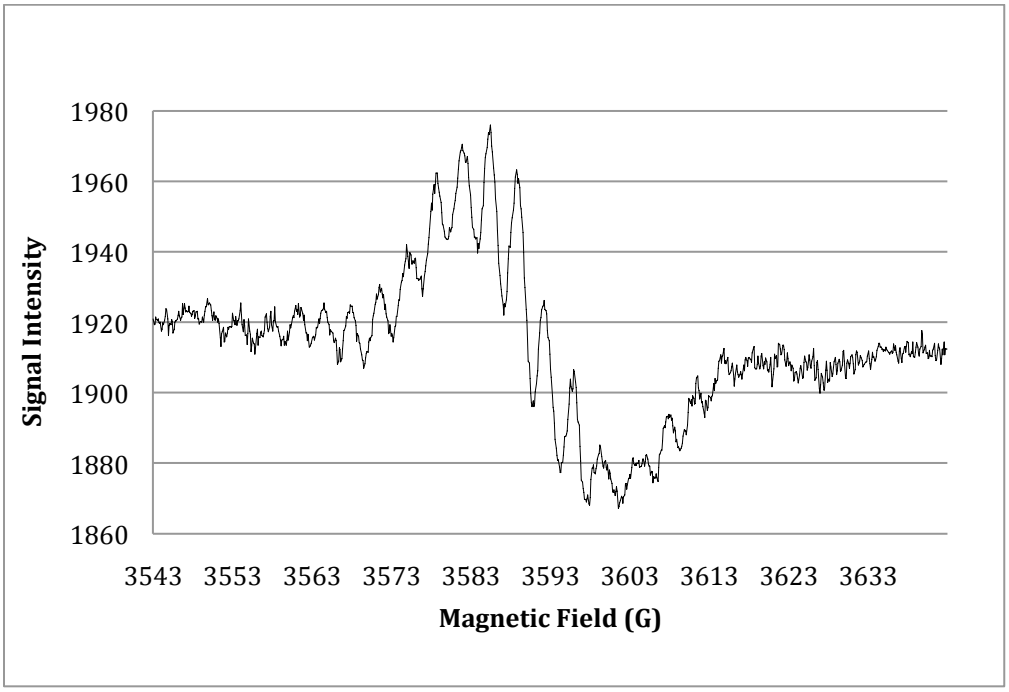

Figure 4-10. EPR recording of the reaction mixture in air. The spectrum shows the reaction of 3MLF 25 mM and TMMP 50 mM in dried acetonitrile-d_3 in anaerobic conditions.

It is worth mentioning the solubility characteristics of **42** in acetonitrile. When the reaction was initiated, both **42** and **4** were well dissolved in acetonitrile. However, as the reaction progressed, some particles precipitated out of the solution by the conclusion at t = 48 hours. A portion of the reaction mixture was submitted to X-ray crystallography, which revealed that that the particles consisted of **42**. The reason that 3MLF precipitates out of the solution under a reaction is unclear. It is possible that the prepared solution was supersaturated.

4.3 Conclusions

In summary, the above results suggest the catalytic oxidation of a tertiary allylamine **4** with **42** at room temperature in normal conditions. The present study also showed that a SET is involved in the oxidation mechanism, which is supported by the EPR data. The SET involvement with **42** is a remarkable finding because **42** is more structurally related to the flavin in a FAD compared to the flavinium salt $\mathbf{43^+ClO_4^-}$; the C4a position of **42** is not as electrophilic as the C4a position of $\mathbf{43^+ClO_4^-}$. Moreover, dioxygen plays a role in the oxidation of **4** with **42**, which most likely occurs in a step immediately after the SET involvement, which is followed by the radical formation in the reaction. Also, the evidence strongly indicates that water is associated with the oxidation of **4** with **42**. How water contributes to the oxidation should be studied further.

Scheme 4-2 shows a proposed mechanism of the oxidation of **4** with **42** in the presence of air. The 3MLF radical anion ($\mathbf{42^{\bullet -}}$) removes a proton from TMMP radical cation ($\mathbf{4^{\bullet +}}$), leading to the generation of the neutral 3MLF radical ($\mathbf{42H^{\bullet}}$) and neutral TMMP radical ($\mathbf{4^{\bullet}}$). The reaction between the oxygen molecule and $\mathbf{42H^{\bullet}}$ yields a C4a peroxy radical ($\mathbf{60^{\bullet}}$), which is followed by the formation of a C4a,10a-dioxetane (**60H**) by internal cyclization. This flavin C4a, C10a-dioxenane derived from the C4a-hydroperoxyl adduct was reported with $\mathbf{43^+ClO_4^-}$ previously.[72] When the reduced form of 3MLF ($\mathbf{42H_2}$) is oxidized with dioxygen, the oxidized form of 3MLF (**42**) and H_2O_2 are regenerated. In addition, the oxidation of **4** proceeds via the intermediate $\mathbf{49^+}$ and generates the oxidation product of $\mathbf{50^+}$ (see Chapter 3 for detail).

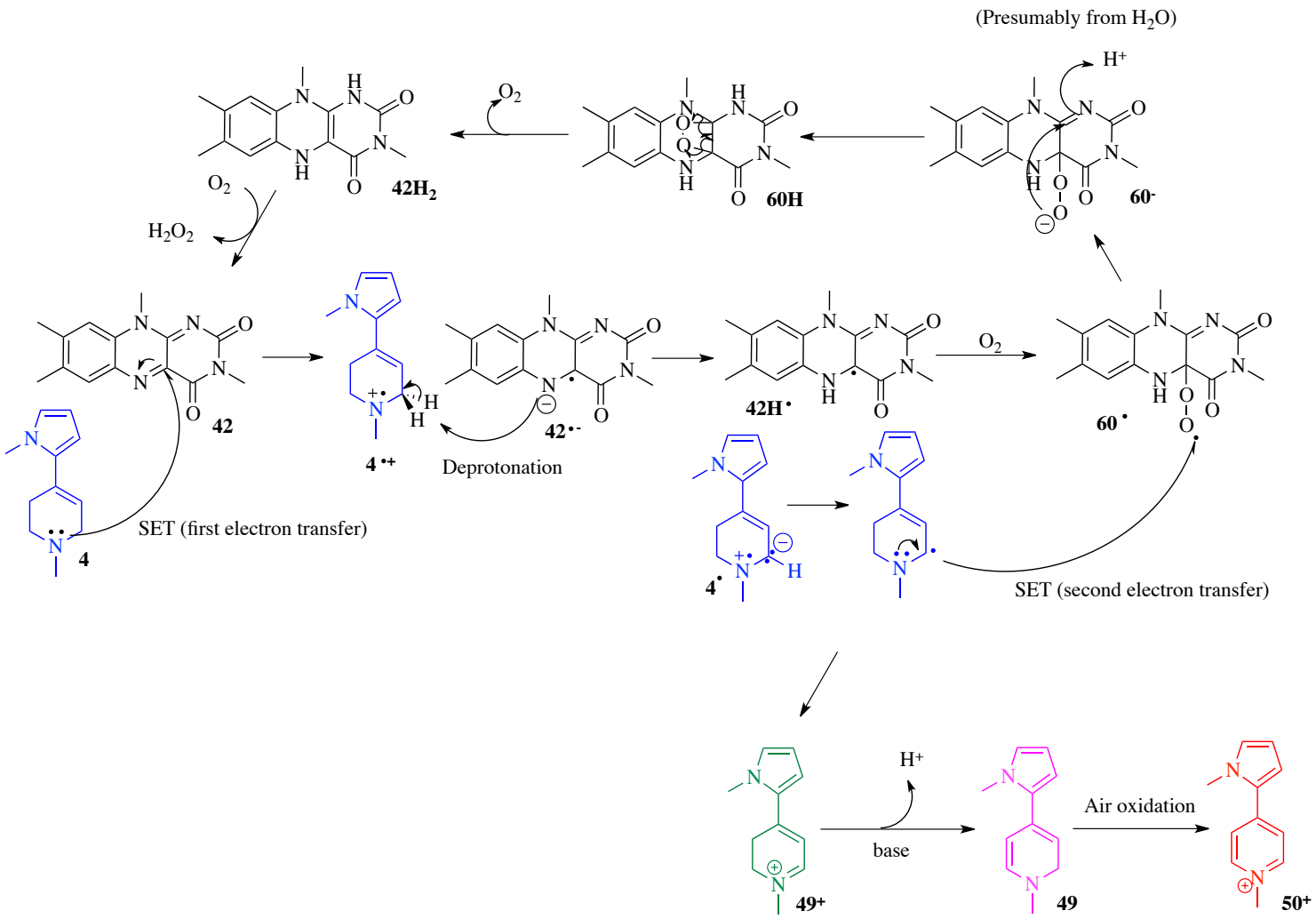
(Presumably from H2O)
H+
O2
42H2
60H
60-
O2
H2O2
42
4 •+
Deprotonation
42 •-
42H •
O2
60 •
4
SET (first electron transfer)
4 •
SET (second electron transfer)
49+
H+
base
49
Air oxidation
50+

Scheme 4-2

CHAPTER FIVE

EFFECT OF WATER ON 5-ETHYL-3-METHYLLUMIFLAVINIUM PERCHLORATE

5.1 Interaction of 5-Ethyl-3-methyllumiflaivnium perchlorate and Water

The effect of water on 5-ethyl-3-methyllumiflavinium perchlorate [5Et3MLF$^+$ClO$_4^-$, (**43$^+$ClO$_4^-$**)] is the focus of this section's discussion. The interaction between the hydroxide anion and the **43$^+$ClO$_4^-$** species was first observed unexpectedly while examining the reaction of **43$^+$ClO$_4^-$** with **4**. Because 1-methyl-4-(1-methyl-1*H*-pyrrol-2-yl)-1,2,3,6-tetrahydropyridine [TMMP (**4**)] is stored as TMMPH$^+$ oxalate (**4H$^+_{ox}$**), a base was added to the mixture in order to deprotonate **4H$^+_{ox}$** and produce a free base **4**. Triethylamine [Et$_3$N (**53**)] was added to the mixture of **43$^+$ClO$_4^-$** and **4H$^+_{ox}$** (experimental solution) to promote a reaction between **43$^+$ClO$_4^-$** and TMMP (structures shown below).

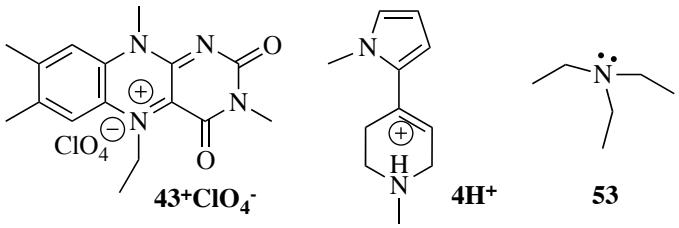

The solution of **43$^+$ClO$_4^-$** alone was dark purple, and the solution of **4H$^+_{ox}$** alone and the solution of **53** alone were both colorless. The concentrations of **43$^+$ClO$_4^-$** and **4H$^+_{ox}$** were 1.25 mM, and the concentration of **53** was 2.75 mM (1 to 2.2 molar ratio reaction). The solvent used for these reactions was commercial grade acetonitrile (anhydrous 99.9%, AcroSeal™) unless described otherwise. In order to validate that there were no side reactions, control samples were also prepared to facilitate comparison: a mixture of **4H$^+_{ox}$** and **53** (control #1) and a mixture of **43$^+$ClO$_4^-$** and **53** (control #2).

First, after mixing **43$^+$ClO$_4^-$** and **4H$^+_{ox}$** in commercial grade acetonitrile, no color changes were observed. When the compounds **43$^+$ClO$_4^-$**, **4H$^+_{ox}$**, and **53** are combined in a reaction mixture, color changes in the reaction mixture were apparent, from purple into green. The control 1 solution (mixture of **4H$^+_{ox}$** and **53**) was colorless, whereas the control 2 solution (mixture of **43$^+$ClO$_4^-$** and **53**) changed in color from purple to a lemon-yellow shade. It is distinctly possible that compounds **43$^+$ClO$_4^-$** and **53** had reacted within the control 2 solution. Consequently, the

mixture of **43^{+}ClO$_4^{-}$** and **53** was further monitored using UV/vis spectroscopy.

Figure 5-1 shows a comparison between the UV/vis spectra for the compounds **43^{+}ClO$_4^{-}$** and **53** in the reaction mixture, dissolved in acetonitrile at room temperature. The chromophores for **43^{+}ClO$_4^{-}$** were found at λ_{max} of 278 nm, 412 nm and 555 nm, and addition of compound **53** to that solution caused color changes observable in the spectrum; the bands at 412 nm and 555 nm disappeared at t = 1 min, while new peaks at 278 nm, 302 nm, and 350 nm appeared on the spectrum. The compound **53** chromophore at λ_{max} of 200 nm could not be monitored because of it absorbs at too low a wavelength.

At t = 1 min after mixing **43^{+}ClO$_4^{-}$** and **53** together, the chromophores for **43^{+}ClO$_4^{-}$** were missing on the reaction mixture spectra (Figure 5-1), suggesting that the conversion of **43^{+}ClO$_4^{-}$** in the presence of **53** occurs rapidly and the disappearance of the chromophores follows subsequentially. The spectrum of the reaction mixture remains unchanged between t = 1 min and t = 24 hours. Therefore, the UV/vis results indicate that some chemical change occurs when **43^{+}ClO$_4^{-}$** and **53** are mixed. The same chromophores still were present 24 hours later.

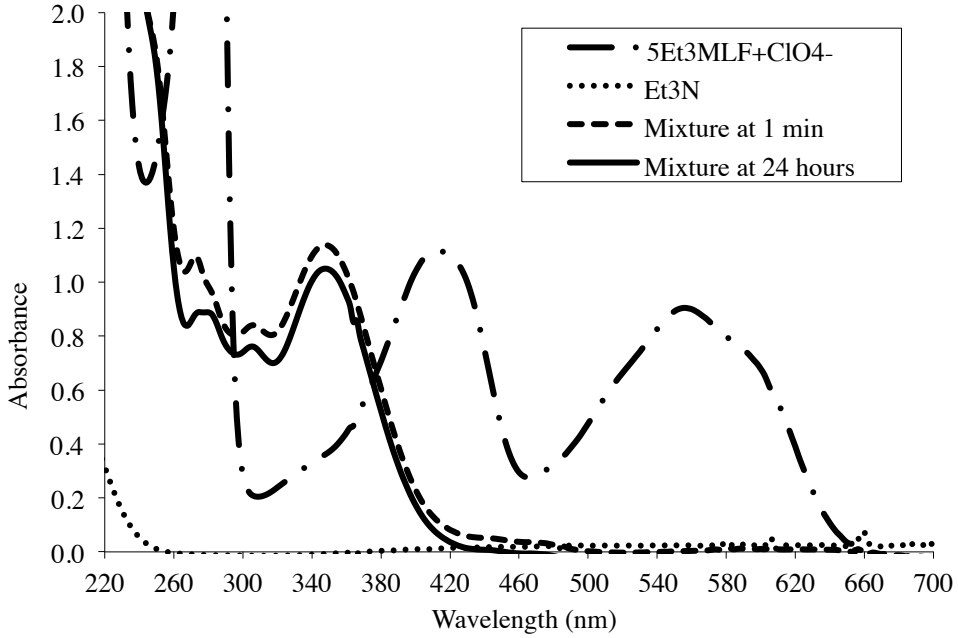

Figure 5-1. UV/vis spectra of the reaction mixture (5Et3MLF^{+}ClO$_4^{-}$ and Et$_3$N). The spectra show the reaction between 5Et3MLF^{+}ClO$_4^{-}$ (1.25 mM) and triethylamine (2.75 mM) with the molar ratio of 1 to 2.2, respectively, in acetonitrile. Dashed-dotted line flavinium only; dotted line, Et$_3$N only; dashed line mixture (5Et3MLF^{+}ClO$_4^{-}$ and Et$_3$N) t = 1 min; solid line, mixture (5Et3MLF^{+}ClO$_4^{-}$ and Et$_3$N) t = 24 hours.

The nature of the species formed in in the reaction mixture of **43$^+$ClO$_4^-$** and **53** were investigated using accurate-mass ESI$^+$/MS spectroscopy (Figure 5-2). The starting materials **43$^+$ClO$_4^-$** and **53** were detected; the ions at *m/z* 299.1485 and 102.1270 correspond to **43$^+$** and **53**, respectively and **43$^+$ClO$_4^-$** with mass accuracies of -6.85 ppm (2.4 mDa) and -8.02 ppm (2.6 mDa), respectively. The species at *m/z* 317 and 331 correspond to the compound at *m/z* 299 plus water [C4a hydroxyl adduct (C4a-OH)](**51H$^+$**)(MH$^+$) and methanol [C4a methoxyl adduct (C4a-OMe)](**63H$^+$**)(MH$^+$), respectively. The peak at *m/z* 331 might have resulted from the interaction between **43$^+$ClO$_4^-$** and the mobile phase (methanol/water) of the instrument and to form the C4a-OMe adduct (**63H$^+$**).[§§§]

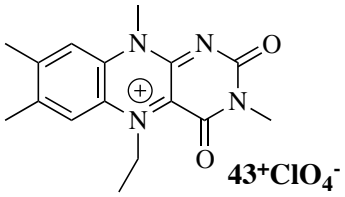

43$^+$ClO$_4^-$

Chemical Formula: $C_{16}H_{19}N_4O_2^+$
Exact Mass: 299.1503

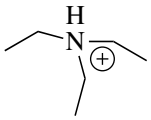

53H+

Chemical Formula: $C_6H_{16}N^+$
Exact Mass: 102.1277

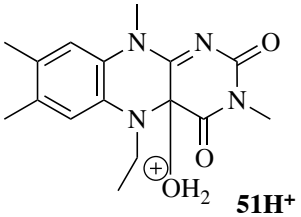

51H$^+$

Chemical Formula: $C_{16}H_{21}N_4O_3^+$
Exact Mass: 317.1608

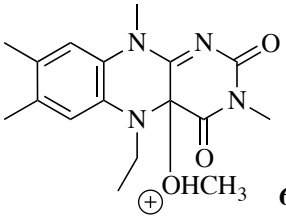

63H$^+$

Chemical Formula: $C_{17}H_{23}N_4O_3^+$
Exact Mass: 331.1765

[§§§] Results indicated that the mobile phase (methanol) could interact with 5Et3MLF$^+$ and/or the C4a-OH adduct, leading the formation of C4a-OMe adduct. Therefore, after this experiment, acetonitrile alone was used for investigations involving the 5Et3MLF$^+$ species.

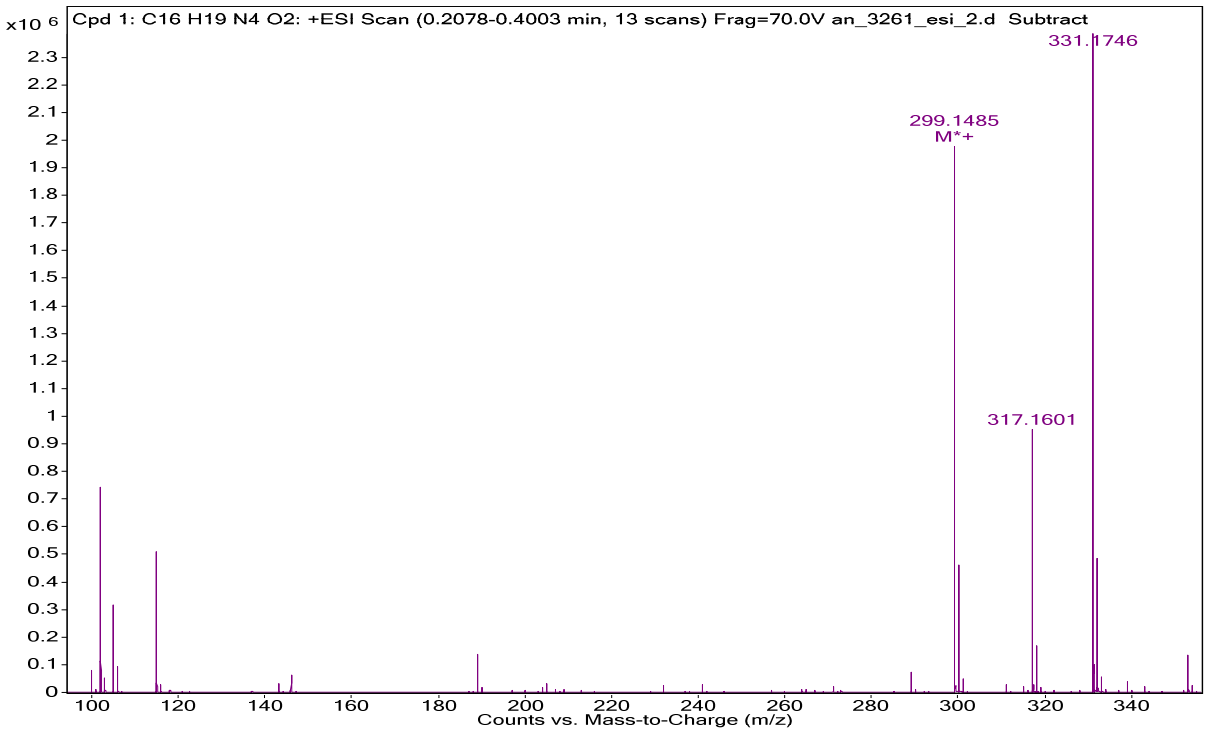

Figure 5-2. Accurate-mass ESI^+/MS spectra of the reaction mixture of $5Et3MLF^+ClO_4^-$ with triethylamine. ESI^+ mass spectrum (*x*-axis: *m*/*z*; *y*-axis: relative abundance) with a closer view of 290 – 340 *m*/*z* regions.

The ESI^+/MS data demonstrated the formation of the C4a-OH adduct (**51**). It is possible that $\mathbf{43^+ClO_4^-}$ in a solution containing acetonitrile and moisture reacts with the hydroxide anion to form **51**,[61b] which is unable to undergo further reaction (Scheme 5-1). To test this hypothesis, addition of D_2O to a solution of $\mathbf{43^+ClO_4^-}$ in acetonitrile-d_3 (30 mM, 500 μL) was monitored using ^{1}H-NMR. Figure 5-3 depicts the images of the compound $5Et3MLF^+$ in acetonitrile-d_3 (top) and with addition of ten drops of D_2O (bottom), which equaled approximately 176 μL. Results illustrate that the marker signal of $\mathbf{43^+ClO_4^-}$, the triplet (3H) at δ 1.80 ppm, shifted to 1.05 ppm after the addition of D_2O. Also, the aromatic protons at δ 7.96 ppm and 8.22 ppm shifted to δ 7.05 ppm and 7.17 ppm, respectively. Figure 5-4 compares ^{1}HNMR spectra between $\mathbf{43^+ClO_4^-}$ with water drops and with the isolated **51** (the isolation and identification of the adduct **51** is discussed later in this chapter, Section 5.3). Notice that the methylene protons in the product are diastereotopic and thus non-equivalent, and that these protons appeared as a multiplet

at δ 3.36 - 3.56 ppm on the NMR spectrum. Therefore, results indicated that the addition of water drops to a **43^{+}ClO$_4^{-}$** solution yields the hydroxyl adduct **51** of 5Et3MLF^{+}.

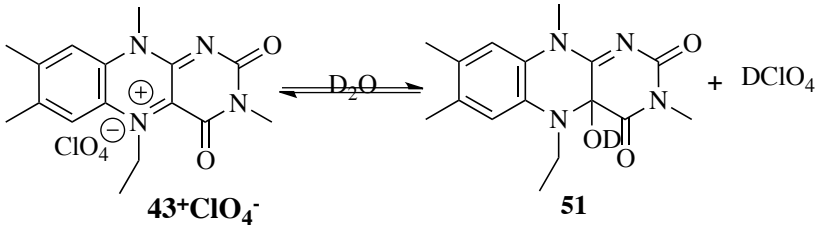

Scheme 5-1

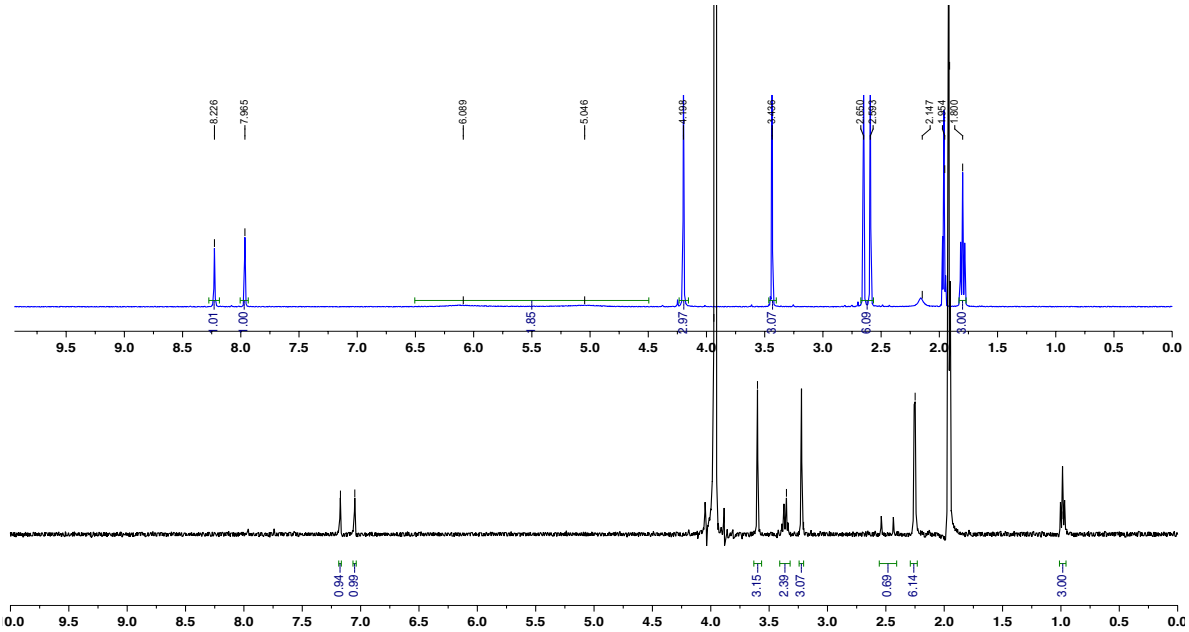

Figure 5-3. Effect of D_2O addition to 5Et3LF^{+}ClO$_4^{-}$ solution on NMR spectra. Comparison of ^{1}H NMR spectra of 5Et3LF^{+}ClO$_4^{-}$ in acetonitrile-d_3 (top, blue)(500 MHz) and after the addition of D_2O (10 drops) to that flavinium solution(bottom, black)(400 MHz, CD_3CN).

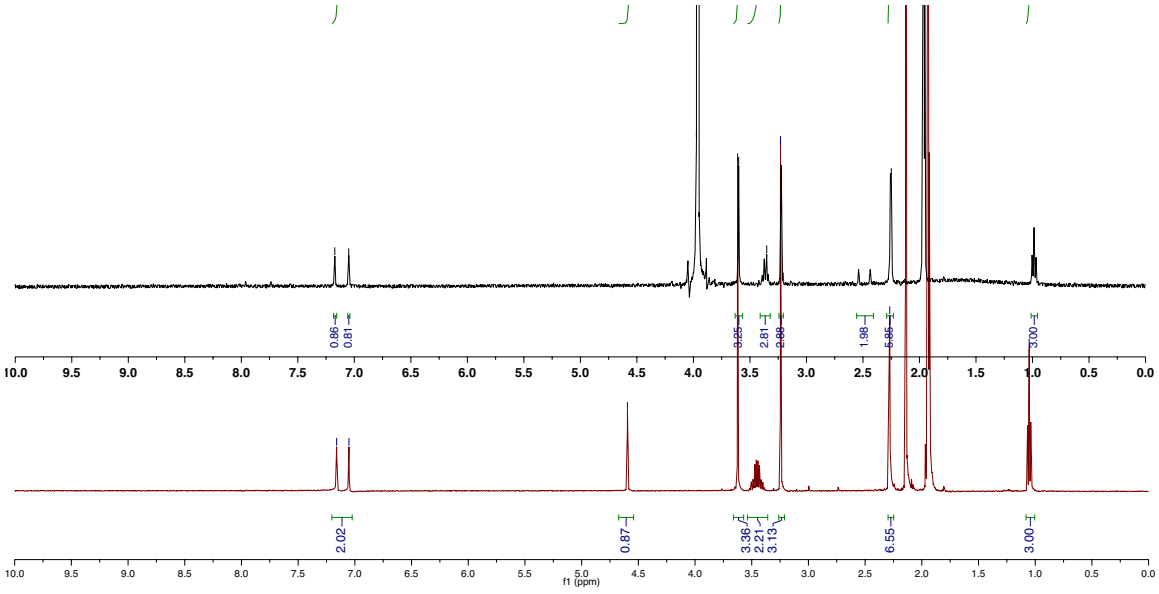

Figure 5-4. Formation of C4aOH adduct by D_2O addition. Superimposed image of the ^1H NMR spectrum showing $5Et3MLF^+$ in CD_3CN with **ten** drops of D_2O (black)(400 MHz) on the ^1H NMR spectrum of the 5Et3MLF-C4aOH adduct (maroon)(500 MHz).

To characterize further the effect of water on **$43^+ClO_4^-$**, UV/vis spectra in acetonitrile were obtained. First, 0.08 mM of **$43^+ClO_4^-$** solution in acetonitrile was prepared, and then ten drops of either water (experimental) or acetonitrile (control) was added to that flavinium solution (**$43^+ClO_4^-$**). Addition of acetonitrile to the flavinium solution (**$43^+ClO_4^-$**) was subsequently tested as a control study. After adding either water or acetonitrile, the solution was well mixed, and the UV/vis spectra of the compounds were then recorded. Figure 4 displays a comparison between spectra for the admission of acetonitrile and of water. Ten drops of water added to the flavinium solution (**$43^+ClO_4^-$**, 0.08 mM) significantly changed the UV/vis spectrum (Figure 5-5 A). The chromophores at λ_{max} 412 nm and 555 nm disappeared upon addition of water, and new peaks around 280 nm, 302 nm, and 350 nm appeared on the later spectrum. On the other hand, the control spectrum did not show any differences (Figure 5-5 B).

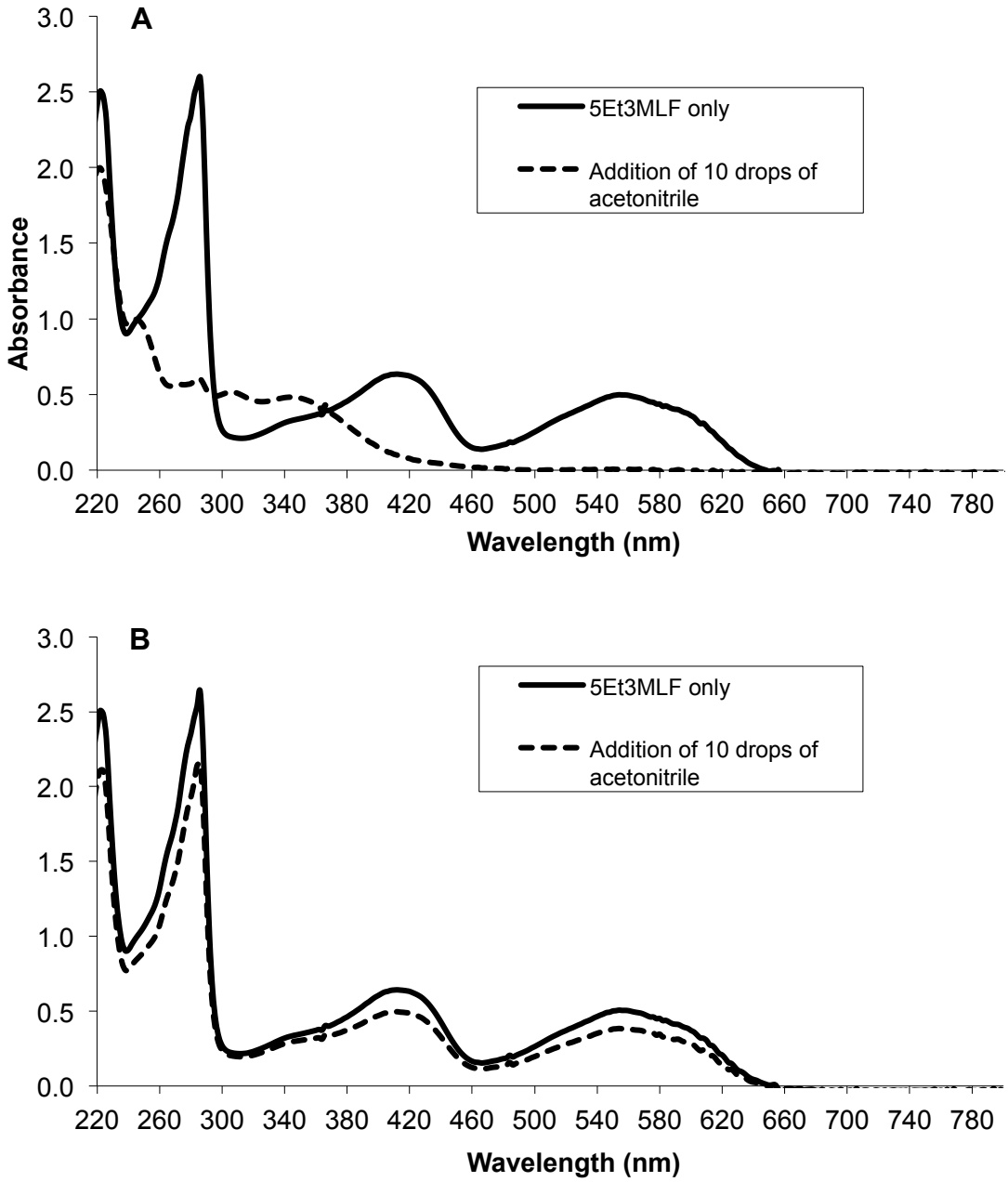

Figure 5-5. Effect of water addition on the absorbance bands of $5Et3MLF^{+}ClO_4^{-}$. The $5Et3MLF^{+}ClO_4^{-}$ solution was made in commercial grade acetonitrile (0.08 mM): (A) after the addition of H_2O (10 drops) and (B) after the addition of acetonitrile (10 drops).

In brief, the disappearance of the chromophores resulted from the presence of the hydroxyl adduct rather than the dilution of the solution. Both NMR and UV/vis data support the hydroxyl adduct formation with a solution of $\mathbf{43^{+}ClO_4^{-}}$ in wet acetonitrile.

Following the UV/vis study, the interaction of **43$^+$ClO$_4^-$** with water was examined using accurate-mass ESI$^+$/MS (Figure 6). A solution of **43$^+$ClO$_4^-$** was made in H_2O/acetonitrile (1 to 1 ratio) and incubated for 48 hours at room temperature in the dark. The accurate-mass ESI$^+$ mass spectrum displays the ions at *m*/*z* 317, 246, and 189 corresponding to **51H$^+$** (MH^+)(mass accuracy of – 4.10 ppm, δ 1.3 mDa), 2-acetamido-3-ethyl-1,5,6-trimethyl-1*H*-benzo[*d*]imidazol-3-ium (**64$^+$**)(mass accuracy of -7.31 ppm, δ 1.8 mDa), and 3-ethyl-1,5,6-trimethyl-1*H*-benzo[*d*]imidazol-3-ium (**47$^+$**)(mass accuracy of -6.34 ppm, δ 1.2 mDa), respectively. The accurate mass numbers for these compounds are listed below. The 246 species (**64$^+$**) might be a fragment ion for one of the intermediates in the proposed mechanism shown in Scheme 3. Assignments for the fragment ions at *m*/*z* 300 and 274 are not obvious. Isolation of the imidazolium from the solution was attempted using extraction and prep-TLC, however, this effort was not successful.

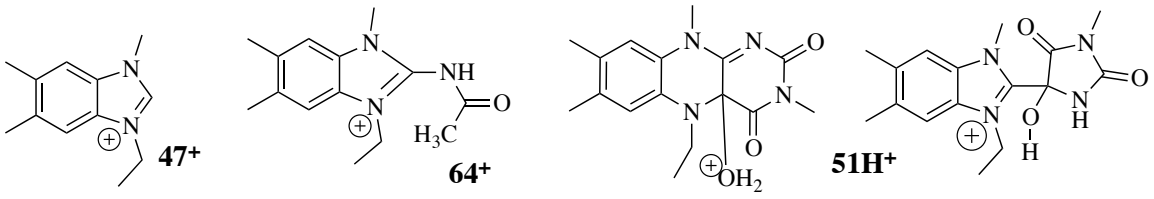

Exact Mass: 189.1386 Exact Mass: 246.1601 Exact Mass: 317.1608 Exact Mass: 317.1608

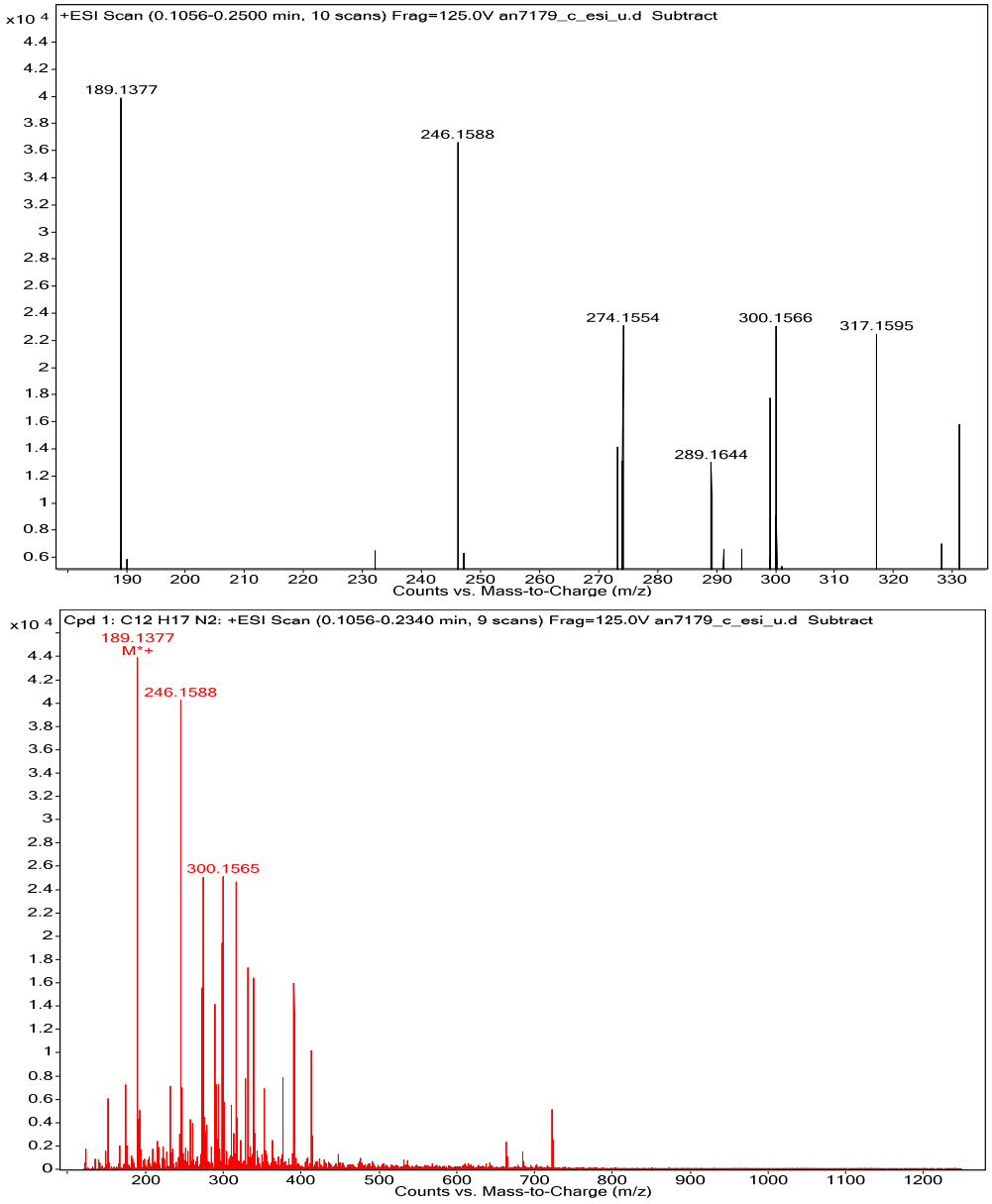

Figure 5-6. Accurate-mass ESI$^+$ mass spectra of 5Et3MLF$^+$ClO$_4^-$ in water/acetonitrile. 5Et3MLF$^+$ClO$_4^-$ was dissolved in 1 to 1 water/acetonitrile: an expansion of the spectrum from *m/z* 180 to *m/z* 330 (A) and a whole spectrum from *m/z* 100 to 1300 (B) (*x*-axis: *m/z*; *y*-axis: relative abundance). Solution was incubated at room temperature in the dark for 48 hours.

Previously, the imidazolium species was reported to be part of the fate of the flavinium;[35, 70] however, the characterization of the imidazolium was not reported, and to my knowledge, the species has never been studied elsewhere subsequent to this report. In the present study, the investigation of the transformation of **43$^+$ClO$_4^-$** into the imidazolium in the presence of a reducing agent $Na_2S_2O_4$ (1 to 1 molar ratio) in acetonitrile was examined using accurate-mass ESI$^+$/MS. The objective of this experiment was to identify potential intermediates of the fate of the **43$^+$ClO$_4^-$** species with the presence of a reducing agent. The first step was to dissolve **43$^+$ClO$_4^-$** in commercial grade acetonitrile, and add a few drops of deionized water containing $Na_2S_2O_4$ to the **43$^+$ClO$_4^-$** solution at room temperature. Possible fragment ions are listed below. Aside from the 189 ion (**47$^+$**), 3MLF (**42**)(MH$^+$) was observed at *m/z* 271.1190 (δ 0.0 mDa) (Figure 5-7). The observation of **42** as a product of N-dealkylation of the flavinium is consistent with a previous finding.[69a] The 232 ion (**58$^+$**) may be one of the intermediate forms of the flavinium salt (**43$^+$**)(δ 0.4 mDa). In addition, the imidazolium ion (**47$^+$**) at *m/z* 189 arose from both the interaction of **43$^+$ClO$_4^-$** with water and the reduction of **43$^+$ClO$_4^-$** with $Na_2S_2O_4$. However, fragment ions (possible intermediates) do not match themselves well; therefore, the formation of the imidazolium salt appears to proceed via different mechanisms.

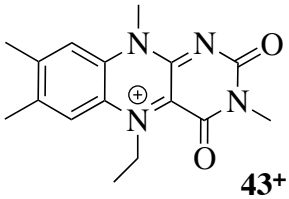

43$^+$

Exact Mass: 299.1503

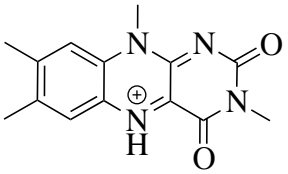

42H$^+$

Exact Mass: 271.1190

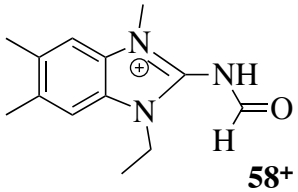

58$^+$

Exact Mass: 232.1444

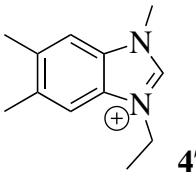

47$^+$

Exact Mass: 189.1386

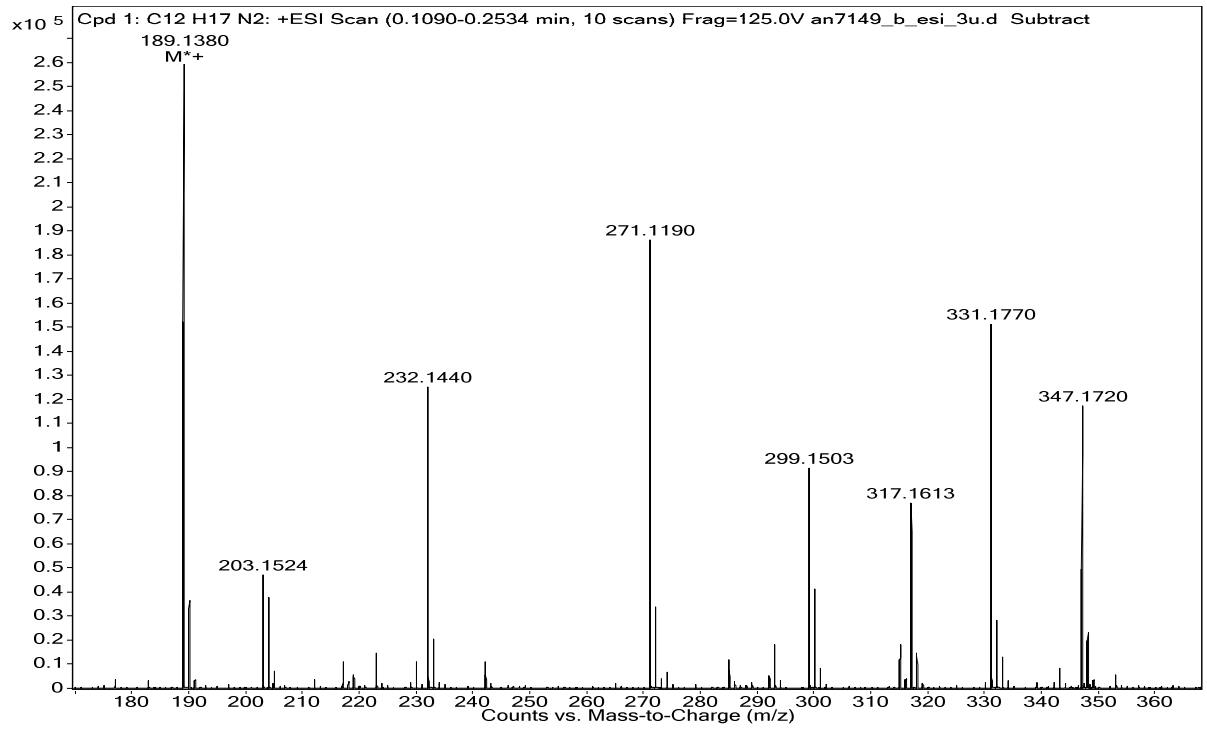

Figure 5-7. Accurate-mass ESI^+ mass spectrum of the reduced 5Et3MLF. Reaction between $5Et3MLF^+ClO_4^-$ and $Na_2S_2O_4$ (1 to 1 molar ratio) proceeds in commercial grade acetonitrile (*x*-axis: *m*/*z*; *y*-axis: relative abundance). An expansion of the spectrum from *m*/*z* 170 to *m*/*z* 370 is shown.

Scheme 5-3 illustrates a proposed mechanism for the transformation from $\mathbf{43^+ClO_4^-}$ to the imidazolium in the presence of $Na_2S_2O_4$. Initially, $\mathbf{43^+ClO_4^-}$ was reduced by dithionite. Following the protonation at the C10a position, the interaction of the compound and water causes ring re-arrangement of pyrazine and ring opening of pyrimidine in the $\mathbf{43^+ClO_4^-}$ salt, followed by a cleavage of the imidazolium. Note that this proposed mechanism involving the presence of dithionite could apply to the reaction of $\mathbf{43^+ClO_4^-}$ with TMMP or benzylamine. In the redox reaction, the amines, TMMP and benzylamine, are the reducing reagents and pass two electrons to the oxidizing reagent $\mathbf{43^+ClO_4^-}$.

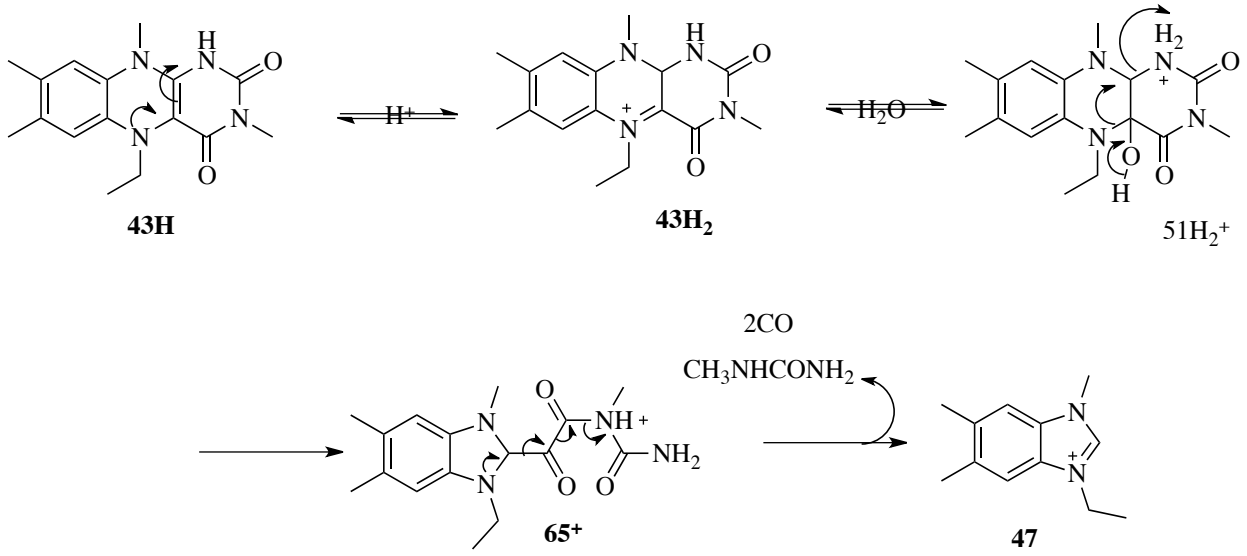

Scheme 5-3

5.2 Effect of Water on Reaction Mechanisms

In Chapter 3, the oxidation of **4** with **43$^+$ClO$_4^-$** was reported. Immediately after mixing these two compounds in commercial grade acetonitrile, color changes in the reaction mixture were apparent; the markers of the flavinium salt **43$^+$ClO$_4^-$** at λ_{max} of 412 and 555 nm disappear without delay. However, there was a delay in detecting the final product (50^+) using NMR. The solvent acetonitrile is known to contain some moisture. Therefore, the effect of water on the oxidation of **4** with **43$^+$ClO$_4^-$** was anticipated.

To examine the effect of water, an excess amount of water (0.5 M) was added to the reaction mixture of **43$^+$ClO$_4^-$** (25 mM) with **4** (25 mM), and the effect of this added water on the product formation (MMP^+, λ_{max} of 370 nm) was investigated using UV/vis spectroscopy. Figures 5-8 A and B show the results of the absence or presence of 0.5 M water, respectively. The spectra of both reactions showed a decrease in the chromophore for **43$^+$ClO$_4^-$** at λ_{max} of 412 nm and 555 nm immediately after water addition, accompanied by the appearance of a chromophore at λ_{max} of 350 nm. The difference appeared after t = 15 min; the chromophore at λ_{max} of 370 nm (marker of MMP^+) was only observed with the reaction lacking any water addition (Figure 5-8A). The formation of MMP^+ was not detected in the reaction mixture to which water had been added over

the course of 2 hours (Figure 8B). Therefore, these results suggest that 0.5 M water stops the reaction of **43**$^{+}$**ClO**$_4^-$ with TMMP and inhibits the oxidation of **4**.

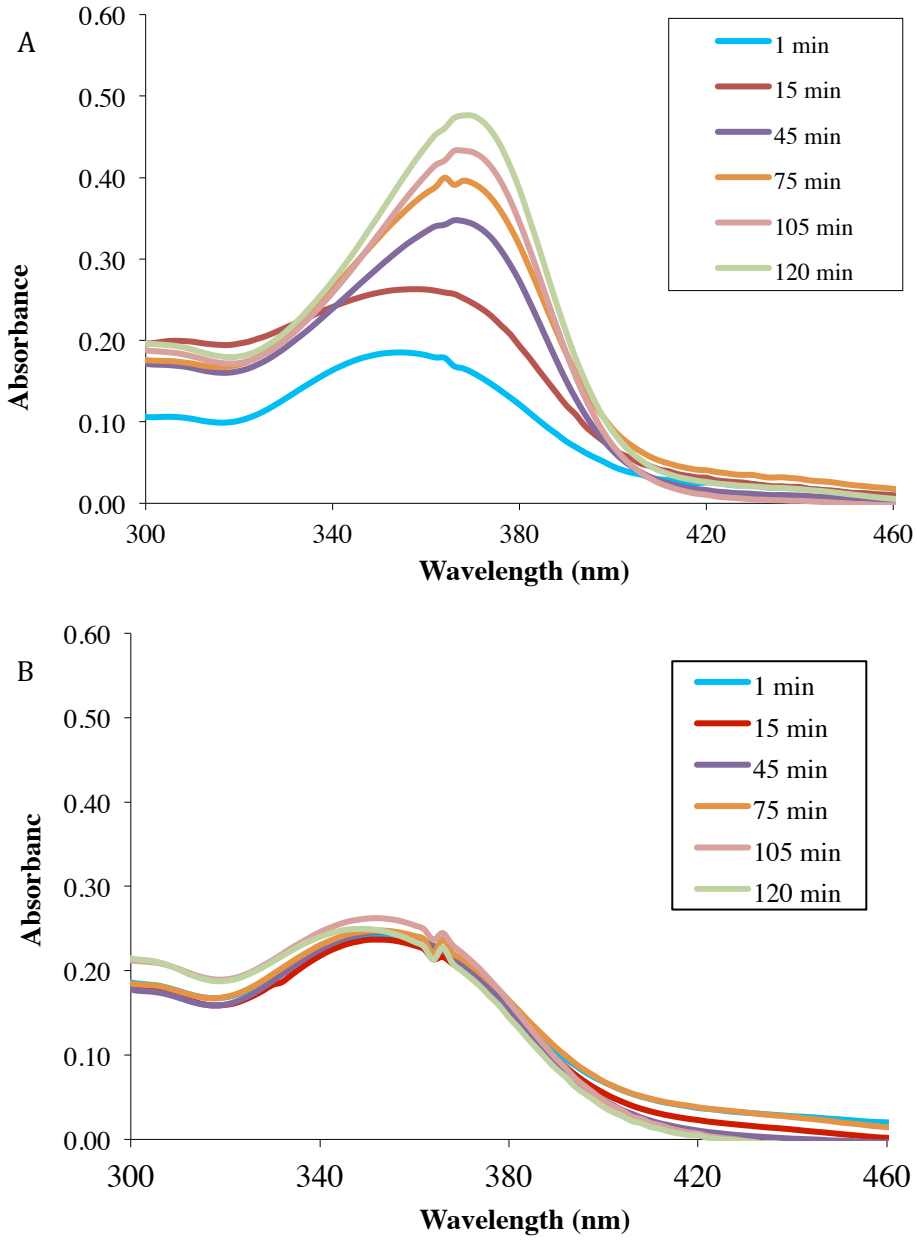

Figure 5-8. UV/vis spectra of the reaction between 5Et3MLF^{+}ClO$_4^-$ and TMMP in commercial grade acetonitrile at room temperature. Change in the concentration of MMP^{+} with the time-dependent reaction between 5Et3MLF^{+}ClO$_4^-$ (25 mM) and TMMP (25 mM) (A), and Formation of C4a-OH adduct by water addition (0.5 M)(B).

Scheme 5-4 shows the formation of the adduct **51** that occurs with the reaction between 5Et3MLF$^+$ and water. A large excess of in the acetonitrile solution of **43$^+$ClO$_4^-$** shifts the equilibrium to the right and the flavinium oxidation is shut down since the C4a position is occupied with the hydroxyl group. Additionally, as long as water is not physically added to commercial grade acetonitrile, acetonitrile wetness does not cause quenching the reactivity of **43$^+$ClO$_4^-$**. When the equilibrium is favored to the left, **43$^+$ClO$_4^-$** undergoes the oxidation of TMMP, leading to the generation of MMP$^+$.

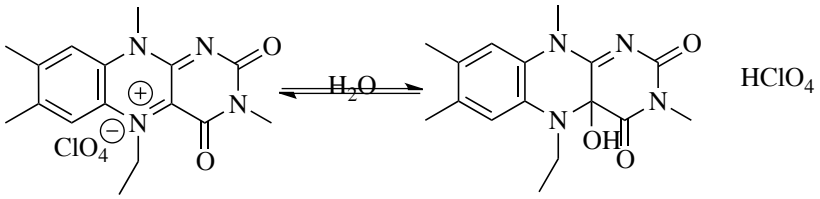

Scheme 5-4

5.3 Identification of C4a Hydroxyl Adduct

In order to isolate the 5Et3MLF-C4aOH adduct (**51**), the flavinium salt **43$^+$ClO$_4^-$** (40 mg) was mixed with triethylamine (**53**, 14 μL) in commercial grade acetonitrile. By adding a bulky base **53** to the solution of **43$^+$ClO$_4^-$**, **53** would deprotonate water molecule to yield a hydroxide anion, which then reacts with the electrophilic carbon at the C4a position of **43$^+$ClO$_4^-$**. The color of the solution changes from purple to a lemon-yellow shade. This solvent was then evaporated from the mixture by purging with N_2. The remaining white/greenish compound was isolated and characterized using NMR and accurate mass ESI$^+$/MS (Scheme 5-5).

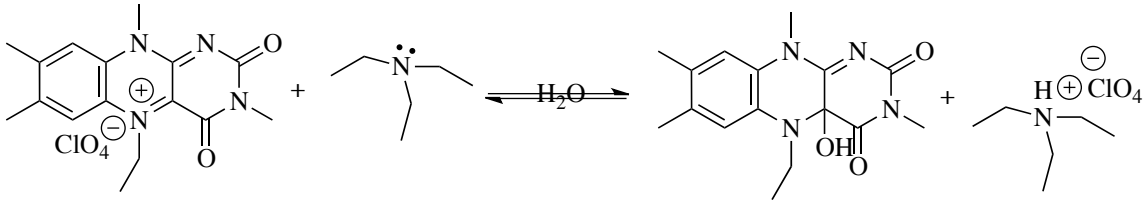

Scheme 5-5

Figure 5-9 displays the accurate-mass ESI$^+$ mass spectrum of the white/greenish solid; the ion observed at *m/z* 317.1625 was confirmed to be **51** (the exact mass of MH$^+$ is 317.16082 amu; the structure is shown below). The two masses differ by 1.7 mDa, and the general rule is to consider

signals occurring within 10 mDa of each other as the same compounds or isomers. Thus, the white/greenish solid is either the adduct **51** or the isomer of the flavin.

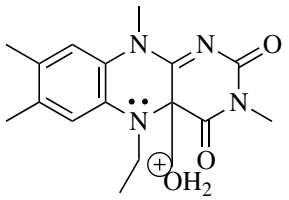

Exact Mass: 317.1608

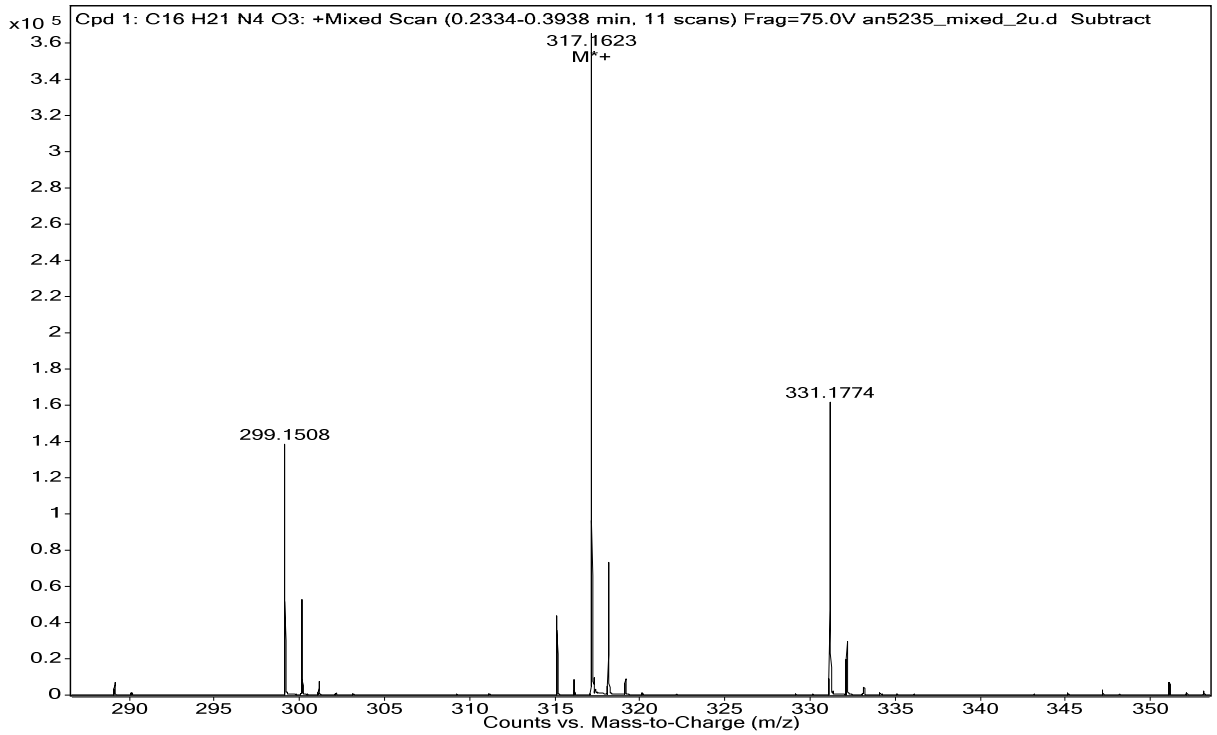

Figure 5-9. Identification of white/greenish solid by the accurate-mass ESI^+/MS. White/greenish solid was dissolved in commercial grade acetonitrile. The mobile phase was acetonitrile alone, and MeOH or water was not used in the mobile phase.

Figures 5-10 and 5-11 display ^1H NMR spectra of the **43$^+$ClO$_4^-$** salt and the adduct **51**, respectively. The ^{1}H-NMR spectrum of **43$^+$ClO$_4^-$** in CD3CN (Figure 4): δ = 8.226 ppm and 7.965 (2H, 2Ar-H), 6.089 and 5.046 (2H, CH_2CH_3), 4.198 and 3.463 (6H, 2N-CH_3), 2.650 and 2.593 (6H, 2Ar-CH_3), and 1.800 (3H, CH_2CH_3). The more detailed characteristics of the salt **43$^+$ClO$_4^-$** are discussed in Chapter 6.

The ^{1}H-NMR spectrum of isolated white/green solid in CD_3CN (Figure 5): δ = 7.1607 ppm (1H, Ar-H_d) and 7.0436 (1H, Ar-H_c), 4.5961 (1H, OH), 3.6244 and 3.2365 (6H, 2N-CH_3), 3.4521 (2H, CH_2CH_3), 2.2995 and 2.2827 (6H, 2Ar-CH_3), 1.0531 (3H, CH_2CH_3). The formation of the adduct **51** caused upfield shifts of the methyl protons on the N5 ethyl from 1.800 ppm to 1.0531 ppm. The methylene protons (H_a and H_b) on the ethyl group are diastereotopic and are thus non-equivalent. The CH_2CH_3 protons have appeared as two doublets of quartets on the NMR spectrum. Also, the nucleophilic addition of a hydroxyl group to the C4a position of 5Et3MLF$^+$ caused its geometric structure to change, which may then give the ethyl group freedom to spin in the space.

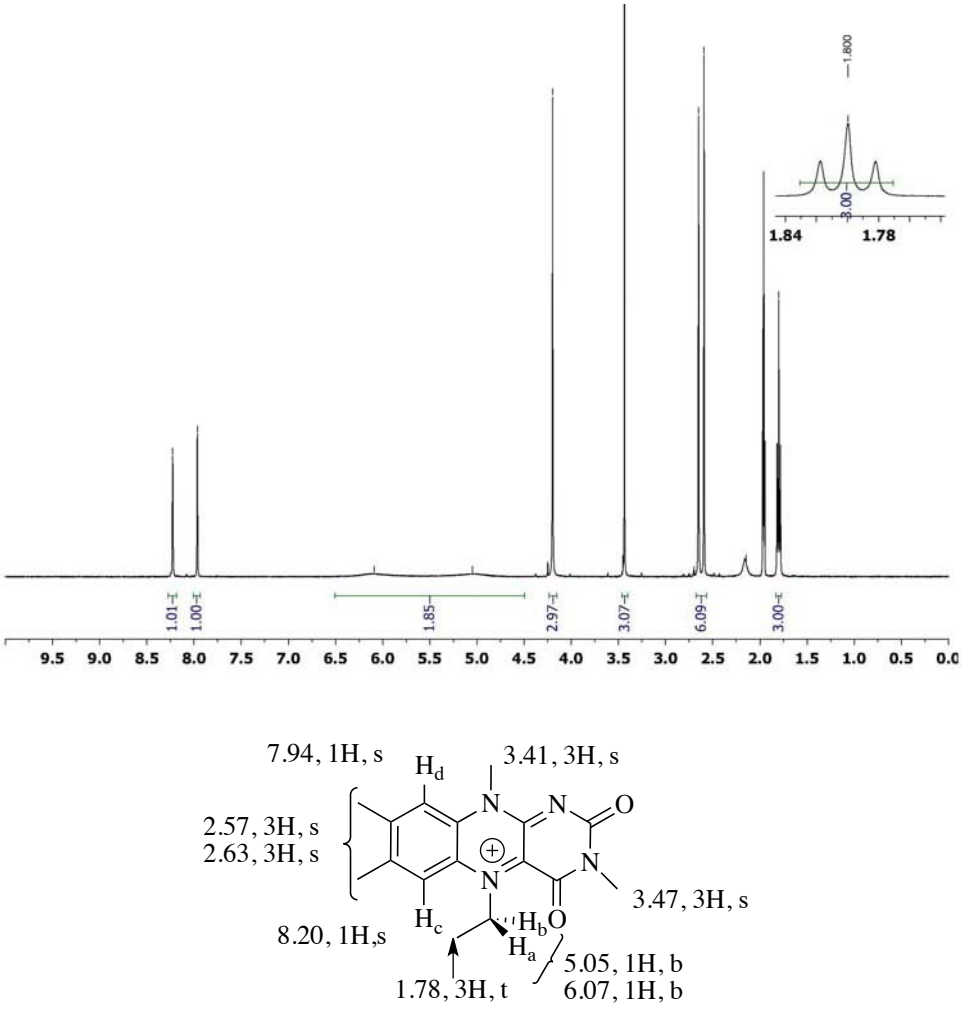

Figure 5-10. ^{1}H-NMR spectrum of 5Et3MLF$^+$$ClO_4^-$ alone and peak assignments. 5Et3MLF$^+$$ClO_4^-$ was dissolved in acetonitrile-d_3 (500 MHz).

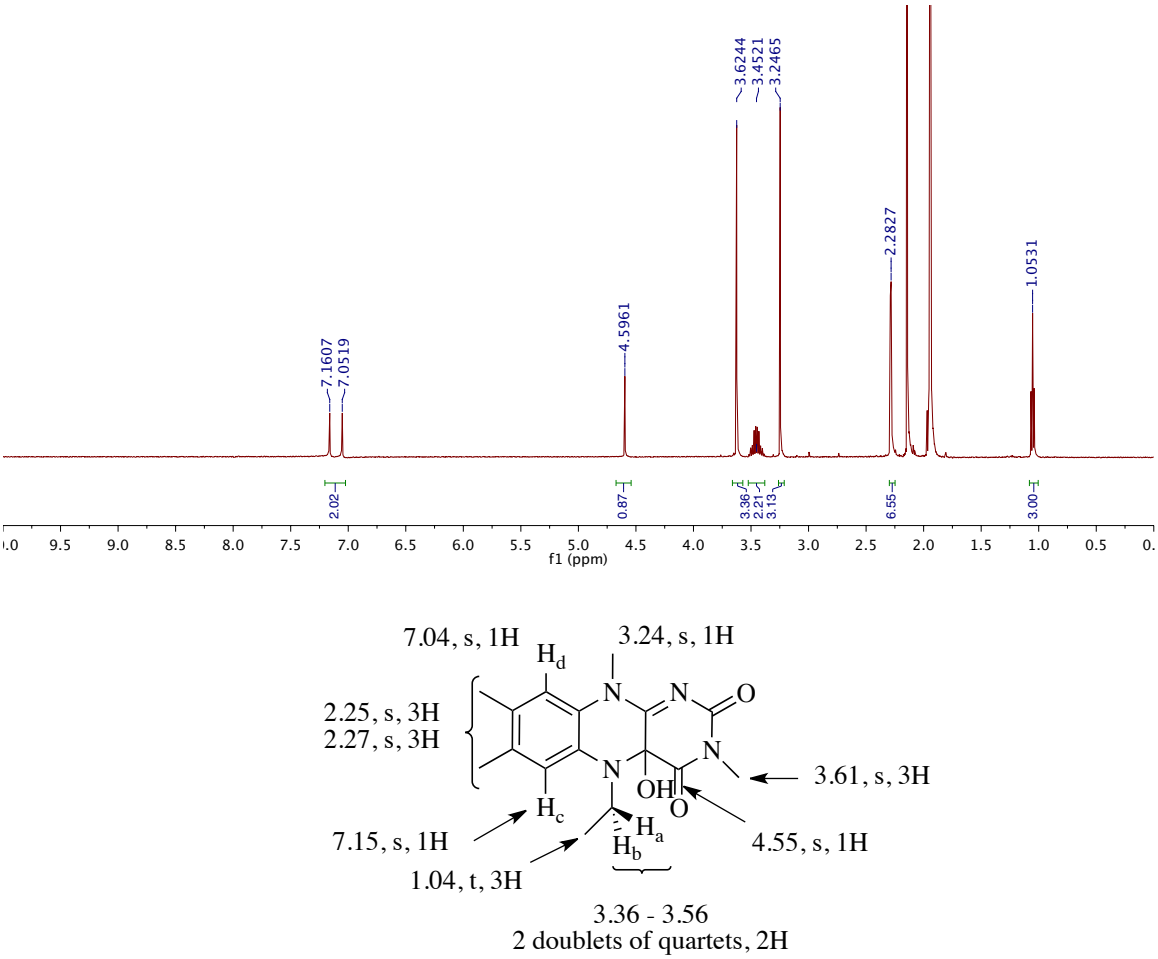

Figure 5-11. ^{1}H-NMR spectrum of the C4a-OH adduct and NMR signal assignments. The white/greenish solid was dissolved in acetonitrile-d_3 (500 MHz).

Accordingly, the results suggest that **43^{+}ClO$_4^{-}$** equilibrates with the adduct **51** in the presence of a base (Scheme 5-4). Thus, in an attempt to recover the starting material **43^{+}ClO$_4^{-}$**, trifluoroacetic acid (TFA) was applied to the reaction mixture of **43^{+}ClO$_4^{-}$** with either **4** or **53** in commercial grade acetonitrile (Scheme 5-6). The addition of TFA would favor the equilibrium toward the starting material **43^{+}ClO$_4^{-}$**. TFA was chosen on account of its strong acidity (p*Ka* 0.23) in order to protonate the oxygen on the C4a adduct to promote loss of H_2O. Also, due to its steric bulk, TEA does not interact with the C4a position of **43^{+}ClO$_4^{-}$**. To supply a sufficient quantity of the acid in the reaction mixture, 10 times more of the acid than the base was added.

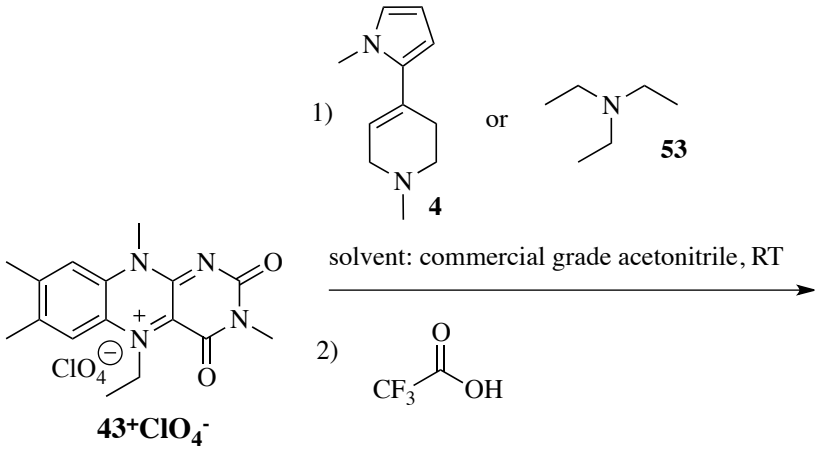

Scheme 5-6

The reaction mixture was produced according to these combinations of constituents: a) **43$^+$ClO$_4^-$** and **4** or b) **43$^+$ClO$_4^-$** and **53** (1 to 1 molar ratio, 0.075 mM) in air using commercial grade acetonitrile. Six minutes after mixing **43$^+$ClO$_4^-$** with the base **4** or **53**) together, TFA was added to the reaction mixture (final concentration of TFA was 0.75 mM).

Figure 5-12 displays the UV/vis spectrum of the effect of TFA on the reaction between **43$^+$ClO$_4^-$** and **53**. Figure 5-13 shows the UV/vis spectrum of the effect of TFA on the reaction between **43$^+$ClO$_4^-$** and **4**. Results indicated that the addition of TFA to both **53** and TMMP reaction mixtures six minutes after its preparation led to the reappearance of the purple color, the markers of **43$^+$ClO$_4^-$** (λ_{max} at 412 nm and 555 nm), for both reactions. Data interpretations are illustrated in Schemes 5-7 and 5-8.

The reaction of **53** did not show the same spectra between at t = 30 sec and at t = 6 min after adding a base. Also, the UV/vis spectra indicated that **43$^+$ClO$_4^-$** equilibrates with **3** in the presence of TFA. The green line (6 min after base) has the λ_{max} value of 350 nm, which is the marker of **51**. In brief, the addition of TFA restored the chromophores of 5Et3MLF$^+$ at λ_{max} 412 and 555 nm, suggesting that **43$^+$ClO$_4^-$** equilibrates with **43$^+$ClO$_4^-$** or **53** with the presence of air.

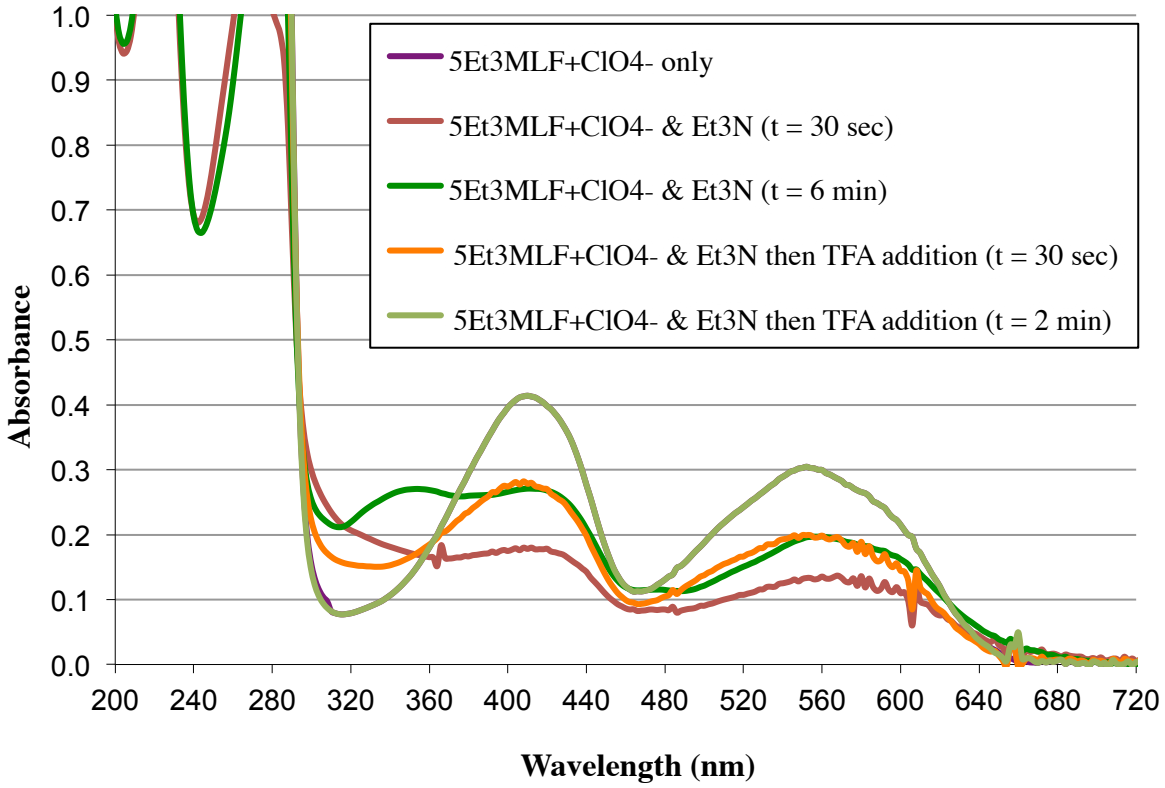

Figure 5-12. UV/vis spectrum of the effect of TFA on the reaction mixture (5Et3MLF$^+$ClO$_4^-$ and TMMP). Mixture of 5Et3MLF$^+$ClO$_4^-$ and TMMP (0.075 mM, 1 to 1 ratio) was made in commercial grade acetonitrile.

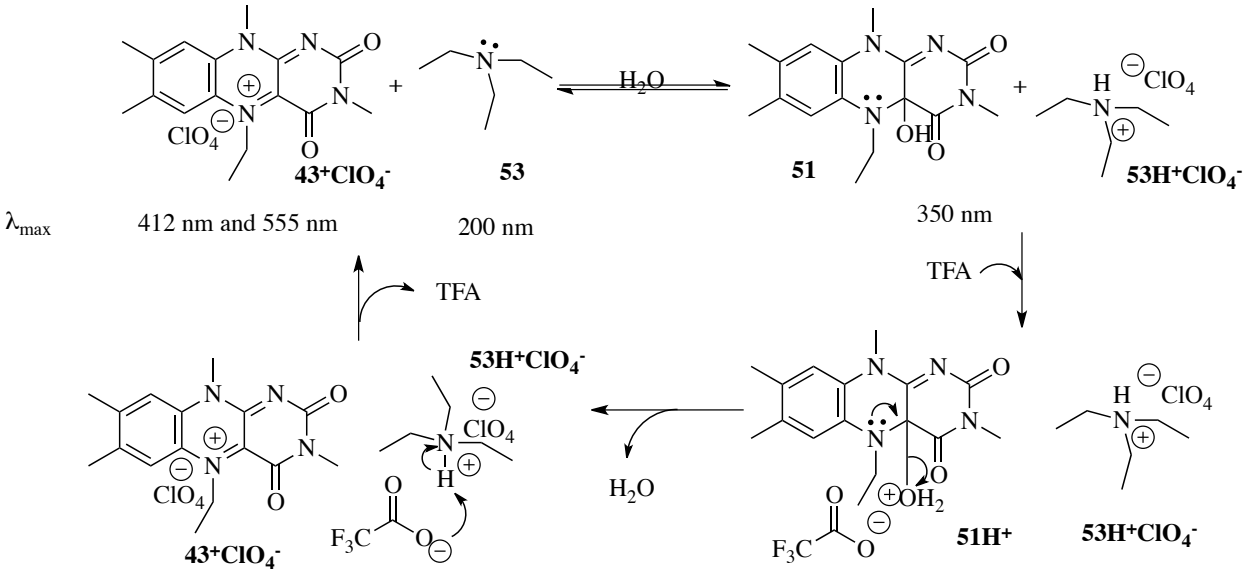

Scheme 5-7

In the course of the reaction between **43^{+}ClO$_4^{-}$** and **4**, the spectra at t = 30 sec and at t = 6 min after adding a base have the same chromophores, which indicates that the initial reaction proceeds at a relatively high rate so that further reaction does not occur by t = 6 min. With the addition of TFA, the chromophores of **43^{+}ClO$_4^{-}$** at λ_{max} 412 and 555 nm reappeared, suggesting that the protonation of its intermediates (λ_{max} at 340 nm, 420 nm, and 560 nm) favors the equilibrium towards **43^{+}ClO$_4^{-}$**. The possible intermediate **51** has λ_{max} of 350 nm, and DHP^{+} has λ_{max} of 420 nm. The reaction appears to proceed via **51** as described in Scheme 5-8.

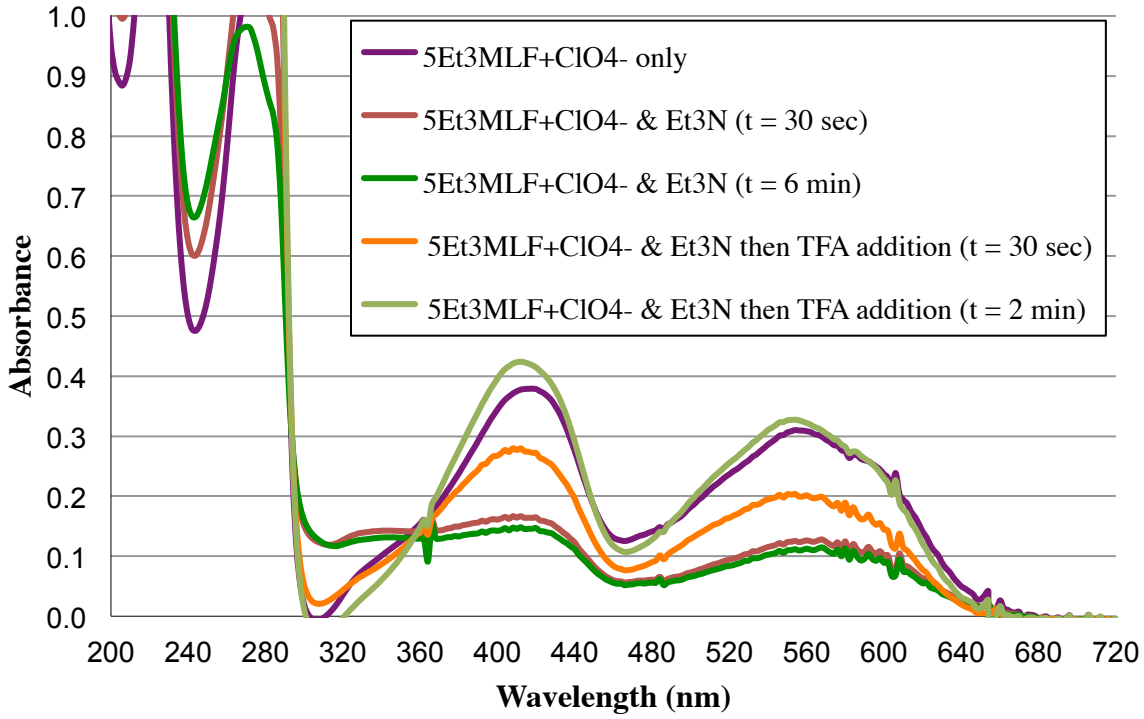

Figure 5-13. UV/vis spectrum of the effect of TFA on the reaction mixture (5Et3MLF^{+}ClO$_4^{-}$ and Et$_3$N). Mixture of 5Et3MLF^{+}ClO$_4^{-}$ and Et$_3$N (0.075 mM, 1 to 1 ratio) was made in commercial grade acetonitrile.

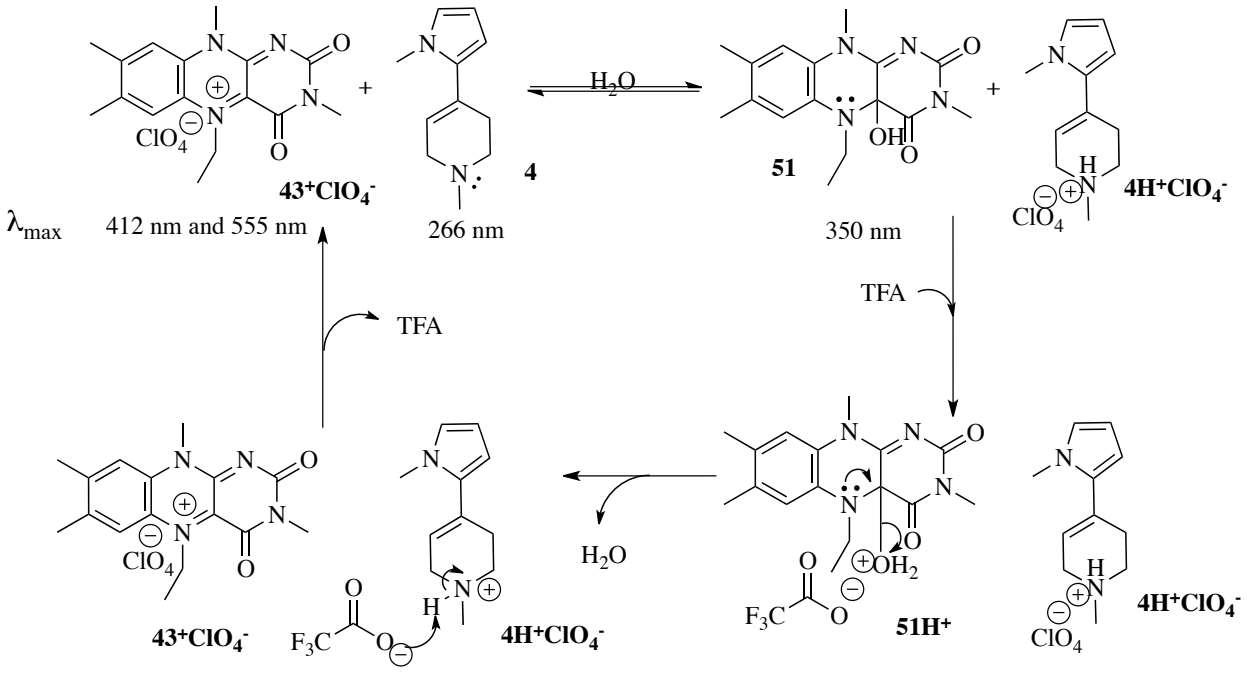

Scheme 5-8

5.4 Conclusions

In summary, the above results suggest the reaction between **$43^{+}ClO_4^{-}$** and water. The hydroxyl anion could react with the C4a position of the $5Et3MLF^{+}$ species, leading to the formation of **51**. Also, an excess amount of water (0.5 M) could diminish the reactivity of **$43^{+}ClO_4^{-}$**. Therefore, the solvent wetness needs to be taken under consideration with the flavinium research.

CHATPTER SIX
METHODOLOGY AND SYNTHESES

6.1 Experimental Section

Caution. MPTP and its structural analog 1-methyl-4-(2-methylpyrrol-2-yl)-1,2,3,6-tetrahydropyridine [TMMP (**4**)] used in the present study are known or potential neurotoxins and should be handled with care using disposable gloves and protective eyewear in a properly ventilated hood. Safe handling information on MPTP has been reported previously.[73]

6.1.1 Chemicals

All starting materials were obtained from Sigma–Aldrich and were used without purification, unless described otherwise. Syntheses of 3-methyllumiflavin [3MLF (**42**)] and 5-ethyl-3-methyllumiflavinium perchlorate [5Et3MLF$^+$$ClO_4^-$ (**43$^+$$ClO_4^-$**)] are described in Section 6-2. All solvents used were ACS grade solvents unless otherwise specified. The synthesis of the oxalate salt of TMMP has been described previously (Nimkar 1996). The solution of **43$^+$$ClO_4^-$** was prepared anew in acetonitrile prior to each experiment. The oxalate salt of TMMP[62] was free-based using Na_2CO_3 as needed.

6.1.2 Instrumentation

UV-vis absorption spectra were recorded using a Hewlett Packard 8452A Diode Array spectrophotometer (1 cm pathway length) and an Ocean Optics S2000 USB spectrophotometer (0.2 cm path length). Proton (^{1}H) and carbon (^{13}C) NMR (500 MHz) spectra were recorded in CD_3CN on a JEOL 500 spectrometer. Gas chromatography was carried out using a Hewlett-Packard 5890A GC equipped with an FID detector and an HP 3393A integrator. Accurate-mass ESI$^+$ mass spectra were recorded on Agilent Technologies 6220 Accurate-Mass TOF LC/MS. X-ray crystallography was used to aid with investigating molecular structures using an Oxford Diffraction Nova diffractometer. Electron Paramagnetic Resonance spectra were recorded using a Bruker ER 200D spectrometer equipped with a Bruker ER 4102ST cavity. For anaerobic sample preparations, an Innovative Technologies nitrogen glove box was utilized. This glove box contains a high capacity purifier for maintaining an oxygen level below 1 ppm.

6.2 Syntheses

The synthesis of **43$^+$ClO$_4^-$** was accomplished by the multi-step reaction sequence first described by Ghisla *et al*. (1973).[74] Although the subject of several literature reports,[35, 45a, 46, 54a, 75] a detailed NMR spectrum of **43$^+$ClO$_4^-$** has not been previously reported. Scheme 6-1 displays the steps involved in the synthesis of the flavinium salt **43$^+$ClO$_4^-$**.

6.2.1 Synthesis of *N*-Methylbarbituric Acid (67)[76]

A mixture of methylurea (180 mmol), malonic acid (212 mmol), and acetic acid (35 mL) was prepared (Scheme 2). This solution was warmed to 60°C while stirring, and all solids were dissolved into the solution. Acetic anhydride (72 mL) was added to the solution one drop at a time; the solution was heated at 70 – 80 °C for 30 min. This solution was then left to sit overnight at room temperature. By the next morning, the solution was clear orange, and there was white precipitation on the bottom. The white precipitation was removed using gravity filtration. The solution was dried (evaporated) using a rotavapor, and then hot filtration was subsequently performed using ethanol (50 mL). The filtrate was placed in the refrigerator overnight before isolating the product, *N*-methylbarbituric acid (**67**)**.** The resulting solid was recrystallized in ethanol to give a fine white power. The averaged percent yield was 85%: mp 131 – 132 °C and reported mp 131 °C; ^{1}H NMR (400 MHz, DMSO) δ 11.28 (s, 1H), 3.52 (s, 2H), 3.00 (s, 3H)

6.2.2 Synthesis of 6-Chloro-3-methyluracil (68)[76]

Compound **67** (10 g, 70 mmol) was added to 40 mL of acetonitrile and heated to 70 °C. Next, 10 mL of $POCl_3$ (16.7 g, 109 mmol) was added dropwise with constant stirring, and the reaction mixture was refluxed for an additional 2 hours. After cooling, the product (solid precipitation), 6-chloro-3-methylouracil, was separated using suction filtration. The crude product was recrystallized using water to obtain an averaged percent yield of 92%: mp 280 – 282 °C.

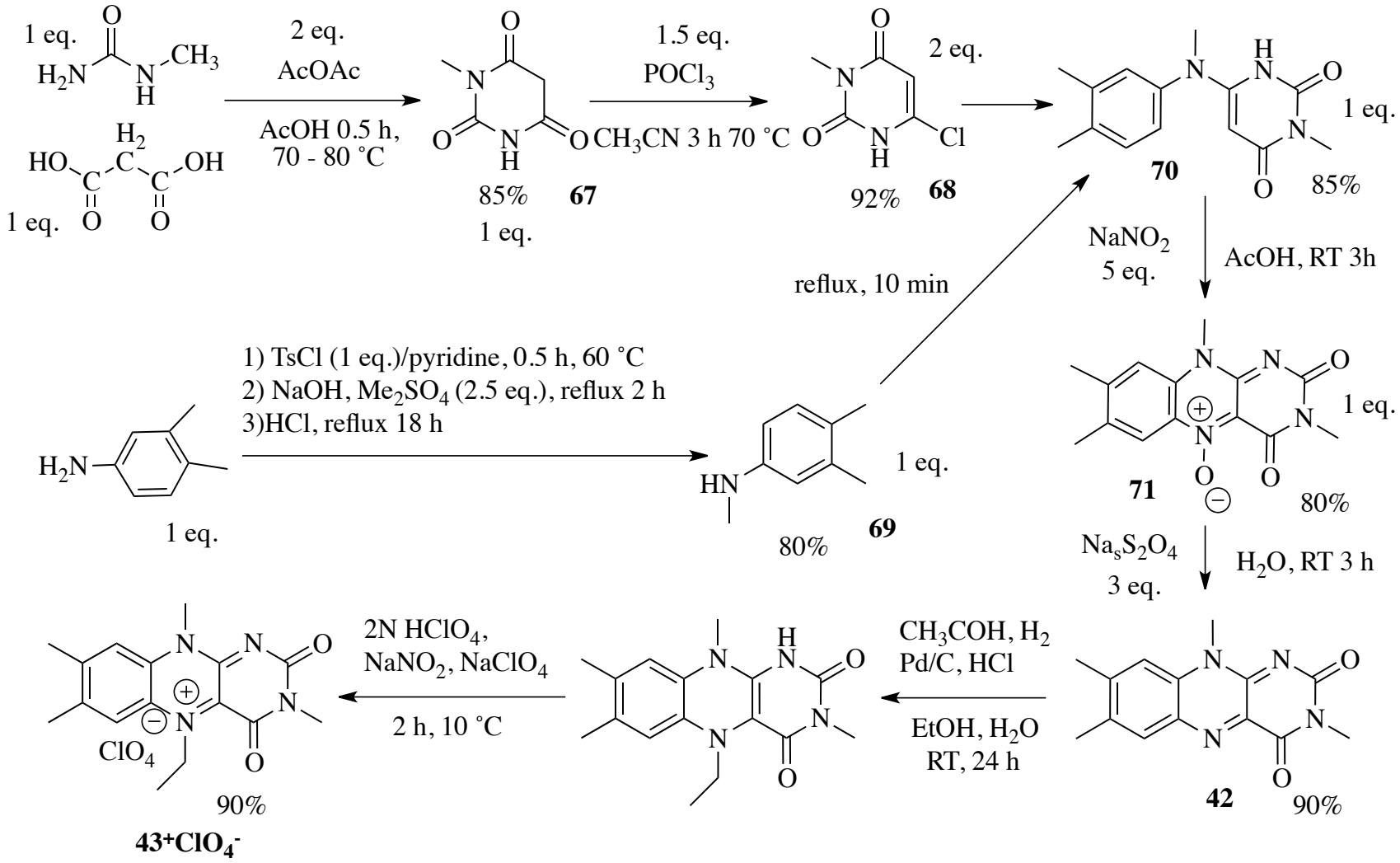
1 eq.
2 eq.
AcOAc
AcOH 0.5 h,
70 - 80 °C
85%
67
1 eq.
1.5 eq.
POCl3
CH3CN 3 h 70 °C
92%
68
2 eq.
70
85%
1 eq.
NaNO2
5 eq.
AcOH, RT 3h
71
80%
1 eq.
Nas2S2O4
3 eq.
H2O, RT 3 h
42
90%
CH3COH, H2
Pd/C, HCl
EtOH, H2O
RT, 24 h
2N HClO4,
NaNO2, NaClO4
2 h, 10 °C
90%
43+ClO4-
reflux, 10 min
1) TsCl (1 eq.)/pyridine, 0.5 h, 60 °C
2) NaOH, Me2SO4 (2.5 eq.), reflux 2 h
3)HCl, reflux 18 h
1 eq.
80%
69
1 eq.

Scheme 6-1

6.2.3 Synthesis of *N*,3,4-Trimethylaniline (69)[77]

Dimethylaniline (9.2 g, 76 mmol) and pyridine (22.7 cm^3) were mixted with constant stirring, and then toluene-tosyl-chloride (13.2 g, 79 mmol) was added. The reaction mixture was then heated at 60 °C for 30 min and 120 °C for 60 min. After standing overnight at room temperature, pyridine was removed by evaporation. Water is added to the remaining reaction mixture in order to stimulate the precipitation of the product. The product N-tosyl-3,4-dimethylaniline was recrystallized using isopropyl alcohol from the resulting reaction mixture: mp 70 - 71°C and reported mp 70.5 – 71.0 °C.

N-tosyl-3,4-dimethylaniline (8 g, 67 mmol), 2N NaOH (40 ml), and H_2O (40 ml) were mixed and warmed to 60 °C. Then, MeOH was slowly added until a slight turbidity was evident. Dimethyl sulfate (10g, 7.5 ml) was added dropwise while stirring the solution, and the reaction mixture was refluxed for 1 hour. Additional 2N NaOH along with 7.5 ml of dimethyl sulfate was added to the reaction mixture. This mixture was further refluxed for an additional 2 hours. The resulting solution was subsequently distilled. For distillation, the oil bath temperature was at 190 – 195 °C, and the temperature inside of the distill system was 90 °C. The collected aqueous (product) was acidic (pH = 1 – 2), and once the collected product cooled down to room temperature, K_2CO_3 was added to it to make to basic at pH 10. The averaged percent yield was 80%: ^{1}H NMR (400 MHz, $CDCl_3$) δ 6.93 (d, 1H), 6.45 (d, 1H), 6.39 (dd, 1H), 2.80 (s, 3H), 2.20 (s, 3H), and 2.15 (s, 3H) .

6.2.4 Synthesis of 6-((3,4-Dimethylphenyl)(methyl)amino)-3-methylpyrimidine-2,4(1*H*,3*H*)-dione (70)[78]

3-methyl-6-chlorouracil (**68**)(0.01 mol) and *N*,3,4-trimethylaniline (**69**)(0.03 mol) were mixed and heated to 170 - 180 °C for 10 min with constant stirring. After cooling to room temperature, the reaction mixture was crushed in ether. The product (crystals) was collected by filtration and washed with water. The crushed solid from ethanol was then recrystallized to yield colorless crystals of 6-(*N*-alkylanilino)uracil (**70**). The averaged percent yield was 85%.

6.2.5 Isoalloxazine-5-oxide (71)[78]

Compound **70** (0.01 mol) was dissolved in 20 mL of acetic acid following which a solution of sodium nitrite (3.5 g, 0.05 mol) in what was added to the reaction mixture. This mixture was stirred at room temperature for 2 to 3 hours, and then diluted with water. The product, isoalloxazine-5-oxide, was collected by filtration and washed several times with water. The crude product was recrystallized with ethanol and the averaged percent yield was 85%: ^{1}H NMR ($CDCl_3$) δ 8.21 (s, 1H), 7.37 (s, 1H), 3.99 (s, 3H), 3.41 (s, 3H), 2.47 (s, 3H), 2.40 (s, 3H).

6.2.6 Synthesis of 3-Methyllumiflavin (42)[78]

Isoalloxazine-5-oxide (**71**)(0.01 mol) from the previous step was added to the solution of sodium dithionite (5.2g, 0.03 mol in water 10 ml) and stirred for 2 to 3 hours at room temperature. Hydrogen peroxide (30%, 2 mL) was then added to the reaction mixture. After overnight stirring, 3-methyllumiflavin was separated by filtration. The crude product was recrystallized using acetic acid, which resulted in orange needle crystals. The averaged percent yield was 90%: ^{1}H NMR (CD_3CN) δ 7.91 (s, 1H), 7.64 (s, 1H), 4.00 (s, 3H), 3.35 (s, 3H), 2.53 (s, 3H), 2.43 (s, 3H); Anal. Calcd for C14H14N4O2: C, 62.21; H, 5.22; N 21.73. Found: C, 59.47; H, 5.38; N 18.25 (containing acetic acid as contamination). Figure 6-1 shows the X-ray crystal image of 3MLF and acetic acid.

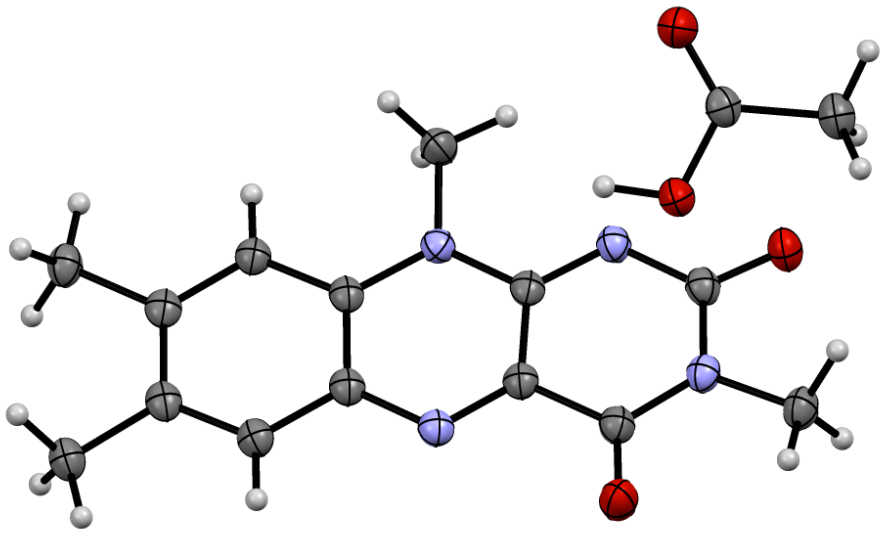

Figure 6-1. X-ray crystal image of 3MLF and acetic acid. Thermal ellipsoid plot of the molecular structure of the C4a-SO_3 adduct and benzoimidazolium at 50 % probability. The solvent was CH_3CN.

6.2.7 Synthesis of 5-Ethyl-3-methyllumiflavinium perchlorate ($43^+ClO_4^-$)[61b]

1) Formation of Reduced 5Et3MLF

3-methyllumiflavin (**42**)(600 mg; 2.22 mmol) was hydrogenated over 10% Pd-C (200 mg) in a mixture of ethanol (50 ml), H_2O (46 ml), concentrated HCl (4 ml) and acetaldehyde (4 ml) at room temperature and at atmospheric pressure. The reaction mixture was degassed, and hydrogenation was conducted using an H_2 balloon. The reaction progress was monitored using TLC. The reaction was allowed to proceed for 24 hours. The catalyst was filtered from the solution to yield a light yellow-red filtrate, which was evaporated to dryness in a vacuum.

2) Conversion of Reduced 5Et3MLF into the $5Et3MLF^+$ salt (**$43^+ClO_4^-$**)

The residue from the previous reaction (light yellow-red filtrate) was dissolved in 2 N $HClO_4$ (10 ml) as well as 2 mL 70% $HClO_4$ plus 8 mL H_2O. Solid $NaClO_4$ (3 g) was added in small portions followed by $NaNO_2$ (1 g). The mixture was cooled at 10 °C with stirring for 2 hours. The violet crystals were filtered off and washed with ice-cooled water; drying them in vacuo at room temperature over P_2O_5 yields at about 80%. The mother liquid was refrigerated overnight and any additional precipitation was collected next day. The crude product was crystallized from acetonitrile and was ether.[74] The averaged percent yield was 90%: mp 234 °C – 237 °C (reported mp 223 °C - 227 °C); ^1H NMR (CD_3CN) δ 8.23 (s, 1H), 7.95 (s, 1H), 6.05 (b, 1H), 5.05 (b, 1H), 4.20 (s, 3H), 3.43 (s, 3H), 2.89 (s, 3H), 2.85 (s, 3H), 1.80 (t, 3H).

6.3 Troubleshooting and Modifications

6.3.1 Identification of Byproducts in the Synthesis of *N*-Methylbarbuturic Acid

During the course of the synthesis of *N*-methylbarbuturic acid (**67**), white solids precipitated out as a by-product. To investigate whether these solids were formed from the product, the authentic *N*-methylbarbituric acid (desired product)(0.5 g) was mixed with acetic acid (solvent)(1.5 mL) and acetic anhydride (reactant)(3 mL). The reaction mixture was then heated at 90 °C for 30 min and left overnight at room temperature. Next, the remaining reaction mixture was crystallized using methanol. The crystals and the by-product were then analyzed using negative ion FAB^- LC/MS and the ion *m/z* 209 $(M-H)^-$ was detected (structure shown below), which indicated that

the byproduct had arisen from overreaction (a reaction between the product and one of the reactants).

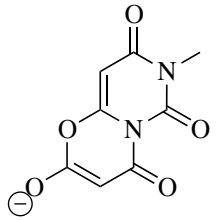

Exact Mass: 209.0204

Scheme 6-2 shows a proposed mechanism for the by-product formation in which *N*-methylbarbituric acid (desired product) was mixed with acetic anhydride (reactant).

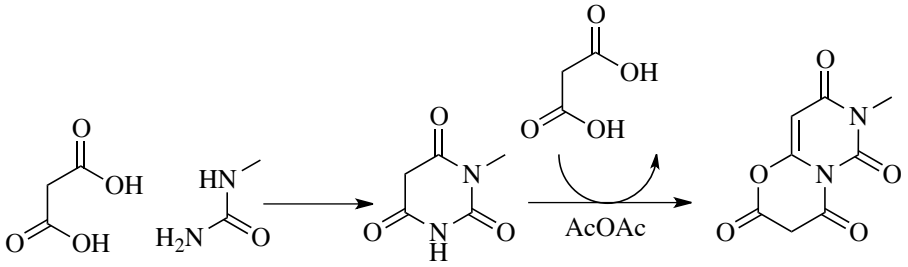

Scheme 6-2

To minimize the by-product generation, the reaction duration was reduced from 6 hours to 30 min, and the temperature was modified from 90 °C to 70 – 80 °C. The reaction progress was monitored using the TLC system, and results indicated that 30 min at 70 – 80 °C was sufficient for the synthesis of *N*-methylbarbituric acid (**67**).

6.3.2 Modification in the Synthesis of 6-Chloro-3-methyluracil

The initial percent yield was 33 % with the original procedure (Scheme 6-3).[76]

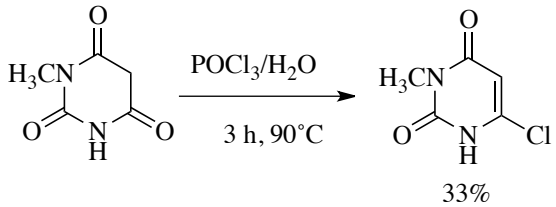

Scheme 6-3

The original solvent suggested was water;[76] however, water reacts with $POCl_3$, consequently generating $POCl_2OH$ and HCl (Scheme 6-4). These side reactions reduced the yield percent of the desired product, 3-chlorobabuturic acid.

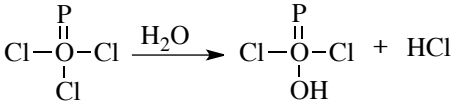

Scheme 6-4

Thus, in order to investigate how to maximize the percent yield, the reaction was carried out with different solvents: $POCl_3$ (without water addition), acetic acid, tetrahydrofuran (THF), and acetonitrile. Reaction of the *N*-methylbarbituric acid (**67**) with $POCl_3$ without water addition was not successful; the reaction mixture was burned out and no useful residues were found.

Next, the reaction in acetic acid proceeded to give a white solid with a sharp melting point 212-213 °C (percent yield of 78%). GC/MS analysis indicated that the nominal mass of the white solid was 184 (AN1121 for GCMS). Scheme 6-5 is a proposed pathway to account for the formation of the compound with the nominal mass of 184. Acetic acid was activated to the acetyl dichlorophoshonyl intermediate (**72**) that acetylated *N*-methylbarbituric acid (**67**) to give HCl, PO_2Cl (**73**), and the product 1-acetyl-3-methylpyrimidine-2,4,6(1*H*,3*H*,5*H*)-trione (**74**). Thus, the reaction in acetic acid did not yield the desired product **68**.

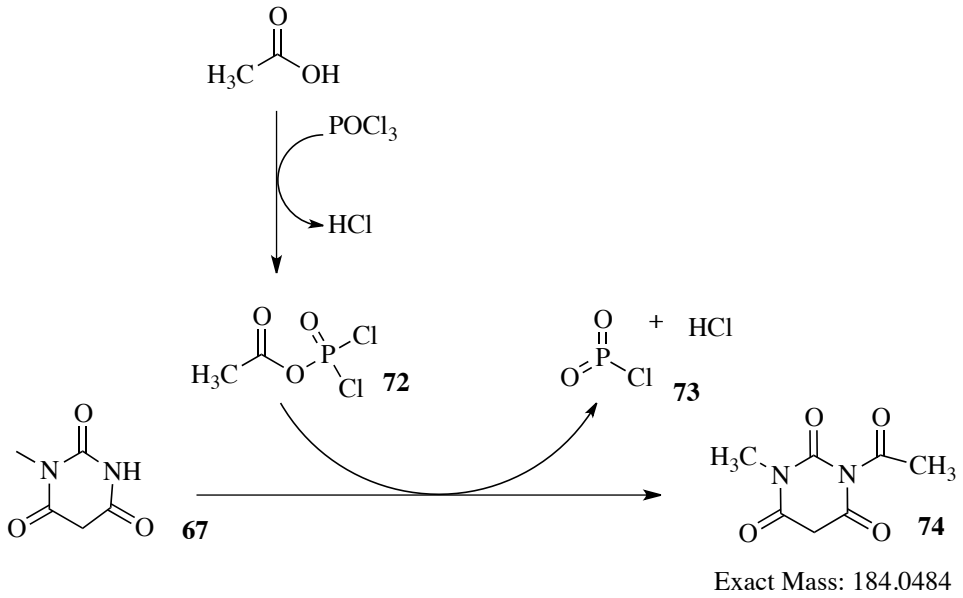

Scheme 6-5

Both acetonitrile and THF are polar aprotic solvents; however, only the reaction in acetonitrile gave essentially quantitative yield of the desired product. Scheme 6-6 illustrates a rationale for failure of THF. Even though solvents can potentially react with HCl, the equilibrium favors the left side for acetonitrile.

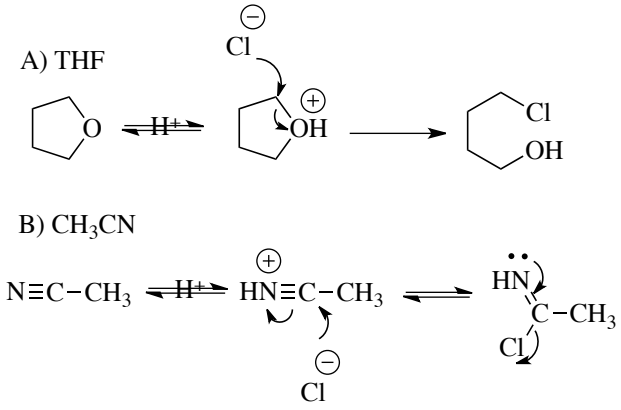

Scheme 6-6

Finally, the reaction of *N*-methylbarbituric acid (**67**) with $POCl_3$ in acetonitrile successfully gave the desired product 6-chloro-3-methyluracil (**68**) with the percent yield of 92%. The percent yield was improved from 33% to 92% by these modifications.

6.3.3 Identification of By-product in the Synthesis of 5-Ethyl-3-methyllumiflavinium perchlorate

Attempts to convert 3MLF **(42)** to 5Et3MLF$^+$ (**43$^+$ClO$_4^-$**) were pursued (Scheme 6-7), and white/pink precipitants were observed during the course of Step 2. After Step 1, solvents (water/ethanol) were evaporated, and the residue was mixed with 2N $HClO_4$ in commercial grade acetonitrile; the precipitation (white/pink solid) came out at the bottom of the reaction solution (reddish).

Everything in the RBF (both the pink solid and reddish liquid) was used for Step 2. After Step 2, dark purple solids precipitated; however the identification of the precipitants using accurate-mass ESI$^+$/MS indicated that the solids were not **43$^+$ClO$_4^-$** (Figure 6-2). Results indicated that there was a major peak at *m/z* 300.1574, which matches the signal for the flavin radical cation **43$^{\bullet+}$**. The desired product of **43$^+$** at *m/z* 299.1503 was not observed. The ion at *m/z* 317 corresponds to the C4a-OH adduct (**51H$^+$**)(0.7 mDa), possibly forming an adduct between the flavin radical salt and water. The ion at *m/z* 289 may possibly be the quinoxalinium (**75$^+$**) shown below.

Step 1: Formation of Reduced Flavin

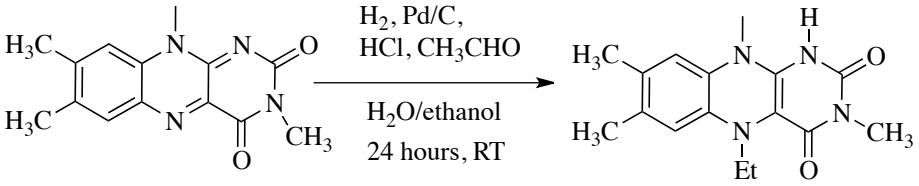

Step 2: Oxidation of Reduced Flavin

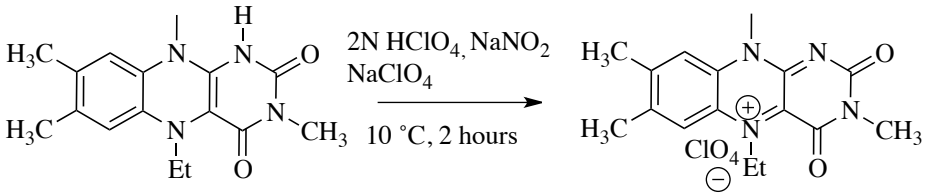

Scheme 6-7

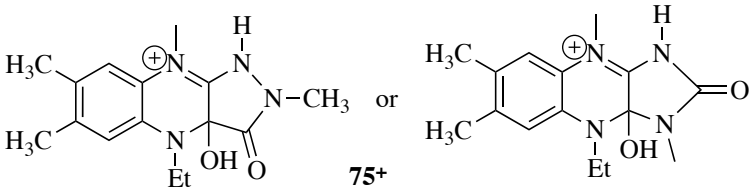

75+

Exact Mass: 289.1659
(0.5 mDa)

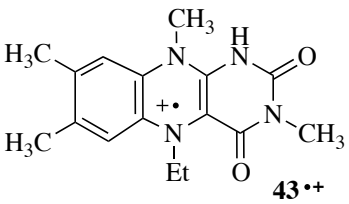

43•+

Exact Mass: 300.1581
(0.7 mDa)

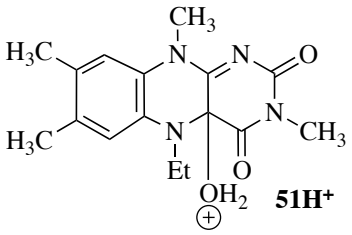

51H+

Exact Mass: 317.1608
(0.2 mDA)

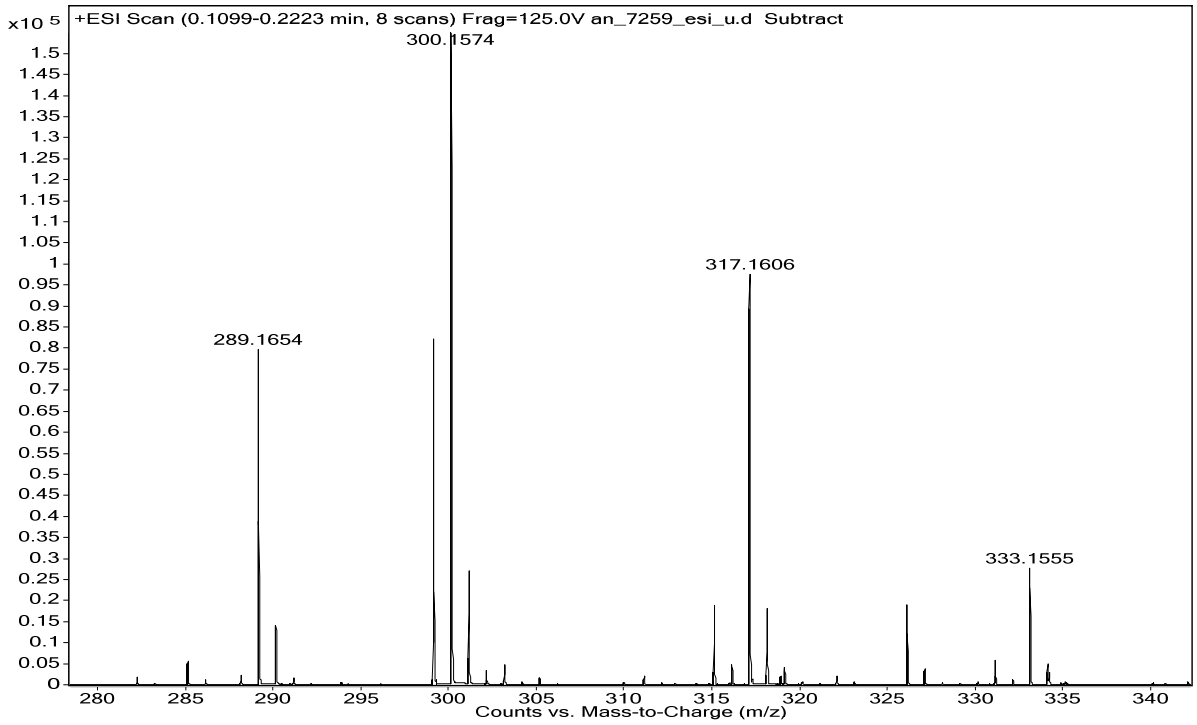

Figure 6-2. Accurate mass ESI+ mass spectrum of the crude product.

Next, the pink/white precipitant was also analyzed using NMR; as shown in Figure 6-3, broad peaks were identified on the ^{1}HNMR spectrum, which indicates radical impurities. This finding is consistent with the ESI+ analysis.

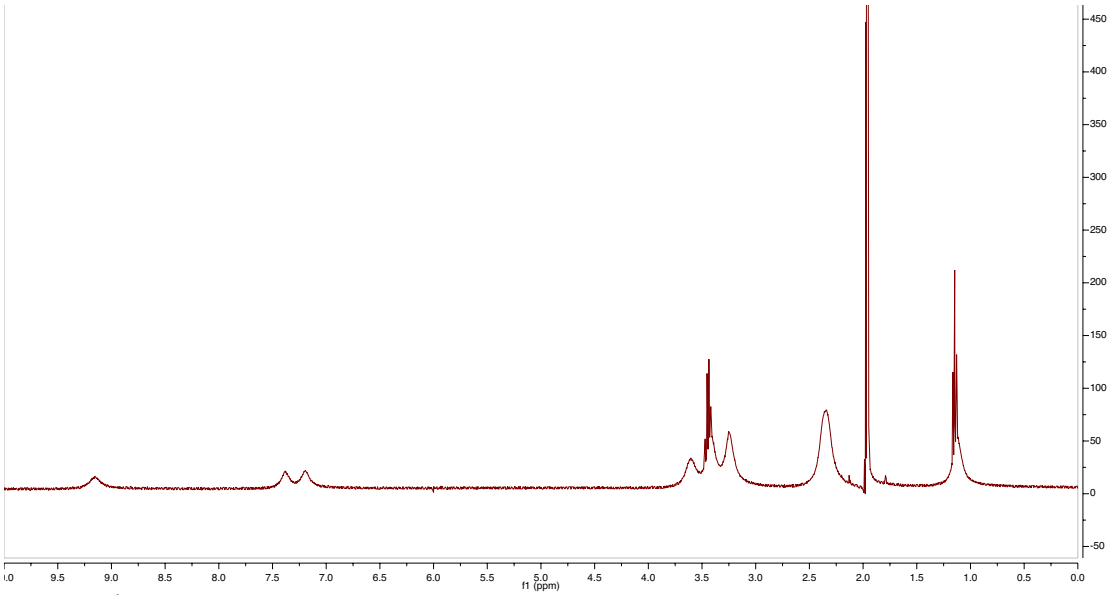

Figure 6-3. ^{1}H-NMR spectrum of the white/pink precipitation (400 MHz, CD_3CN).

The next goal was to crystallize the pink/white precipitant. This precipitant was not particularly stable, and it gradually turned into a dark brown/blackish crystalline solid with air exposure. Therefore, it was handled carefully and stored under argon in the dark.

The pink/white precipitant was dissolved in commercial grade acetonitrile and transferred to an NMR tube. Another organic solvent, diethyl ether, was placed onto the top of the solution. Diethyl ether has the advantage in that it is miscible with acetonitrile. After many attempts, a crystalline solid with excellent quality was obtained. Figure 6-4 shows the X-ray crystal image of the side product. The result revealed that the pink/white precipitant was protonated form of reduced 5Et3MLF (**43H$^+$**). A rationale for the formation of the undesired product is that when $HClO_4$ was added to the reaction solution, protonated reduced flavin **43H$^+$** crashed out of that solution because it is not soluble in ethanol (Scheme 6-8). Some ethanol might have remained from Step 1, which might have not evaporated completely as intended. The majority of the side product is possibly **43H$^+$**. During ESI analysis, an electron and proton were bombarded out, leading to the identification of the flavin cation radical (**43$^{\bullet+}$**) using accurate-mass ESI$^+$/MS.

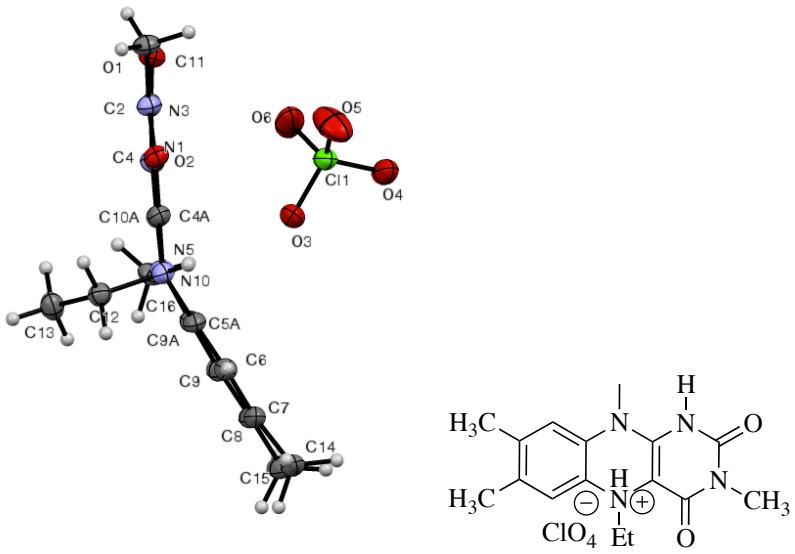

Figure 6-4. Thermal ellipsoid plot of the molecular structure of the protonated reduced 5-ethyl-3-methyllumiflavin at 50 % probability.

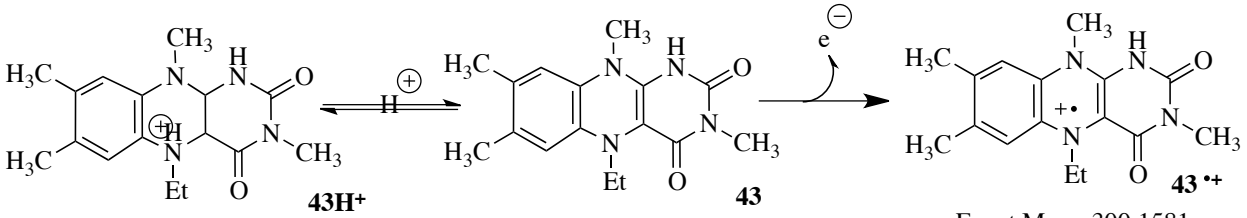

Scheme 6-8

Also, it should be noted that the X-ray crystal structure showed the bent at N5 – N10 (116.80 °), indicating that those N atoms are more sp^3 than sp^2 hybridized, at least in the crystal lattice structure. Previously, the conformation of the reduced 5Et3MLF was studied using the Gaussian computational analysis, and the bent at the N5-N10 (110.96 °) was also found in a proposed global minimum conformation (Figure 6-5). The x-ray crystal image confirmed that the sp^3 hybridization at N5 and N10 is thermodynamically favorable in the reduced flavin, whereas the majority of the oxidized flavin is found in planner and in the sp^2 hybridization.

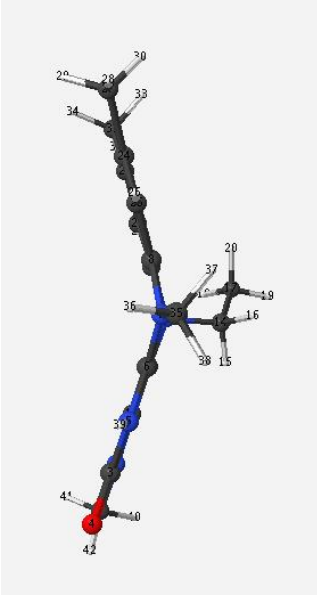

Figure 6-5. A proposed global minimum conformation of the reduced 5Et3MLF conformation.

Lastly, the crude product was again mixed with $NaNO_2$ and $NaClO_4$ (Step 2 in Scheme 6-7), and the desired product **43**$^{+}$**ClO**$_4^{-}$ was isolated and identified successfully.

In summary, the white/pink precipitation during the synthesis of **43**$^{+}$**ClO**$_4^{-}$ was the reduced 5Et3MLFH^{+}. It was precipitated in the solution because it is not soluble in ethanol, indicating that the solvent had not evaporated completed after Step 1.

6.4 Characteristics of 5-Ethyl-3-methyllumiflavinium perchlorate and Associated Species.

6.4.1 Restricted Rotation in 5-Ethyl-3-methyllumiflavinium perchlorate

This section discusses the characteristics of the species **$43^{+}ClO_4^{-}$** and its associated compounds. First, it is important to appreciate the numbering of atoms in $5EtMLF^{+}$; the structure below includes numbered atoms for reference in the text.[79] The flavinium salt **$43^{+}ClO_4^{-}$** consists of three rings: xylene (the A ring), pyrazine (the B ring), and pyrimidine (the C ring).[21]

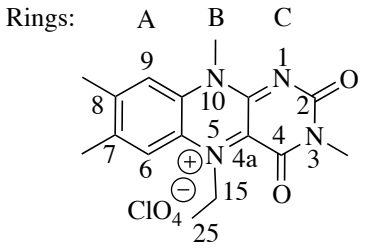

Figure 6-6 displays the ^{1}H-NMR spectrum of **$43^{+}ClO_4^{-}$**. ^{1}H-NMR results demonstrated that the triplet signal for $NCH_2\mathit{CH_3}$ protons is centered at 1.80 ppm. The signal for the $N\mathit{CH_2}CH_3$ protons is complex (non-equivalence due to hindered rotation about the N-CH_2 bond, see a later section for details) and appears as the broad (geminal and vicinal coupled) peaks center at δ 6.09 and 5.05 ppm. The complete assignments for the spectrum are shown below.

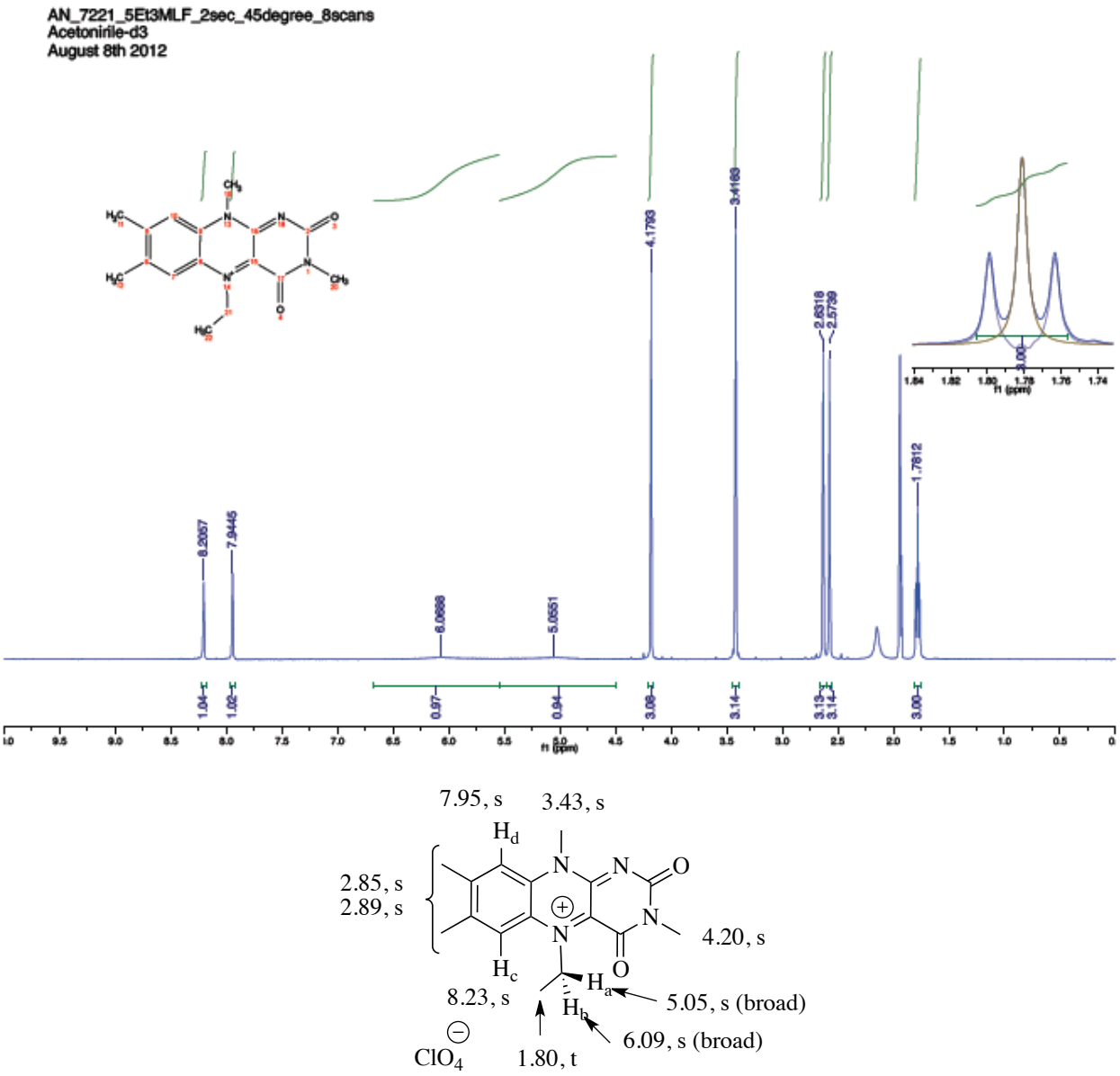

Figure 6-6. ^{1}H-NMR spectrum of 5Et3MLF^{+}ClO$_4^{-}$ (500 MHz, CD_3CN).

Initially, these very weak signals escaped detection and in fact previous reports failed to make assignments for H_a and H_b. Because the signal for the methyl protons of the N5 ethyl group is clearly shown at 1.80 pm as a triplet, one would expected to find two multiplet peaks for the methylene protons, as reported in one of the Mariano papers.[35] However, the present study did not obtain this result. Instead, two very broad, weak signals were observed that centered at δ 5.05 and 6.09 ppm. To determine whether these signals correspond to the methylene protons of the *N*-ethyl group, the species **43^{+}ClO$_4^{-}$** was examined using the 2D Total Correlation

Spectroscopy (TOCSY) experiment (Figure 6-7). The results demonstrated that there was a correlation between the N-$CH_2$$CH_3$ protons (broad peaks) centered at δ 5.05 and 6.09 ppm and the N-CH_2CH_3 protons (triplet) centered at δ 1.80 ppm. This indicates that these protons are adjacent to each other. As shown in Figure 1, the nearly symmetrical triplet for the N-CH_2CH_3 signal may indicate that the coupling constants of the non-equivalent methylene protons and the methyl protons are very nearly the same.

One interpretation of these spectral characteristics assumes that restricted rotation about the N-ethyl bond leads to the non-equivalency observed for the methylene protons. To examine this possibility, temperature dependent studies were undertaken. The hypothesis tested in this section is that the two broad signals described above belong to the methylene protons. Upon heating to 60 ˚C, these two broad signals merged into one peak, a result that is consistent with the increased rate of rotation about the N-ethyl bond. NMR results demonstrated that the chemical shift difference between those two broad signals center at 5.05 ppm (H_a) and 6.09 ppm (H_b) declined with heating and merged at 60 ˚C (δ 5.68 ppm), while the two broad signals were clearly separated at 23 ˚C (δ 5.00 and 6.00 ppm)(Figure 6-8).

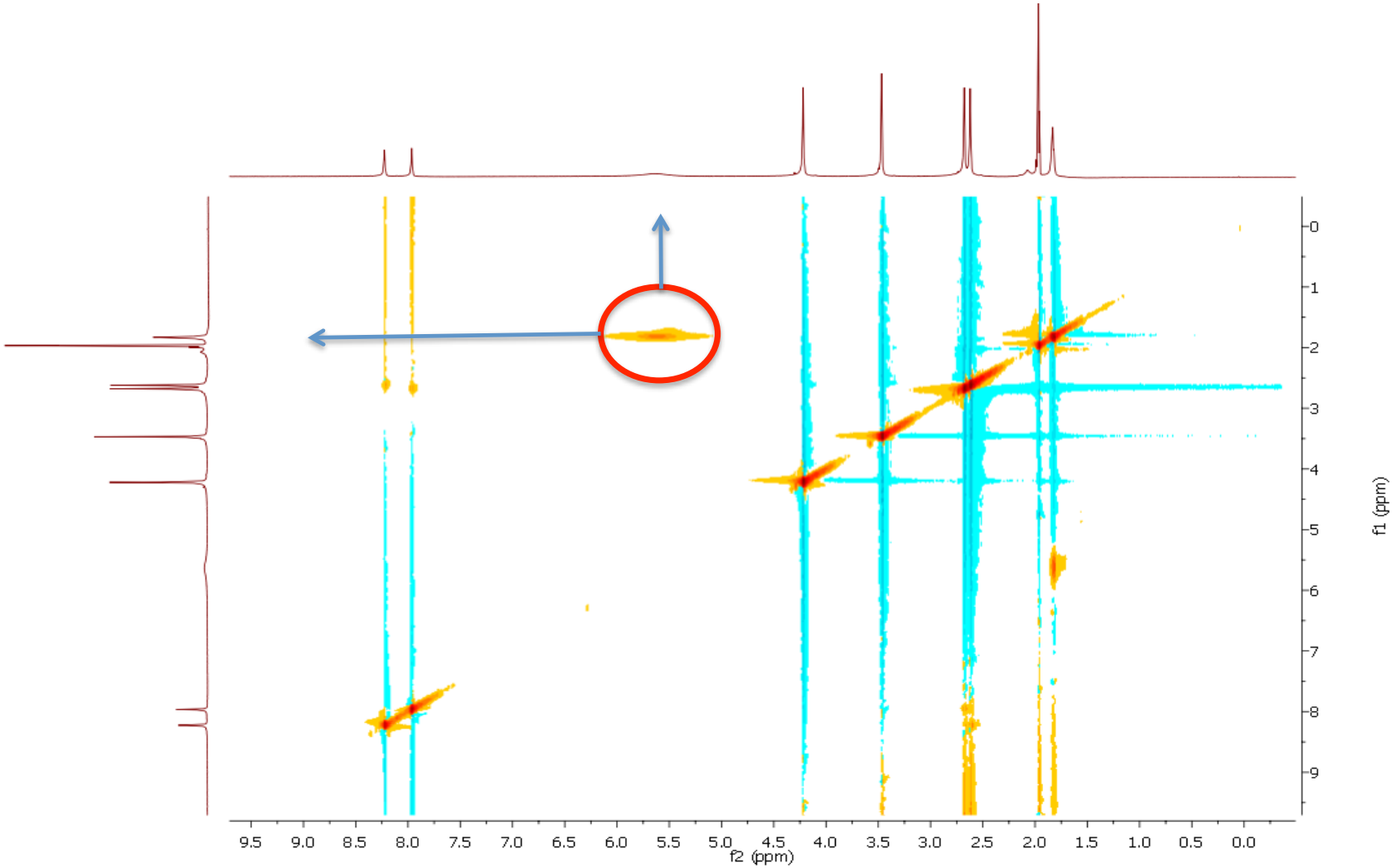

Figure 6-7. 2D TOCSY spectrum of the 5Et3MLF^{+} salt (CD_3CN, 600 MHz). Correlation lines for the methylene protons (δ 5.05 and 6.09 ppm) and methyl protons (δ 1.80 ppm) of N-ethyl group are drawn in the figure.

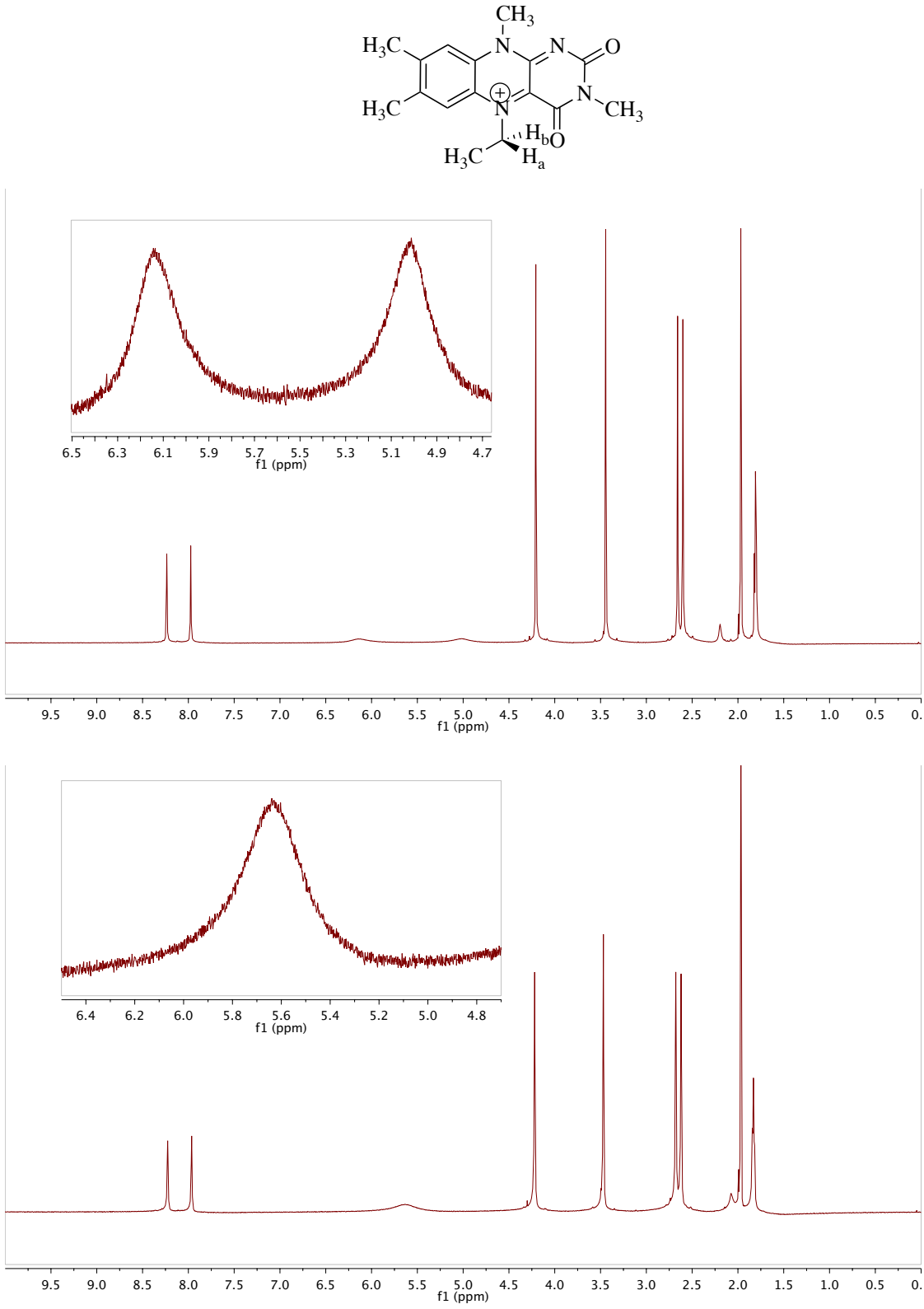

Figure 6-8. Effect of temperature on the methylene protons of 5Et3MLF^{+}ClO_4^{-}. ^{1}H NMR spectra (CD_3CN, 600 MHz) of 5Et3MLF^{+}ClO_4^{-} at 23 °C (A) and 60 °C (B).

This temperature effect was further examined at lower temperatures from 0 to -35 °C. An even more relevant observation was that the broad signals resolved into two multiplets each consisting of six peaks upon cooling to -35 ˚C (Figure 6-9). These signals are most likely a doublet of quartets for each methylene proton (see the diagram below).

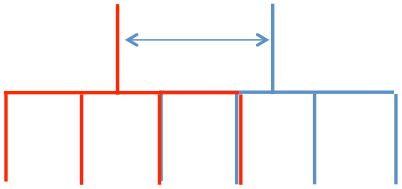

Recall that the two broad signals coalesced into a broad signal centered at δ 5.65 ppm upon heating to 60 ˚C (Figure 6-8). Energy calculations estimate the rotational energy barrier for this bond (assuming a flat structure) to be 19 kcal/mol (see calculation below). In brief, the NMR results indicated that the restricted rotation about the N-ethyl bond causes the non-equivalency observed for the methylene protons.

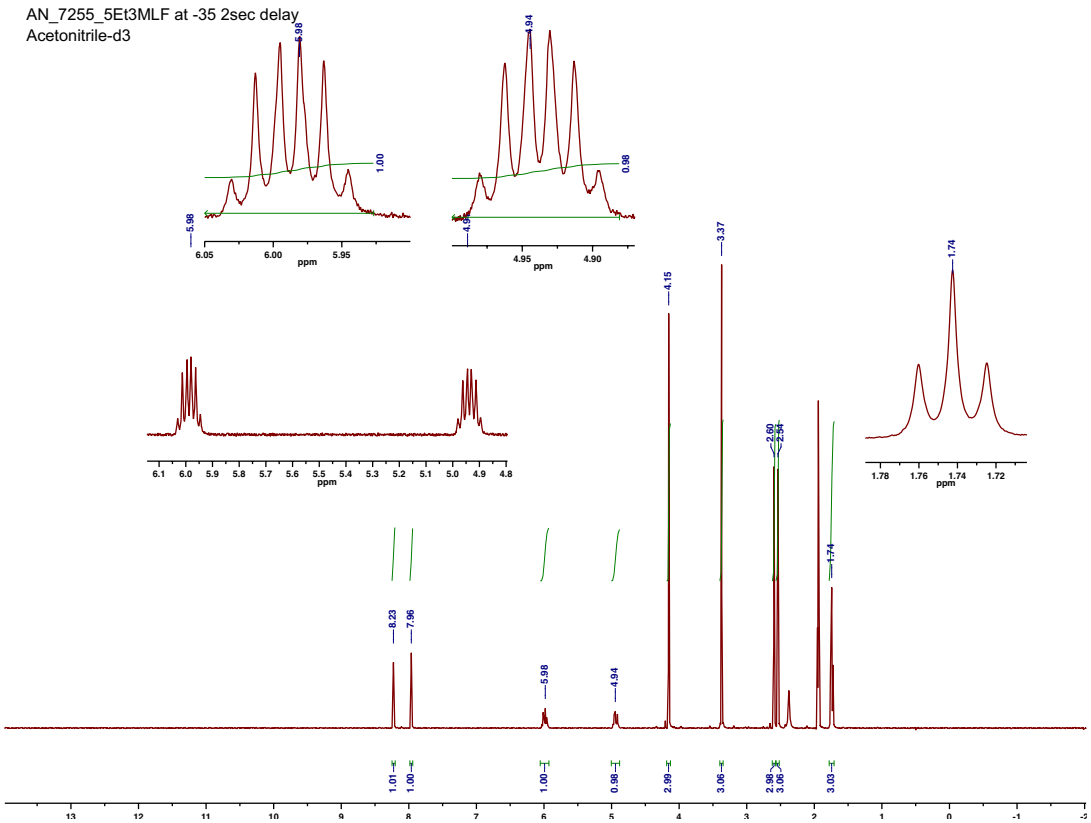

Figure 6-9. NMR spectrum of 5Et3MLF^{+}ClO_4^{-} at -35 ˚C (CD_3CN, 400 MHz).

The rate constant of rotation using the following equation,

$$k_c = 2.22\ \Delta v$$

where k_c represents the rate constant at the coalescence temperature and Δν represents the difference in Hz between the two signals at low temperature. The energy barrier to rotation (in J/mol) is calculated by the equation listed below.[80]

$$Energy\ barrier\ \left(\frac{J}{mol}\right) = 19.14\ T_C\ [10.32 + \log\left(\frac{T_c}{k_c}\right)]$$

Where k_c = 2.22 × the difference in distance in Hz between the two signals at low temperature (1.1 Hz) and T_c = the coalescence temperature in K (333 K). The energy barrier is in J/mol

T_c = 273 K+ 60 K = 333 K
$logT_c/k_c$ = log(333/(222 × 1.1))

Energy barrier = (19.14 J/K/mol × 333 K) × (10.32 + 2.14) = 74467.06 J/mol

Thus, energy barrier in kcal/mol is

74467.06 J/mol × 0.00024 kcal/J = 17.87 kcal/mol

Because the coalescence temperature can be ≤ 60 K, the estimated energy barrier to rotate the N-ethyl bond is ≤ 17.87 kcal/mol.

6.4.2 Reduced Form: 5-Ethyl-3-methyllumiflavin

Because there is a possibility that the reduced 5Et3MLF (**43H$_2$**) may be involved in the reaction between **43$^+$ClO$_4^-$** and **4**, recording the ^{1}H NMR spectrum of the reduced 5EtMLF in acetonitrile-d_3/D_2O containing $Na_2S_2O_4$ was attempted. The first step was to dissolve the flavinium salt **43$^+$ClO$_4^-$** in acetonitrile-d_3 (approximately 500 μL), which was treated with $Na_2S_2O_4$ in D_2O under argon (a few drops as needed)(Scheme 6-9). The solution was degassed and prepared under argon. The NMR tube was then glass-sealed to prevent any air exposure to the sample.

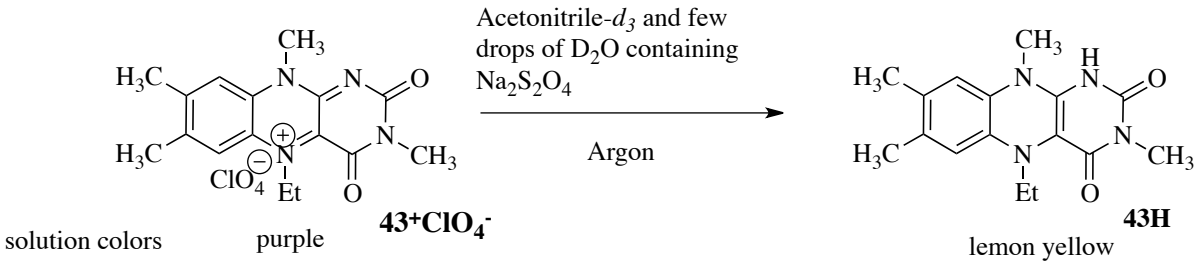

Scheme 6-9

The complete ^{1}HNMR assignment of the reduced 5Et3MLF (**43H$_2$**) is provided in Figure 6-10: ^{1}H NMR (CD_3CN was layered with $D_2O/Na_2S_2O_4$): δ = 6.66 (1H, ArH_a)**,** 6.57 (1H, ArH_b), 3.20 ppm (q, 2H, CH_2CH_3), 3.12 ppm (s, N-CH_3), 3.11 ppm (s, N-CH_3), 2.14 ppm (s, Ar-CH_3), 2.10 ppm (s, Ar-CH_3), and 0.98 ppm (t, CH_2CH_3). Note that the signal for the N(5)CH_2CH_3 protons in the reduced form (**43H$_2$**) is equivalent and appears as a quartet centered at δ 3.20 ppm. Recall that the signal for the N(5)CH_2CH_3 protons in **43$^+$ClO$_4^-$** are non-equivalent and appear as two broad peaks (Figure 6-6).

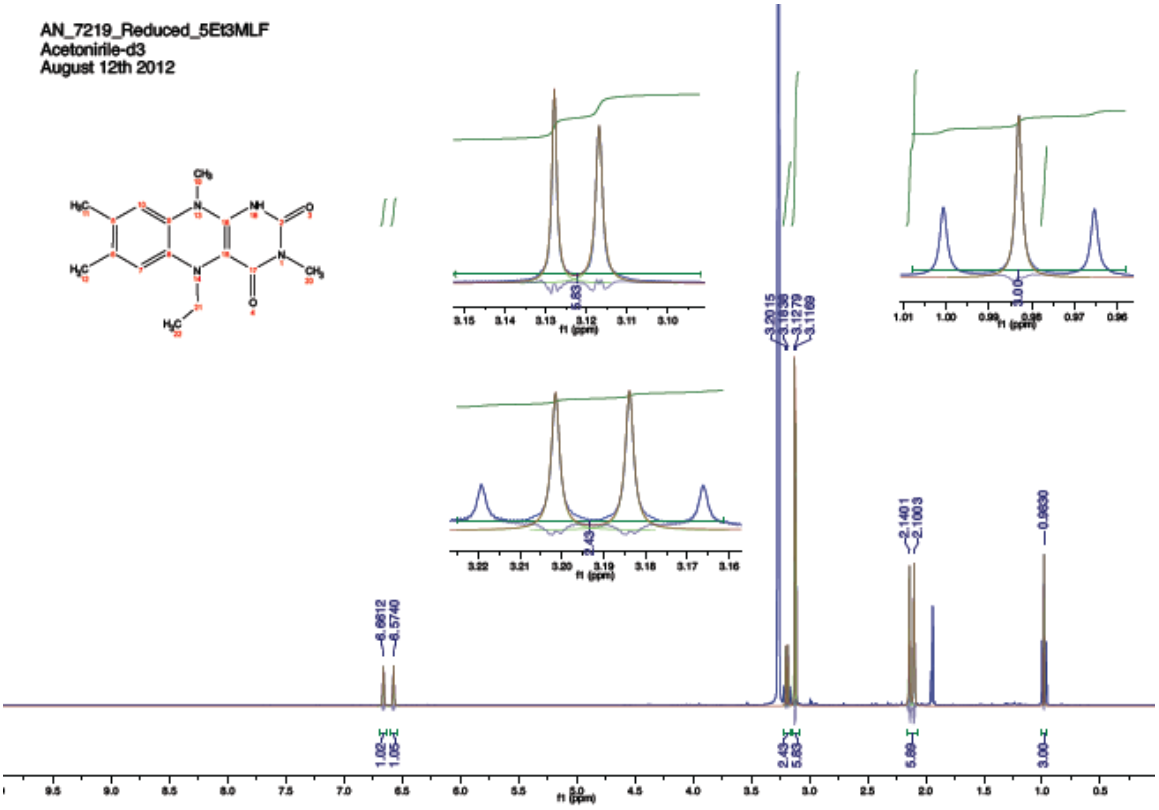

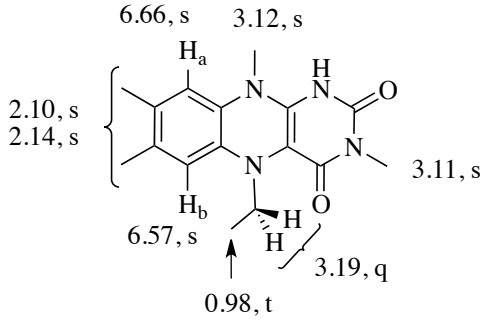

Figure 6-10. ^{1}H-NMR spectrum of 5Et3MLF^{+}ClO$_4^{-}$ with $Na_2S_2O_4$. The spectrum shows the addition of a few drops of D_2O containing $Na_2S_2O_4$ to the 5-ethyl-3-methyllumiflavinium perchlorate solution (500 MHz, CD_3CN).

One interpretation of the change in the coupling constant is that it results from the difference in the hybridization of the N(5) atom. The N(5) atom of **43^{+}ClO$_4^{-}$** whereas the N(5) atom has *sp*^{3} characteristics in the reduced 5Et3MLF (**43H$_2$**). This avoids antiaromaticity (the Breslow concept)[81] of the ring system. The center pyrazine ring is bent at the N5-N10 axis, which creates the angle between the xylene and pyrimidine rings.[65] Therefore, the NMR results suggest the freedom of rotation about N-ethyl bond in the reduced 5Et3MLF (**43H$_2$**).

As discussed in the previous section, the N-ethyl bond of 5Et3MLF$^+$ shows restricted rotation. In the oxidized form, the atoms are sp^2 hybridized, and the three rings are coplanar. Hence, the aromatic proton at C(6) on the xylene ring (the A ring in Section 6-3-1), on the methylene protons of N(5)-CH_2CH_3 on the pyrazine ring (the B ring), and the oxygen atom of C(4)=O in the pyrimidine ring (the C ring) could be located in the same plane in the compound **43$^+$ClO$_4^-$** but not in **43H$_2$**.

In the case of compound **43H$_2$**, the methylene protons are equivalent, and the signal for N(5)-CH_2CH_3 appears as a quartet at the center δ 3.20 ppm. Because the N(5) atom has sp^3 hybridized characteristics, the flavin rings are no longer present in the coplanar in **43H$_2$**. The pyramidal inversion of the N(5)-centre was reported with reduced flavins using the NMR analysis.[82] Reduced flavins were found in two boat conformations with interconvertion of ring inversion and N inversion. As a result, the distances from the methylene protons of N(5)-CH_2CH_3 to the aromatic proton at C(6) and to the oxygen atom of C(4)=O are not close enough to cause the restricted rotation about the N-ethyl bond in **43H$_2$**. The flavin conformational change from the co-planar (the oxidized form) to bent (the reduced form) has also been observed in the flavoenzymes' structures.[83] For example, the bending angle between xylene (the A ring) and pyrimidine (the C ring) was observed as 34° in the reduced thiredoxin reductase using X-ray crystallography.[83b]

6.5 X-ray Crystallography of C4a-Sulfonate Adduct of 5-Ethyl-3-methyllumiflavin

Observations of a sulfur-5Et3MLF adduct occurred unexpectedly while obtaining the ^{1}H NMR spectra of the 5Et3MLF. Scheme 6-10 shows the overall reaction of the formation of C4a-sulfonate adduct as determined by X-ray crystallography. The difference between Schemes 1 and 2 involves whether the sample was kept under argon or with air exposure, respectively. The sulfonate-adduct was prepared in the presence of air using the same chemicals as with the preparation of **43H$_2$**: treating the 5Et3MLF$^+$ solution in acetonitrile with a few drops of D_2O containing $Na_2S_2O_4$.

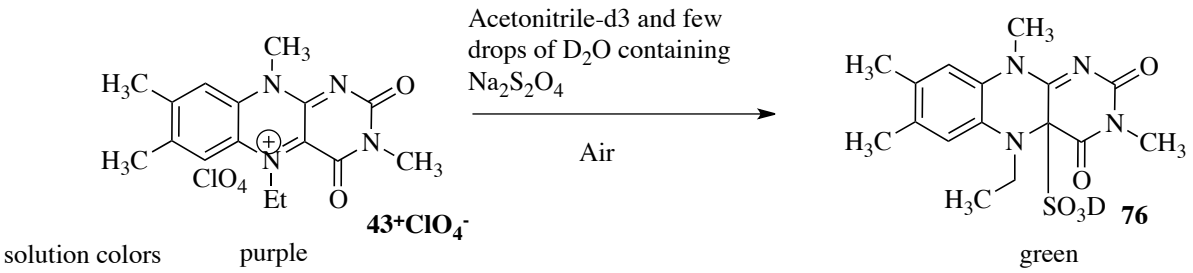

Scheme 6-10

To prepare a sample for NMR analysis, the flavinium salt 5Et3MLF$^+$ was dissolved in acetonitrile-d_3 and mixed with D_2O containing the reducing reagent $Na_2S_2O_4$; after the two layers were clearly separated, only the acetonitrile layer was removed for NMR analysis. The ^{1}H NMR spectrum of the product is given in Figure 6-11: ^{1}H NMR (CD_3CN was layered with $D_2O/Na_2S_2O_4$): δ = 6.92 (1H, ArH_c)**,** 6.81 (1H, ArH_d), 4.17, (1H, CH_2CH_3), and 3.14 ppm (1H, CH_2CH_3), 3.53 ppm (s, N-CH_3), 3.14 ppm (s, N-CH_3), 2.20 ppm (s, Ar-CH_3), 2.10 ppm (s, Ar-CH_3), and 1.07 ppm (t, CH_2CH_3). However, the recorded NMR was different from what was expected (the reduced 5Et3MLF), and the product was uncertain at the time. This is too complicated for me to follow.

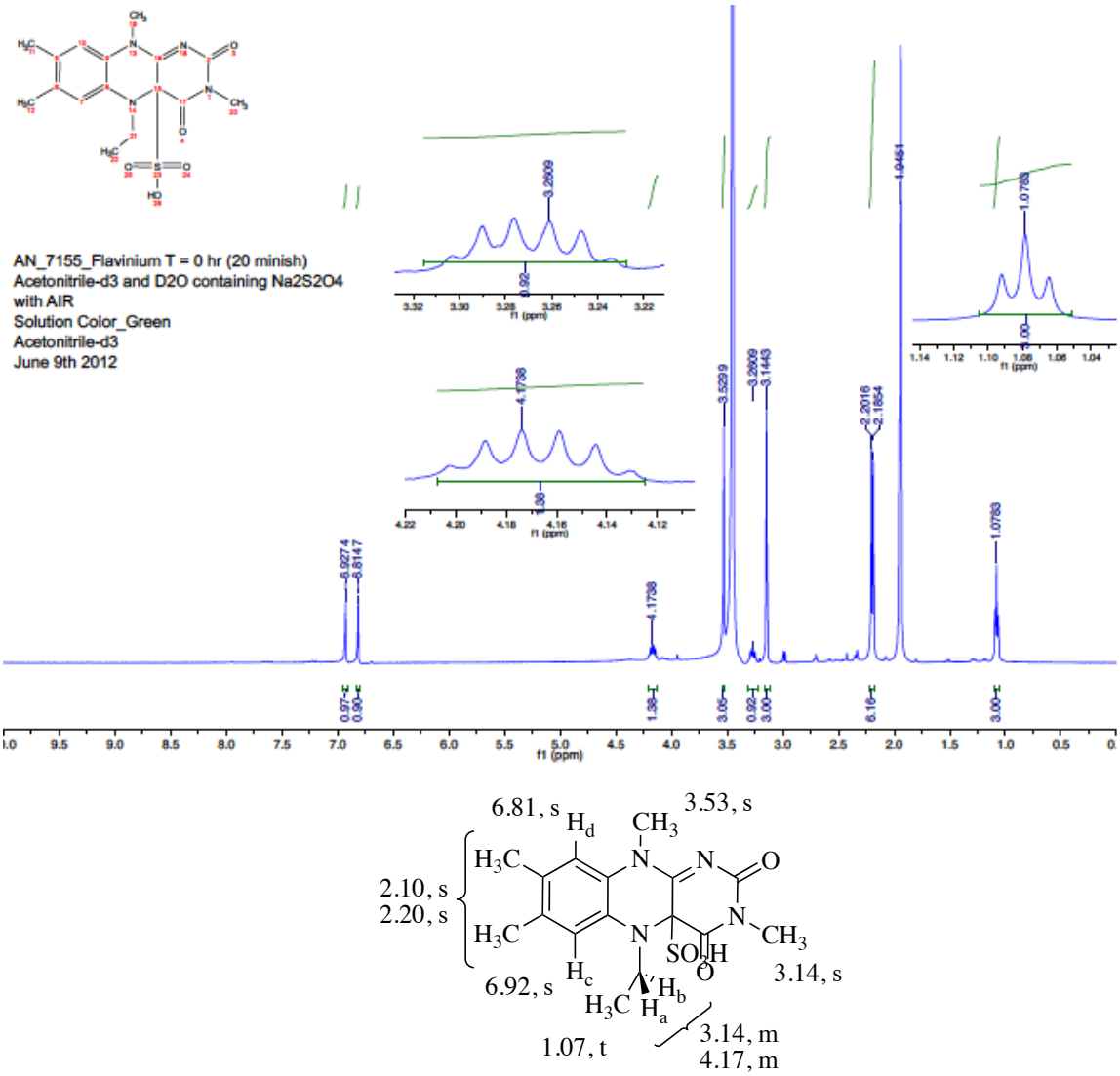

Figure 6-11. ^{1}H-NMR spectrum of the 4a-sulfonated adduct and NMR signal assignments (CD_3CN, 500 MHz).

On the next day, white crystals in the remaining D_2O layer were observed in the leftover solution, which were analyzed using X-ray diffraction. It may be that the formation of the adduct takes some time (in this case, overnight) and that the sulfonate adduct is not water soluble, even though it is a charged species. Also, the sulfonate adduct formation was only observed with the reaction in air, suggesting dioxygen dependency. Note that the NMR spectrum given in Figure 6-12 is interpreted as 5-ethyl-3,7,8,10-tetramethyl-2,4-dioxo-2,3,4,4a,5,10-hexahydrobenzo[*g*]pteridine-4a-sulfonic acid [C4a 5Et3MLF-SO_3H adduct (**76**)]

whereas the crystal image shows the C4a sulfonate anion (**76**$^-$) and the benzoimidazolium species **47**$^+$ (structures shown below).

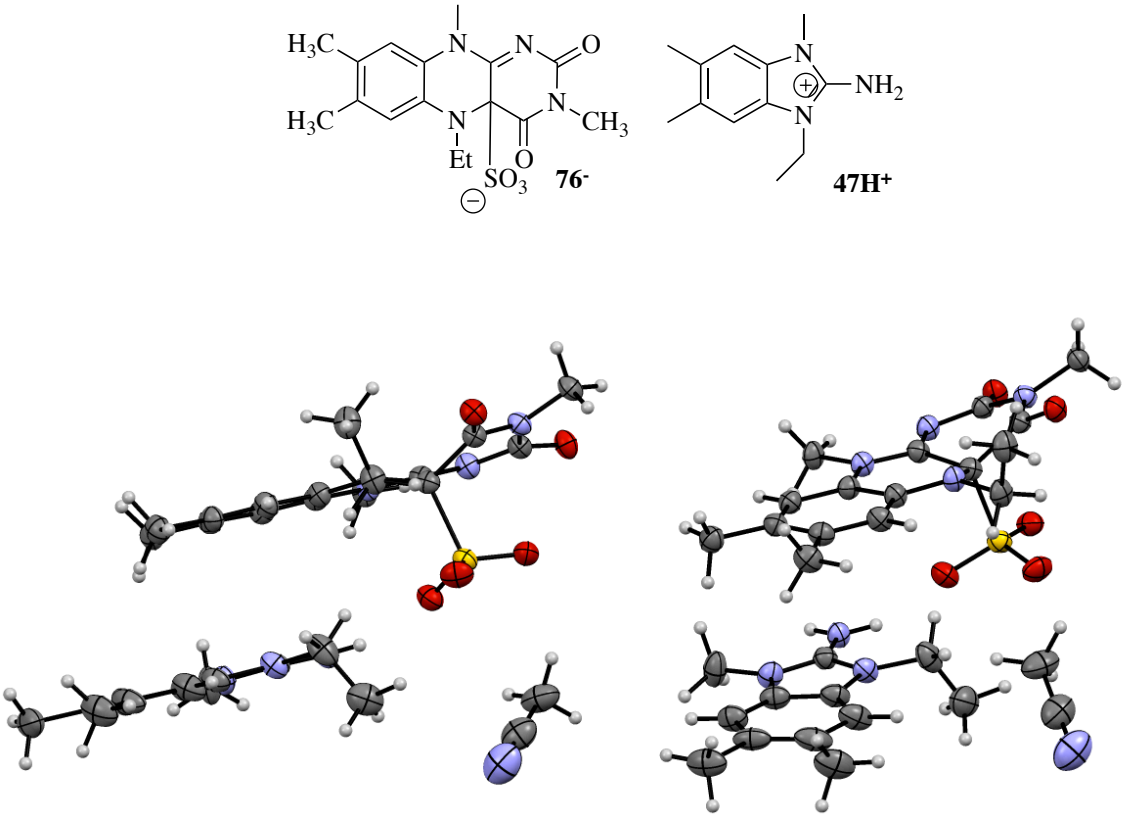

Figure 6-12. X-ray crystal images of the C4a-SO_3 adduct and benzoimidazolium. Views from the side (left) and form the top (right) are shown. Thermal ellipsoid plot of the molecular structure of the C4a-SO_3 adduct and benzoimidazolium at 50 % probability. The solvent was CH_3CN.

In summary, this section presents details of the characteristics of the 5Et3MLF$^+$ and associated compounds. The methylene protons at the N(5) position are non-equivalent and lead to interesting NMR characteristics that have not been described before. On the otherhand, in the reduced 5Et3MLF, the signal for the methylene protons of reduced 5Et3MLF are equivalent. It seems as though the flavin conformational change at N5 (from sp^2 to sp^2/sp^3) increased the freedom of the rotation around the N-ethyl group.

6.6 Experimental Protocols

6.6.1. Experimental Section for the Reaction Between 5Et3MLF$^+$ClO$_4^-$ and TMMP

Prior to the experiment, CD_3CN was dried over CaH_2 for 2 days with continuous stirring. For this experiment, valve NMR tubes were used since these are designed to improve the safety of sample handling for volatile, air-sensitive compounds. These valved NMR tubes were cleaned and dried in the oven overnight. **5Et3MLF$^+$ClO$_4^-$** (**43$^+$ClO$_4^-$**) was placed in a desiccator with P_2O_5. Five mg of **43$^+$ClO$_4^-$** was dissolved in 0.5 mL of de-gassed acetonitrile. **TMMP** (**4**) was added (4.5 μL) to the **43$^+$ClO$_4^-$** solution in a glove box. The molar ratio of **43$^+$ClO$_4^-$** and **4** was 1 to 2 for the present study with 25.12 mM and 50.12 mM being the final concentrations. Altogether, four samples were prepared. Immediately after mixing the starting materials, all samples were subjected to an NMR analysis with the first NMR spectra (T_{argon} = 0 min) taken using Bruker Avance II 500MHz NMR. To monitor time-dependent formation of the product **MMP$^+$** (**50$^+$**), spectra were recorded every 30 min for the first 6 hours. Subsequently, a new spectrum was recorded every 24 hours for a week. After spectra were taken at T_{argon} = 0 min, dried air (10 mL each) was added to two samples (aerobic samples) with the reaction in air being monitored over time. Two other sample solutions remained under argon (anaerobic samples).

For UV analyses, 20 μL of an NMR sample (reaction mixture) was diluted into three mL of commercial grade acetonitrile. For ESI analyses, 20 μL of an NMR sample (reaction mixture) was diluted into three mL of commercial grade acetonitrile, 20 μL of which was then further diluted in two mL of commercial grade acetonitrile.

6.6.2. Experimental Section for the Reaction Between 3MLF and TMMP

First, 3.5 mg of **3MLF (42)** was dissolved in 0.5 mL of de-gassed acetonitrile. The 3MLF solution in valve NMR tubes was heated to 65 °C in order to dissolve all the 3MLF in dried acetonitrile. After the solution decreased to room temperature, no 3MLF particles were evident in the solution. Compound **4** (4.5 μL) was added to the solution of **42** in a glove box. The molar ratio of **42** and **4** was 1 to 2 for the present study with 25 mM and 50 mM being the final concentrations. The NMR recording procedure is identical to that described for the experiment in Chapter 3-2.

CHAPTER SEVEN

SUMMARY

7.1 Final Thoughts and Conclusion

One of the goals of this project was to examine whether FAD chemical models are suitable for studying the mechanism of MAO-B oxidation. Two FAD chemical models are investigated in this project: 5-ethyl-3-methyllumiflavinium perchlorate ($5Et3MLF^+ClO_4^-$) and 3-methyllumiflavin (3MLF). Both FAD models at ground state demonstrated oxidation of TMMP and generation of the corresponding pyridinium product MMP^+ at room temperature. These findings provide evidence that the oxidation of TMMP proceeds via the obligatory intermediate DHP^+, which is converted to the corresponding free base species DHP, and ultimately DHP is air oxidized to MMP^+. These mechanisms are consistent with the oxidation of TMMP via MAO-B. Also, the results indicated that the FAD chemical models require dioxygen for the first 2-electron oxidation of TMMP, while MAO-B catalyzes amine substrates anaerobically. Because the MAO-B oxidation does not require dioxygen, these FAD models may not demonstrate the redox process of MAO per se. However, 3MLF and $5Et3MLF^+ClO_4^-$ may be good chemical models with which to study both SET and nucleophilic polar mechanisms for other oxygen-dependent flavoenzymes.

The other goal was to investigate the pathway of the alpha-carbon oxidation of the cyclic tertiary amine using the FAD chemical models. Proposed pathways are the single electron transfer, nucleophilic polar, and hydrogen atom transfer pathways. EPR analysis detected the formation of radicals concurrent with the oxidation of TMMP in the presence of both 3MLF and $5Et3MLF^+ClO_4^-$ at room temperature, which suggests that a single electron transfer mechanism is involved in the oxidation. In addition, previous findings and the X-ray crystal image generated in the course of the present study reveal that the initial reaction of benzylamine with $5Et3MLF^+ClO_4^-$ proceeds via the formation of an adduct at the C4a position of $5Et3MLF^+$ to form the corresponding Schiff base. These results demonstrate that a single electron pathway may be involved in the alpha-carbon oxidation in the reaction between $5Et3MLF^+ClO_4^-$ and TMMP; a nucleophilic polar pathway is likely involved in the reaction between $5Et3MLF^+ClO_4^-$ and benzylamine. The steric effect of the cyclic tertiary allylamine TMMP might explain the tendency toward single electron transfer rather than polar or hydrogen atom transfer. In brief,

use of the FAD chemical models is a useful tool for studying the oxidation of primary and secondary amines as well as tertiary amines.

Lastly, the effect of water on the reactivity of $5Et3MLF^+ClO_4^-$ is reported in this dissertation. The results indicate that water forms an adduct with $5Et3MLF^+$, and that an excess amount of water halts the oxidative reactions of $5Et3MLF^+ClO_4^-$. These findings suggest that the moisture content of solvents needs to be taken into consideration in research using the FAD model $5Et3MLF^+$.

7.2 Suggested Future Work

This study has demonstrated that investigation of other cyclic tertiary allylamines with the FAD chemical models is a promising direction for future work. Preliminary observations of the oxidation of *N*-cyclopropyl TMMP (**81**) in the presence of the flavinium salt $\mathbf{43^+ClO_4^-}$ were recorded using EPR, NMR, and X-ray crystallography. EPR spectroscopy detected the formation of radicals concurrent with the reaction at t = 2 hours. Also, the reaction between $\mathbf{43^+ClO_4^-}$ and **81** was monitored by ^{1}H NMR. The formation of cyclopropyl MMP^+ $\mathbf{82^+}$ was demonstrated by NMR spectra obtained during the course of the reaction. The NMR results demonstrate that the cyclopropyl group (ring closed form) does not undergo ring opening as would have been predicted from earlier reports of the behavior of cyclopropylaminyl radical cations.

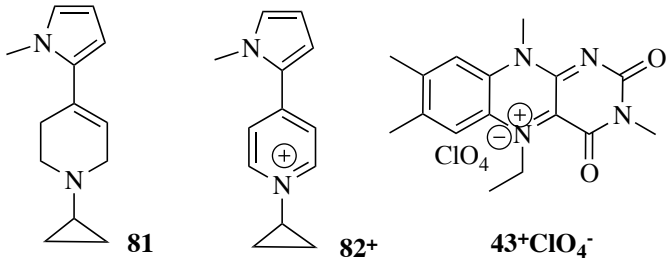

Furthermore, the crystal of the final product was analyzed using X-ray crystallography. The results indicated the intact cyclopropyl group attached to the N1 position of MMP^+ (Figure 7-1).

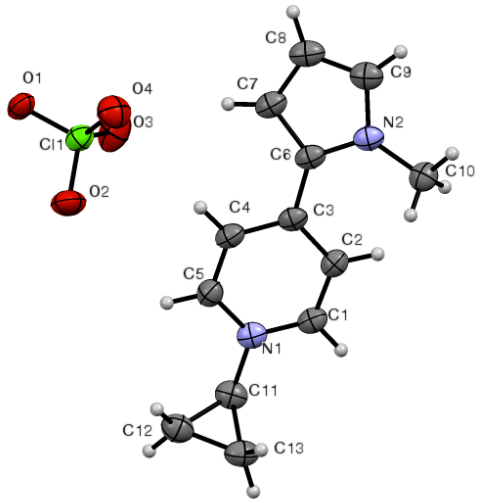

Figure 7-1. X-ray crystal image of *N*-cyclopropyl MMP^+. Thermal ellipsoid plot of the molecular structure of *N*-cyclopropyl MMP^+ at 50 % probability. The crystal of *N*-cyclopropyl MMP^+ was obtained from the reaction mixture of $5Et3MLF^+ClO_4^-$ and *N*-cyclopropyl TMMP in acetonitrile-d_3.

These remarkable findings have opened Pandora's box. This EPR result supports an SET pathway for the oxidation of cyclopropyl TMMP with $5Et3MLF^+$. NMR results demonstrated the formation of cyclopropyl MMP^+ as the final product, which was also supported by the X-ray crystal structure image.

These findings raise questions since the cyclopropyl system is expected to be ultrasensitive for single electron transfer; thus, electron transfer from cyclopropyl TMMP is anticipated to give the cycloproyl ring opened product. The EPR results indicated radical formation, suggesting an SET mechanism. However, the observation that an intact cyclopropyl group is attached to the N1 position of MMP^+ suggests a mechanism other than SET. This area needs further examination.

Also, the comparison of TMMP (**1**) and the corresponding piperidine (**80**) with regard to the reactivity towards the FAD models might lend new insight on the structurally unique feature of MPTP derivatives with the oxidation of MAO.

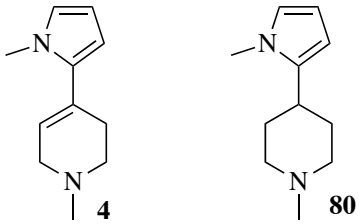

4 **80**

7.3 Contributions

Contributions to this dissertation are as follows: Dr. Carla Slebodnick performed the X-ray crystallography for all X-ray crystal images. Mr. Bill Bebout performed accurate-mass ESI^+/MS analysis. Dr. Paul Deck performed distillation of acetonitrile-d_3 and sample preparation in a glove box for experiments under anaerobic conditions. Dr. James Mahaney performed EPR analysis. Dr. James M. Tanko, Dr. Neal Castagnoli Jr. and Dr. Arthur Stiles, IV contributed to the writing and editing of this dissertation.

REFERENCES

1. Reynolds, A.; Laurie, C.; Mosley, R. L.; Gendelman, H. E., Oxidative stress and the pathogenesis of neurodegenerative disorders. *Int. Rev. Neurobiol.* **2007,** *82*, 297-325.
2. Parkinson, J., An essay on the shaking palsy. 1817. *J. Neuropsychiatry Clin. Neurosci.* **2002,** *14* (2), 223-36; discussion 222.
3. Savitt, J. M.; Dawson, V. L.; Dawson, T. M., Diagnosis and treatment of Parkinson disease: molecules to medicine. *J. Clin. Invest.* **2006,** *116* (7), 1744-54.
4. Dorsey, E. R.; Constantinescu, R.; Thompson, J. P.; Biglan, K. M.; Holloway, R. G.; Kieburtz, K.; Marshall, F. J.; Ravina, B. M.; Schifitto, G.; Siderowf, A.; Tanner, C. M., Projected number of people with Parkinson disease in the most populous nations, 2005 through 2030. *Neurology* **2007,** *68* (5), 384-6.
5. Shih, J. C.; Chen, K.; Ridd, M. J., Monoamine oxidase: from genes to behavior. *Annu. Rev. Neurosci.* **1999,** *22*, 197-217.
6. (a) Youdim, M. B.; Edmondson, D.; Tipton, K. F., The therapeutic potential of monoamine oxidase inhibitors. *Nature Rev. Neurosci.* **2006,** *7* (4), 295-309; (b) Youdim, M. B.; Bakhle, Y. S., Monoamine oxidase: isoforms and inhibitors in Parkinson's disease and depressive illness. *Brit. J. Pharmacol.* **2006,** *147 Suppl 1*, S287-96.
7. Reynolds, M. S.; Holm, R. H., Iron-sulfur-thiolate basket clusters. *Inorg. Chem.* **1988,** *27* (24), 4494-9.
8. Mandemakers, W.; Morais, V. A.; De Strooper, B., A cell biological perspective on mitochondrial dysfunction in Parkinson disease and other neurodegenerative diseases. *J. Cell Sci.* **2007,** *120* (Pt 10), 1707-16.
9. Carlsson, A.; Lindqvist, M.; Magnusson, T., 3,4-Dihydroxyphenylalanine and 5-hydroxytryptophan as reserpine antagonists. *Nature* **1957,** *180* (4596), 1200.
10. Bernheimer, H.; Birkmayer, W.; Hornykiewicz, O.; Jellinger, K.; Seitelberger, F., Brain dopamine and the syndromes of Parkinson and Huntington. Clinical, morphological and neurochemical correlations. *J. Neurol. Sci.* **1973,** *20* (4), 415-55.
11. (a) Langston, J. W., Parkinson's disease: current and future challenges. *Neurotoxicology* **2002,** *23* (4-5), 443-50; (b) Langston, J. W.; Ballard, P.; Tetrud, J. W.; Irwin, I., Chronic Parkinsonism in humans due to a product of meperidine-analog synthesis. *Science* **1983,** *219* (4587), 979-80.
12. Vila, M.; Przedborski, S., Targeting programmed cell death in neurodegenerative diseases. *Nature Rev. Neurosci.* **2003,** *4* (5), 365-75.
13. Yu, J.; Castagnoli, N., Jr., Synthesis and monoamine oxidase B substrate properties of 1-methyl-4-heteroaryl-1,2,3,6-tetrahydropyridines. *Bioorg. Med. Chem.* **1999,** *7* (12), 2835-42.
14. (a) Heikkila, R. E.; Manzino, L.; Cabbat, F. S.; Duvoisin, R. C., Protection against the dopaminergic neurotoxicity of 1-methyl-4-phenyl-1,2,5,6-tetrahydropyridine by monoamine oxidase inhibitors. *Nature* **1984,** *311* (5985), 467-9; (b) Ramsay, R. R.; Krueger, M. J.; Youngster, S. K.; Gluck, M. R.; Casida, J. E.; Singer, T. P., Interaction of 1-methyl-4-phenylpyridinium ion (MPP+) and its analogs with the rotenone piericidin binding-site of NADH dehydrogease. *J. Neurochem.* **1991,** *56* (4), 1184-1190.
15. (a) Dawson, T. M.; Dawson, V. L., Molecular pathways of neurodegeneration in Parkinson's disease. *Science* **2003,** *302* (5646), 819-22; (b) Vila, M.; Perier, C., Molecular pathways of programmed cell death in experimental Parkinson's disease. *Parkinsonism. Relat. Disord.* **2008,** *14 Suppl 2*, S176-9.

16. Fuller, R. W.; Hemrick-Luecke, S. K., Persistent depletion of striatal dopamine and its metabolites in mice by TMMP, an analogue of MPTP. *J. Pharm. Pharmacol.* **1987,** *39* (8), 667-9.
17. (a) Anderson, A. H.; Kuttab, S.; Castagnoli, N., Jr., Deuterium isotope effect studies on the MAO-B catalyzed oxidation of 4-benzyl-1-cyclopropyl-1,2,3,6-tetrahydropyridine. *Biochemistry* **1996,** *35* (10), 3335-40; (b) Castagnoli, K.; Petzer, J. B.; Steyn, S. J.; Van Der Schyf, C. J.; Castagnoli, N., Jr., Inhibition of human MAO-A and MAO-B by a compound isolated from flue-cured tobacco leaves and its neuroprotective properties in the MPTP mouse model of neurodegeneration. *Inflammopharmacology* **2003,** *11* (2), 183-188.
18. Castagnoli, K.; Murugesan, T., Tobacco leaf, smoke and smoking, MAO inhibitors, Parkinson's disease and neuroprotection; are there links? *Neurotoxicology* **2004,** *25* (1-2), 279-91.
19. Castagnoli, N., Jr.; Castagnoli, K.; Magnin, G.; Kuttab, S.; Shang, J., Studies on the oxidation of 1,4-disubstituted-1,2,3,6-tetrahydropyridines. *Drug Metab. Rev.* **2002,** *34* (3), 533-47.
20. Elbaz, A.; Bower, J. H.; Maraganore, D. M.; McDonnell, S. K.; Peterson, B. J.; Ahlskog, J. E.; Schaid, D. J.; Rocca, W. A., Risk tables for parkinsonism and Parkinson's disease. *J. Clin. Epideiol.* **2002,** *55* (1), 25-31.
21. Ghisla, S.; Edmondson, D. E., Flavin Coenzymes. *Encyclopedia of Life Science* **2009**.
22. Hemmerich, P., The present status of flavin and flavocoenzyme chemistry. *Fortschr. Chem. Org. Naturst* **1976,** *33*, 451-527.
23. Binda, C.; Newton-Vinson, P.; Hubalek, F.; Edmondson, D. E.; Mattevi, A., Structure of human monoamine oxidase B, a drug target for the treatment of neurological disorders. *Nature Struct. Biol.* **2002,** *9* (1), 22-6.
24. (a) Barsky, J.; Pacha, W. L.; Sarkar, S.; Zeller, E. A., Amine oxidases. XVII. Mode of action of 1-isonicotinyl-2-isopropylhydrazine on monoamine oxidase. *J Biol Chem* **1959,** *234* (2), 389-91; (b) Weyler, W.; Hsu, Y. P.; Breakefield, X. O., Biochemistry and genetics of monoamine oxidase. *Pharmacol. Ther.* **1990,** *47* (3), 391-417.
25. Wu, E.; Shinka, T.; Caldera-Munoz, P.; Yoshizumi, H.; Trevor, A.; Castagnoli, N., Jr., Metabolic studies on the nigrostriatal toxin MPTP and its MAO B generated dihydropyridinium metabolite MPDP+. *Chem. Res. Toxicol.* **1988,** *1* (3), 186-94.
26. Bach, A. W.; Lan, N. C.; Johnson, D. L.; Abell, C. W.; Bembenek, M. E.; Kwan, S. W.; Seeburg, P. H.; Shih, J. C., cDNA cloning of human liver monoamine oxidase A and B: molecular basis of differences in enzymatic properties. *Proc. Natl. Acad. Sci. U.S.A.* **1988,** *85* (13), 4934-8.
27. Grimsby, J.; Chen, K.; Wang, L. J.; Lan, N. C.; Shih, J. C., Human monoamine oxidase A and B genes exhibit identical exon-intron organization. *Proc. Natl. Acad. Sci. U.S.A.* **1991,** *88* (9), 3637-41.
28. Lieberman, A. N., *Monoamine oxidase inhibitors in neurological diseases*. Marce Dekker: New York, 1994; p xviii, 371 p.
29. Silverman, R. B.; Hawe, W. P., SAR studies of fluorine-substituted benzylamines and substituted 2-phenylethylamines as substrates and inactivators of monoamine oxidase B. *J. Enzyme Inhib.* **1995,** *9* (3), 203-15.

30. Binda, C.; Li, M.; Hubalek, F.; Restelli, N.; Edmondson, D. E.; Mattevi, A., Insights into the mode of inhibition of human mitochondrial monoamine oxidase B from high-resolution crystal structures. *Proc. Natl. Acad. Sci. U.S.A.* **2003,** *100* (17), 9750-5.
31. Knoll, J., Pharmacological basis of the therapeutic effect of (-)deprenyl in age-related neurological diseases. *Med. Res. Rev.* **1992,** *12* (5), 505-24.
32. Glover, V.; Halket, J. M.; Watkins, P. J.; Clow, A.; Goodwin, B. L.; Sandler, M., Isatin: identity with the purified endogenous monoamine oxidase inhibitor tribulin. *J. Neurochem.* **1988,** *51* (2), 656-9.
33. Kalman, T. I., *Drug action and design : mechanism-based enzyme inhibitors : proceedings of the Twentieth Annual Medicinal Chemistry Symposium, Amherst, New York, U.S.A., on May 21-23, 1979*. Elsevier/North Holland: New York, 1979; p xvii, 309 p.
34. Silverman, R. B., Effect of alpha-methylation on inactivation of monoamine oxidase by N-cyclopropylbenzylamine. *Biochemistry* **1984,** *23* (22), 5206-13.
35. Kim, J. M.; Bogdan, M. A.; Mariano, P. S., Mechanistic analysis of the 3-methyllumiflavin-promoted oxidative deamination of benzylamine. A potential model for monoamine oxidase catalysis. *J. Am. Chem. Soc.* **1993,** *115* (23), 10591-5.
36. (a) Walker, M. C.; Edmondson, D. E., Structure-Activity Relationships in the Oxidation of Benzylamine Analogs by Bovine Liver Mitochondrial Monoamine Oxidase B. *Biochemistry* **1994,** *33* (23), 7088-98; (b) Ottoboni, S.; Caldera, P.; Trevor, A.; Castagnoli, N., Jr., Deuterium isotope effect measurements on the interactions of the neurotoxin 1-methyl-4-phenyl-1,2,3,6-tetrahydropyridine with monoamine oxidase B. *J. Biol. Chem.* **1989,** *264* (23), 13684-8.
37. (a) Silverman, R. B.; Hoffman, S. J., Mechanism of Inactivation of Mitochondrial Monoamine Oxidase by N-Cyclopropyl-N-arylalkyl Amines. *J. Am. Chem. Soc.* **1980,** *102* (2), 884-6; (b) Silverman, R. B.; Hoffman, S. J.; Catus, W. B., III, A mechanism for mitochondrial monoamine oxidase catalyzed amine oxidation. *J. Am. Chem. Soc.* **1980,** *102* (23), 7126-8.
38. Simpson, J. T.; Krantz, A.; Lewis, F. D.; Kokel, B., Photochemical and photophysical studies of amines with excited flavins. Relevance to the mechanism of action of the flavin-dependent monoamine oxidase. *J. Am. Chem. Soc.* **1982,** *104* (25), 7155-61.
39. Rigby, S. E.; Basran, J.; Combe, J. P.; Mohsen, A. W.; Toogood, H.; van Thiel, A.; Sutcliffe, M. J.; Leys, D.; Munro, A. W.; Scrutton, N. S., Flavoenzyme catalysed oxidation of amines: roles for flavin and protein-based radicals. *Biochem. Soc. Trans.* **2005,** *33* (Pt 4), 754-7.
40. Barnes, K. K.; Mann, C. K., Electrochemical oxidation of primary aliphatic amines. *J. Org. Chem.* **1967,** *32* (5), 1474-1479.
41. Jurva, U.; Bissel, P.; Isin, E. M.; Igarashi, K.; Kuttab, S.; Castagnoli, N., Jr., Model electrochemical-mass spectrometric studies of the cytochrome P450-catalyzed oxidations of cyclic tertiary allylamines. *J. Am. Chem. Soc.* **2005,** *127* (35), 12368-77.
42. Andrieux, C. P.; Dumasbouchiat, J. M.; Saveant, J. M., Homogeneous Redox Catalysis of Electrochemical Reactions .4. Kinetic Controls in the Homogeneous Process as Characterized by Stationary and Quasi-Stationary Electrochemical Techniques. *J. Electroanal. Chem.* **1980,** *113* (1), 1-18.

43. Brown, L. E.; Hamilton, G. A., Some model reactions and a general mechanism for flavoenzyme-catalyzed dehydrogenations. *J. Am. Chem. Soc.* **1970,** *92* (24), 7225-7.
44. Walsh, C. T.; Schonbrunn, A.; Abeles, R. H., Studies on the mechanism of action of D-amino acid oxidase. Evidence for removal of substrate -hydrogen as a proton. *J. Biol. Chem.* **1971,** *246* (22), 6855-66.
45. (a) Hoegy, S. E.; Mariano, P. S., Mechanistic and synthetic aspects of amine oxidations promoted by 3-methyl-5-ethyllumiflavinium perchlorate. *Tetrahedron* **1997,** *53* (14), 5027-5046; (b) Miller, J. R.; Edmondson, D. E., Structure-activity relationships in the oxidation of para-substituted benzylamine analogues by recombinant human liver monoamine oxidase A. *Biochemistry* **1999,** *38* (41), 13670-83.
46. Ball, S.; Bruice, T. C., Oxidation of amines by a 4a-hydroperoxyflavin. *J. Am. Chem. Soc.* **1980,** *102* (21), 6498-503.
47. Kim, J.-M.; Hoegy, S. E.; Mariano, P. S., Flavin Chemical Models for Monoamine Oxidase Inactivation by Cyclopropylamines, a-Silylamines, and Hydrazines. *J. Am. Chem. Soc.* **1995,** *117* (1), 100-5.
48. Chiba, K.; Peterson, L. A.; Castagnoli, K. P.; Trevor, A. J.; Castagnoli, N., Jr., Studies on the molecular mechanism of bioactivation of the selective nigrostriatal toxin 1-methyl-4-phenyl-1,2,3,6-tetrahydropyridine. *Drug Metab. Dispos.* **1985,** *13* (3), 342-7.
49. Miller, A. E.; Bischoff, J. J.; Bizub, C.; Luminoso, P.; Smiley, S., Electronic and steric effects in oxidations by isoalloxazine 4a-hydroperoxides. *J. Am. Chem. Soc.* **1986,** *108* (24), 7773-8.
50. Erdem, S. S.; Karahan, O.; Yildiz, I.; Yelekci, K., A computational study on the amine-oxidation mechanism of monoamine oxidase: Insight into the polar nucleophilic mechanism. *Org. Biomol. Chem.* **2006,** *4* (4), 646-658.
51. (a) Miller, J. R.; Edmondson, D. E.; Grissom, C. B., Mechanistic probes of monoamine oxidase B catalysis: Rapid-scan stopped flow and magnetic field independence of the reductive half-reaction. *J. Am. Chem. Soc.* **1995,** *117* (29), 7830-1; (b) Franot, C.; Mabic, S.; Castagnoli, N., Jr., Chemical model studies on the monoamine oxidase-B catalyzed oxidation of 4-substituted 1-methyl-1,2,3,6-tetrahydropyridines. *Bioorg. Med. Chem.* **1997,** *5* (8), 1519-29.
52. (a) Cerny, M. A.; Hanzlik, R. P., Cytochrome P450-catalyzed oxidation of N-benzyl-N-cyclopropylamine generates both cyclopropanone hydrate and 3-hydroxypropionaldehyde via hydrogen abstraction, not single electron transfer. *J. Am. Chem. Soc.* **2006,** *128* (10), 3346-54; (b) Dinnocenzo, J. P.; Karki, S. B.; Jones, J. P., On Isotope Effects for the Cytochrome-P-450 Oxidation of Substituted N,N-Dimethylanilines. *J. Am. Chem. Soc.* **1993,** *115* (16), 7111-7116.
53. Franot, C.; Mabic, S.; Castagnoli, N., Jr., Chemical model studies on the monoamine oxidase-B catalyzed oxidation of 4-substituted 1-cyclopropyl-1,2,3,6-tetrahydropyridines. *Bioorg. Med. Chem.* **1998,** *6* (3), 283-291.
54. (a) Kim, J. M.; Bogdan, M. A.; Mariano, P. S., SET photochemistry of flavin-cyclopropylamine systems. Models for proposed monoamine oxidase inhibition mechanisms. *J. Am. Chem. Soc.* **1991,** *113* (24), 9251-7; (b) Kim, J. M.; Cho, I. S.; Mariano, P. S., Amine-flavin electron transfer photochemistry. Potential models for monoamine oxidase catalysis and inhibition. *J. Org. Chem.* **1991,** *56* (16), 4943-55.
55. Yano, K., Bicyclo[3.2.0]hept-6-en-2-yl carbonium ion. 2-Methyl substituent effects. *J. Org. Chem.* **1975,** *40* (4), 414-417.

56. Suleman, N. K.; Flores, J.; Tanko, J. M.; Isin, E. M.; Castagnoli, N., Jr., The tert-butoxyl radical mediated hydrogen atom transfer reactions of the Parkinsonian proneurotoxin 1-methyl-4-phenyl-1,2,3,6-tetrahydropyridine and selected tertiary amines. *Bioorg. Med. Chem.* **2008,** *16* (18), 8557-62.
57. Nimkar, S. K.; Anderson, A. H.; Rimoldi, J. M.; Stanton, M.; Castagnoli, K. P.; Mabic, S.; Wang, Y. X.; Castagnoli, N., Jr., Synthesis and monoamine oxidase B catalyzed oxidation of C-4 heteroaromatic substituted 1,2,3,6-tetrahydropyridine derivatives. *Chem. Res. Toxicol.* **1996,** *9* (6), 1013-22.
58. Pretorius, A.; Ogunrombi, M. O.; Fourie, H.; Terre'blanche, G.; Castagnoli, N., Jr.; Bergh, J. J.; Petzer, J. P., Interactions of 1-methyl-3-phenylpyrrolidine and 3-methyl-1-phenyl-3-azabicyclo[3.1.0]hexane with monoamine oxidase B. *Bioorg. Med. Chem.* **2010,** *18* (11), 4111-8.
59. (a) Finnegan, K. T.; Irwin, I.; Delanney, L. E.; Ricaurte, G. A.; Langston, J. W., 1,2,3,6-tetrahydro-1-methyl-4-(methylpyrrol-2-yl)pyridine: studies on the mechanism of action of 1-methyl-4-phenyl-1,2,3,6-tetrahydropyridine. *The Journal of pharmacology and experimental therapeutics* **1987,** *242* (3), 1144-51; (b) Bembenek, M. E., Studies of the in vitro oxidation of 1-methyl-4-(1-methylpyrrol-2-yl)-4-piperidinol and its dehydration product 1,2,3,6-tetrahydro-1-methyl-4-(methylpyrrol-2-yl) pyridine by human monoamine oxidases A and B. *Life Sci.* **1990,** *46* (25), 1873-7.
60. Chiba, K.; Trevor, A.; Castagnoli, N., Jr., Metabolism of the neurotoxic tertiary amine, MPTP, by brain monoamine oxidase. *Biochem. Biophys. Res. Commun.* **1984,** *120* (2), 574-8.
61. (a) Ghisla, S.; Mayhew, S. G., Identification and structure of a novel flavin prosthetic group associated with reduced nicotinamide adenine dinucleotide dehydrogenase from Peptostreptococcus elsdenii. *J. Biol. Chem.* **1973,** *248* (18), 6568-70; (b) Mager, H. I. X.; Tu, S.-C., Aromatic hydroxylations by flavins: evidence of direct attack on phenylalanine by flavin radical species. *Tetrahedron* **1994,** *50* (18), 5287-98.
62. Bai, H. Synthetic and metabolic studies on 1-methyl-4-(1-methylpyrrol-2-yl)-1,2,3,6-tetrahydropyridine, a neurotoxic analog of the Parkinsonian inducing agent MPTP. M s, Virginia Polytechnic Institute and State University, 1991.
63. Hemmerich, P.; Muller, F., Flavin-O2 interaction mechanisms and the function of flavin in hydroxylation reaction. *Ann. N.Y. Acad. Sci.* **1973,** *212*, 13-26.
64. Peterson, L. A.; Caldera, P. S.; Trevor, A.; Chiba, K.; Castagnoli, N., Jr., Studies on the 1-methyl-4-phenyl-2,3-dihydropyridinium species 2,3-MPDP+, the monoamine oxidase catalyzed oxidation product of the nigrostriatal toxin 1-methyl-4-phenyl-1,2,3,6-tetrahydropyridine (MPTP). *J. Med. Chem.* **1985,** *28* (10), 1432-6.
65. Hemmerich, P., Flavin-O2 interaction mechanisms and the function of flavin in hydroxylation reactions. *Ann. N.Y. Acad. Sci.* **1973,** *212*, 13-26.
66. Mager, H. I. X.; Addink, R., Electron transfer - II. Accumulation of 5-ethyl-3-methyllumiflavin radical by spontaneous conversions of 5-ethyl-3-methyllumiflavinium salts. *Tetrahedron* **1985,** *41* (1), 183-90.
67. (a) Nanni, E. J., Jr.; Sawyer, D. T.; Ball, S. S.; Bruice, T. C., Redox chemistry of N5-ethyl-3-methyllumiflavinium cation and N5-ethyl-4a-hydroperoxy-3-methyllumiflavin in dimethylformamide. Evidence for the formation of the N5-ethyl-4a-hydroperoxy-3-methyllumiflavin anion via radical-radical coupling with superoxide ion. *J. Am. Chem. Soc.* **1981,** *103* (10), 2797-802; (b) Muller, F.; Brustlein, M.; Hemmerich,

P.; Massey, V.; Walker, W. H., Light-absorption studies on neutral flavin radicals. *Eur. J. Biochem.* **1972,** *25* (3), 573-80.
68. (a) Vaish, S. P.; Tollin, G., Flash photolysis of flavins. V. Oxidation and disproportionation of flavin radicals. *J. Bioenerg.* **1971,** *2* (2), 61-72; (b) Muller, F., Flavin radicals: chemistry and biochemistry. *Free Radical Biol. Med.* **1987,** *3* (3), 215-30.
69. (a) Kemal, C.; Bruice, T. C., The chemistry of an N5-methyl-1,5-dihydroflavin and its aminium cation radical. *J. Am. Chem. Soc.* **1976,** *98* (13), 3955-64; (b) Bergstad, K.; Jonsson, S. Y.; Bäckvall, J.-E., A New Coupled Catalytic System for Dihydroxylation of Olefins by H2O2. *J. Am. Chem. Soc.* **1999,** *121* (44), 10424–10425; (c) Imada, Y.; Iida, H.; Ono, S.; Masui, Y.; Murahashi, S., Flavin-catalyzed oxidation of amines and sulfides with molecular oxygen: biomimetic green oxidation. *Chem. Asian. J.* **2006,** *1* (1-2), 136-47.
70. Mager, H. I. X., Activation and transfer of oxygen. XV. Evidence for the transient opening of the pyrazine ring in N1- and N5-alkylflavin models, 4A- to 10A-Adduct isomerization and pyrazine and pyrimidine ring contractions. *Tetrahedron Lett.* **1979,** (37), 3549-52.
71. Taga, M. E.; Larsen, N. A.; Howard-Jones, A. R.; Walsh, C. T.; Walker, G. C., BluB cannibalizes flavin to form the lower ligand of vitamin B12. *Nature* **2007,** *446* (7134), 449-53.
72. Muto, S.; Bruice, T. C., Dioxygen Transfer from 4a- Hydroperoxyflavin Anion. 3. Oxygen Transfer to the 3-Position of Substituted Indoles. *J. Am. Chem. Soc.* **1980,** *102*, 7559-7564.
73. Markey, S. P., *MPTP, a neurotoxin producing a Parkinsonian syndrome*. Academic Press: Orlando, 1986; p xiv, 722 p.
74. Ghisla, S.; Hartmann, U.; Hemmerich, P.; Mueller, F., Flavine series. XVIII. Reductive alkylation of the flavine nucleus. Structure and reactivity of dihydroflavines. *Justus Liebigs Annalen der Chemie* **1973,** (8), 1388-415.
75. Powell, M. F.; Wong, W. H.; Bruice, T. C., Concerning 1e- transfer in reduction by dihydronicotinamide: reaction of oxidized flavin and flavin radical with N-benzyl-1,5-dihydronicotinamide. *Proc. Natl. Acad. Sci. U.S.A.* **1982,** *79* (15), 4604-8.
76. Shamim, M. T.; Ukena, D.; Padgett, W. L.; Daly, J. W., Effects of 8-phenyl and 8-cycloalkyl substituents on the activity of mono-, di-, and trisubstituted alkylxanthines with substitution at the 1-, 3-, and 7-positions. *J. Med. Chem.* **1989,** *32* (6), 1231-7.
77. Hemmerich, P.; Fallab, S.; Erlenmeyer, H., Synthesen in der Lumiflavinreihe. *Helvetica Chimica Acta* **1956,** *1242* (S9), 1242-1252.
78. Yoneda, F.; Sakuma, Y.; Ichiba, M.; Shinomura, K., Syntheses of isoalloxazines and isoalloxazine 5-oxides. A new synthesis of riboflavin. *J. Am. Chem. Soc.* **1976,** *98* (3), 830-5.
79. Norrestam, R.; Tillberg, O., Flavine derivatives. Crystal and molecular structure of 5-ethyl-3,7,8,10-tetramethylisoalloxazinium perchlorate. *Acta Crystallogr.* **1972,** *28(B)* (Pt. 6), 1704-12.
80. Dyke, S. F., *Organic spectroscopy : an introduction*. 2d ed.; Longman: London; New York, 1978; p 290 p.
81. Brewslow, R., Small Antiaromatic Rings. *Angew. Chem.* **1968,** *7* (8), 565-570.

82. Tauscher, L.; Ghisla, S.; Hemmerich, P., NMR.-Study of nitrogen inversion and conformation of 1,5-dihydro-isoalloxazines ("reduced flavin"). Studies in the flavin series, XIX. *Helv. Chim. Acta* **1973,** *56* (2), 630-44.
83. (a) Waksman, G., Crystal structure of the phosphotyrosine recognition domain SH2 of the Src oncogene product complexed with tyrosine-phosphorylated peptides. *Cell. Mol. Biol.* **1994,** *40* (5), 611-8; (b) Lennon, B. W.; Williams, C. H., Jr.; Ludwig, M. L., Crystal structure of reduced thioredoxin reductase from Escherichia coli: structural flexibility in the isoalloxazine ring of the flavin adenine dinucleotide cofactor. *Protein Sci.* **1999,** *8* (11), 2366-79.

APPENDICES

Appendix A

License Agreement for Figure 1-1

NATURE PUBLISHING GROUP LICENSE TERMS AND CONDITIONS

Jun 23, 2013

This is a License Agreement between A Nakamura ("You") and Nature Publishing Group ("Nature Publishing Group") provided by Copyright Clearance Center ("CCC"). The license consists of your order details, the terms and conditions provided by Nature Publishing Group, and the payment terms and conditions.

All payments must be made in full to CCC. For payment instructions, please see information listed at the bottom of this form.

License Number	3174861283162
License date	Jun 23, 2013
Licensed content publisher	Nature Publishing Group
Licensed content publication	Nature Reviews Neuroscience
Licensed content title	Targeting programmed cell death in neurodegenerative diseases
Licensed content author	Miquel VilaandSerge Przedborski
Licensed content date	May 1, 2003
Volume number	4
Issue number	5
Type of Use	reuse in a thesis/dissertation
Requestor type	academic/educational
Format	print and electronic
Portion	figures/tables/illustrations
Number of figures/tables/illustrations	1
High-res required	no
Figures	I would like to use Box 2 figure in my dissertation
Author of this NPG article	no
Your reference number	
Title of your thesis / dissertation	Investigation of FAD Chemical Models to Study the Monoamine Oxidase Catalyzed Oxidation of Cyclic Tertiary Allylamines
Expected completion date	Jun 2013
Estimated size (number of pages)	200
Total	0.00 USD
Terms and Conditions	

Appendix B

UV Spectrum of 1-Methyl-4-(2-methylpyrrol-2-yl)-pyridinium in Acetonitrile

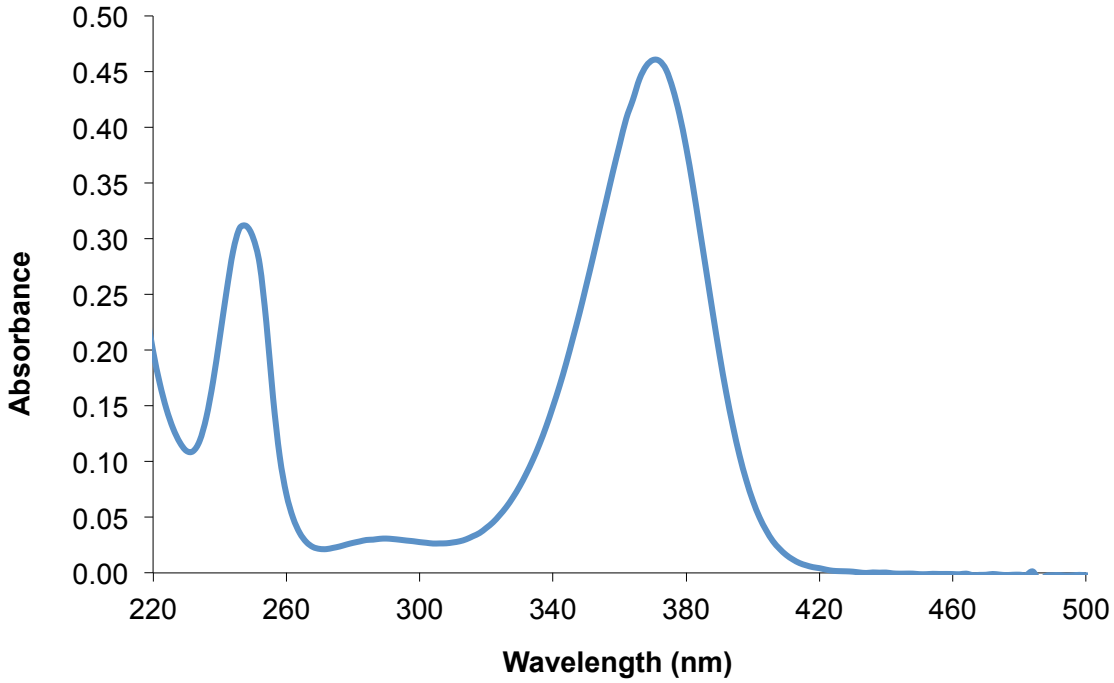

To calculate the molar extinction coefficient of MMP^+, ten mg of MMP^+I^- was dissolved in 25 mL of acetonitrile. That MMP^+I^- solution was diluted in acetonitrile (dilution factor 100), and then the absorbance was recorded three times, and the values were averaged out to calculate the molar extinction coefficient (0.46 at $\lambda_{max} = 370$, $\varepsilon = 34125$).

Appendix C

Sample Calculation for Quantitative Analysis using ^{1}H NMR

To quantify the formation of MMP^{+}, an internal standard hexamethyldisiloxane (HMDSO) was added to the reaction mixture of $5Et3MLF^{+}ClO_4^{-}$ and TMMP.

The concentration of MMP^{+} was calculated using the following equation.

$$\frac{Integration\ area\ of\ compound\ MMP+}{Integration\ area\ of\ compound\ HMDSO} = \frac{(number\ of\ protons\ in\ compound\ MMP+)(concentraion\ of\ compound\ MMP+)}{(number\ of\ protons\ in\ compound\ HMDSO)(concentration\ of\ compound\ HMDSO)}$$

Using the equation, the concentration of MMP+ at t = 300 min was calculated.

$$\frac{0.04}{0.14} = \frac{18\ (0.37)}{2\ (X\ mM)}$$

X = 24.14 mM

Thus, the reaction between $5Et3MLF^{+}ClO_4^{-}$ (25 mM) and TMMP (50 mM) yielded 24.14 mM of MMP^{+} at t = 300 min.

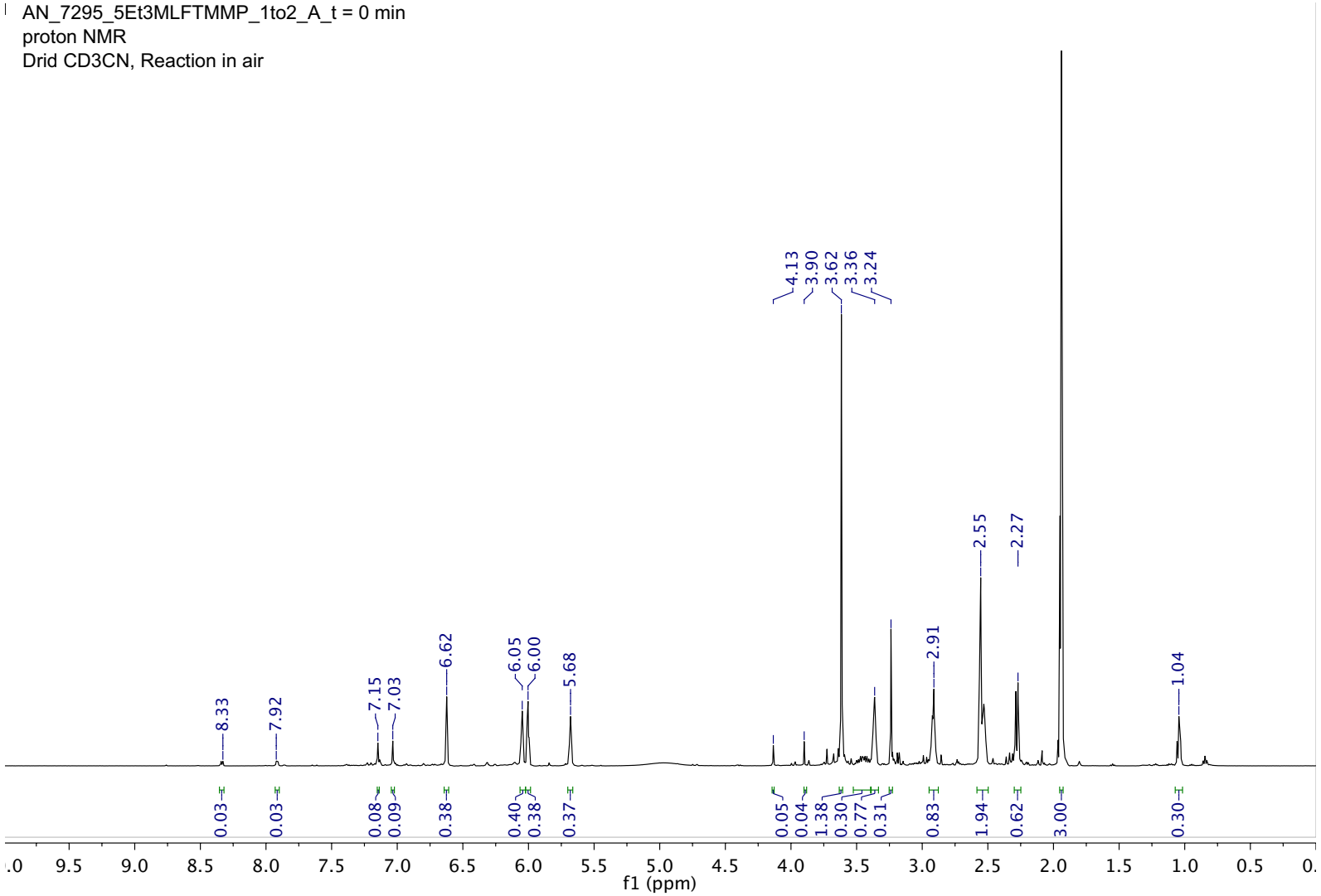
AN_7295_5Et3MLFTMMP_1to2_A_t = 0 min
proton NMR
Drid CD3CN, Reaction in air
8.33
7.92
7.15
7.03
6.62
6.05
6.00
5.68
4.13
3.90
3.62
3.36
3.24
2.91
2.55
2.27
1.04
0.03
0.03
0.08
0.09
0.38
0.40
0.38
0.37
0.05
0.04
1.38
0.30
0.77
0.31
0.83
1.94
0.62
3.00
0.30
f1 (ppm)

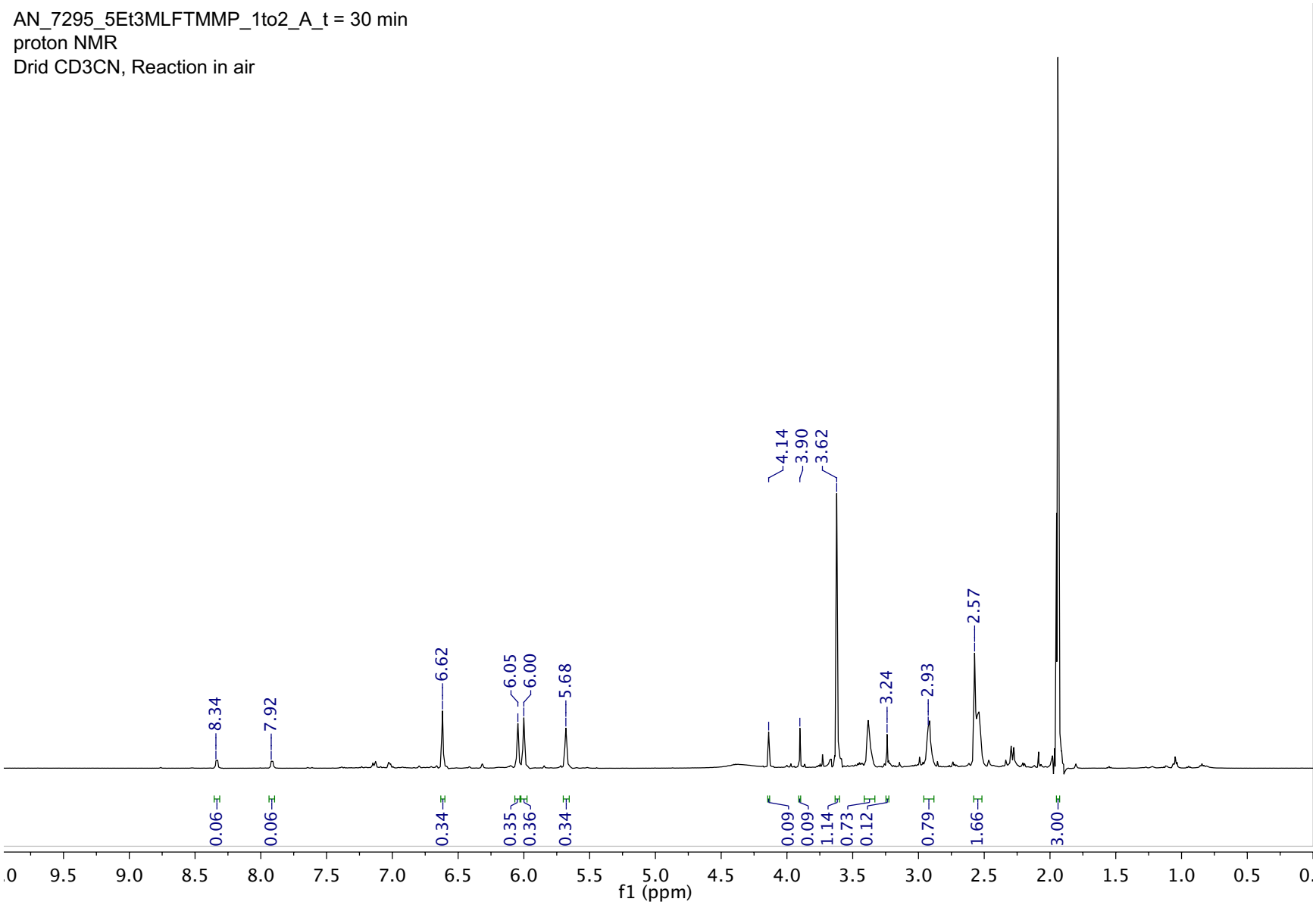
AN_7295_5Et3MLFTMMP_1to2_A_t = 30 min
proton NMR
Drid CD3CN, Reaction in air
8.34
7.92
6.62
6.05
6.00
5.68
4.14
3.90
3.62
3.24
2.93
2.57
0.06
0.06
0.34
0.35
0.36
0.34
0.09
0.09
1.14
0.73
0.12
0.79
1.66
3.00
f1 (ppm)

AN_7295_5Et3MLFTMMP_1to2_A_t = 60 min
proton NMR
Drid CD3CN, Reaction in air

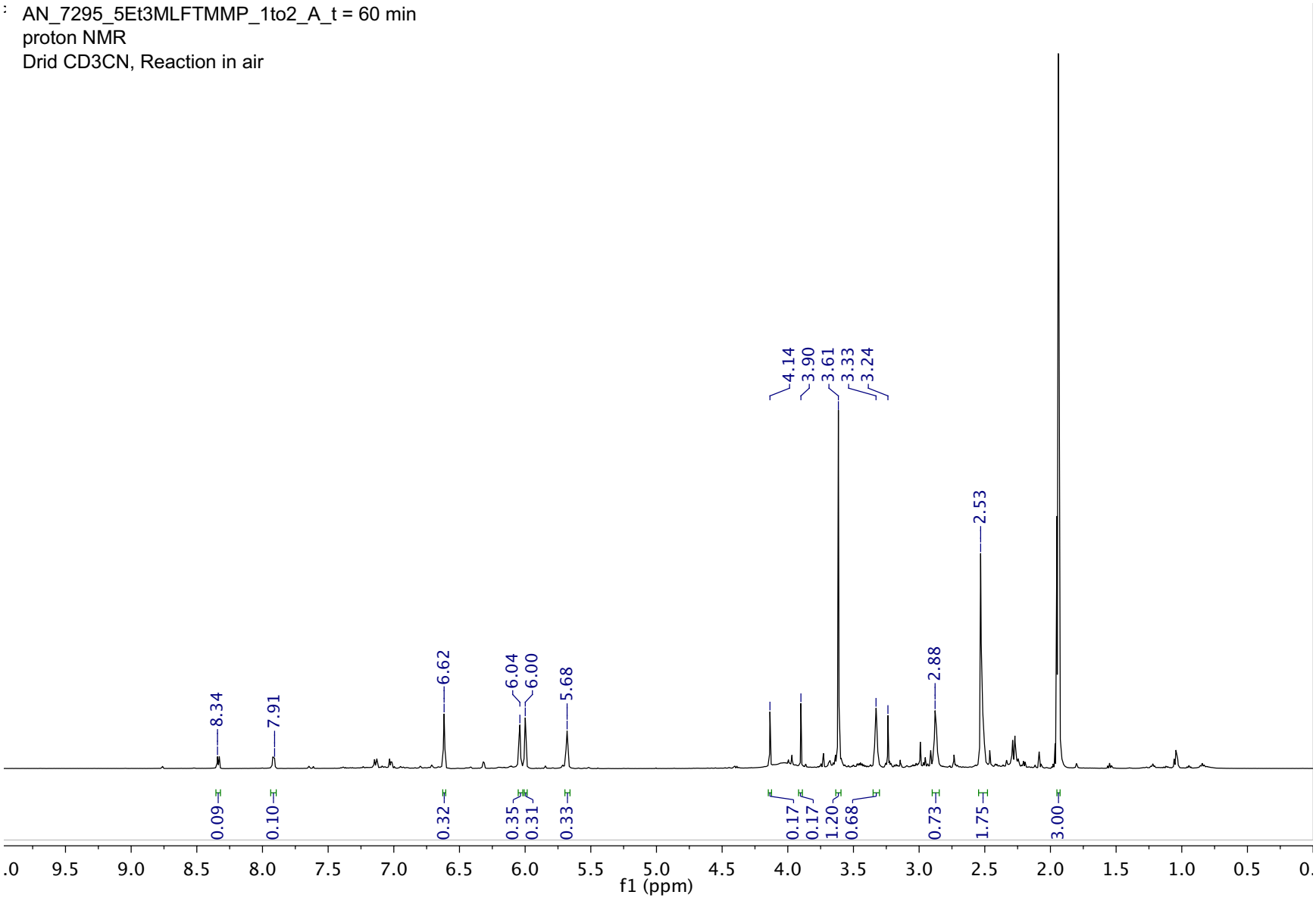

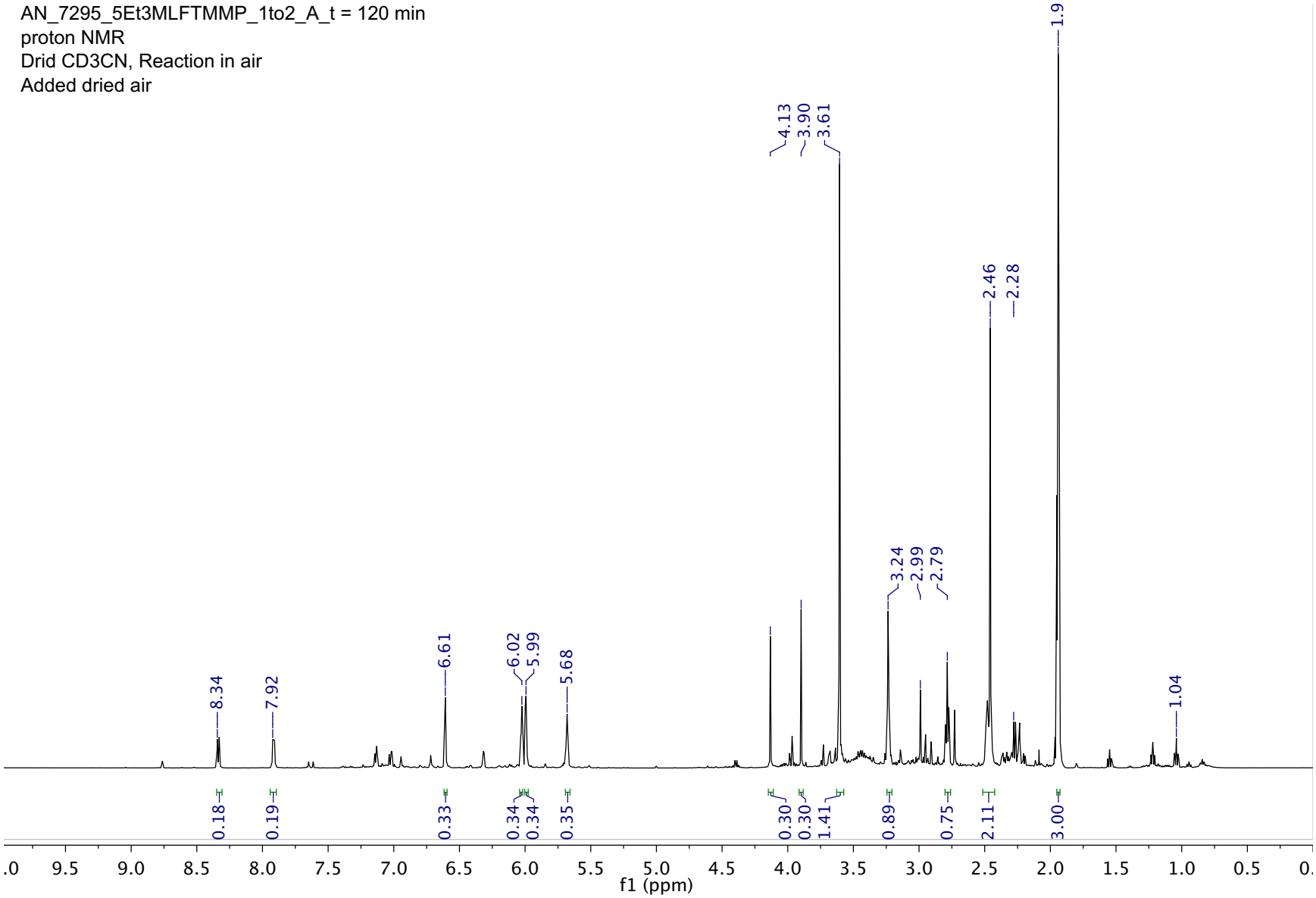
AN_7295_5Et3MLFTMMP_1to2_A_t = 120 min
proton NMR
Drid CD3CN, Reaction in air
Added dried air
8.34
7.92
6.61
6.02
5.99
5.68
4.13
3.90
3.61
3.24
2.99
2.79
2.46
2.28
1.9
1.04
0.18
0.19
0.33
0.34
0.34
0.35
0.30
0.30
1.41
0.89
0.75
2.11
3.00
f1 (ppm)

AN_7295_5Et3MLFTMMP_1to2_A_t = 150 min
proton NMR
Drid CD3CN, Reaction in air
Added dried air

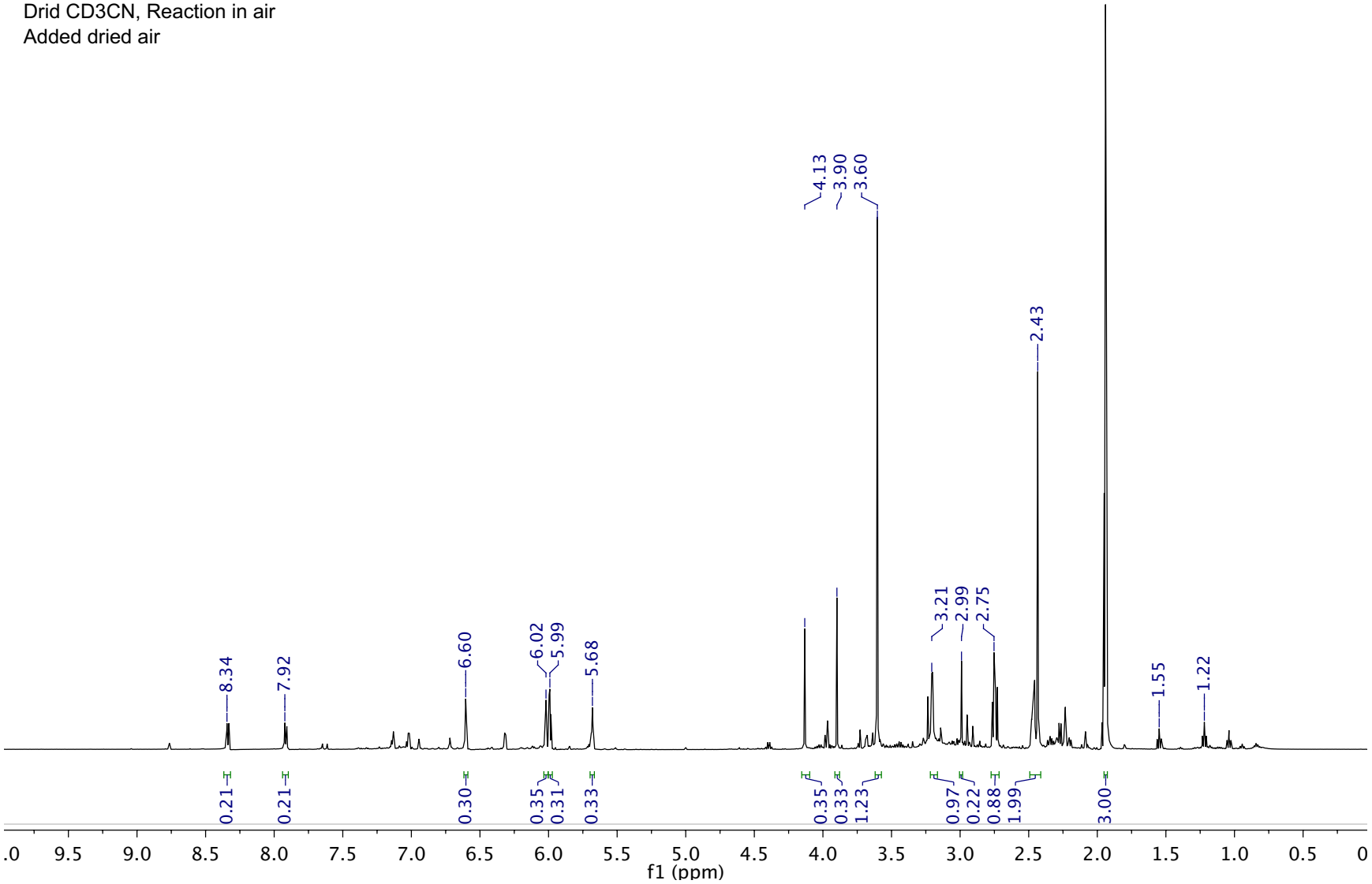

AN_7295_5Et3MLFTMMP_1to2_A_t = 180 min
proton NMR
Drid CD3CN, Reaction in air
Added dried Air

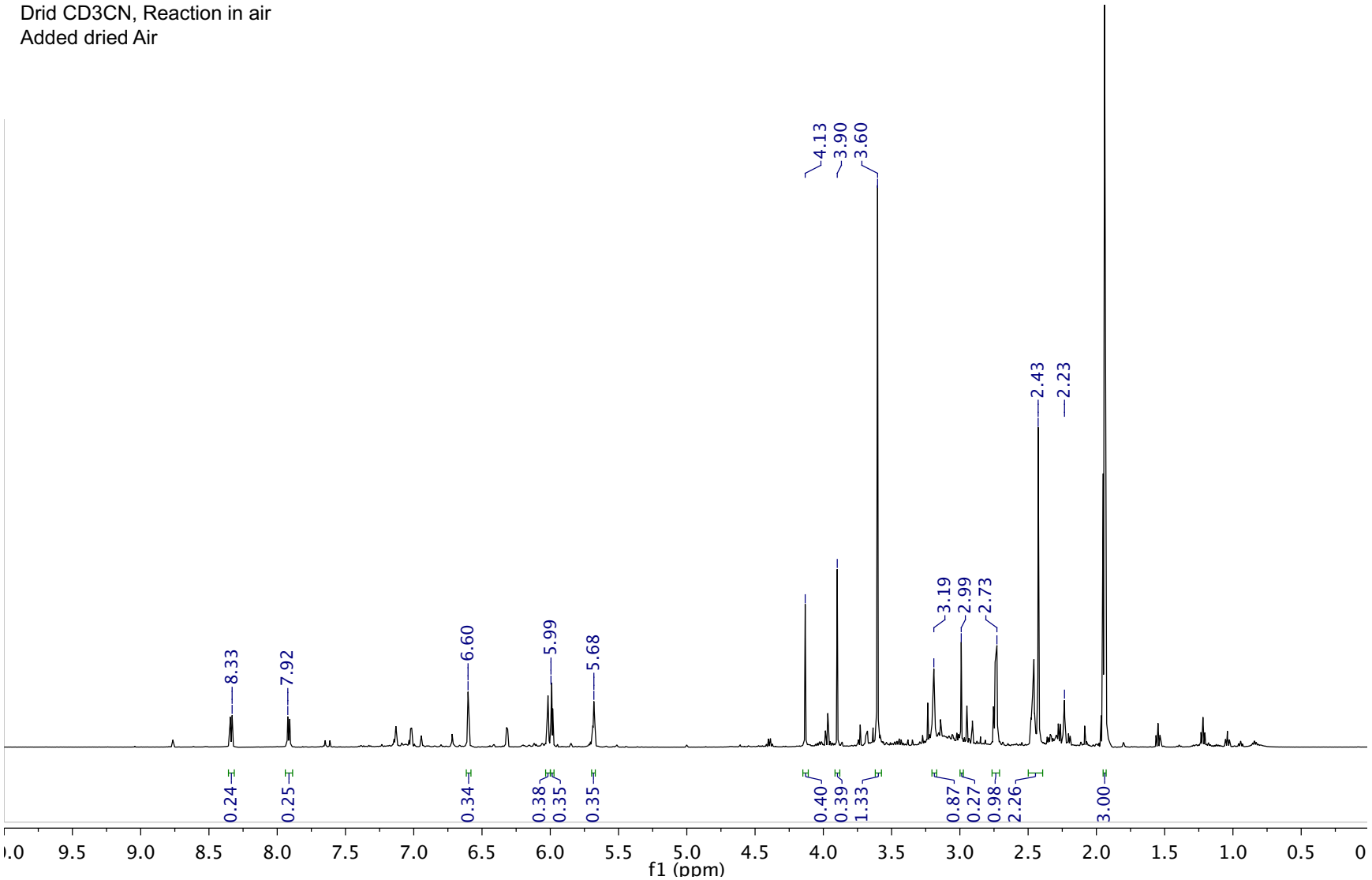

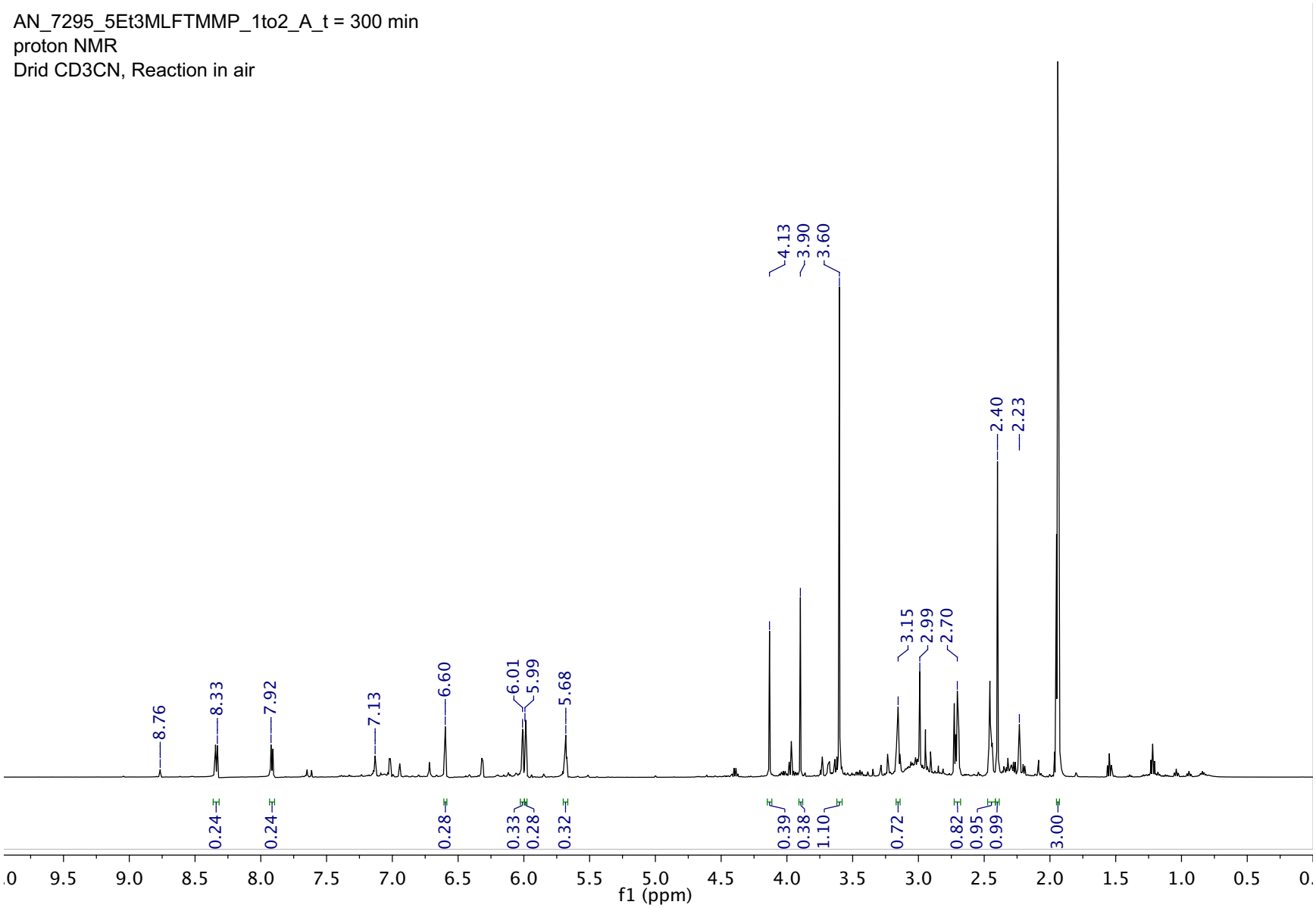
AN_7295_5Et3MLFTMMP_1to2_A_t = 300 min
proton NMR
Drid CD3CN, Reaction in air
8.76
8.33
7.92
7.13
6.60
6.01
5.99
5.68
4.13
3.90
3.60
3.15
2.99
2.70
2.40
2.23
0.24
0.24
0.28
0.33
0.28
0.32
0.39
0.38
1.10
0.72
0.82
0.95
0.99
3.00
f1 (ppm)

AN_7295_5Et3MLFTMMP_1to2_A_t = 24hrs
proton NMR
Drid CD3CN, Reaction in air

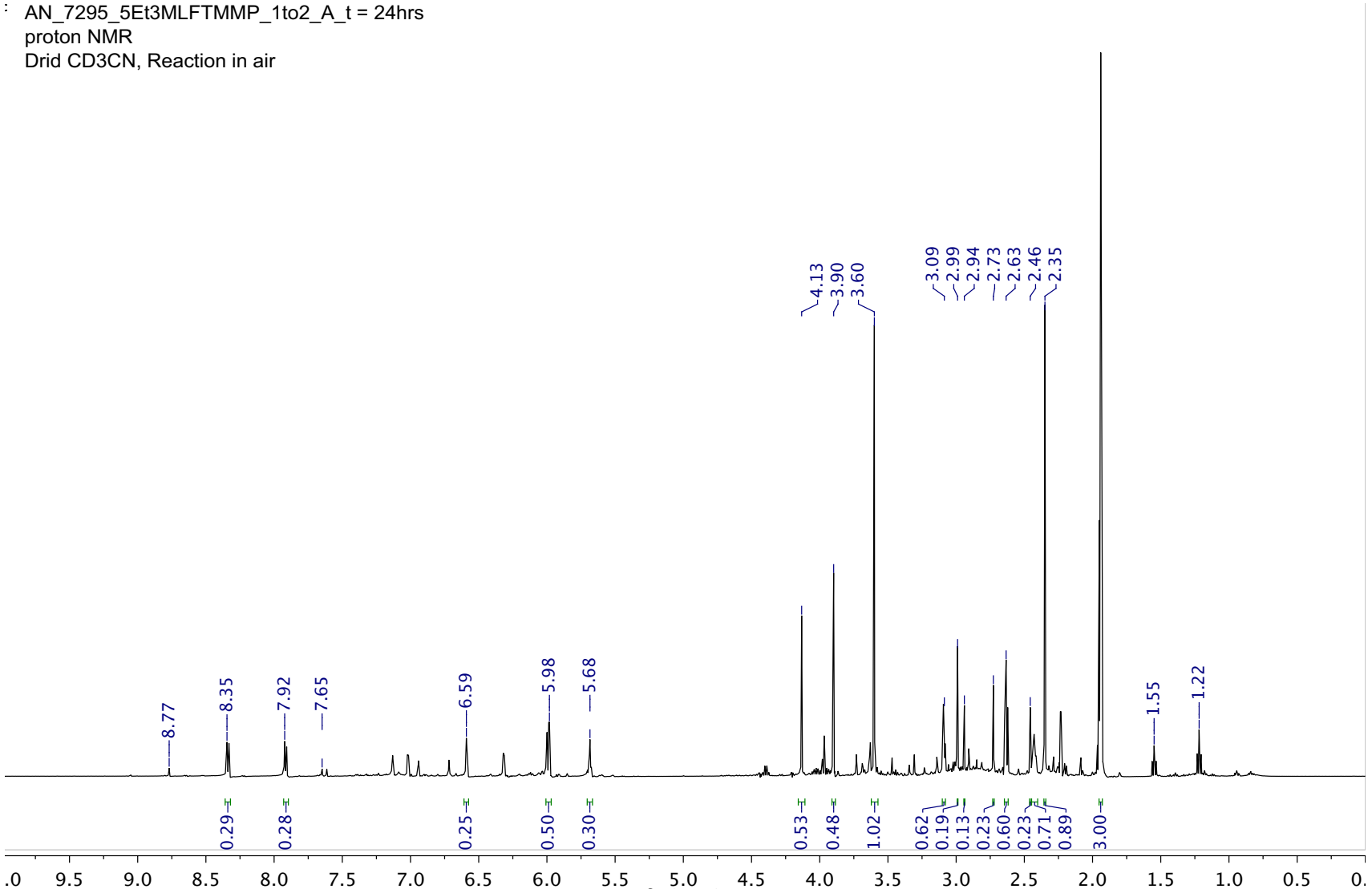

Appendix E: Supplemental Data for Chapter 3-2 (Section 3.2.2.5)

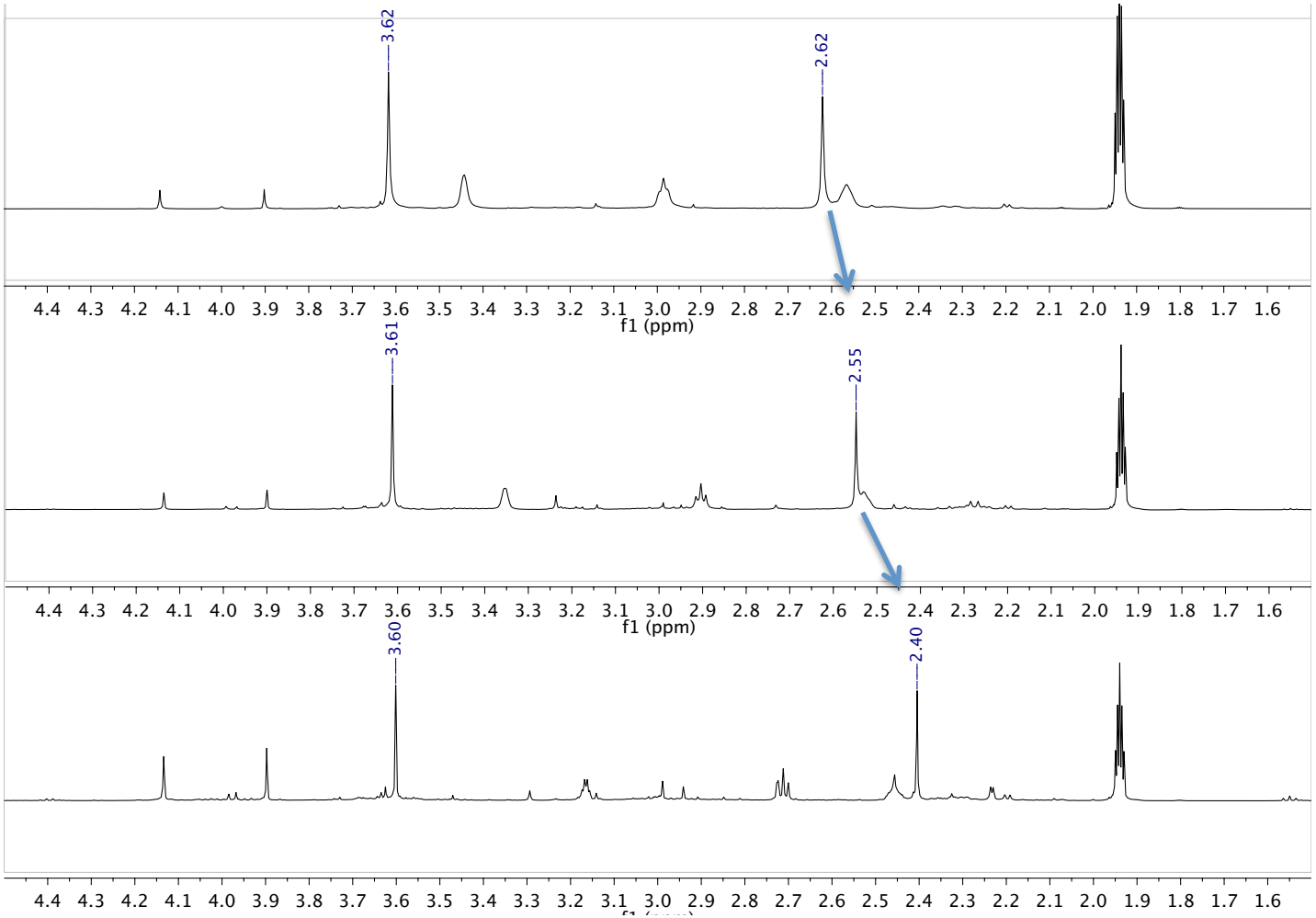

Superimposed ^{1}H NMR spectra of the reaction between 5Et3MLF$^{+}CLO_{4}^{-}$ and TMMP at δ = 4.5 ppm - 1.5 ppm: under argon at T = 0 min (top), immediately after the air was re-introduced (middle), and 24 hours after the air was re-introduced (bottom).

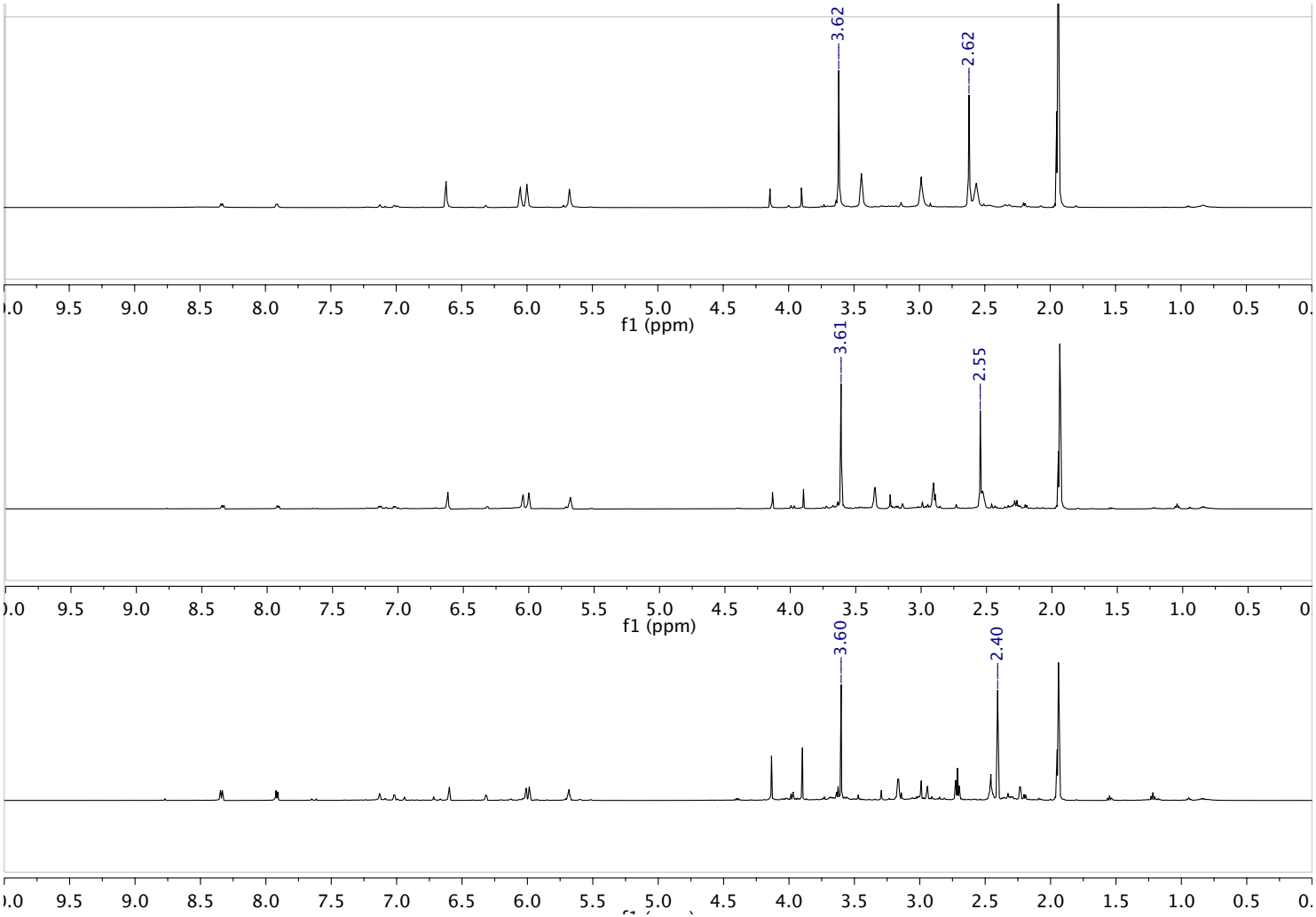

Superimposed ^{1}H NMR spectra of the reaction between $5Et3MLF^{+}CLO_4^{-}$ and TMMP at δ = 10 ppm - 0 ppm: under argon T = 0 min (top), immediately after the air was re-introduced (middle), and 24 hours after the air was re-introduced (bottom).

Appendix F

License Agreement for Figure 3-2-16

ELSEVIER LICENSE
TERMS AND CONDITIONS

Jun 10, 2013

This is a License Agreement between A Nakamura ("You") and Elsevier ("Elsevier") provided by Copyright Clearance Center ("CCC"). The license consists of your order details, the terms and conditions provided by Elsevier, and the payment terms and conditions.

All payments must be made in full to CCC. For payment instructions, please see information listed at the bottom of this form.

Supplier	Elsevier Limited The Boulevard,Langford Lane Kidlington,Oxford,OX5 1GB,UK
Registered Company Number	1982084
Customer name	A Nakamura
Customer address	Department of Chemistry Blacksburg, VA 24061
License number	3165360181994
License date	Jun 10, 2013
Licensed content publisher	Elsevier
Licensed content publication	Tetrahedron
Licensed content title	Electron transfer-II: Accumulation of 5-ethyl-3-methyllumiflavin radical by spontaneous conversions of 5-ethyl-3-methyllumiflavinium salts
Licensed content author	H.I.X. Mager,R. Addink
Licensed content date	1985
Licensed content volume number	41
Licensed content issue number	1
Number of pages	8
Start Page	183
End Page	190
Type of Use	reuse in a thesis/dissertation
Portion	figures/tables/illustrations
Number of figures/tables /illustrations	1

Format	both print and electronic
Are you the author of this Elsevier article?	Yes
Will you be translating?	No
Order reference number	
Title of your thesis/dissertation	Investigation of FAD Chemical Models to Study the Monoamine Oxidase Catalyzed Oxidation of Cyclic Tertiary Allylamines
Expected completion date	Jun 2013
Estimated size (number of pages)	200
Elsevier VAT number	GB 494 6272 12
Permissions price	0.00 USD
VAT/Local Sales Tax	0.0 USD / 0.0 GBP
Total	0.00 USD
Terms and Conditions	

Appendix G

License Agreement for Figure 3-2-18

JOHN WILEY AND SONS LICENSE TERMS AND CONDITIONS

Mar 15, 2013

This is a License Agreement between A Nakamura ("You") and John Wiley and Sons ("John Wiley and Sons") provided by Copyright Clearance Center ("CCC"). The license consists of your order details, the terms and conditions provided by John Wiley and Sons, and the payment terms and conditions.

All payments must be made in full to CCC. For payment instructions, please see information listed at the bottom of this form.

License Number	3110301165108
License date	Mar 15, 2013
Licensed content publisher	John Wiley and Sons
Licensed content publication	FEBS Journal
Licensed content title	Light-Absorption Studies on Neutral Flavin Radicals
Licensed copyright line	Copyright © 2005, John Wiley and Sons
Licensed content author	Franz Müller,Martin Brüstlein,Peter Hemmerich,Vincent Massey,Wolfram H. Walker
Licensed content date	Mar 3, 2005
Start page	573
End page	580
Type of use	Dissertation/Thesis
Requestor type	University/Academic
Format	Print and electronic
Portion	Figure/table
Number of figures/tables	4
Number of extracts	
Original Wiley figure/table number(s)	I would like to use Figure 4 in my doctoral thesis. Thank you.
Will you be translating?	No
Order reference number	
Total	0.00 USD
Terms and Conditions	

Appendix H

License Agreement for Figure 3-2-23

NATURE PUBLISHING GROUP LICENSE
TERMS AND CONDITIONS

Jul 03, 2013

This is a License Agreement between A Nakamura ("You") and Nature Publishing Group ("Nature Publishing Group") provided by Copyright Clearance Center ("CCC"). The license consists of your order details, the terms and conditions provided by Nature Publishing Group, and the payment terms and conditions.

All payments must be made in full to CCC. For payment instructions, please see information listed at the bottom of this form.

License Number	3181161360758
License date	Jul 03, 2013
Licensed content publisher	Nature Publishing Group
Licensed content publication	Nature
Licensed content title	BluB cannibalizes flavin to form the lower ligand of vitamin B12
Licensed content author	Michiko E. Taga, Nicholas A. Larsen, Annaleise R. Howard-Jones, Christopher T. Walsh and Graham C. Walker
Licensed content date	Mar 22, 2007
Volume number	446
Issue number	7134
Type of Use	reuse in a thesis/dissertation
Requestor type	academic/educational
Format	print and electronic
Portion	figures/tables/illustrations
Number of figures/tables /illustrations	1
High-res required	no
Figures	Figure 1
Author of this NPG article	no
Your reference number	
Title of your thesis / dissertation	Investigation of FAD Chemical Models to Study the Monoamine Oxidase Catalyzed Oxidation of Cyclic Tertiary Allylamines
Expected completion date	Jul 2013
Estimated size (number of pages)	200
Total	0.00 USD

Appendix I

Elemental Analysis Data of Benzoimidazolium Compounds

1-ethyl-5,6-dimethyl-1*H*-benzo[*d*]imidazole

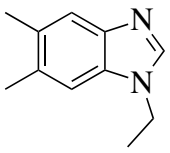

Chemical Formula: $C_{11}H_{14}N_2$
Elemental Analysis: C, 75.82; H, 8.10; N, 16.08

C	H	N	
11	14	2	
%			
Carbon	Hydrogen	Nitrogen	Total
75.81	8.10	16.09	100.00

Atlantic Microlab, Inc.

Sample No. AN 7297A

6180 Atlantic Blvd. Suite M
Norcross, GA 30071
www.atlanticmicrolab.com

Company/School Virginia Tech
Dept. Chemistry
Address
City, State, Zip
Name Akiko Nakamura Date
Phone 540-231-[illegible] 1912

Professor/Supervisor: Tanko
PO# / CC# PO # 30595202

Element	Theory	Found	
C	75.8	75.83	76.01
H	8.1	7.94	8.04
N	16.09	16.08	16.04

Single ☐ Duplicate ☒

Elements Present: C, H, N

Analyze for: C, H, N

Hygroscopic ☐ Explosive ☐ unknown
M.P. B.P.

To be dried: Yes ☒ No ☐
Temp. Vac. Time

Rush Service ☐ Rush service guarantees analyses will be completed and results available by 5 PM EST on the day the sample is received by 11 AM.

Include Email Address or FAX # Below

nakamura@vt.edu.

Date Received JUL 0 8 2013 Date Completed JUL 0 9 2013
Remarks:

3-ethyl-1,5,6-trimethyl-1*H*-benzo[*d*]imidazol-3-ium

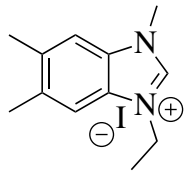

Chemical Formula: $C_{12}H_{17}IN_2$
Elemental Analysis: C, 45.58; H, 5.42; I, 40.14; N, 8.86

C	H	N	I	
12	17	2	1	
%				
Carbon	Hydrogen	Nitrogen	Iodine	Total
45.58	5.42	8.86	40.14	100.00

Atlantic Microlab, Inc.

Sample No. AN7297B

6180 Atlantic Blvd. Suite M
Norcross, GA 30071
www.atlanticmicrolab.com

Company/School Virginia Tech
Dept. Chemistry
Address
City, State, Zip
Name Akiko Nakamura Date
Phone 540-231-1912

Professor/Supervisor: Tanko
PO# / CC# PO# 3059520'2

Element	Theory	Found	
C	45.58	45.58	45.69
H	5.42	5.34	5.49
N	8.86	8.72	8.80

Single ☐ Duplicate ☒
Elements Present: C, H, N, I
Analyze for: C, H, N
Temp.
Rush Service ☐ Rush service guarantees analyses will be completed and results available by 5 PM EST on the day the sample is received by 11 AM.
Include Email Address or FAX # Below
nakamura@vt.edu

Date Received JUL 0 8 2013 Date Completed JUL 0 9 2013
Remarks:

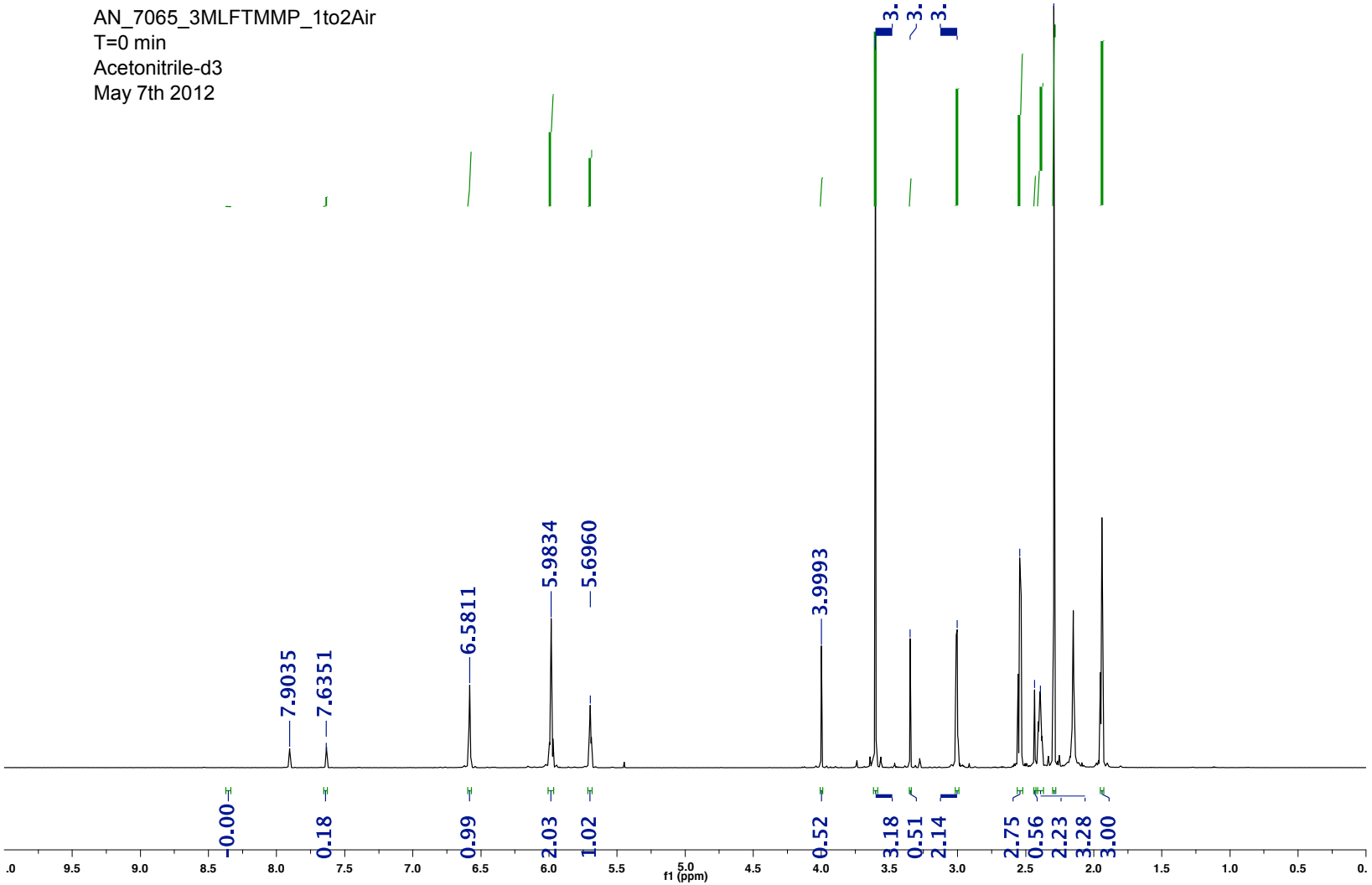
AN_7065_3MLFTMMP_1to2Air
T=0 min
Acetonitrile-d3
May 7th 2012
7.9035
7.6351
6.5811
5.9834
5.6960
3.9993
0.00
0.18
0.99
2.03
1.02
0.52
3.18
0.51
2.14
2.75
0.56
2.23
3.28
3.00
f1 (ppm)

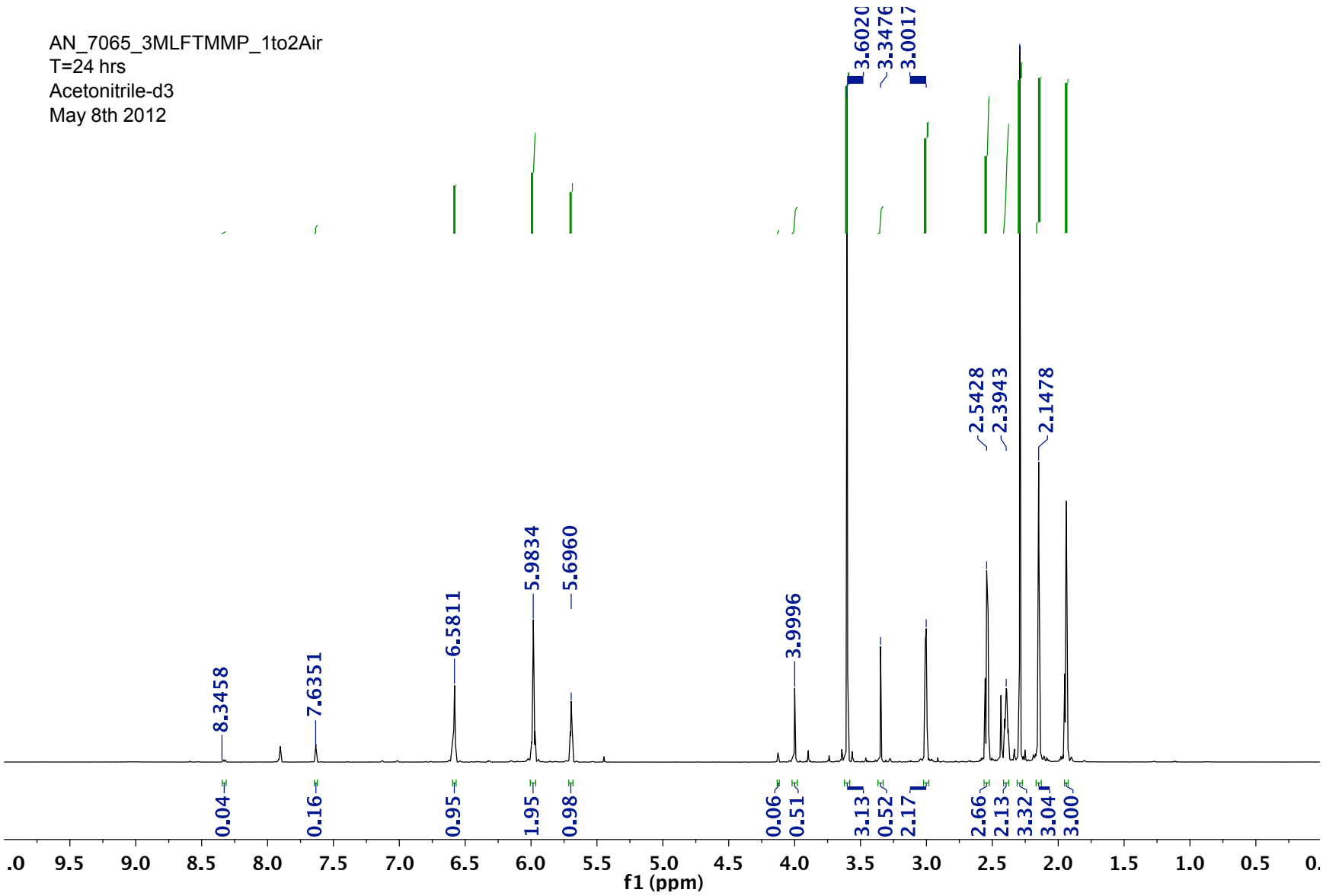
AN_7065_3MLFTMMP_1to2Air
T=24 hrs
Acetonitrile-d3
May 8th 2012
8.3458
7.6351
6.5811
5.9834
5.6960
3.9996
3.6020
3.3476
3.0017
2.5428
2.3943
2.1478
0.04
0.16
0.95
1.95
0.98
0.06
0.51
3.13
0.52
2.17
2.66
2.13
3.32
3.04
3.00
f1 (ppm)

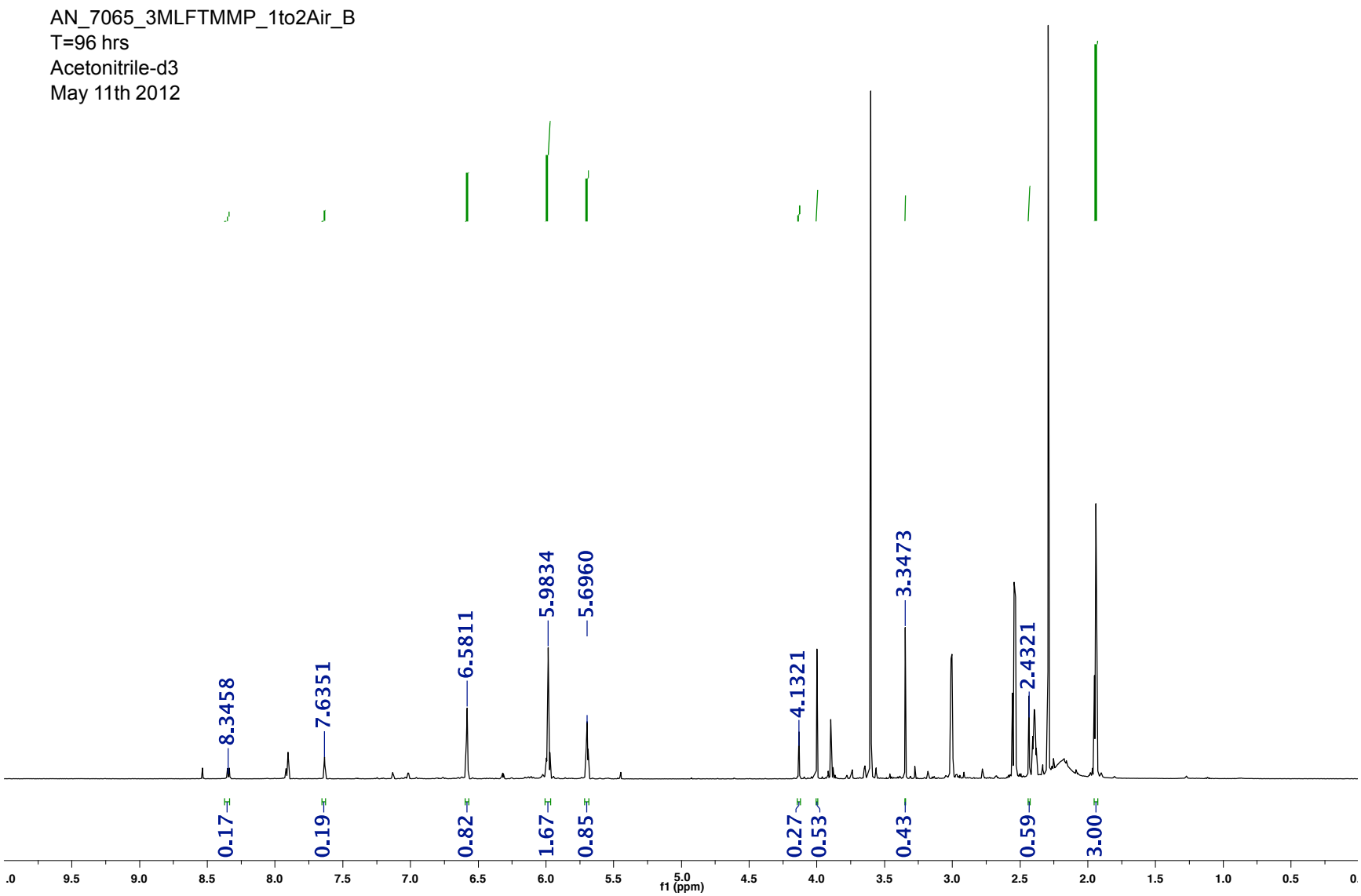
AN_7065_3MLFTMMP_1to2Air_B
T=96 hrs
Acetonitrile-d3
May 11th 2012
8.3458
7.6351
6.5811
5.9834
5.6960
4.1321
3.3473
2.4321
0.17
0.19
0.82
1.67
0.85
0.27
0.53
0.43
0.59
3.00
f1 (ppm)

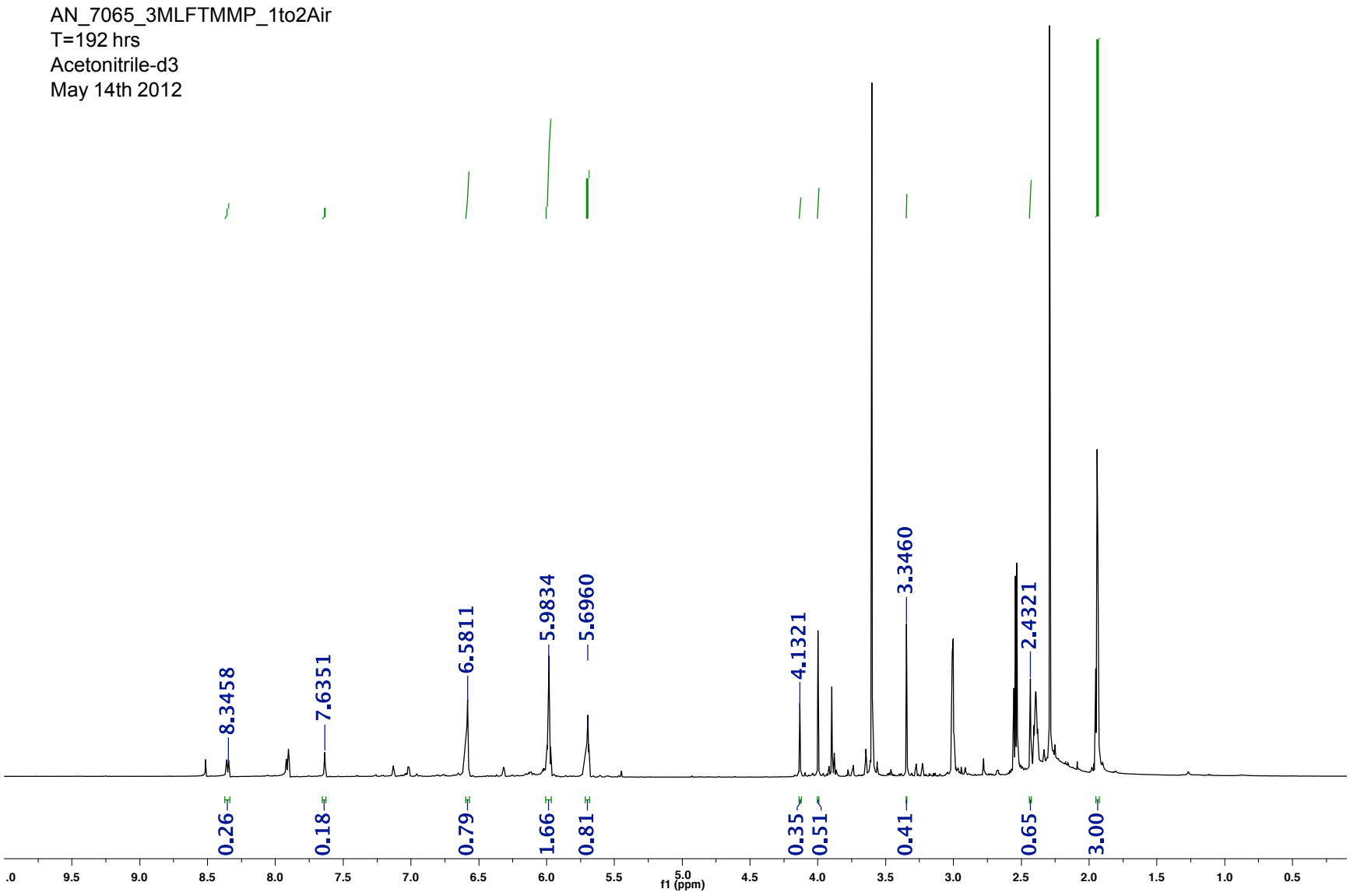
AN_7065_3MLFTMMP_1to2Air
T=192 hrs
Acetonitrile-d3
May 14th 2012
8.3458
7.6351
6.5811
5.9834
5.6960
4.1321
3.3460
2.4321
0.26
0.18
0.79
1.66
0.81
0.35
0.51
0.41
0.65
3.00
f1 (ppm)

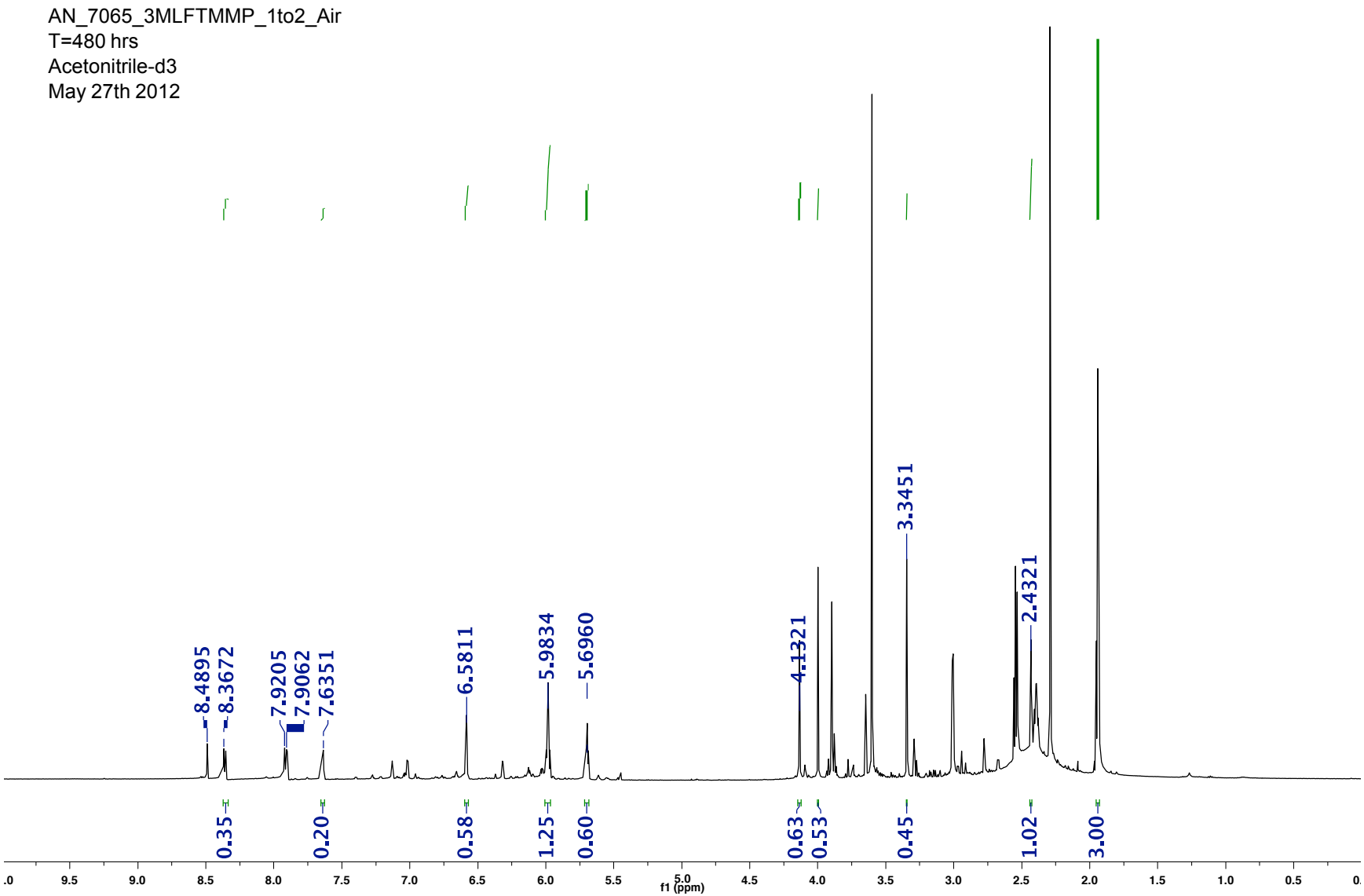
AN_7065_3MLFTMMP_1to2_Air
T=480 hrs
Acetonitrile-d3
May 27th 2012
8.4895
8.3672
7.9205
7.9062
7.6351
6.5811
5.9834
5.6960
4.1321
3.3451
2.4321
0.35
0.20
0.58
1.25
0.60
0.63
0.53
0.45
1.02
3.00
f1 (ppm)

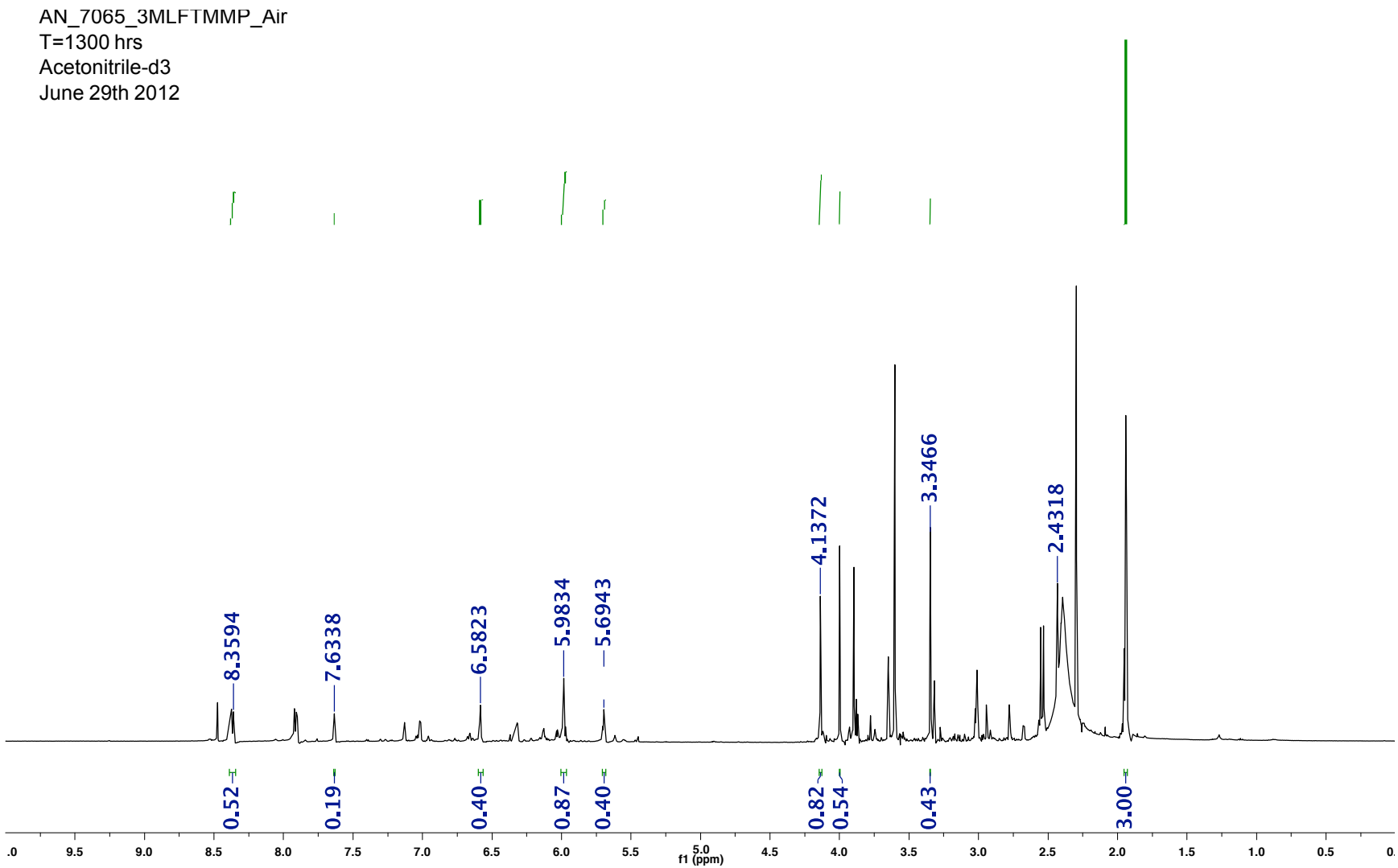
AN_7065_3MLFTMMP_Air
T=1300 hrs
Acetonitrile-d3
June 29th 2012
8.3594
7.6338
6.5823
5.9834
5.6943
4.1372
3.3466
2.4318
0.52
0.19
0.40
0.87
0.40
0.82
0.54
0.43
3.00
f1 (ppm)